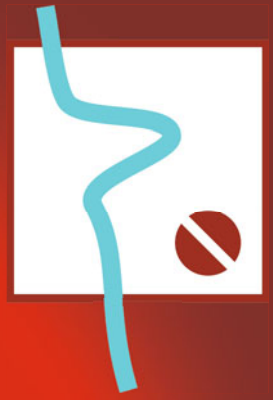


Building Pathology and Rehabilitation



João M.P.Q. Delgado *Editor*

Recent Developments in Building Diagnosis Techniques

 Springer

Building Pathology and Rehabilitation

Volume 5

Series editors

V. Peixoto de Freitas, Porto, Portugal

Aníbal Costa, Aveiro, Portugal

João M.P.Q. Delgado, Porto, Portugal

More information about this series at <http://www.springer.com/series/10019>

João M.P.Q. Delgado
Editor

Recent Developments in Building Diagnosis Techniques

 Springer

Editor
João M.P.Q. Delgado
Faculty of Engineering
University of Porto
Porto
Portugal

ISSN 2194-9832 ISSN 2194-9840 (electronic)
Building Pathology and Rehabilitation
ISBN 978-981-10-0465-0 ISBN 978-981-10-0466-7 (eBook)
DOI 10.1007/978-981-10-0466-7

Library of Congress Control Number: 2015960832

© Springer Science+Business Media Singapore 2016

This work is subject to copyright. All rights are reserved by the Publisher, whether the whole or part of the material is concerned, specifically the rights of translation, reprinting, reuse of illustrations, recitation, broadcasting, reproduction on microfilms or in any other physical way, and transmission or information storage and retrieval, electronic adaptation, computer software, or by similar or dissimilar methodology now known or hereafter developed.

The use of general descriptive names, registered names, trademarks, service marks, etc. in this publication does not imply, even in the absence of a specific statement, that such names are exempt from the relevant protective laws and regulations and therefore free for general use.

The publisher, the authors and the editors are safe to assume that the advice and information in this book are believed to be true and accurate at the date of publication. Neither the publisher nor the authors or the editors give a warranty, express or implied, with respect to the material contained herein or for any errors or omissions that may have been made.

Printed on acid-free paper

This Springer imprint is published by SpringerNature
The registered company is Springer Science+Business Media Singapore Pte Ltd.

Preface

In the distant past, construction solutions were validated empirically through several years of experience, whereas with the onset of further industrialization of the construction process, it was recognized within the construction community that a performance-based selection of materials, components, and systems was required if innovation was to be fostered and progress in the construction domain achieved. However, it was equally apparent to those promoting such novel approaches that the selection on the basis of understanding of performance requirements could only be met if the results of research and development were made available and indeed exploitable by practitioners.

The main purpose of this book, *Recent Developments in Building Diagnosis Techniques*, is to provide a collection of recent research works on building diagnosis techniques to contribute to the systematization and dissemination of knowledge related to construction pathology, hygrothermal behaviour of buildings, durability, and diagnostic techniques and, simultaneously, to show the most recent advances in this domain. It includes a set of new developments in the field of building physics, risk assessment of urban fire, building anomalies in materials and components, new techniques for better energy efficiency analysis, and diagnosis techniques, such as infrared thermography. Building thermography is explained with a lot of thermal images as examples for physical consequences of formulae, and case studies of several kinds of inspections are developed, from moisture and mould, to building energy efficiency and construction defects, etc.

The book is divided into several chapters that intend to be a resume of the current state of knowledge for the benefit of professional colleagues, scientists, students, practitioners, lecturers, and other interested parties to network. At the same time, these topics will be the encounter of a variety of scientific and engineering disciplines, such as civil, materials, and mechanical engineering.

João M.P.Q. Delgado

Contents

Practical Experiences from Several Moisture Performance Assessments	1
Petri J. Annila, Jukka Lahdensivu, Jommi Suonketo and Matti Pentti	
Analysis of Main Parameters that Affect Contact Area Between Mortar Rendering and Substrate: Use of 3D Laser Scanning Technique.	21
Carina Mariane Stolz and Angela Borges Masuero	
The Pathologies of the ETICS	37
Filiberto Lembo and Francesco Paolo R. Marino	
Criteria for Identification of Ceramic Detachments in Building Facades with Infrared Thermography	51
Elton Bauer, Elier Pavón, Cláudio H.F. Pereira and Matheus L.M. Nascimento	
Diagnosis of Moisture Movements in Massive Dolostone Walls of Medieval Churches	69
Lembit Kurik, Targo Kalamees and Urve Kallavus	
The Wind-Driven Rain and the Buildings: Directional Driving Rain, Experimental Simulation and Quantification of Wetness Areas	91
Lais Zucchetti, Patricia Poyastro, Silvia Trein Heimfarth Dapper, Angela Borges Masuero and Acir Mércio Loredou-Souza	
A Performance Assessment of Prefabricated Bathrooms Installed in the 1990s	105
Martin Morelli and Erik Brandt	
Good Practice: Analysis of the Vulnerability of Seven Churches in Monza. From an Information Model to a Geodatabase	127
Cecilia Bolognesi	

**On the Use of Infrared Thermographic Measurements
for Evaluating the Airtightness of the Building Envelope 145**
Katrien Maroy, Nathan Van Den Bossche, Marijke Steeman
and Sven Van De Vijver

**Evaluation of Moisture Transfer to Improve the Conservation
of Tiles Finishing Facades 171**
Silvia Erba, Bruno Daniotti, Elisabetta Rosina, Antonio Sansonetti
and Riccardo Paolini

**Analysis of Microclimate in a Historical Building to Assess
the Probability of Recurrence of Filamentous Fungi 195**
Fernanda Lamego Guerra, Eduardo Grala da Cunha and Fábio Galli

Practical Experiences from Several Moisture Performance Assessments

Petri J. Annila, Jukka Lahdensivu, Jommi Suonketo and Matti Pentti

Abstract This study analysed the moisture performance assessment reports of 76 buildings: 56 schools, nine healthcare buildings, three daycare centres and five office buildings. The researchers' practical experiences from moisture performance assessments were also made use of in the study. The aim of this study was to determine the methods used to detect moisture and mould damage in the building stock. The results of the study show that most moisture and mould damage is detected by a surface moisture indicator (Annila et al. in Proceedings of the 1st international symposium on building pathology, pp 115–122, 2015a). That is an important finding since these indicators enable easy measuring of large sections of structures and targeting of more detailed inspections, moisture measurements and material samplings based on mapping with them.

Keywords Indoor air quality · Moisture · Mould · Sick building syndrome · Condition assessment

1 Introduction

The indoor air quality (IAQ) problems of the building stock are caused by many factors including carbon dioxide (CO₂), carbon monoxide (CO), nitrogen dioxide (NO₂), particulate matter (PM), high indoor temperature and relative humidity, low

P.J. Annila (✉) · J. Lahdensivu · J. Suonketo · M. Pentti
Department of Civil Engineering, Tampere University of Technology,
P.O. Box 600, 33101 Tampere, Finland
e-mail: petri.annila@tut.fi

J. Lahdensivu
e-mail: jukka.lahdensivu@tut.fi

J. Suonketo
e-mail: Jommi.suonketo@tut.fi

M. Pentti
e-mail: matti.pentti@tut.fi

ventilation rate, mould, bacteria, volatile organic compounds (VOC), chemicals, dust, cigarette smoke, pet allergens, radon, asbestos and formaldehyde (HCHO). The most significant factor varies by region and year of construction (Weschler 2009). In the Nordic countries and in North America, indoor air problems are often related to moisture and mould damage in structures and buildings (Bornehag et al. 2001, 2004; Hyvärinen 2002; Mudarri and Fisk 2007).

A recent study (Annila et al. 2015a) established the methods used in Finland to detect moisture and mould damage in buildings and structures. The research material consisted of moisture performance assessment reports on 76 buildings. Moreover, experiences from practical moisture performance assessments were used to find new targets of development. The study was conducted as part of wider research aimed at developing operating procedures and methods for earlier detection of moisture and mould damage. The methods can help prevent moisture and mould damage and ensuing IAQ problems and negative health impacts.

2 Literature Review

2.1 *Moisture Performance Assessment in Finland*

Awareness of moisture and mould damage in the building stock and its impact on IAQ and the health of users increased in the 80s. Subsequently, the subject area was researched a lot and the methods presently used in Finnish moisture performance assessment became established in the 90s. They are partly described, for instance, in Haverinen-Shaughnessy et al. (2008) and Asikainen (2008). An updated guide for moisture performance assessment is currently being prepared as part of the moisture and mould programme of the Ministry of the Environment in Finland.

In Finland, research on moisture and mould damage is referred to either as moisture performance assessment or IAQ research. In practice, their contents are nearly identical, but their aims are different. Moisture performance assessment determines the current condition of structures, any possible damage in them, and their future repair needs. Indoor air research focuses on IAQ and possible impurities in the air. High quality indoor air research, however, also establishes the moisture and mould damage to structures which makes its content practically identical to that of a moisture performance assessment.

Moisture performance assessments generally consist of the four main phases described in Fig. 1 (Annila et al. 2015a): analysis of background and input data, field study, necessary laboratory tests, and analysis and conclusions.

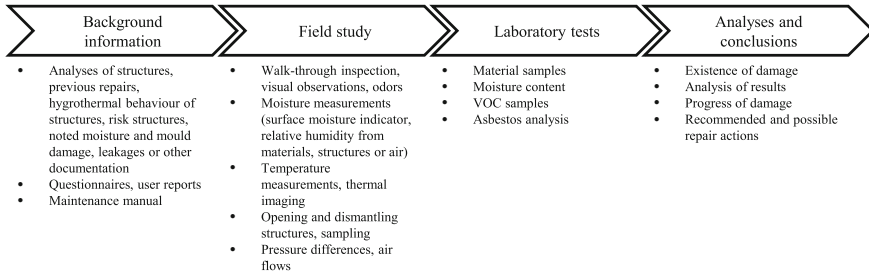


Fig. 1 Four main phases of moisture performance assessment and their main content (Annila et al. 2015a)

2.2 Initiation of Moisture and Mould Damage

Moisture and mould damage and the ensuing indoor air problems and repair need are described in Fig. 2. Damage to structures is initiated by moisture stress. There is wide variation between moisture sources and levels of moisture stress. When moisture stress is sufficiently high and lasts long enough, the capacity of a material subject to moisture stress may be exceeded leading to moisture damage. Depending on the material’s properties and prevailing conditions, the moisture in a structure may further lead to mould damage. The moisture stress and time required for mould growth can be estimated by different mould growth models (Vereecken and Roels 2012; Ojanen et al. 2010; Vinha et al. 2013; Johansson et al. 2005, 2012; Sedlbauer 2002).

Depending on the prevailing conditions, the material layers of a structure, air flows and location of mould damage, impurities may spread from a damaged area into indoor air leading to an indoor air problem and possible health symptoms in users. Due to the complexity of the phenomena, the links between concentrations of indoor air impurities and health symptoms have not been determined, but the correlation between them is clear (Bornehag et al. 2001, 2004).

Usually, only health symptoms of users lead to moisture performance assessments or indoor air studies that determine the repair need of a building.

The period between the various phases is typically very long. Asikainen (2008) estimated that repairs are typically undertaken 2–5 years after the occurrence of health symptoms. Even after repairs, it takes 6–12 months for indoor air conditions to stabilise (Haverinen-Shaughnessy et al. 2008). Thus, depending on the occupancy of the building, the users can be exposed to impurities for quite long periods even after IAQ problems or moisture and mould damage have been identified.

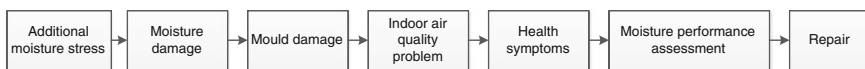


Fig. 2 Development of moisture and mould damage and related repair need

Consequently, there is a clear need for more effective procedures that enable faster identification of moisture and mould damage.

2.3 *Extent of Moisture and Mould Damage in Buildings*

The extent of moisture and mould damage in the building stock has been the subject of many studies, for instance, in Canada (Lawton et al. 1998), Finland (Nevalainen et al. 1998), Sweden (Smedje et al. 1997), Austria (Haas et al. 2007) and Norway (Holme et al. 2008). The results have also been published in scientific journals. Zock et al. (2002) studied the link between moisture and mould damage and asthma in 18 countries, in Europe and elsewhere. Undoubtedly many national studies, whose results have not been presented in English-language scientific journals, have also been conducted. Several studies made in Finland have also been aimed at decision makers, not scientific circles. A comprehensive summary of these Finnish studies was prepared in 2012 (Reijula et al. 2012). An abstract of it is available in English.

Reijula et al. (2012) summarised the major moisture and mould damage occurring in the Finnish building stock as follows: *We estimate that the prevalence of significant damp and mould damage is 7–10 % of the floor area in small and row houses, 6–9 % in multi-storey apartment block, 12–18 % in schools and kindergartens, 20–26 % in care institutions and 2, 5–5 % in offices.*

Although the extent of moisture and mould damage has been examined in several studies, their results are not mutually comparable since the research methods and definitions of moisture and mould damage have varied. Many studies have investigated the extent of moisture and mould damage through questionnaires directed at users (Lawton et al. 1998; Nevalainen et al. 1998; Haas et al. 2007; Holme et al. 2008; Zock et al. 2002). Questionnaires have been complemented for instance by visual observations made by professionals (Lawton et al. 1998; Nevalainen et al. 1998; Haas et al. 2007; Holme et al. 2008), measurements (Lawton et al. 1998) and indoor air samples (Lawton et al. 1998; Haas et al. 2007; Holme et al. 2008). Comparison of these research methods to the thorough Finnish moisture performance assessment of Fig. 1 makes the difference between the methods apparent.

Studies have shown that a significant part (Partanen et al. 1995), up to one-third (Pirinen 2006), of moisture and mould damage may be hidden, that is, not detectable on the surface of structures despite being examined by an expert. Thus, studies of moisture and mould damage to the building stock based on user surveys and partial measurements are not accurate. It is possible that some damage has gone unnoticed which may accentuate the significance of observable damage in such studies where hidden damage may be totally ignored (Asikainen 2008). Yet, visual observations and user reports on moisture and mould damage play a major role in damage identification and moisture performance assessment (Leivo et al. 1998).

Due to the variance in research methods and questions, the picture of the present state of the building stock and its moisture and mould damage is inaccurate. Lawton

et al. (1998) stated in the 90s that information about the condition of a building is the most important factor when planning its repair. The same observation was made in connection with a study on the moisture and mould damage repair projects of Finnish municipalities (Kero 2011). Inadequate moisture performance assessments have led to many failed repair projects (Kero 2011).

A recent study (Annala et al. 2015b) showed that Finnish buildings suffering from indoor air problems often have multiple problems, that is, moisture and mould damage in several structures. In the study the structures were divided into six groups: base floors, roof assembly, intermediate floors, external walls, walls in soil contact and partitions. All examined buildings did not have intermediate floors and walls in soil contact. 68 % of the examined buildings had moisture and mould damage in at least three different structural elements such as the base floor, the roof assembly and an external wall. It was also discovered that individual damaged spots were quite small in area (Annala et al. 2015b).

Thorough moisture performance assessments are necessary to avoid failed repairs (Lawton et al. 1998; Kero 2011; Marttila 2014). Most important from the viewpoint of successful repairs is to know all existing damage despite it being spread across several structures (Annala et al. 2015b) and partly hidden (Partanen et al. 1995; Pirinen 2006). For this reason, more effective identification of moisture and mould damage and development of moisture performance assessment are still topical research areas.

2.4 Definition of Moisture and Mould Damage

For the purposes of this study (Annala et al. 2015a), any damage that meets at least one of the following criteria was considered moisture and mould damage (Annala et al. 2015b):

- I Mould damage visible to the naked eye without magnification.
- II Unrepaired, active water leakage detrimental to the structure or building material that it wets.
- III A structure or building material found to be moist, extremely moist or wet by a surface moisture detector based on a five-step assessment scale: dry, slightly moist, moist, extremely moist and wet.
- IV Relative humidity of the structure exceeds 80 % in a drill-hole measurement.
- V A material sample shows active microbial (fungal or bacterial) growth. The fungal and bacterial colonies are determined by dilution plating on MEA agar and TYG agar.

Criterion I

The occurrence of moisture and mould damage has been examined in several scientific studies based on sensory observations (e.g. Lawton et al. 1998; Nevalainen et al. 1998; Smedje et al. 1997; Haas et al. 2007; Holme et al. 2008; Zock et al. 2002). In a summary of the Finnish building stock (Reijula et al. 2012),

many of the original studies are also based, at least partly, on visual observations of damage in buildings. That research method was considered scientific enough for the purposes of these studies.

The observations of TUT researchers about moisture performance assessments support the assumption that moisture and mould damage can be so clearly visible to the naked eye on the surface of a structure or through an inspection opening without a magnifying glass or microscope that establishment of damage requires no more detailed studies. Figure 3 shows an example of clearly visible mould damage on a chipboard wall. Verbally described observations in moisture performance reports are often illustrated by photos which also allow the reader to see what the target of observation looked like during field study.

Olfactory observations by a condition investigator were not used as a criterion of moisture and mould damage in this study because the existence of a strong mould odour in a space does not necessarily indicate reliably which structure in the said space is damaged. Air flows and leaks can carry odours from other spaces.

Criterion II

Water leaks, which may occur both in pipes and structures, have been made into a separate criterion among visual observations. These leaks have not necessarily led to moisture or mould damage by the time of the moisture performance assessment, but an unrepaired leak is highly likely to damage structures and materials. Thus, repair of observed leaks is as important as that of observed existing moisture and mould damage. Figure 4 shows an example of a leaky roof assembly.

Criterion III

Nevalainen et al. (1998) used surface moisture measurements in their study on moisture and mould damage. The mapping made in TUT moisture performance assessments using a surface moisture indicator was the basis of dividing structures into five classes: dry, slightly moist, moist, extremely moist and wet. Similar classification is used in Finland quite generally. In many moisture performance

Fig. 3 Example of visually observed mould damage to a chipboard structure



Fig. 4 Example of leak in a roof assembly detected during a moisture performance assessment



assessment reports analysed for the study, the results of surface moisture measurements had been complemented with more accurate moisture measurements of structures, which allows comparison of the results of surface moisture measurements and more accurate moisture measurements. The combination of the observations of TUT researchers and performed measurements constitute a reliable method properly used for determining the moisture content of structures although surface moisture measurements do not yield an accurate numerical value.

Criterion IV

The moisture and mould damage in structures and the building materials they contain can be modelled by different mould growth models. Vereecken and Roels (2012) have compared the different models that allow estimating the conditions and speed at which structures develop mould damage. Table 1 shows the mould growth sensitivity classes of the VTT-TUT mould growth model often used in Finnish studies (Ojanen et al. 2010, 2011; Vinha et al. 2013).

Johansson et al. (2005, 2012) have suggested critical moisture contents for various materials at which mould growth is possible. The sensitivity of materials to mould growth based on those critical contents is similar to that of the classification of Table 1. For instance, Johansson et al. (2012) determined that the critical moisture content of pine is 75–80 % RH and that of cement-based boards 90–95 %

Table 1 Mould growth sensitivity classes (Ojanen et al. 2010, 2011; Vinha et al. 2013)

Sensitivity class	Materials
Very sensitive	Sawn spruce and pine, planed pine, pine sapwood
Sensitive	Planed spruce, gluelam board, paper-coated PUR, gypsum boards, paper-based products
Medium resistant	Carbonated concrete, aerated and cellular concrete, glass wool, polyester wool, cement-based products
Resistant	Polished PUR, glass, metals, fresh alkali concrete

RH. Their material is based on an earlier publication used in several studies after the original one (Johansson et al. 2005). Sedlbauer (2002) also presented similar substrate categories for building materials.

Based on a summary of the mould growth models (Ojanen et al. 2010, 2011; Vinha et al. 2013; Johansson et al. 2005, 2012; Sedlbauer 2002), mould growth in the most sensitive materials, such as organic building materials, is possible at about 80 % RH at normal temperature of the structures.

A survey of the typical structures found in the Finnish building stock shows that the structures themselves or their component materials fall into the two most sensitive classes of Table 1. Therefore, the critical value of 80 % RH was used in this study to assess Finnish structures.

Criterion V

Material samples detached from building materials can be used with the direct culture or diluted culture method to determine whether there is microbial (fungal or bacterial) growth in the sample. The fungal and bacterial colonies were determined by dilution plating on MEA agar (20.0 g of malt extract, 20.0 g of saccharose, 1.0 g of peptone, 20.0 g of agar, and 0.1 g of chloramphenicol in 1 l of deionized water) and TYG agar (5.0 g of tryptone, 2.5 g of yeast extract, 1.0 g of glucose, 15.0 g of agar, and 0.5 g of cycloheximide in 1 l, of deionized water). The colonies were counted on day 7 (fungal) and day 10 (bacterial) after incubation. The fungal genera were identified microscopically. Furthermore, bacteria were classified as actinomycetes and other bacteria. This is a customary material sample analysis method in Finland (Pessi et al. 2002).

3 Research Materials and Methods

3.1 Research Material

Researchers at TUT Department of Civil Engineering have performed moisture performance assessments of 76 municipality-owned buildings: 59 schools, nine healthcare buildings, three daycare centres and five office buildings. The originally independent studies were later summarised in various ways. Users of all examined buildings have had different health symptoms and other negative sensations of poor IAQ. In the case of 49 buildings, the date of completion of the plan for the moisture performance assessment, the field study and reporting could be determined.

The studied buildings represent well the age distribution of the Finnish building stock. The oldest individual buildings had been built in the 1800s while the majority had been completed in the 50s, 60s and 70s—the period when school construction was especially brisk in Finland. The age distribution of the research material is shown in Fig. 5. The research material included all conventional structures, building materials and building systems used in Finland.

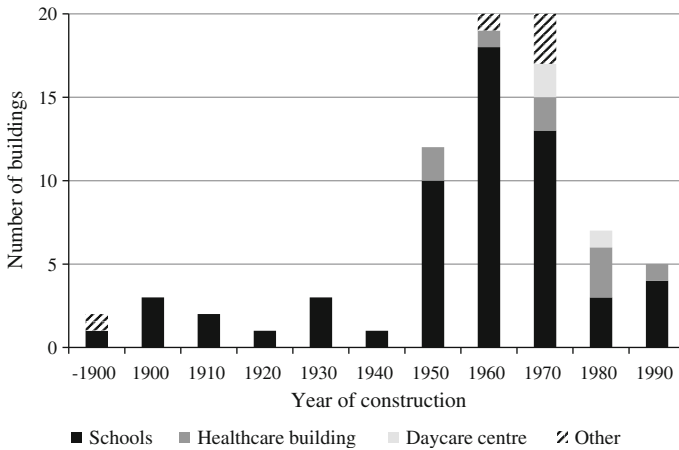


Fig. 5 Age distribution of examined buildings (Annala et al. 2015a)

3.2 Research Method

The 76 buildings of the study were originally examined as individual units. However, the content of the moisture performance assessments had been the same with all buildings (as shown in Fig. 1). At the outset of the study, the content of the moisture performance assessment reports on the 76 buildings, especially as concerns moisture and mould damage, was transferred to a database. All observed moisture and mould damage mentioned in the reports including related basic data, such as structure, material and used research methods, was entered. Basic data of each building such as year of construction, material of bearing frame, occupancy, location, time of assessment, number of storeys, roof type and foundation method were also recorded.

A total of 1784 observations suggesting moisture and mould damage had been made about the studied buildings. After their recording, observations were classified into two groups: “0 = undamaged” and “1 = damaged” based on the below definition of acute moisture and mould damage. An observation was classified as acute moisture and/or mould damage (class 1 = damaged) if it met at least one of the following criteria (Annala et al. 2015b):

- I Mould damage visible to the naked eye without magnification.
- II Unrepaired, active water leakage detrimental to the structure or building material that it wets.
- III A structure or building material found to be moist, extremely moist or wet by a surface moisture detector based on a five-step assessment scale: dry, slightly moist, moist, extremely moist and wet.

Table 2 Basic structure of the database and four examples

Example	Visual observation	Active leakage	Surface moisture detector	Relative humidity	Mould growth	Class: undamaged or damaged
1	Discolouration		Dry			0
2	Paint peeling off		Moist	86.3 % RH		1
3	Discolouration		Extremely moist		Actinomycetes	1
4	Visible damage	Yes				1

IV Relative humidity of the structure exceeds 80 % in a drill-hole measurement.

V A material sample shows active microbial (fungal or bacterial) growth. The fungal and bacterial colonies were determined by dilution plating on MEA agar and TYG agar.

Table 2 shows examples of entries in the database. They are related to observations and measurements made in the buildings to detect moisture and mould damage in structures.

The examples in Table 2 may correspond, e.g., to observations like the following.

1. The wall surfacing material had discolouration that was dry according to the surface moisture indicator. The discolouration was the result of normal soiling of the structure.
2. The coat of paint on the wall in soil contact was peeling off. Drill-hole measurements on the concrete structure indicated a moisture content of 86.3 % RH.
3. Moisture stains were visible in the ceiling and the structure was extremely moist according to the surface moisture indicator. A material sample from the roof assembly showed strong growth of actinomycetes.
4. The partition had visually observable damage around a leaking tap water pipe.

Of the above described observations and those presented in Table 2, nos. 2, 3 and 4 have been classified as damage in accordance with the used acute moisture and mould damage definition.

3.3 *Scope of the Study*

The study was limited to moisture and mould damage occurring in structures. A similar approach was followed also in the original moisture performance assessments. They examined what types of damage occur in structures and their repair need.

Moisture and mould damage has been found to have a negative impact on the health of users (Bornehag et al. 2001, 2004). The 76 moisture performance assessment reports used as research material did not, however, focus on the health symptoms experienced by users, which is why this study also excludes them. The original moisture performance assessment reports also dealt with ventilation and shortcomings and observations related to its performance. Yet, this study excludes building systems.

The scope of the study is based on the following hypothesis: When all moisture and mould damage in structures is repaired, the building cannot cause any health symptoms or indoor air problems related to moisture and mould damage to structures.

4 Results

4.1 Length of Moisture Performance Assessment Process

Different mould growth models (Vereecken and Roels 2012; Ojanen et al. 2010; Vinha et al. 2013; Johansson et al. 2005, 2012; Sedlbauer 2002) can be used to estimate the time required for mould damage to occur. Generally it is weeks, even months, depending on the level of moisture stress and the sensitivity of a material to mould growth.

Presently, there is not sufficient research data on how quickly and what types of mould damage spread impurities into indoor air which may cause health symptoms in users. The spreading is influenced by many factors such as pressure ratios, location of damage, materials of structure and air flows. Moreover, people react differently to spreading impurities. TUT has conducted user surveys and interviewed building users in connection with moisture performance assessments. According to users, health problems have generally continued for quite long before investigation of the cause of symptoms and the building's condition has started.

The analysed moisture performance assessment reports have been used to determine the time between (1) the start of planning the research and the first day of field study, (2) the start of field study and reporting, and (3) the start of planning the study and reporting.

The length of the first period indicates the slowness of municipal decision-making processes although the users experience health symptoms related to a building. The length of the second period indicates the time taken by a moisture performance assessment. The third criterion represents the length of the overall process, being the sum of the two previous ones. Figure 6 shows the length distribution of these three periods for the 49 buildings for which the data in question could be determined.

In the case of 31 (63.3 %) buildings, the moisture performance assessment was launched within 2 months of submission of tender. The moisture performance assessment proper including reporting may take several months: according to the study material, the shortest time it took to write the report was 1–2 months after the field study. A total of five (10.2 %) condition assessments were completed that

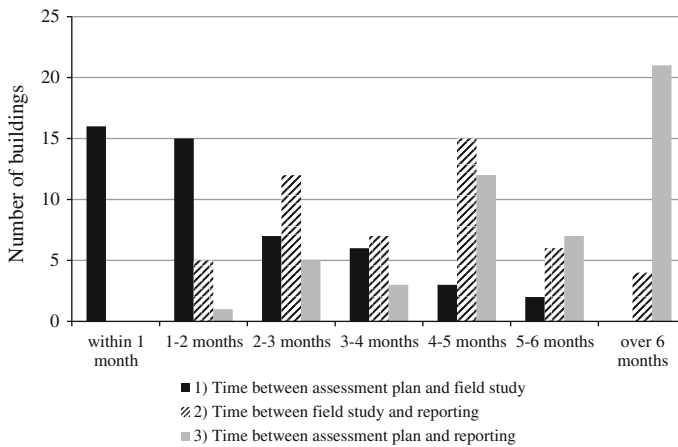


Fig. 6 Lengths of different phases of moisture performance assessments in research data

quickly. The period between the planning and reporting of the assessment was over six months in the case of 21 buildings (42.9 %).

Asikainen (2008) found that it can take 2–5 years between the occurrence of health symptoms and the completion of repairs. In addition, Haverinen-Shaughnessy et al. (2008) found that it takes 6–12 months after repairs for the impurity content to stabilise.

Due to the slowness of the processes, the exposure times to indoor air impurities caused by moisture and mould damage are long. Therefore, there is a clear need to develop moisture and mould damage detection methods so that damage can be observed more effectively before health symptoms appear.

4.2 Detection Methods

Based on the used criteria, a total of 920 observations on acute moisture and mould damage were made in the examined 76 buildings. The number of detected damage was great since the moisture performance assessments examined the extent of damage to determine the extent of required repairs. Thus, for instance, the base floor may have been investigated from different spaces whereby several observations about moisture and mould damage in an individual structural element of a building may have been made.

Figure 7 shows the distribution of observed moisture and mould damage in examined buildings by structures.

Figure 8 shows the methods used to detect the 920 moisture and mould damage in question. Part of the damage was detected by several methods, for example, surface moisture measurement and material samples. A single method was used to

Fig. 7 Locations of moisture and mould damage by structures

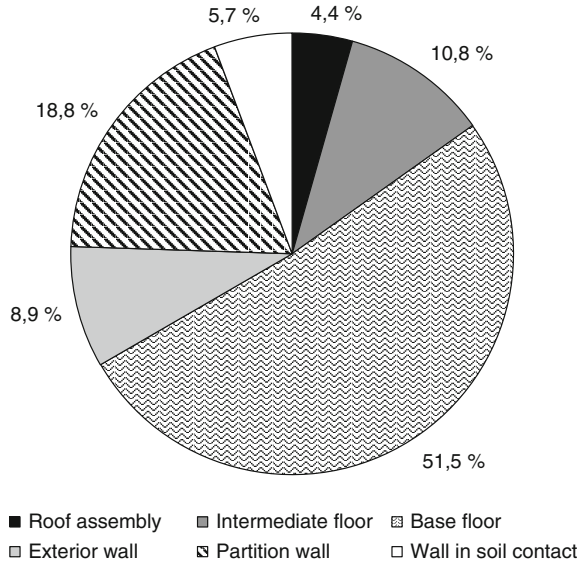


Fig. 8 Methods used to detect moisture and mould damage

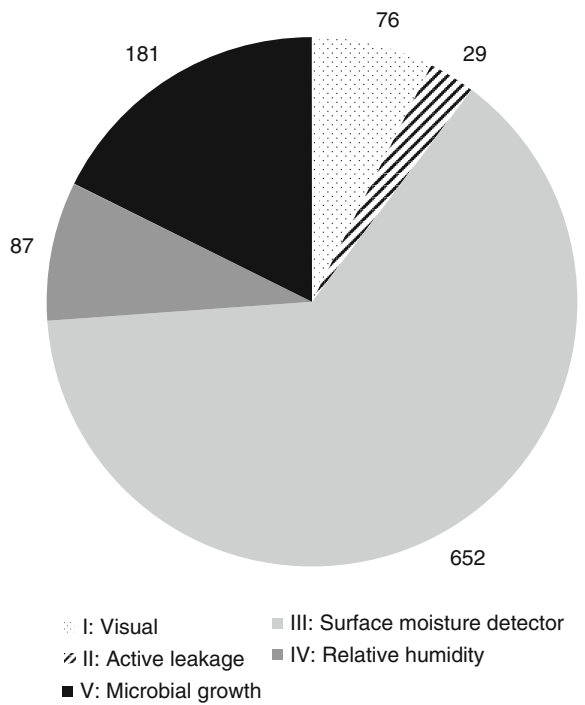


Table 3 Methods used to detect moisture and mould damage

Detection method	Number of detections	Share of all detections (%)	Confirmed measurements or observations (%)
I Visual: clear damage	76	7.4	47.4
II Visual: active leakage	29	2.8	13.8
III Surface moisture detector	652	63.6	12.1
IV Relative humidity	87	8.5	34.5
V Material sample test	181	17.7	30.4

detect 821 (89.2 %) damage while two or more methods were used for the other 99 (10.8 %).

The number of confirmed measurements and observations (99 damage) is small. This is due to the fact that measurements at one spot are rarely made by several methods. For example, if damage is suspected in the base floor, the moisture content of the structure can be measured from a different spot than the material sample taken. If both methods indicate damage in the base floor, the base floor of the space in question has two damaged areas according to the calculation method, the existence of neither having been confirmed by the other. When the base floor is examined as a unit, more confirming measurements are made, but at different points of the structure.

Table 3 shows the number and share of detections by different methods as well as how often measurements and observations have been confirmed by another method. According to Table 3, moisture and mould damage was detected 652 times with a surface moisture indicator. Some other method was used to confirm 12.1 % of these measurements.

Visually observed clear mould damage, RH measurements and material samples have most often been confirmed by other methods: in 47.4, 34.5 and 30.4 % of the cases, respectively. The used confirmation method has often been surface moisture measurement.

Table 3 shows that surface moisture measurements (63.6 %) are clearly the most used method for detecting moisture and mould damage. The second most popular method is material samples (17.7 %)—the large difference between their use is due to the fact that surface moisture measurements yield a value that indicates the moisture content of a structure quickly and cost-effectively.

A total of 589 sensory observations by condition investigators had been recorded in the assessment reports on the 76 buildings involved in the study. Of these observations 258 (43.8 %) were linked to 920 detected moisture and mould damage. Moisture and mould damage could be detected by a single sensory observation in 105 instances. It is highly likely that considerably more sensory observations

Table 4 Methods used to detect moisture and mould damage in different structures

Detection method	Roof assembly (%)	Intermediate floor (%)	Base floor (%)	Exterior wall (%)	Partition wall (%)	Wall in soil contact (%)	Average (%)
I Visual: clear damage	13.3	7.5	5.7	8.8	11.5	3.5	8.4
II Visual: active leakage	13.3	0.9	2.1	0.0	0.5	1.8	3.1
III Surface moisture detector	13.3	65.4	67.9	48.4	68.8	77.2	56.8
IV Relative humidity	11.1	9.3	11.8	3.3	2.1	5.3	7.2
V Material sample test	48.9	16.8	12.4	39.6	17.2	12.3	24.5

were made in connection with field studies. If sensory observations were found to be unconnected to moisture and mould damage, they have not necessarily been entered in the moisture performance assessment report. Moreover, the sensory observation may not have been recorded either if a structure had been subjected to moisture measurements or material sample tests. Yet, the significance of an investigator's sensory observations is high.

Table 4 shows the method used to detect damage in different structures. The shown deviation between moisture and mould damage detection methods for different structures is wide.

5 Discussion

5.1 Length of Moisture Performance Assessment Process

The time from the beginning of moisture stress and the occurrence of moisture and mould damage is long in Finland. The process may take several years as found in earlier studies (Asikainen 2008). The observations of this study and that by Haverinen-Shaughnessy et al. (2008) support the view of the long duration of the process phases. In the case of the 76 moisture performance assessments included in this study, the date of completion of the condition assessment plan, the field study and the report could be established. In 21 (42.9 %) cases, the interval between the completion of the moisture performance assessment plan and reporting was over six months, 358 days at the longest.

All phases of the process need to be developed in order that repair of moisture and mould damage becomes faster and exposure of users to indoor air impurities

due to moisture and mould damage becomes shorter. Moisture performance assessments also need to be developed and studied further and the best phase for launching assessments determined. Presently, they often start only after a building's users start to show health symptoms. Yet, we should be able to act before these health symptoms occur. Early detection of moisture and mould damage and management of moisture risks require more effective methods and approaches.

The study showed that moisture performance assessments take a long time: based on the research material the period between completion of the assessment plan and the report was on average 183 days. Of that, the completion of the assessment plan and the field study took 63 days, on average, while the remaining 120 days were spent completing the report and analyses after field study.

The shortest time required for the actual moisture performance assessment process (from field study to reporting) is about one month, since the analysis of material samples generally takes at least two weeks. In the case of five buildings (10.2 % of research material), the moisture performance assessment report was finished in 1–2 months after the field study. However, the longest time required was over six months (in 4 of 49 cases). The length of the moisture performance assessment process is probably due to the fact that the results of material sample tests are not known during field study but have to be waited for. That may lead to a situation where further samples from a building are needed, which naturally doubles the time needed to complete the report.

5.2 Moisture and Mould Damage Detection Methods

Based on the research results, the sensory observations of the condition investigator and surface moisture measurements play a significant role in the detection of moisture and mould damage. That is also suggested by the fact that many studies on the damage suffered by the building stock have searched for moisture and mould damage especially by sensory observations (e.g. Lawton et al. 1998; Nevalainen et al. 1998; Smedje et al. 1997; Haas et al. 2007; Holme et al. 2008; Zock et al. 2002). An expert opinion and surface moisture measurements can indeed establish quickly and cost-effectively the repair need of buildings. It is not a novel finding since Lappalainen et al. (2001) have shown that the order of importance of school building repairs can be set based on sensory observations and surface moisture measurements.

However, an expert's observations reflect only the conditions at isolated spots of a building. The regular users of a building make observations over the long term. Leivo et al. (1998) recognised that users play an important role in the detection of moisture and mould damage. The significance of users has also been noted in studies on the damage suffered by the building stock and their impact (Zock et al. 2002; Howden-Chapman et al. 2005). The subject requires further study in order for us to know how well building users without expertise in moisture and mould damage and IAQ problems can detect related damage and risks compared to an expert.

Based on the results of this study, 73.9 % of detected moisture and mould damage could be detected from the surface of structures as clear mould damage (Detection method I), a water leak (II) or by surface moisture measurements (III). As previously stated, visual observations have probably been made in connection with moisture measurements (IV) and material sample tests (V), which were not necessarily always recorded in moisture performance assessment reports, or that by themselves were not sufficiently clear indicators of the existence of damage.

Partanen et al. (1995) found that a significant portion of the moisture and mould damage in the Finnish building stock is hidden. Pirinen (2006) estimated that one-third of all moisture and mould damage is hidden. The results of this study support the results and observations of those two earlier studies since about a quarter of the damage could not be detected from the surface of structures but required using destructive methods.

The moisture and mould damage of different structures were detected by very different methods as Table 3 indicates. This can probably be largely explained by the differences between structures. For example, a concrete slab with a moist soffit that is part of the base floor probably also has a moist top due to its capillarity, whereby its moistness can be detected by a surface moisture detector. On the other hand, the thermal insulation of a roof assembly is generally external to the air/vapour barrier which may prevent detecting damage from the surface of the structure. That may require, for instance, a mould sample from the thermal insulation of the roof assembly.

In the study 73.9 % of all damage was detected on the surface of structures (Detection methods I-III). Yet, it is important to note (Table 3) that only 39.9 % of the damage in roof assembly could be detected from the surface of structures. The share was highest at 82.5 % in walls in soil contact. Further study on detection methods suitable for different structures is needed.

The scope of the study was limited based on the hypothesis that if a building has no moisture and mould damage, related health symptoms and indoor air problems cannot occur there. Excessive repairs are not generally economically feasible, or even profitable. Thus, we should have criteria for the kinds of moisture and mould damage that should be repaired to avoid the occurrence of health symptoms. Repair of the smallest and slightest damage is not necessarily needed. Currently, we do not know what impurity-content level in relation to moisture and mould damage causes health symptoms for groups or individual users. This has been recognised earlier (Bornehag et al. 2001, 2004), but the research problem remains unsolved and further medical research is needed.

6 Conclusions

This study determined on the basis of moisture performance assessment reports on 76 buildings the methods used to detect moisture and mould damage in Finland. It also sought targets of development related to moisture performance assessments

based on these condition assessment reports and the practical experiences of researchers who have conducted moisture performance assessments.

According to the study, 73.9 % of moisture and mould damage can be detected on the surface of structures by sensory observations or surface moisture measurements. However, the share can be significantly smaller depending on the assessed structure: in roof assembly 39.9 % of the damage could be detected on the surface of a structure.

The study found that the mere time taken by a moisture performance assessment is long: the period between the completion of the assessment plan and the report was, on average, 183 days. Moisture and mould damage processes are long also in other respects and can take several years. All phases certainly have areas that can be improved so that the processes and the exposure of users to the impurities caused by moisture and mould damage can be shortened. The moisture performance assessment process also requires development.

References

- Annala PJ, Lahdensivu J, Suonketo J, Pentti M (2015a) Practical experiences from several moisture performance assessments. In: Proceedings of 1st international symposium on building pathology, ISBP2015. Porto, Portugal, pp 115–122. 24–27 Mar 2015
- Annala PJ, Hellemaa M, Pakkala TA, Lahdensivu J, Suonketo J, Pentti M (2015b) Extent of moisture and mould damage in structures of public buildings. *Indoor and Built Environment*. (submitted)
- Asikainen V (2008) Sisäilmaongelmaisten koulurakennusten korjaaminen. Osa 1 Kiinteistön omistajan opas sisäilmaongelmaisten koulurakennusten kunnan tutkimiseen ja korjaushankkeisiin. Opetushallitus, 43 p. (in Finnish)
- Bornehag C-G, Blomquist G, Gyntelberg F, Järholm B, Malmberg P, Nordvall L, Nielsen A, Pershagen G, Sundell J (2001) Dampness in buildings and health. Nordic interdisciplinary review of the scientific evidence on associations between exposure to “Dampness” in buildings and health effects. *Indoor Air* 11:72–86
- Bornehag CG, Sundell J, Bonini S, Custovic A, Malmberg P, Skerfving S, Sigsgaard T, Verhoeff A (2004) Dampness in buildings as a risk factor for health effects, EUROEXPO: a multidisciplinary review of the literature (1998–2000) on dampness and mite exposure in buildings and health effects. *Indoor Air* 2004 14:243–257
- Haas D, Habib J, Galler H, Buzina W, Schlacher R, Marth E, Reinthaler FF (2007) Assessment of indoor air in Austrian apartments with and without visible mold growth. *Atmos Environ* 41 (2007):5192–5201
- Haverinen-Shaughnessy U, Hyvärinen A, Putus T, Nevalainen A (2008) Monitoring success of remediation: seven case studies of moisture and mold damaged buildings. *Sci Total Environ* 399(2008):19–27
- Holme J, Geving S, Jenssen JA (2008) Moisture and mould damage in Norwegian Houses. Nordic Symposium on Building Physics 2008, Copenhagen, Denmark, 8 p
- Howden-Chapman P, Saville-Smith K, Crane J, Wilson N (2005) Risk factors for mold in housing: a national survey. *Indoor Air* 15:469–476
- Hyvärinen A (2002) Characterizing moisture damaged buildings—environmental and biological monitoring. Publications of National Public Health Institute A8/2002, 121 p

- Johansson P, Samuelson I, Ekstrand-Tobin A, Mjörnell K, Sandberg PI, Sikander E (2005) Microbiological growth on building materials: critical moisture levels. State of the Art. SP Swedish National Testing and Research Institute
- Johansson P, Ekstrand-Tobin A, Svensson T, Bok G (2012) Laboratory study to determine the critical moisture level for mould growth on building materials. *Int Biodeterior Biodegradation* 73(2012):23–32
- Kero P (2011) Evaluating of moisture and mold renovation process in municipal buildings. Master of Science Thesis. Tampere University of Technology, 62 p (in Finnish)
- Lappalainen S, Kähkönen E, Loikkanen P, Palomäki E, Lindroos O, Reijula K (2001) Evaluation of priorities for repairing in moisture-damaged school buildings in Finland. *Build Environ* 36 (2001):981–986
- Lawton MD, Dales RE, White J (1998) The influence of house characteristics in a canadian community on microbiological contamination. *Indoor Air* 8:2–11
- Leivo V, Pirinen J, Reiman M, Ruotsalainen R, Rautiala S, Suojanen P (1998) Opas kosteusongelmiin – Rakennustekninen, mikrobiologinen ja lääketieteellinen näkökulma. Tampere University of Technology publication 95, Talonrakennustekniikka, 157 p. (in Finnish)
- Marttila T (2014) Assessment of state-supported mould renovations. Master of Science Thesis, 45 p +55 appendix p. (in Finnish)
- Mudarrí D, Fisk WJ (2007) Public health and economic impact of dampness and mold. *Indoor Air* 2007(17):226–235
- Nevalainen A, Partanen P, Jääskeläinen E, Hyvärinen A, Koskinen O, Meklin T, Vahteristo M, Koivisto J, Husman T (1998) Prevalence of moisture problems in Finnish houses. *Indoor Air (Suppl 4)*: 45–49
- Ojanen T, Viitanen H, Peuhkuri R, Lähdesmäki K, Vinha J, Salminen K (2010) Mold growth modelling of building structures using sensitivity classes of materials. In: *Proceedings Buildings XI, Florida*
- Ojanen T, Peuhkuri R, Viitanen H, Lähdesmäki K, Vinha J, Salminen K (2011) Classification of material sensitivity e new approach for mould growth modeling. In: *9th Nordic symposium on building physics, vol 2, pp 867–874*
- Partanen P, Jääskeläinen E, Nevalainen A, Husman T, Hyvärinen A, Korhonen L, Meklin T, Miller K, Forss P, Saajo J, Röning-Jokinen I, Nousiainen M, Tolvanen R, Henttinen I (1995) Pientalojen kosteusvauriot – yleisyyden ja korjauskustannusten selvittäminen. Osa A: Kosteusvaurioiden yleisyys. Kansanterveyslaitoksen julkaisuja, B6/1995. 31s. (in Finnish)
- Pessi A-M, Suonketo J, Pentti M, Kurkilähti M, Peltola K, Rantio-Lehtimäki A (2002) Microbial growth inside insulated external walls as an indoor air biocontamination source. *Appl Environ Microbiol* 2002:963–967
- Pirinen J (2006) Pientalojen mikrobivauriot. Lähtökohtana asukkaiden kokemat terveyshaitat. Dissertation. Hengitysliiton julkaisuja 19/2006. Tampere University of Technology, 96 p +28 appendix p. (in Finnish)
- Reijula K, Ahonen G, Alenius H, Holopainen R, Lappalainen S, Palomäki E, Reiman M (2012) Rakennusten kosteus- ja homeongelmat. Eduskunnan tarkastusvaliokunnan julkaisu 1/2012, 178 p +28 appendix p. (in Finnish)
- Sedlbauer K (2002) Prediction of mould growth by hygrothermal calculation. *J Therm Environ Build Sci* 25(4):321–336
- Smedje G, Norbäck D, Edling C (1997) Subjective indoor air quality in schools in relation to exposure. *Indoor Air* 7:143–150
- Vereecken E, Roels S (2012) Review of mould prediction models and their influence on mould risk evaluation. *Build Environ* 51(2012):296–310
- Vinha J, Laukkarinen A, Mäkitalo M, Nurmi S, Huttunen P, Pakkanen T, Kero P, Manelius E, Lahdensivu J, Köliö A, Lähdesmäki K, Piironen J, Kuhno V, Pirinen M, Aaltonen A, Suonketo J, Jokisalo J, Teriö O, Koskenvesa A, Palolahti T (2013) Ilmastonmuutoksen ja lämmöneristyksen lisäyksen vaikutukset vaipparakenteiden kosteusteknisessä toiminnassa ja rakennusten energiankulutuksessa. Tutkimusraportti 159. Tampere, Tampere University of Technology, Department of Civil Engineering. 354 p +43 appendix p. (in Finnish)

- Weschler CJ (2009) Changes in indoor pollutants since the 1950s. *Atmos Environ* 43 (2009):153–169
- Zock J-P, Jarvis D, Luczynska C, Sunyer J, Burney P (2002) Housing characteristics, reported mold exposure, and asthma in the European Community Respiratory Health Survey. *J Allergy Clin Immunol* 110(2):285–292

Analysis of Main Parameters that Affect Contact Area Between Mortar Rendering and Substrate: Use of 3D Laser Scanning Technique

Carina Mariane Stolz and Angela Borges Masuero

Abstract The objective of this research is to analyze the influence of granulometric composition of sand, application energy, and substrates superficial tension on the contact area of rendering mortars. Three different substrates were selected with distinct wetting behaviors: polyethylene, acrylic, and glass. The contact angle of drop water was measured by goniometer. Mortars were prepared with cement:lime:sand ratios of 1:0:3, 1:1:6, and 1:2:9, by content converted in mass, with sand composition of 25 % of each 0.15, 0.3, 0.6, and 1.2 mm grain sizes. Characterization tests in fresh and hardened mortars were performed to provide the technological control of mortars and concretes, as well as the characterization of the different rheological behaviors of the mortars by squeeze-flow and rotational rheometer methods. Mortars were applied to substrates with two different energies, and after curing time were parted from substrates and submitted to scanner 3D digitalization of interfacial area. Results showed that both mortar proportion and substrate superficial tension exercise influence on interfacial contact area development. Additionally, interaction between application energy and substrates superficial tension was significantly influent on contact area. Finally, 3D scanning is a promising new method that shows good performance to measure contact area to improve the understanding of bond strength.

Keywords Contact area · Mortar rendering · Laser 3D scanner · Application energy

C.M. Stolz (✉) · A. Borges Masuero
Federal University of Rio Grande do Sul, Porto Alegre, Rio Grande do Sul, Brazil
e-mail: carimstolz@yahoo.com.br

A. Borges Masuero
e-mail: angela.masuero@ufrgs.br

1 Introduction

In several countries, as Brazil, most building constructions use mortar rendering. However, poor technological control and the lack of technical expertise in the production of mortars rendering often produce pathological manifestations that may compromise the functions of renderings like protection, waterproofing, and aesthetic appearance of constructions.

In order to mitigate the onset of pathological manifestations, many researchers (Hall 1977; Hall and Yau 1987; Yates et al. 1994; Sugo et al. 2001; Ramos et al. 2012) have focused attention on the adhesion of rendering mortars.

Texture characteristics of substrates, the physical/chemical characteristics may influence the development of the contact area at the interface between mortar and substrate, exerting direct influence on adhesion. In this way of thinking, some researches focused on parameters related to substrates characteristics, as porosity (Pagnussat 2013) and rugosity (Holla et al. 2015; Santos et al. 2007; Pretto 2007; Stolz 2011), both the study of the interface between mortar and substrates, as in the study of the interface between layers of concrete structures. However, it is rare to find studies researching the influence of surface tension of cementitious materials on adherence at the interface between materials (Stolz and Masuero 2015).

In addition, researchers (Pretto 2007; Stolz 2011; Carasek 1996) have published images that indicate that increasing the surface texture of a substrate is not enough to increase adhesion if the mortar applied to the surface cannot penetrate the texture and wet the substrate. In this context, the rheological characteristics of mortar flows (Banfill 2003; Bauer et al. 2007; Senff et al. 2009) have been investigated in order to understand their influence on the phenomenon of adhesion and effective interfacial contact area.

Analogously, the adequate energy of mortars application that is fundamental to improve the flow and wet property of mortars on substrates has been investigated by many researchers.

The techniques of adhesion measurement are, generally, destructive. The most common technique is to apply a tensile strength on a mortar coating sample, measuring their tensile bond strength with a pull-off tester. However, some researchers look to correlate the bond strength behavior with the parameters measured in nondestructive testing.

Some nondestructive techniques found in technical researches consist of measure faults on interfacial contact area with ultrasound, correlating bigger times of wave's passage with failures presence (Tan et al. 1996; Davis and Brough 1972). Nevertheless, values measured by this technique are only comparative, and have influence of the heterogeneous characteristics of cementitious materials and substrate and rendering voids.

Other researches investigate interfacial failures by using thermographic cameras (Kylili et al. 2014; Freitas et al. 2014). This technique is effective to identify zones

with coating detachment, because of voids' difference in temperature; however, this does not demonstrate the quantitative values of adhesion in interface.

Thus, the path to find nondestructive techniques to estimate adhesion at the interface between systems, appears to thoroughly investigate the properties that affect this property and develop mathematical models for predicting the behavior of building systems.

In this line, the use of 3D laser scanning for characterizing surfaces appears as an accurate and easy to use tool. Some authors (Hola et al. 2015; Santos et al. 2007; Pretto 2007; Stolz 2011; Logins and Torims 2015; Deltombe et al. 2014) have used it to characterize surface roughness, using parameters provided by this device. The measurement of failures present at the mortar/substrate interface in order to quantify the real interfacial contact area is innovatory.

Considering all the variables that can influence the interface contact between surfaces, this study aims to analyze the influence of mortar proportioning and application energy of rendering mortar on interfacial contact area, when applied to substrates with different superficial tensions.

2 Methodology

The experimental program consists of producing three different mortars, with the same binder: aggregate ratio of 1:3, ranging lime hydrated percentage. So, mortars were produced in the proportions of 1:0:3, 1:1:6, and 1:2:9 (cement:hydrated lime:sand, in volume, dry materials, converted in mass in laboratory). These mortars were applied with two application energies in three different no porous and no rough (smooth) substrates, with distinct characteristics of wettability.

Experimental matrix is shown in Fig. 1.

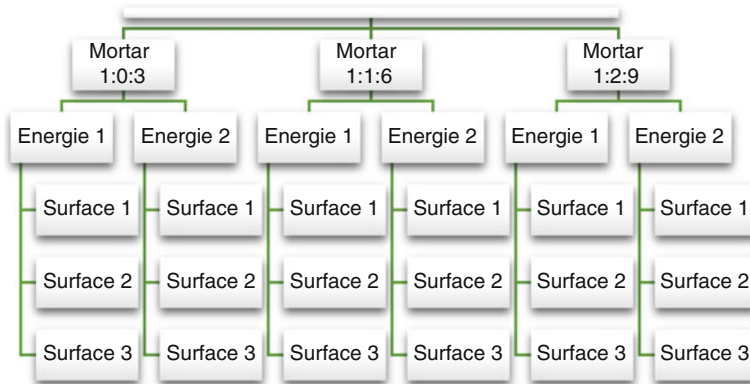


Fig. 1 Experimental matrix

2.1 Mortars Production

Three mortars prepared with compositions of 1:0:3, 1:1:6, and 1:2:9 (cement:hydrated lime:dry sand) were produced according to the Brazilian Standard NBR 13276/2005, for a 240 mm consistence index. The quartz sand used (specific mass: 2.50 g/cm^3) consist of the composition of sand with grains retained in sieves #1.2, 0.6, 0.3, and 0.15 mm, with equal fractions of each sieve, 25 % each (Unitary mass: 1.51 g/cm^3).

The cement used was Portland cement type IV (equivalent to the American IP (MS) grade), and the calcitic lime (specific mass 2.37 g/cm^3 , mean particle size $22.4 \text{ }\mu\text{m}$) complied by Brazilian standards limits.

2.2 Mortars Characterization

Characterization tests of fresh and hardened mortars were performed to provide the technological control of the materials, in addition to the characterization of the different rheological behaviors. In fresh state, bulk density, water retentivity, and air content characterization were performed, all of them according to Brazilian standards. In hard state, 28 days before mortars production, were performed flexural strength, compressive strength, dynamic elasticity modulus, density and capillary water absorption characterization tests, all according to Brazilian standards.

A Brookfield Rotational Rheometer R/S plus was used for the rheological characterization. The vane type V 30×15 was used, with a height of 30 mm and a diameter of 15 mm, in a standard container for all mortars. This type of vane is the most suitable for rheological tests on mortar coating suspensions and high-viscosity materials. The size of the vane was determined in preliminary tests. The rotational rheometer data was then treated with the Rheo3000 Software.

The routine chosen for mortar analysis consists of four lectures levels, each 20 s, reaching a maximum of 100 1/s shear rate (Fig. 2). The objective of this characterization was to take an apparent viscosity in a fixed point to compare different mortars.

2.3 Mortars Application

Mortars were applied to the substrates by means of a device called “drop box,” illustrated in Fig. 3, from two fixed fall heights of 30 cm and 1 m. A “drop box” is a simple device, used by some researchers (Pagnussat 2013; Stolz 2011; Stolz and Masuero 2015; Carasek 1996; Antunes 2005; Paes 2004), which allows users to

Fig. 2 Rheometer routine

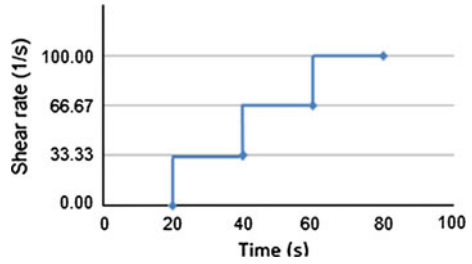
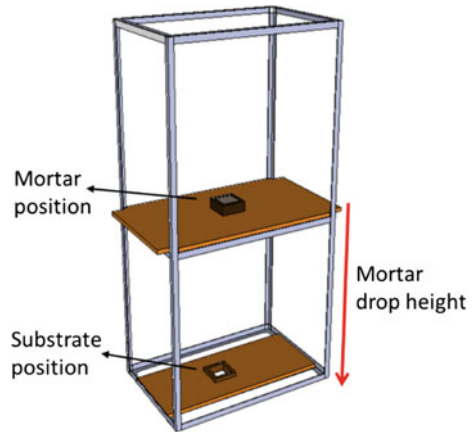


Fig. 3 Schematic figure of “drop box” device



adjust the height from which the mortar will be dropped into the substrate, therefore controlling the applied energy.

2.4 Substrates Selection

Through preliminary analysis, three nonabsorbent substrates with different wettability ratings were chosen: glass, acrylic, and polyethylene. These substrates were characterized by measuring the contact angle of a drop of water projected on their surface, through a goniometer. Table 1 presents the chosen surface with their respective contact angles. The glass surface can be considered hydrophilic, with a contact angle of 27° , the acrylic surface is an intermediary surface, with 52° of contact angle, and the polyethylene surface is hydrophobic, with 96° of contact angle.

Using the Young–Laplace equation, the superficial tension of the surfaces was evaluated, which are presented in Table 2.

Table 1 Contact angle of a water drop with selected surfaces


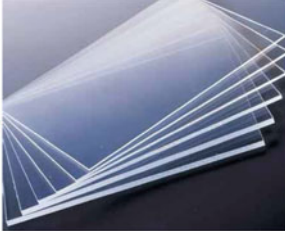




Glass	Acrylic	Polyethylene
		
		
$\theta_m = 27^\circ$	$\theta_m = 52^\circ$	$\theta_m = 96^\circ$

Table 2 Superficial tension calculated by Young-Laplace equation

Surface	Superficial tension (dynes/cm)
Water (20 °C)/air (liquid/steam)	$\gamma_{LS} = 72.8$
Glass (solid/steam)	$\gamma_{SS} = 1000$
Acrylic (solid/steam)	$\gamma_{SS} = 41$
Polyethylene (solid/steam)	$\gamma_{SS} = 31$
Glass (solid/liquid)	$\gamma_{SL} = 935.13$
Acrylic (solid/liquid)	$\gamma_{SL} = -3.82$
Polyethylene (solid/liquid)	$\gamma_{SL} = -38$

3 Results

The results of mortar characterization and contact area quantification are presented in this section.

3.1 Mortar Characterization

Mortars proportioning are presented in Table 3.

Tables 4 and 5 present fresh and hardened (28 days) states characterization of mortars, respectively.

Table 3 Mortars proportioning

Mortar	Water (g)	Consistency (mm)	Water/cement ratio	Water/binder ratio
1:0:3	214	245	0.95	0.95
1:1:6	222	244	1.91	1.19
1:2:9	250	250	3.21	1.44

Table 4 Characterization tests of fresh rendering mortars

Mortar	Bulk density of fresh mortar NBR 13278/05 (kg/m ³)	Water retentivity NBR 13277/05 (%)	Air content NBR NM 47/02 (%)
1:0:3	2064	97	2.57
1:1:6	2062	98	2.20
1:2:9	2039	95	2.00

Table 5 Characterization tests of hardened rendering mortars

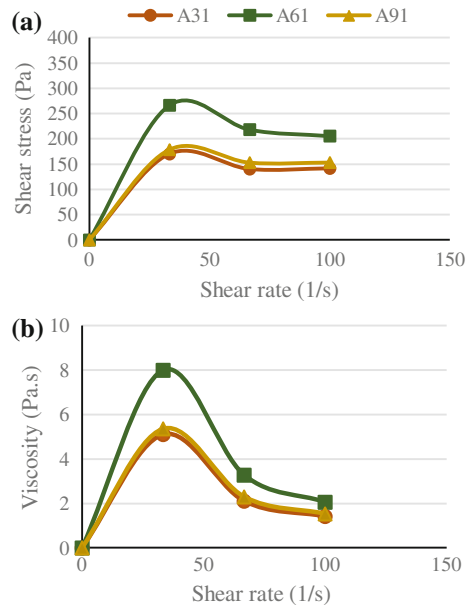
Mortar	Compressive strength NBR 3279/05 (MPa)	Flexural strength NBR 13279/05 (MPa)	Dynamic elasticity modulus NBR 15630/08 (GPa)	Density of hardened mortar NBR 13280/05 (kg/m ³)	Capillary water absorption NBR 15259/05 (g/dm ² min ^{1/2})
1:0:3	7.63	2.34	14.66	1908	8.89
1:1:6	2.27	0.25	7.31	1880	15.67
1:2:9	0.73	0.35	3.45	1810	24.43

In fresh state, it was possible to observe that the hydrated lime presence on mortars proportioning exerted influence on air content and bulk density. The more the content of lime, the smaller the bulk density, as the density of lime density is less. The greater presence of lime decreases the air content. It can result in small grains of mortar fill of voids in admixture. Water retentivities of all mortars were similar, and it does not seem to be influenced by these mortar proportionings.

The hardening state characterization shows that hydrated lime's presence significantly reduced the mechanic strength of mortars, reducing also the dynamic elasticity modulus and density, as expected. On the other hand, capillary water absorption was increased by lime presence on mortars proportioning.

Rheological characterization with rotational rheometer is presented in Fig. 4. The 1:1:6 mortar showed a viscosity and yield stress increase fairly sizeable. It is believed that a set of phenomena may have caused this behavior, the most evident was interaction between the proportioning associated with a uniform particle size of sand, generating a worst packaging.

Fig. 4 Curves resulting of rotational rheometry of mortars: **a** Shear stress (Pa s) versus Shear rate (1/s); **b** Viscosity (Pa s) versus Shear rate (1/s). Where: A31 = 1:0:3; A61 = 1:1:6; A91 = 1:2:9



This fact reaffirms that the understanding of how the flow occurs in heterogeneous suspensions, such as coating mortars, is quite complex. So that, apparently, it should be considered not only the packaging and the particle size distribution of the aggregates, but its interaction with the paste of all the dispersion and how the particles react when subjected to tension, flowing in a homogeneous or heterogeneous way (with particles segregation).

Calculating void volume (V_v) of all mortars it was observed that mortar 1:1:6 presented bigger V_v percentage (41.87 %), followed by 1:2:9 mortar with $V_v = 41.66$ % and 1:0:3 with $V_v = 40.56$ %. So, it can be concluded that bigger V_v mortar has also bigger viscosity values.

The grains friction of heterogeneous suspensions and their influence on mortars rheology was subject of Mendes' (2008) study. The author states that particle size distribution of aggregates has influence on suspension rheological behavior. However, for the variables evaluated by the author, it was not possible to establish direct correlation between the coefficient of friction of the aggregates and the suspensions viscosity. Olhero and Ferreira (2004) corroborate with this statement, emphasizing that the rheological behavior can not only be based on the suspension particles' size, but also on the distribution of particle sizes, which plays a more important role in this behavior.

Another phenomenon that may be occurring on the 1:1:6 mortar, which has lime in its composition, however, showed high viscosity and flow resistance, which can be related to the content of fines having reached a "critical value." This theory has

been reported by some authors (Zahia et al. 2005; Benabed et al. 2012; Zhang and Han 2000), who observed that, for the same cement content (constant w/b ratio), the adding of fine particles reduces the viscosity of the paste before increasing this property. It happens, when the fines content exceeds a certain critical value, which is the water/cement ratio dependence.

Lee et al. (2003) and Kashani et al. (2014) complement that, when a mineral admixture with a large particle dispersion is added to the cement paste, the smaller particles fill the pores, enhancing packing, while increasing the free water of cement pastes fluidity. In smaller dispersion particle size distributions case, pores among particles are greater, thus reducing fluidity.

In the 1:0:3 mortar case, the lack of fine aggregates on composition could result in more easier exit of water present in porous mortar that is accumulated on vane surrounding, generating a small viscosity.

3.2 *Three-Dimensional Laser Scanning*

After curing time, mortars were separated from the substrates and digitized with a tridimensional laser scanner. The results were treated with the Geomagic Studio 10 Software to generate a tridimensional image. This image was saved in the PNG (Portable Network Graphics) format and opened with the Photoshop CS5 Software, where contact and noncontact areas were quantified. It is important to emphasize that the images were not altered, but only treated to connect 3D scanned points and highlight the noncontact areas.

One example of the results of these treatments is presented in Fig. 5, where dark blue and black points represent the noncontact areas.

The results for the contact area measurement of mortars are presented in Table 6, for mortars 1:0:3, 1:1:6, and 1:2:9, respectively. The technique of 3D laser scanning proved to be adequate for interface contact area measurement, considering that variation coefficients resultant of the method were lower than 10 %.

In order to verify the statistical significance of the obtained values, an analysis of variance (ANOVA) was performed with the Software Statistica 7 (Table 7). It is possible to observe that mortar proportioning and fall heights are significant factors on contact area development, with 95 % of reliability. In addition, the interaction between surface \times fall heights is significant on interface contact area development.

The graphs of significant interactions, i.e., mortar, fall heights, and the interaction between mortar/surface/fall heights, are presented in Figs. 6, 7 and 8. Figure 6 shows that mortar 1:1:6 presented worst behavior in relation to contact area. This fact can be related with the viscosity of this mortar, which was higher than the others, as presented on rheological results.

Fig. 5 Images resulting from the 3D scan. The noncontact area points are shown in *dark blue* and *black*: **a** 3D image resulting from treatment in Geomagic Studio 10 Software, **b** 2D image treated in Geomagic Studio 10 Software, **c** 2D image treated in Photoshop CS5 Software

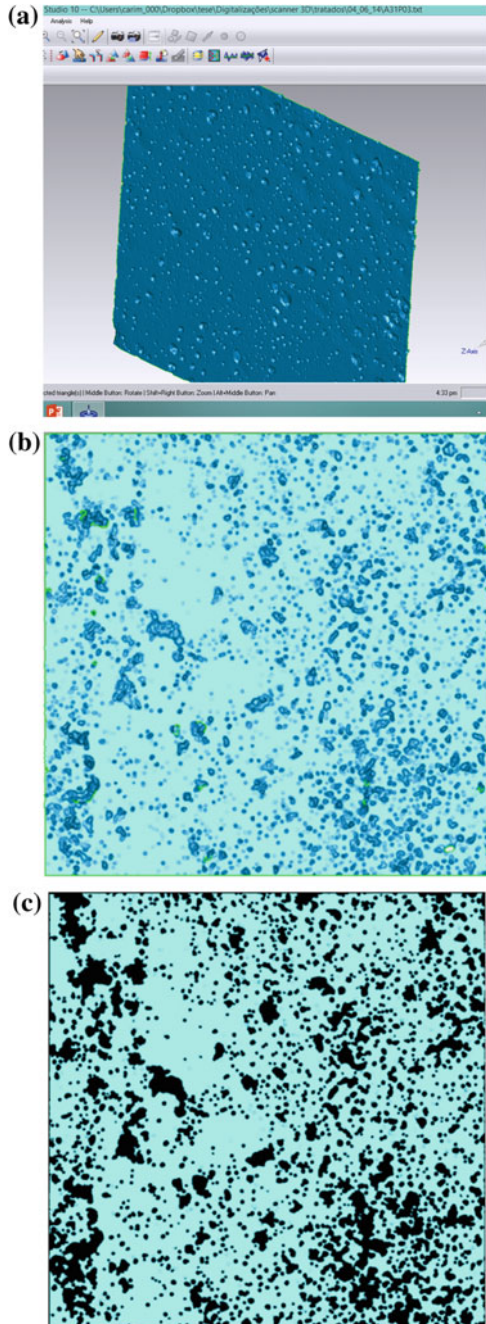


Table 6 Measurement of contact areas of mortars 1:0:3, 1:1:6, and 1:2:9, applied to the polyethylene, acrylic, and glass substrates with fall heights of 30 and 100 cm

Mortar	Surface	Fall heights (cm)	Mean contact area (%)	SD (%)	VC (%)
1:0:3	Polyethylene	100	79.32	2.89	4
1:0:3	Acrylic	100	90.53	3.07	3
1:0:3	Glass	100	89.53	3.72	4
1:0:3	Polyethylene	30	83.34	6.67	8
1:0:3	Acrylic	30	78.33	5.23	7
1:0:3	Glass	30	78.89	7.89	10
1:1:6	Polyethylene	100	75.92	3.14	4
1:1:6	Acrylic	100	87.11	2.17	2
1:1:6	Glass	100	81.98	5.24	6
1:1:6	Polyethylene	30	71.77	1.56	2
1:1:6	Acrylic	30	73.29	2.44	3
1:1:6	Glass	30	74.37	3.57	5
1:2:9	Polyethylene	100	84.66	4.66	6
1:2:9	Acrylic	100	81.71	3.36	4
1:2:9	Glass	100	92.19	1.42	2
1:2:9	Polyethylene	30	87.77	4.63	5
1:2:9	Acrylic	30	82.12	6.22	8
1:2:9	Glass	30	79.57	7.13	9

SD Standard deviation; VC Variation coefficient

Table 7 Controlled factors and contact area data factorial analysis of variance (ANOVA)

Factor	SS	DOF	MS	Calc.F	P factor
Mortar	984.7	2	492.4	12.46	0.000028
Surface	4.0	2	2.0	0.05	0.950539
Fall heights (cm)	504.0	1	504.0	12.75	0.000688
Mortar*surface	169.5	4	42.4	1.07	0.377863
Mortar*fall heights (cm)	42.5	2	21.3	0.54	0.586510
Surface*fall heights (cm)	424.8	2	212.4	5.37	0.006997
Mortar*surface*fall heights (cm)	258.5	4	64.6	1.64	0.176483
Error	2490.0	63	39.5		

SS Sum of square, DOF Degree of freedom, MS Mean square

Figure 7 shows that greater energy application of rendering mortar results in greater percentage of contact area, i.e., less contact failures.

Analogously, as can be seen in Fig. 8, it is possible to conclude that, for the lower application energy, the surface hydrophobicity was not a significant influent

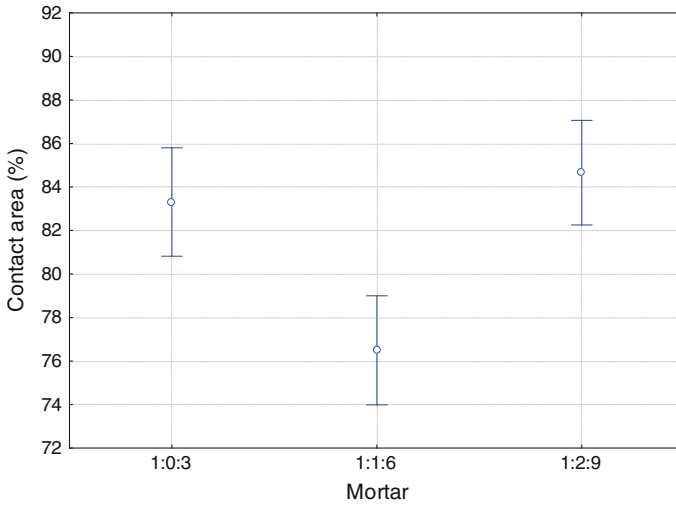


Fig. 6 ANOVA of mortars proportioning influence on interfacial contact area

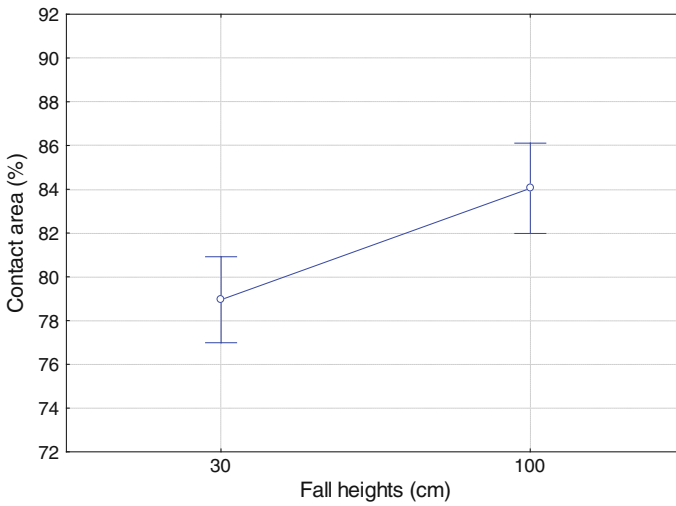


Fig. 7 ANOVA of fall heights (energy of application) influence on interfacial contact area

in contact area development. On the other hand, the greater fall height evidences how bigger is the contact angle of the drop water on surface, i.e., the greater the degree of hydrophobicity, the lower the contact area percentage.

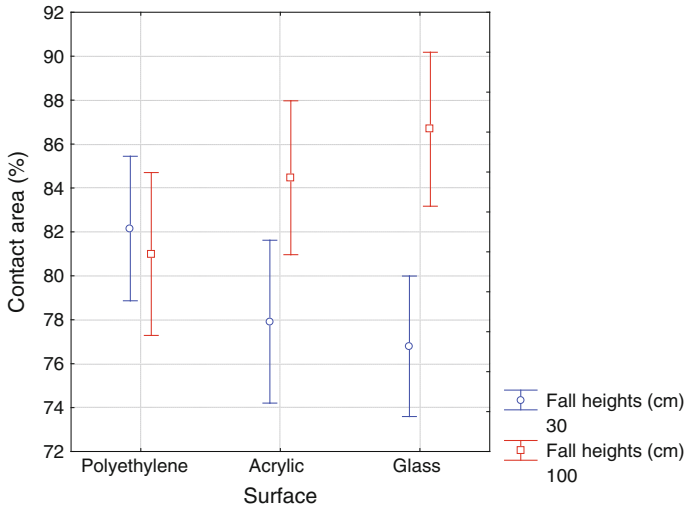


Fig. 8 ANOVA of fall heights (energy of application) and surface angle of contact interaction on interfacial contact area

4 Conclusions

Based on the results of this experimental program, it is possible to establish the following conclusions, for variables studied:

- the mortar proportioning is the most influent variable on substrate/mortar interface contact area, presenting lower p factor on statistical analysis;
- application energy of mortars have to be controlled and measured looking for a bigger interfacial contact area. In practice, it is important to standardize as much as possible this variable, using mechanized application instead of manual (which is frequent in most Brazilian works);
- superficial tension of substrates is a property that deserves more attention from researchers studying adhesion. This property can be affected by the substrate composition or mold release agents used in concrete, for example, and its interaction with application energy of mortar has a significant influence on interfacial contact area;
- packing of all grains present in mortar composition have to be measured, not only for sand or aggregates, since there is an interaction between aggregates and binders grains that can modify flow;
- 3D laser scanning is an important and innovative technique to quantify interfacial contact area, showing a good potential for further improvements.

Acknowledgments The authors appreciate the financial support of CNPq (Conselho Nacional de Desenvolvimento Tecnológico—Brazilian Council of Technological Development) and CAPES (Fundação Coordenação de Aperfeiçoamento de Pessoal de Nível Superior—Brazilian Ministry of Education).

References

- Antunes RPN (2005) Influence of rheology and the impact energy on the adhesive strength of mortar coatings, 187 p. Phd thesis (PhD in Civil Engineering)—Polytechnic School of São Paulo University, São Paulo (In Portuguese)
- Banfill PFG (2003) The rheology of fresh cement and concrete—a review. In 11th International congress on cement chemistry, Proceedings. Duban
- Bauer E, Sousa JGG, Guimarães EA, Silva FGS (2007) Study of the laboratory Vane test on mortars. *Build Environ* 42:86–92
- Benabed B, Kadri E, Azzouz L, Kenai S (2012) Properties of self-compacting mortar made with various types of sand. *Cem Concr Compos* 34:1167–1173
- Carasek H (1996) Portland cement mortars adherence to porous substrates: assessing of the influence factors and contribution to the study of the linkage mechanism, 285 p. Thesis (Doctoral)—Polytechnic School of São Paulo University, São Paulo (In Portuguese)
- Davis WR, Brough R (1972) Ultrasonic techniques in ceramic research and testing. *Ultrasonics* 10 (3):118–126
- Deltombe R, Kubiak KJ, Bigerelle M (2014) How to select the most relevant 3D roughness parameters of a surface. *Scanning* 36:150–160
- Freitas S, Freitas VP, Barreira E (2014) Detection of façade plaster detachments using infrared thermography—a nondestructive technique. *Constr Build Mater* 70:80–87
- Hall C (1977) Water movement in porous building materials-I. Unsaturated flow theory and its applications. *Build Environ* 12:117–125
- Hall C, Yau MHR (1987) Water movement in porous building materials—IX. The water absorption and sorptivity of concretes. *Build Environ* 22:77–82
- Hola J, Sadowski L, Reiner J, Stach S (2015) Usefulness of 3D surface roughness parameters for nondestructive evaluation of pull-off adhesion of concrete layers. *Constr Build Mater* 84:111–120 1 June 2015
- Kashani, A, Nicolas RS, Qiao GG, Van Deventer JSJ, Provis JL (2014) Modelling the yield stress of ternary cement–slag–fly ash pastes based on particle size distribution. *Powder Technol* 266:203–209
- Kylili A, Fokaides PA, Christou P, Kalogirou SA (2014) Infrared thermography (IRT) applications for building diagnostics: a review. *Appl Energy* 134:531–549
- Lee SH, Kim HJ, Sakai E, Daimon M (2003) Effect of particle size distribution of fly ash–cement system on the fluidity of cement pastes. *Cem Concr Res* 33(5):763–768
- Logins A, Torims T (2015) The Influence of high-speed milling strategies on 3d surface roughness parameters. In: 25th DAAAM international symposium on intelligent manufacturing and automation. vol 100, pp 1253–1261
- Mendes TM (2008) Influence of the aggregate friction coefficient and the matrix viscosity in the rheological behavior of concentrated heterogeneous suspensions, 122 p. Master (Master in Civil Engineering)—Polytechnic School of São Paulo University, São Paulo (In Portuguese)
- Olhero SM, Ferreira JMF (2004) Influence of particle size distribution on rheology and particle packing of silica-based suspensions. *Powder Technol* 139:69–75
- Paes INL (2004) Evaluation of the mortar coatings water transport in the initial post-application times, 265 p. Phd thesis (PhD in Civil Engineering)—Brasília University, Brasília (In Portuguese)

- Pagnussat D (2013) Effect of production burning temperature of ceramic blocks and its influence in the tensile bond strength of mortar renderings under ceramic block walls. 2013. Thesis (Doctoral)—Federal University of Rio Grande do Sul, Porto Alegre (In Portuguese)
- Preto MEJ (2007) Influence of the rugosity produced by concrete substrate treatment in adherence of mortar coverings, 180 p. Thesis (Master)—Federal University of Rio Grande do Sul, Porto Alegre (In Portuguese)
- Ramos NMM, Simões ML, Delgado JMPQ, de Freitas VP (2012) Reliability of the pull-off test in situ evaluation of adhesion strength. *Constr Build Mater* 31:86–93
- Santos PMD, Júlio ENBS, Silva VD (2007) Correlation between concrete-to-concrete bond strength and the roughness of the substrate surface. *Constr Build Mater* 21(8):1688–1695
- Senff L, Barbeta PA, Repette WL, Hotza D, Paiva H, Ferreira VM, Labrincha JA (2009) Mortar composition defined according to the rheometer and flow table tests using factorial designed experiments. *Constr Build Mater* 23:3107–3111
- Stolz CM (2011) Interaction between mortar rheological parameters and surface potential contact area on mortar renderings bond strength, 212 p. Thesis (Master)—Federal University of Rio Grande do Sul, Porto Alegre (In Portuguese)
- Stolz CM, Masuero AB (2015) Analysis of main parameters affecting substrate/mortar contact area through tridimensional laser scanner. *J Colloid Interface Sci* 455:16–23
- Sugo HO, Page AW, Lawrence SJ (2001) The development of mortar/unit bond. In: Canadian masonry symposium, 9th, fredericton. Proceedings of department of civil engineering—University of New Brunswick
- Tan KS, Chan KC, Wong BS, Guan LW (1996) Ultrasonic evaluation of cement adhesion in wall tiles. *Cement Concr Compos* 18(2):119–124
- Yates M, Martin-Luengo MA, Cornejo J, González V (1994) The importance of the porosity of mortars, tiles and bricks in relation to their bonding strengths. *Stud Surf Sci Catal* 87:781–790
- Zahia T, Roussel N, Lanos C (2005) The squeezing test: a tool to identify firm cement-based material's rheological behaviour and evaluate their extrusion ability. *Cem Concr Res* 35 (10):1891–1899
- Zhang X, Han J (2000) The effect of ultra-fine admixture on the rheological property of cement paste. *Cem Concr Res* 30(5):827–830

The Pathologies of the ETICS

Filiberto Lembo and Francesco Paolo R. Marino

Abstract The use of the ETICS is covered by a specific technical standard: the ETAG 004 *Guideline for Technical Approval of External Thermal Insulation Composite Systems With Rendering*, issued by EOTA *European Organization for Technical Approvals*; so, all applications should include approved systems, with the ETA *European Technical Approval* marking, which are raised from an approval body. From the design point of view, ETICS are differentiated according to the methods of fixing: bonded ETICS, bonded ETICS with supplementary mechanical fixings, mechanically fixed ETICS with supplementary adhesive, and purely mechanically fixed ETICS. There are also different types of substrates (masonry walls [made from units of clay, concrete, calcium silicate, autoclaved aerated concrete or stone]); in situ or prefabricated concrete walls; wood structures. ETICS components are many and can be very different from one system to the other: they are basically adhesive (dry mortar, powder requiring addition of extra binder, paste requiring addition of cement, ready-to-use paste), with more or less organic resin; insulation product (basically EPS, mineral wool, and wood wool; but also cork, XPS, polyisocyanurate (PIR), phenolic foam, and others); rendering system, made by reinforcement (glass fiber, or plastic mesh – standard or reinforced – or metal lath, or dispersed fibers embedded or dispersed in render coating), render, formed by base coat, key coat, finishing coat, and/or decorative/protective coat; mechanical fixing devices and ancillary materials and components, as window's sill, corners,

Contributions. The contribution of the authors in the research and in editing and writing the text of the paper, were equal.

F. Lembo (✉) · F.P.R. Marino
School of Engineering, University of Basilicata, 10 Viale dell'Ateneo Lucano,
85100 Potenza, Italy
e-mail: filiberto.lembo@unibas.it

F.P.R. Marino
e-mail: francesco.marino@unibas.it

joint-covers, sealants, mastics, and so on. So, due to the complexity of the structure and the number of performances required, in the case of emerging pathologies, checking for causes is very difficult.

Keywords ETICS · Pathologies · ETAG 004 · Diagnosis techniques

1 Grounds for a Research

Probably, there is no “non-traditional” building technique that, as *External Thermal Insulation Composite Systems* (ETICS), is concerned with a technical standard that pays as much attention to “*verification methods used to examine the various aspects of performance, the assessment criteria used to judge the performance for the intended use and the presumed conditions for the design and execution*” (ETAG 004 2000). The *Guideline* is, on the other hand, the result of a long evolution that dates back to *UEAtc Technical Guide for the Assessment of External Wall Insulation Systems Faced with Mineral Render* of the April 1992, and before to the *UEAtc Directives for the Assessment of External Insulation Systems for Walls (Expanded Polystyrene Insulation Faced with a Thin Rendering)* of June 1988; and more before to the researches from 1959, on the one hand in France (Lembo 1990), especially from C.S.T.B., and on the other in Germany (Riedel et al. 2010).

The ETAG “*has been established in compliance with the provisions of the Council Directive 89/106/EEC (CPD)...is a basis for ETAs, i.e. a basis for technical assessment of the fitness for use of a product for an intended use*” (ETAG 004 2000, p. 14). Therefore, from the point of view of pathologies, an ETICS homologated through an ETA and executed in respect to limitations and prescriptions stated in the ETA (Cahier du CSTB 2013), should be *by definition* pathologies’ exempt or, at least, immune from heavy pathologies, as to bring into question his functionality, in a long time (25 years or so on). And, on the other hand, a system set in place in a way different from that stated in the ETAG 004 and in the ETA (for instance, bonded on minus than 20 % of surface, with components which are different from that scheduled in the ETA, with different thickness of the layers, with differing composition) (for instance, without key coat if scheduled), is therefore “*outlaw*,” and hence bound to be subject to most different pathologies. It should be banned from the market. It should not exist.

In actual fact, this is not true. On the contrary, you can see the diffusion of “*do-it-yourself systems*,” in which components are chosen on the free market on the basis of economic convenience, and assembled according to the convenience of designers or of builders (CRESME RICERCHE SpA 2014) by subjects who often have a very limited design culture, a limited knowledge of the defects before studied and known, and who often have the economic interest to adopt a pre-determined solution, rather than the best solution for a specific situation. In this case, to have an ETA becomes only the covering for being on the market, in a condition

of *laissez faire, laissez passer*. On the other hand, in particular, systems durability appears to be not exactly determinable, despite the extent and the close examination of experimental tests scheduled by ETAG 004; most of all, these tests are unable to provide a system's *qualitative assessment*: once exceeded requirement's established threshold, every system looks like equal, all perfectly adherent to substrate, weather proof, nonhydrophilic, not subject to cracks, and so on.

Simply, it is not true. Some between them last 10 years without problems, and others every time, also if as soon as realized look like perfect, after some years appear fatally and systematically compromised. At the extent that today, recovering and upgrade works on the ETICS already existing are nearly in the same quantity of new ETICS works. But in the building sector, economic interests are much too strong to have somebody who says "*Artemidoro's papyrus is a false.*" The situation is similar to that which occurs in Italy with precast facing reinforced concrete industrial buildings, they continue to realize with coverings that normally satisfies standards for static security, but not durability requirements. They can be tried out from the structural point of view, and they are; but as durability, it is another subject, and 20 years later they are a fresco of rust drippings and spalling of concrete.

Actually, under the unique ETICS's acronym are collected systems extremely different, born from very different requirements. To deeply analyze them, you must subdivide them into types and examine them one by one and compare one type with another. Only in this way can you understand why they exist, and why they are proposed on the market. But we can only touch on this in the few pages of this contribute.

2 The ETICS Are Responses to Different Performance Requirements

ETICS were born at the end of the 1950s because only then were available non-saponifying organic resins that make traditional mineral renders enough elastic, to become warp without cracking due to great thermal deformations, peculiar of a thin layer adherent, applied on an insulation product, warmed up by the sun and straight after cooled by icy rain. Only in this way renders can follow thermal movements of synthetic insulation products below, characterized by an " α " much greater than traditional ones. In fact, despite wood wool was industrially produced from the first decades of the century, as insulation product the interest was in these years in particular to the EPS that, being not hydrophilic in an outstanding way, give to the exterior walls further weather tightness.

France is, especially, the only country that has, yet in that moment, and today too, a standard (D.T.U. 20.11 and D.T.U. 23.1) which classify water tightness to the rain of buildings external walls, identifying four different building typologies of different rain screen performance, and establish that (according to the exposition of

the wall, on wind zone; on nearness to lakes or seaside; on the height of the wall on the ground; and on being “sheltered” or not) you must adopt very specific wall typologies, or even you must study and implement specific solutions *purpose-made* (Lembo 1990, Vol. I, pp. 49–59). In France, an ETICS realized with a nonhydrophilic material such as EPS which led to the upgrading of the external walls of *Ist type to IInd a-type* [the worst, that with lower weather tightness, realized with hydrophilic materials in contact between them (for instance, units of clay or concrete, rendered or not, but also in reinforced concrete, also with hydrophilic insulation in contact or at range shorter than 2 cm from other hydrophilic layers of the wall)].

Therefore, the advantage of realizing an ETICS with EPS was double: the insulation and the water tightness. From here, the great diffusion in France, Germany, and in general in countries with stormy weather, of the ETICS founded on EPS.

This standard in France has been even further specified, in March 1983 (we are speaking of 31 years ago) with the Deliberation of *Groupe Spécialisé n. 7 (produit et systèmes d'étanchéité et d'isolation complémentaire de parois verticales)* of the *Commission chargée de formuler des Avis Techniques*: “*Conditions générales d'emploi des systèmes d'isolation thermique des façades par l'extérieur faisant l'objet d'un avis technique*” (Cahier du CSTB n° 237, Livraison 1833), which at point 3 *Choix des types de murs isolés par l'extérieur en fonction de leur exposition à la pluie*, has defined four wall types, with water tightness increasing from XI to XII, to XIII, to XIV, and establish that the water tightness depends on both the quality of supporting wall, the insulation material and quality of exterior skin, setting ETICS polystyrene based in types XII and XIII, depending on being dressed with mineral base coat and finishing coat (XII) or organic base coat and finishing coat (XIII).

But for buildings more than three floors high, or with a higher fire risk, mainly if the thickness of EPS insulation is more than 10 cm, in England, in France and in Germany, for a long time it is necessary to provide for cut-flame architraves on doors and windows, and/or cut-flame rings all building round at the most every two floor, realized with material reacting to fire A1 or A2; and here comes the diffusion of ETICS with insulation products in nonhydrophilic mineral wool, in different types (MW and L). But, also if in tests preview from ETAG 004 water absorption after 1 h or after 24 h of the base coat or of the all system is corresponding to the required performance, the hydrophilic behavior of material is undoubtedly different, and inferior to that of an EPS (Pearson 2010).

Therefore, you need base coats and finishing coats especially waterproof, and with a higher content of organic resin, to obtain a high water tightness. But higher content of organic resin makes renders more inflammable, and lowers their reaction to fire. Hence, the requirement of defense from fire risk and water tightness are in contradiction between them. In a high-rise building it is difficult to conciliate the two performances, and you need systems especially studied for satisfying both these requirements.

In the same way, the use of wood wools that today have their principal reason in the search of materials with greater sustainability; they are normally characterized by reaction to fire E, as the EPS, and they are undoubtedly more hydrophilic than EPS; with water they decay. Therefore, an ETICS with insulation product made in wood wool should be made up by components especially refined for obtaining at the same time the necessary water tightness and the appropriate reaction to fire.

Analogously, for solving particular acoustic problems, often determined by systems of building “light and dry” of opaque parts of walls, now in fashion; for they have been necessary to implement particular solutions, with insulation products elasticated and heavy renders, very thick, in way to take the best advantage of mass-string-mass effect. But heavy renders, very thick, are basically more rigid and brittle than thin renders, and crack’s risk become greater, and you must pay a greater attention in the design phase, providing break-up joints, which are expensive and can be not appreciated (Lembo 1990, Vol. II, pp. 38–39) (see Figs. 1 and 2).

That is what occurs for the colors of the façades, which must be clear if you want to keep down the risk of cracks, in particular for mineral renders. That which shuffles between strips of beige and dark brown, without scheduling break-up joints on the contact line between the two colors, in 10 years will find the façade systematically cracked (see Figs. 3 and 4). Which ETAG 004, which ETA can remedy to pathologies coming up for the lack of design culture of project managers?

And so on, with other insulation products, for the most part implemented for other productive sectors, and that industries urge for inserting in the building sector of the exterior insulation of façades, like the cork, the extruded polystyrene foam XPS, the rigid polyurethane foam PUR, the products of phenolic foam PF, the polyisocyanurate PIR, the expanded glass foam, and many others.



Fig. 1 Building with ETICS in PIR in Torrette di Mercogliano (Avellino). Insulation thickness: 3 cm; cementitious render: 2.0–2.5 cm; finishing coat: paint



Fig. 2 Wall facing west

Fig. 3 New building under construction in the University Campus of Macchia Romana in Potenza. ETICS ISOL-K8 (ETA-05/0195)



Fig. 4 Walls are painted in *light beige* and *dark brown*, in vertical alternate strips



Some of these materials, as the XPS, the PUR, the PF, the PIR, are characterized by thermal expansion ratio greater than EPS, and therefore make difficult the task of reinforcement meshes and of base coats, for preventing that system, with the passing of time, breaks (as it can be seen in Figs. 1 and 2). Or else, like the cork, the PU or the PIR, have the tendency, as time goes by, to absorb and to hold back the moisture, chiefly through the not protected edges, changing their thermal and weather tightness characteristics (Pearson 2010, p. 74).

Otherwise, they are subject to phenomenon of long-term withdrawal, which can cause cracking of base coat and finishing coat. Each of ETICS produced with these new and different materials, which answer more to productive and market requirements, than to constructive ones, has his own characteristics very different from these of the systems of the beginning, on which we have 50 years of experience; and the risk of heavy pathologies with the passing of time increases.

We have had an illuminating example, in Canada, with uncritical use, for wooden houses, of ETICS implemented for buildings in massive systems, that caused pathologies very serious and irretrievable on tens thousands houses, that has been demolished few years after their completion, because decayed and at risk of collapse (Horvat and Fazio 2004). But in Italy, today, they make the same errors.

Otherwise, the companies that want to assure superior qualities to their systems issue technical requirements much more restrictive than that of ETAG 004 for the materials and components to insert in their systems (for instance, the Sto AG Company has a proprietary disciplinary “*Quality requirements for Sto polystyrene insulation boards,*” through which they request performances especially high for all important parameters and characteristics). This means that systems seemingly equals can have in reality technical characteristics deeply different, and can be designed for long lasting, or not.

3 Research Methodology: A Comprehensive Examination of European Valid ETA, Focused on Comparison with Italian Valid ETA

For understand causes of ETICS’ pathologies, identify those predictable and distinguish those “structural” from those coming from design or execution mistakes, is in progress since 3 years at Constructions Technology Laboratory *La.Te.C.* of Engineering School of Basilicata University, Potenza, a research program that examined every valid ETA, issued in whole Europe from National Approval Body (C.S.T.B. in France, D.I.B.t. in Germany, IETcc in Spain, ITC in Italy, LNEC in Portugal, O.I.B. in Austria, SITAC in Sweden, TZÙS in the Czech Republic, TSUS in Slovakia, UBAtc in Belgium, Z.A.G. in Slovenian Republic, and so on). They are many hundreds. Systems have been classified by typologies, by principal characteristics and performances, and they have been confronted between them, on the basis of data emerging from ETA analysis.

The classification of the systems, useful to operate the comparison between them, was made considering the following properties and characteristics: system name, European technical assessment, system holder, short description, finishing, reinforcement mortar (after 1 h, Kg/m^2 ; after 1 die Kg/m^2), finishing coatings (after 1 h, Kg/m^3 ; after 1 die Kg/m^3), type of wall, wind resistance (glued, PVC profiles, dowels), percentage of fireproofing agent declared, reaction to fire Eurocode EN 13501-1, vapor permeability (air thickness, m), EPD, material safety data sheet, resistance of the screws (category, notes, records), gluing surface percentage, bonding and reinforcing mortar, insulating, dowels, PVC profiles, reinforcement mesh, primer, mineral finishing, and organic finishing.

An example of a comparative table that has been made is shown below in Fig. 5. Given the considerable size, it is reported only as an extract and divided into several parts (see Fig. 5).

Operationally, it proceeded in the following way. First, we find that information contained in the ETA issued from different approval bodies, as well in the fixed frame of ETAG 004 (2000, pp. 116–143), have different degrees of close examination. Whereas, for instance, the ETA of CSTB show often the year of introduction on the market of the system and the amount of surfaces yearly done, many

Order number	System Name	European Technical Assessment	System Holder	Short description	Finishing
1	KNAUF WARMWAND SYSTEM EPS/SM300	CSTB ETA - 13/0555 27/06/2013 - 26/06/2018	Société Knauf Gips KG DE - 97346 Iphofen	Malta di armatura spessa a base di calce aerea e di legante idraulico (polvere da mescolare con acqua), rete in fibre di vetro, EPS incollato (fino a 300 mm di spessore) o fissato meccanicamente (tasselli o profili, fino a 200 mm)	Intonaco sottile a base di legante idraulico o acriliossano Intonaco spesso a base di calce aerea
2	FASSATHERM CLASSIC F	CSTB ETA - 13/0532 26/06/2013 - 25/06/2018	FASSA SpA IT - 31027 Spresiano	Malta di armatura sottile a base di cemento (polvere da mescolare con acqua), rete in fibre di vetro, EPS incollato (fino a 300 mm di spessore) o fissato meccanicamente (tasselli o profili, fino a 200 mm)	intonaci sottili con legante acrilico
3	THERMOCOVER	ITC ETA - 13/0514 27/05/2013 26/05/2018	VALT PLASTIC Srl 23010 Barbeno in Valtellina (SO)	Collante e malta di armatura sottile a base di cemento (polvere da mescolare con acqua), rete in fibre di vetro R117 saint Gobain Vertex, EPS incollato	intonaco sottile con legante acrilico "SILACRYL COMPACT ANTIALGA" 1,5
4	SIGMA ISOL ST	ITC ETA - 13/0513 27/05/2013 26/05/2018	PPG UNIVER SpA 28010 Cavallino (NO)	Collante e malta di armatura sottile a base di cemento (polvere da mescolare con acqua) min. 40%, rete in fibre di vetro R117 saint Gobain Vertex, EPS incollato	intonaco sottile con legante acrilico "SILACRYL COMPACT ANTIALGA" 1,5
5	UNIVERCAP	ITC ETA - 13/0512 27/05/2013 26/05/2018	PPG UNIVER SpA 28010 Cavallino (NO)	Collante e malta di armatura sottile a base di cemento (polvere da mescolare con acqua) min. 40%, con fissaggio meccanico supplementare, rete in fibre di vetro R117 saint Gobain Vertex, EPS	intonaco sottile con legante acrilico 1,2 "DURPLAST COMPACT FIM" (cancellato) intonaco sottile con legante acrilico 1,5 "DURPLAST COMPACT ACRIFLOSSANICO FIM" (cancellato)
6	THERMIX	ITC ETA - 13/0511 27/05/2013 26/05/2018	CUGINI SpA 24027 Nembro (BG)	Collante e malta di armatura sottile a base di cemento (polvere da mescolare con acqua) min. 40%, con fissaggio meccanico supplementare, rete in fibre di vetro R117 saint Gobain Vertex, EPS	paste pronte all'uso con legante acrilico, da utilizzare con primer con lo stesso numero

Reinforcement mortar		Finishing coatings		Type of wall	Wind resistance			Percentage of fireproofing agent declared	Reaction to fire Eurocode, EN 13501-1	Vapor permeability Air thickness (m)	EPD
after 1 h Kg/m ²	after 1 die Kg/m ²	after 1 h Kg/m ²	after 1 die Kg/m ²		glued	PVC profiles	dowels				
				28m - 18m XI - XII	nessuna limitazione	limitazioni	limitazioni		B-s2, d0		NO
< 1,0	< 0,5		< 0,5					nella malta di armatura 20% nei rivestimenti di finitura: 0%	B-s2, d0	malta di armatura + rivestimento 0,6 + 0,7	
< 1,0	< 0,5		< 0,5						F nessuna prestazione determinata	0,42	
< 1,0	< 0,5		< 0,5						F nessuna prestazione determinata	0,29	
< 1,0	< 0,5		> 0,5	→ prova gelo /disg, non eseg. NPD					F nessuna prestazione determinata	0,28 + 0,29	
< 1,0	< 0,5		3 finiture < 0,5						F nessuna prestazione determinata	0,18+0,42	
			1 finitura > 0,5	→ prova gelo /disg, non eseg. NPD					F nessuna prestazione determinata		

Fig. 5 Example of a complete synoptic table of ETICS cataloging and characterization

Material Safety Data Sheet	Resistance of the screws			Gluing surface percentage	Bonding and reinforcing mortar	Insulating	
	cat.	notes	records				
NO	II - III	rischi bombature	spessore minimo della malta di arm.: 7 mm	30 ± 25%	SM300, SM700, SM700 Pro Duo-Kleber: polvere a base di cemento da mescolare con acqua. Colla: min 4 Kg/m ² . Malta di armatura min. 7,5+3 Kg/m ² .	EPS bianco o grigio	solb EPS bianco
						Incollato o tassellato E, max 300 mm Ia2 Sa4 O=3 Lx3(120) E=2	Mecanico con profili E, max 200 mm Ia2 S=5 O=3 L=4 E=2
	II - III	con armatura semplice	nelle note sulla posa in opera, al punto 4.2.2, si ribadisce che l'incollaggio deve essere 40%	20% Resistenza a trazione perpendicolare ≥ 200 kPa	CG/11F collante in polvere a base di cemento CEM II/A-L 42,5 R, da mescolare con 24,5-27,5% di acqua. Colla: 3-5 kg/m ² (cancellato). Malta: 3,5-4 kg/m ² (cancellato).	EPS "Standard" s 16 kg/m ² E, da 20 a 300 mm	EPS "Standard" E, da 60 a 200 mm
		con armatura doppia					
	II	con armatura standard	nelle note sulla posa in opera, al punto 4.2.2, si ribadisce che l'incollaggio deve essere 40%	20% Resistenza a trazione perpendicolare ≥ 200 kPa	Collante e malta di armatura SIGMA (ISOL PW FINE, polvere a base di cemento CEM II/A-L 42,5 R, da mescolare con 24,5-27,5% di acqua. Colla: 3-5 kg/m ² (cancellato). Malta: 3,5-4 kg/m ² (cancellato).	EPS "Standard" s 20 kg/m ² E, da 50 a 200 mm λ=0,035	"EXPANDIT EPS 100 ETICS"
II	con armatura standard	nelle note sulla posa in opera, al punto 4.2.2, si ribadisce che l'incollaggio deve essere 40%	20% Resistenza a trazione perpendicolare ≥ 200 kPa	Collante e malta di armatura UNIVERCAP, Cugini SpA (BG), polvere a base di cemento CEM II/A-L 42,5 R, da mescolare con 24-27,5% di acqua. Colla: 3-5 kg/m ² (cancellato). Malta: 3,5-4 kg/m ² (cancellato).	EPS "Standard" s 20 kg/m ² E, da 50 a 200 mm λ=0,035	"EXPANDIT EPS 100 ETICS"	
							con armatura standard
II	con armatura standard	nelle note sulla posa in opera, al punto 4.2.2, si ribadisce che l'incollaggio deve essere 40%	20% Resistenza a trazione perpendicolare ≥ 200 kPa	Collante e malta di armatura ADEMIX P200, Cugini SpA (BG), polvere a base di cemento CEM II/A-L 42,5 R, da mescolare con 24-27,5% di acqua. Colla: 3-5 kg/m ² (cancellato). Malta: 3,5-4 kg/m ² (cancellato).	EPS "Standard" s 20 kg/m ² E, da 50 a 200 mm λ=0,035	"EXPANDIT EPS 100 ETICS"	
							con armatura standard

Dowels	PVC profiles	Reinforcement mesh	Primer	Mineral finishing	Organic finishing
vari (14)	Knuf	incollato o tassellato T≥1 Ra=1 M=2 E=1 meccanico con profili T≥1 Ra=2 M=2 E=2 R 131 A 101 C+ Saint Gobain Adfors R 131 A 102 C+ Saint Gobain Adfors Armiergewebe 4x4 mm (03 - 1C+) Asflatex	QUARZGRUND legante acrilico pronto all'impasto	SP 260, RP 240, SM 700 Pro NoBo, paste pronte all'impasto, a base di calce aerea	CONNIS, ADDIS paste pronte all'impasto, a base di legante ari/lissanico <i>nota: - data delle prime applicazioni: 2010 - in Europa, circa 1,4 milioni di m²</i>
vari (4)	disegni sull'ETA	4 armature normali, anche Saint Gobain, tra 160 e 170 gr/m ² : R 131 A 101C+ (160), R 131 A 102 C+ (170), SSA-1363 F+ (160), FASSANET-160 (0161-CA) (170) 2 armature rinforzate, da 350 e 700 gr/m ² : FASSANET-370 (0370-A) (350), R 565 A 101 (700)	FA 249 legante acrilico, con 6 volumi d'acqua FA 526, legante acrilico, da mescolare con 5% in peso d'acqua		n.4 tipi di pasta pronta all'impiego, con legante acrilico, ciascuna in quattro varianti di granulometria. Per tutti, dal 9,6% al 10,3% di materia organica
1 6/m ² (cancellato)	TER-11-2218N Dakota Italia SpA (cancellato)	R117 Valplastic Sd (150), Italy, 4 x 4,5 mm	DUE IN UNO, emulsione acrilica in fase acquosa (pronta all'uso)		SYLACRIL COMPACT ANTIALGA pasta pronta all'uso con legante acrilico 1,2 gr., 2+3 kg/m ² (cancellato), spessore 1,5 mm
1 6/m ² (cancellato)	TER-11-2218N Dakota Italia SpA (cancellato) polipropilene 8 mm chiodo nylon	R117 Sain Gobain Vertex-Litomysl, Czech Republic, 4 x 4,5 mm	SIGMA SILOXAN FX, soluzione acquosa di resine acriliche e silossaniche, da diluire con acqua 1:1		SIGMA FA=ADE PUTZ AS 1,5 mm pasta pronta all'uso con legante acrilico. 2 x 2,2 kg/m ² ogni strato (cancellato), spessore 1,5 mm
1 6/m ² (cancellato)	TER-11-2218N Dakota Italia SpA (cancellato) polipropilene 8 mm chiodo nylon	R117 Sain Gobain Vertex-Litomysl, Czech Republic, 4x4,5 mm	ISOACRIL, emulsione stirolo acrilica in fase acquosa, da diluire con acqua 1:7 LIBRA PRIMER, soluzione acquosa di resine acriliche e silossaniche, pronta o da diluire 1:1		DURPLAST COMPACT F/M 1,2 mm pasta pronta all'uso con legante acrilico DURPLAST COMPACT F/M 1,5 mm pasta pronta all'uso con legante acrilossabico
1 6/m ² (cancellato)	TER-11-2218N Dakota Italia SpA (cancellato) polipropilene 8 mm chiodo nylon	R117 Sain Gobain Vertex-Litomysl, Czech Republic, 4 x 4,5 mm	1 - DUE IN UNO, emulsione acrilica in fase acquosa (pronta all'uso) 2 - ISOACRIL, emulsione stirolo acrilica in fase acquosa, da diluire con acqua 1:7 3 - SIGMA SILOXAN FX, soluzione acquosa di resine acriliche e silossaniche, pronta o da diluire 1:1		Paste pronte all'uso, legante acrilico 1 - SYLACRIL COMPACT ANTIALGA 1,2 mm, 2-3 kg/m ² 1,5 kg/m ² 2 - RESTAUR MIX F/EI ETICS 1,0 mm, 1,5 kg/m ² 3 - DURPLAST COMPACT F/M 1,2 mm, 2-2,2 kg/m ² 4 - SIGMA FA=ADE PUTZ AS 1,5 mm

Fig. 5 (continued)

others do not contain this information; and therefore systems that still must be tested through realizations are treated like others, on the market from many years and with which are realized yearly millions of square meters.

Most part of systems (more than 80 % in number of ETA) has EPS as insulation product; follows mineral wool (about 10 % in number of ETA); every other insulation product occupies the residual percent. For the most part, systems forecast bonds and base coats as powder requiring addition of cement as extra binder, and have organic resin ratio very low, about 3–3.5 % in the base coat, 5–9.5 % in finishing coat.

Therefore, are present mainly these that already in 1980 in France were defined “*hydraulic render of first generation*,” in opposition to “*thin render, organic base, of second generation*” (Lembo 1990, Vol. I, p. 93). But thicknesses of base coats according to schedules of ETA’s are as a general rule very thin, and normally is specified only the minimum thickness, but not the maximum. This is a problem, because properties of a material depend on his thickness that cannot be freely changed, without altering its behavior (as it can be seen in Figs. 1 and 2).

Hence we are talking, in general, of materials quite cheap, not particularly refined, and therefore you invent that many companies, holders of approval, produce only insulation product, or on the contrary the base coat and the finishing coat, while the elements with greater technological complexity (for some system they seem to be the meshes and the fixing devices; for others, the insulation products; for others more, base coat and finishing coat) are produced by few specialized industries, and cement is bought directly by the company that applies the system, on the free market, normally CEM II/A-LL 42,5 R.

The most part of systems is fixed whether bonded, or bonded with supplementary mechanical fixings. But, while French or German standards constitute precise reference frame for typifying the wind load resistance system must offer in different site conditions, in Italian ETA all is entrusted to project manager and to executive director, who every time should establish system’s wind load security conditions, on the basis of valid standard NTC 2008.

The result is that for many Italian systems ETA foresees to use only one type of supplementary anchors, that obviously makes unfeasible the system’s use in the different situation you can find, and usually entrusts to the anchors an improper ancillary function, with diction: “*mechanical fixing devices are utilized to give stability up to the moment in which the bond is dried and act as temporary connection*;” in some cases, the fixing capacity of the anchor is scheduled in the ETA as “*F – No Performance Determined*” (ETA-13/0134, CAPTHERM). How it is possible to issue an ETA in these conditions, is not so much understandable.

It strikes us that many systems, mainly Italian, based on MW insulation products, that should be implemented just for the use in situations in which there is a great fire risk, obtain the ETA without being tested to the fire reaction tests, and therefore the system has an ETA with the assessment of reaction to fire “*F – No Performance Determined*.”

It must be highlighted, compared to European panorama, the general solution's poverty of finishing/decorative coats of Italian systems: many of Italian ETA concern systems with only one finishing coat, with only one particles size. It is truly difficult to trust the unique operational mode of the system's interventions. That is, it looks like that in this domain too spread the custom, very Italian, to the "slip of paper": the ETA serves to shelter a realization dissimilar, that you carry out the following requirements of client of the specific building work, regardless the provisions of the ETA.

So the ultimate pathology of the ETICS, almost of these Italians, appears plain: in a system like this, very awkward, in which many elements carry out in the same time many functions, the alteration also of only one characteristic of one of layers compared to the system issued through the ETA can easily bring the system get out of hand, and become the origin of pathologies you can easily observe, and are well documented in the literature (Riedel et al. 2010, Chap. 7, pp. 132–181).

The remedy appears to be as much plain: to deny every form of warranty, in unequivocal way, to every design solution not according to schedule in the ETA (for instance, to bond claddings in bricks or ceramics of stone plates to ETICS which has not that prevision in their ETA; or to change the type of finishing coat and/or decorative coat, or else to substitute the XPS to the EPS, or the EPS to the XPS, and so on), and not into compliance with *best practices* everywhere plasticized. Sure enough, the in progress research proves that local conditions can have a catalytic function for pathological phenomena.

In places that look like Avellino, already famous in the literature (Massari and Massari 1985), almost as Holzkirken in Germany, for the very high humidity ratio all year long and for the rain that, pressed by the wind, "*hit in horizontal*" the walls of buildings facing West (giving birth to a "*Bastard Cold*": evaporation cooling of the walls of 3–4 °C in respect with air temperature), every applied physics phenomenon is amplified, and only the ETICS of superior quality are able to give performances required from the hostile environment.

4 Conclusions

The study of the ETICS is particularly tricky due to the complexity of the structure and the number of performances required and the checking for causes is very difficult in the case of emerging pathologies.

The paper shows a method for doing this, based on the respect or not, from every layer and from the relationship between the layers, of the characteristics and performances fixed by ETAG 004 and by Technical Specifications made by other Specialized Body, as the *Groupe Spécialisé n° 7* of C.S.T.B., or extracted by *best practices* and by case studies known in the literature or observed by the authors; the study of the influence of local conditions.

References

- Cahier du CSTB 3035_V2 – Juillet (2013) Systèmes d'isolation thermique extérieure par enduit sur polystyrene expansé – Cahier des Prescriptions Techniques d'emploi et de mise en oeuvre
- CRESME RICERCHÉ SpA (2014) Indagine sull'attuale posizionamento e sulle prospettive di mercato del "Sistema a cappotto", CORTEXA, May 2014, Analisi SWOT, pp 51–53
- ETAG 004 (2000) Guideline for European technical approval of external thermal insulation composite systems (ETICS) with rendering, Brussels, EOTA, edn 2000, Amended Aug 2011, Feb 2013, p 10
- Horvat M, Fazio P (2004) Protocol and assessment tool for performance evaluation of light-frame building envelopes. In: Proceedings of CIB world building congress 2004, Toronto, Canada, 2–7 May 2004, Paper n. 352, p 2
- Lembo F (ed) (1990) *Isolare dall'esterno*, vol I, Teoria, and vol II, Tecniche e manutenzione, Bologna, Edizioni C.E.L.I., 1990, Introduzione, pp VII–XV, *Premessa*, p XXVII e *Bibliografia*, pp XXI–XXV
- Massari G, Massari I (1985) *Risanamento dei locali umidi*, Milano, U. Hoepli Editore, pp 297–301
- Pearson CJ (2010) External wall insulation, 1st edn 2006, eVersion 2010, Wellgarth Publishing, ISBN No 978-0-9553636-2-7, p 69: mineral fibre slabs should not be left exposed to the weather, if it does become saturated, it should be allowed to dry out naturally before the finishes are used
- Riedel W, Oberhaus H, Frössel F, Haegle W (2010) *Wärmedämm-Werbundsysteme – Von der Thermohaut bis zur transparenten Wärmedämmung*, Baulino Verlag – Fraunhofer IRB Verlag, 2nd edn, p 16

Criteria for Identification of Ceramic Detachments in Building Facades with Infrared Thermography

Elton Bauer, Elier Pavón, Cláudio H.F. Pereira
and Matheus L.M. Nascimento

Abstract Infrared thermography is a nondestructive technique with great application potential to study the pathologies of buildings. The use of passive thermography to evaluate building facades subjected to sun incidence has allowed interesting advances in the identification of regions with initial detachments that are not visible on the facade surfaces. There are, however, several difficulties in the methodology, especially regarding the best moment to visualize the anomalies. These moments depend mainly on the heat flow in the facade, which is not constant. The objective of this study is to identify the best conditions to visualize the anomalies by performing field and laboratory studies to evaluate delta-T and contrast functions. To this end, a laboratory study was developed. It consisted of heating and cooling experimental base plates with manufactured internal defects, which were monitored by a sequence of thermograms obtained continuously. The field study consisted of evaluating an area of a building facade with detachment patches. The thermal evolution of the facade was monitored continuously by thermography for 10 h. The results indicate that delta-T cannot be used as the sole parameter to identify the anomalies. It is also highlighted that knowing the direction of heat flow is important since the contrast functions have shown that the anomalies are best visualized at the beginning of the heat flow, heating or cooling. It proved that the criteria obtained in the laboratory are applicable to field studies, especially if it is possible to analyze previously the heat flow on the facade.

E. Bauer (✉) · E. Pavón · C.H.F. Pereira · M.L.M. Nascimento
Department of Civil and Environmental Engineering, Faculty of Technology, University of Brasília (UnB), Campus Darcy Ribeiro, Brasília, DF 70910-900, Brazil
e-mail: elbauerlem@gmail.com

E. Pavón
e-mail: elierpavon@gmail.com

C.H.F. Pereira
e-mail: claudiochp@gmail.com

M.L.M. Nascimento
e-mail: leoni.matheus@gmail.com

Keywords Infrared thermography · Detachment · Facades · Contrast · Delta-T

1 Introduction

The studies of buildings' degradation seek to measure and map the anomalies; therefore, it is necessary to identify and quantify the pathological manifestations present in each of the building elements. The identification of anomalies in the building facades is often a complex activity, which requires elaborate logistics and difficult to implement procedures (Bauer and Pavón 2015). Thus, the aim is to implement and refine experimental techniques, preferably nondestructive, so that the routine inspection can be improved and the evaluation is quicker and more precise. One of these techniques is the infrared thermography, which can be used to identify detachment and cracks on walls, the most important defects found in inspections (Edis et al. 2012, 2014a). It should be emphasized that the thermographic inspection allows a nondestructive evaluation, which may be performed at a distance, without requiring complex logistics to access the facade. It is also noteworthy the immediacy of the technique since the thermograms are captured in real time and immediate analysis of the images allows to identify the potential problems in the image-making process (reflections, improper angulation) and observe potential abnormalities as well. This can be done continuously during the inspection, and the subsequent study of the images allows a conclusive analysis and definition of the studied aspects.

In addition to investigating detachment problems (Cerdeira et al. 2011; de Freitas et al. 2014), thermography allows to evaluate abnormalities due to humidity (Lerma et al. 2011, 2013; Edis et al. 2014b, 2015; Menezes et al. 2015), cracks (Dufour et al. 2009; Broberg 2013; Freitas et al. 2014), and other pathologies of different coating systems (Lai et al. 2010, 2012; Pascu 2011). This is true for laboratory studies performed under relatively controlled conditions and field studies under different exposure conditions. The results obtained mainly in the studies of building facades are not yet highly applicable due to the lack of a standard procedure and analysis criteria for the application of thermography (Bauer et al. 2015a). It is, therefore, necessary to establish a significant set of criteria and standards to identify safely the anomalies of the facades under different exposure situations (Bauer and Pavón 2015).

Most research presents several case studies with quantitative results using delta-T values (temperature difference on the surface between the region of the anomaly and the surrounding area) as a criterion for identifying defective areas (Bauer et al. 2015a). This temperature difference between the defective region and its surrounding area is easily identified in some thermograms. The surface temperature of the facade depends on a very large set of climatic variables (solar irradiance, incidence of winds, shading, among others), and on the characteristics of facade elements (absorbance, thermal conductivity, surface texture, among many others).

Thus, the delta-T detected on a facade may be different from that obtained in relation to another, especially if there is heat flow differentiation.

The more detailed studies correlate the delta-T with the wall temperature gradient (between the outer and internal surface) (Cerdeira et al. 2011), and show correlations with numerical simulations (Taylor et al. 2014) and field measurements (Edis et al. 2015). However, the results are still specific to the systems and conditions of each study, since they depend heavily on specific exposure conditions. It is, therefore, necessary to analyze the behavior of surface temperatures, gradients, and the evolution of heat flow, to establish the criteria that can be used to plan the inspection and subsequent analysis of thermograms.

Thus, this work discusses the most important variables for applying the technique and how the field conditions influence the results, contributing to the applicability of thermography to study facades, by improving the accuracy of the analysis and applying the definition criteria to identify the anomalies. The methodologies found in recent studies to identify and quantify pathological manifestations in building facades using infrared thermography are presented. Also, the results of laboratory and field experiments are used to establish appropriate criteria to identify detachment in facades.

2 Thermography in Detection of Defects in Facades

The infrared thermography enables quick inspections (in real time), without contact measurements, and from a distance. The infrared camera transforms the thermal energy emitted by the surface of an object in the infrared range of the electromagnetic spectrum into a visible image (Madruga et al. 2010). Thus, the thermogram allows identifying an entire temperature distribution in the various elements that make up the facade.

To identify the anomalies, the analysis and the result do not depend only on the characteristics, geometry, and depth of the defect. Objects in thermal or hygroscopic equilibrium cannot be investigated by thermography since the temperature difference is required (surface temperature) for thermographic identification (Barreira and de Freitas 2007). The intensity and direction of the heat flow through the wall, inwards or outwards, determine the moment when the anomaly is visible while appearing on the thermogram as the coldest or hottest zone (Fig. 1). The temperature difference that identifies the probable anomalies arise from the flow of heat that develops in the facade. The presence of defects such as voids, heterogeneities, and detachments locally modify the heat transport rate of the element or material, which can be detected in the surface temperature (Bauer et al. 2014). Thus, defects or anomalies can be identified by comparing the near or surrounding regions. Important pathological manifestations that must be mapped in the inspection can be detected, such as detachments, cracks, moisture, the presence of occluded materials, structural elements, components of the facade, and internal elements.

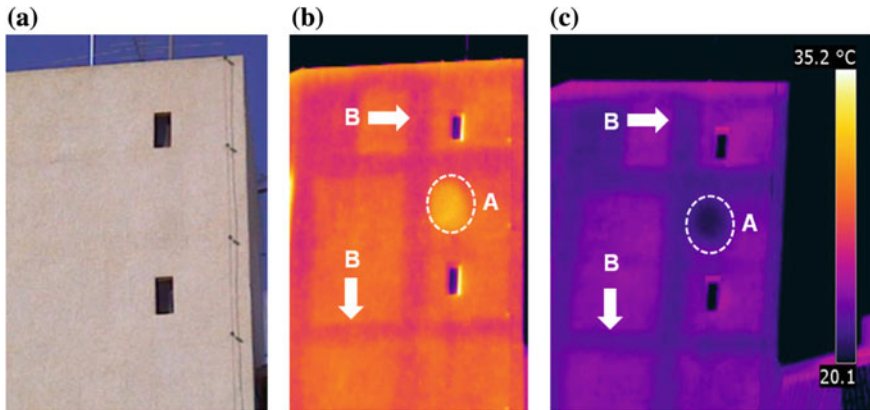


Fig. 1 Thermographic inspection detail: **a** facade image; **b** thermogram obtained during the heating up by the sun; **c** thermogram during cooling, without sunlight

In the case of detachment, the relatively small thickness of most of the coating materials (5–10 mm) and the presence of air between the coating layers as a result of loss of adhesion with the substrate (empty space) are two facts that enable the study of this phenomenon. The presence of air in the voids near surface layers creates a significant flow disturbance in the heat flow causing differences in the surface temperature, which compared to a normal, defect-free neighboring area allows identifying these anomalies in the thermogram (Fig. 1).

The moisture detection depends on the thermal properties of the material, especially the specific heat capacity. The higher the specific heat capacity, the more the energy is needed to heat or cool a particular material. Water has a specific heat capacity higher than that of common building materials such as wood or brick. Consequently, the water loses or gains heat slower than these materials in similar conditions, causing the specific heat capacity of the wet material to increase. This results in areas with high moisture content to appear warmer or cooler than the surrounding structure (Kominsky et al. 2007). The moisture in porous materials increases the thermal conductivity and decreases the thermal resistance, thus creating a kind of thermal bridge (Kylili et al. 2014). Another important point concerns the water evaporation from the surface. Evaporation rate is higher or lower depending on ambient temperature and relative humidity. It should be remembered that the evaporation mechanism involves loss of energy at the surface (specific enthalpy of evaporation) which causes a significant temperature reduction in the wet surface. The identification of the moistened area becomes very difficult when there is no evaporation. Furthermore, these complexities make it very difficult to measure the moisture content by thermography, since the temperature distribution captured by thermogram depends on a specific set of characteristics and properties related to the condition of the target object studied. These conditions vary depending on the degree of exposure of the studied object to the environment and throughout the day (temperature and relative humidity).

The identification of elements or components internal to the facade becomes possible as long as there are differences in the thermal resistance between these elements. The thermal resistance difference causes changes in the heat flow so that the thermogram identifies regions with different surface temperatures. Therefore, a proper analysis can identify internal elements that are colder or warmer than the neighboring regions, depending on the direction of heat flow (heating or cooling).

Figure 1 illustrates these observations. Figure 1a shows a digital image of the inspected facade with no observed anomalies. The thermogram of Fig. 1b shows the heating up of the surface temperature due to the incidence of sunlight, with the heat flow moving from outside to inside (direct flow). Region (A) shows a detachment with higher temperature than the surrounding region. It is also possible to identify the concrete structure (internal component), (B), where the temperature is lower than the surrounding region at that time. It should be noted that as the heat flow changes over time, the patterns observed in the thermogram also change. Figure 1c shows the same facade during cooling and the heat flow is inverse (from the facade to the environment). It is possible to identify the detachment region (A), which is cooler than the surrounding areas. The internal components of the structure (B) are identified by colder regions at this time.

It is observed that the visualization of the defect on the facade becomes either easier or more difficult depending on the physical phenomena and particular conditions. However, the identification and assessment of these phenomena is a complex task due to the number of variables related to the material and the element, the position of the element on the facade, and especially, the environmental conditions that are involved.

3 Thermography Inspection Variables and Conditions

The infrared thermography requires great care while obtaining the data and analyzing the results due to the number of variables involved in measurements. The failure in observing important points can lead to errors in the images, inaccuracies, and misdiagnosis. The thermographer should be aware of this set of variables to ensure the accuracy of the analysis and interpretation of results.

3.1 *Thermographic Inspection Variables*

There are two main groups of variables: those that depend on the equipment and those related to the target object. In the case of variables related to the equipment, the IFOV (Instantaneous Field Of View) and the resolution of the thermographic camera are the most important. These variables define the scope of the thermographic inspection in relation to the size of the defect to be studied and the clarity of

the image to facilitate its identification. The studies to identify defects in facades use cameras with IFOV between 0.6 and 2 and resolution of 240×180 px (Edis et al. 2014a, 2015), 320×240 (Lerma et al. 2011, 2013), 640×480 px (Fox et al. 2014, 2015), and 752×480 px (de Freitas et al. 2014).

Emissivity, distance, and reflection are the most important variables related to the target. The quantitative thermography requires the knowledge of the emissivity of all the materials of the facade surface for an accurate assessment. The use of tabulated data or data assumed to be identical between materials can lead to considerable errors (Bauer et al. 2015b). Regarding the distance, Barreira et al. (2015) reported no major differences up to 10 m, but concluded that the image clarity and precision are affected, thus directly influencing the display of the defects. Reflection is a major limitation in the field measurements (Edis et al. 2012). Construction materials with very smooth and bright finishes reflect the infrared radiation of other surrounding elements, leading to wrong temperature values in the thermograms, and misinterpretation of the results. For these reasons, the thermographer should be experienced and able to choose carefully the most appropriate position to acquire the image (thermogram) and avoid reflections. This issue is very common in assessments of building facades, especially when the measurements are conducted under strong sunlight.

3.2 Conditions for the Thermographic Inspection

In addition to the variables involved in the measurements, the facade hygrothermal conditions and behavior also help define when it is possible to perform the measurements successfully. It is necessary to examine the incidence of solar radiation, surface and environment temperatures, humidity, among other variables since the heat flow depends on and affects these variables. The heat flow surrounding the building is not static or constant throughout the day and depends largely on the air temperature, the heating up by the sun incidence and the cooling down of the facade (Bauer et al. 2014). In a thermographic inspection, how and when a particular defect is identified depends on the direction and magnitude of the heat flow. Often it is recommended that the thermographic inspections be conducted at the moment when the heat flow through the facade is high, thus maximizing the surface temperature differences (Cerdeira et al. 2011).

This analysis requires studying the solar trajectory to identify sun incidence and shade conditions, which define the thermal flow and, consequently, the best conditions to detect the anomalies.

The facades receive morning or afternoon sunlight depending on their cardinal orientation. The building facade heats up under the strong sunlight causing a direct heat flow moving from outside to inside. When the facade stops receiving the sunlight, the heating process stops, possibly starting an inverse heat flow, from the warm facade to the environment.

Therefore, these different flow behaviors used to identify the anomalies in different directions, make it necessary to study both direct, and inverse heat flow to define the testing criteria for each inspection. For these reasons, a previous analysis of the predicted flow regimes on the facade throughout the day and night should be performed previously. The use of hygrothermal simulation of the different facades of the building is a very useful tool to define these flow conditions.

4 Thermographic Analysis for Identifying Detachments

The most important analyses used to identify anomalies with infrared thermography are the visual difference in the thermogram (qualitative thermography) and the delta-T (quantitative thermography). Recent studies have linked delta-T to the time of day or heat flow parameters to identify and evaluate more precisely the defects. The defects are identified from the visual differences in the thermogram. The color differences (temperatures) in areas that in principle should be homogeneous are warning signs of possible defects in the material or element (Fig. 1). The visual differences in the thermograms allow identifying the cold and hot areas on the facades of buildings, thermal bridges that result from the structural elements (beams and pillars) or different materials (mortar, brick), and defects in insulation materials (Larsen and Hongn 2012).

Martinez et al. (2013) used the infrared thermography as a nondestructive testing technique and a complement to the visual inspection in areas of difficult access. These authors detected moisture by locating areas of lower temperature in the thermal image areas; these areas underwent local cooling effect due to water evaporation. Furthermore, they detected cracks by observing the high temperatures on both sides of the crack since heat transfer by conduction does not occur in this area because of discontinuity in the material.

Kominsky et al. (2007) also employed thermography as a supplement to visual inspection to identify moisture in ceramic brick and wood walls. The visual analysis of the thermogram was the criterion for selecting the areas where the invasive test using moisture meters was performed. They concluded that the qualitative infrared thermography coupled to visual inspection, along with the quantitative confirmation using moisture meters, is an effective procedure to detect anomalous humidity in the building envelope.

Bisegna et al. (2014) compared the visual information and thermographic images of a historic building in different years and could recognize the area that had been repaired due to differences in the masonry texture. Furthermore, between the various materials, areas with cracks and lack of homogeneity were also identified.

Most of the studies on quantitative analysis use the delta-T as a defect identifying parameter. The delta-T is given by the temperature difference between the defective area and the regular area, i.e., without any defect. This parameter has been

used as a preliminary tool to detect moisture in ceramic tile facades, being able to detect moisture for temperature gradient values less than $0.5\text{ }^{\circ}\text{C}$ (Edis et al. 2014b). In this case, the results of infrared thermography, the measurement of surface moisture, and numerical simulations showed that the higher moisture content of the ceramics in some areas generally coincided with the highest surface temperatures, when inspected after the sunset.

Laboratory studies conducted to detect detachments of plaster coats on facades yielded values of about $2.5\text{ }^{\circ}\text{C}$ (de Freitas et al. 2014). Also, field studies conducted in Porto, Portugal showed that the maximum delta-T values were obtained at 12 h 30 min.

Another laboratory study evaluated the delta-T values for concrete slabs with cubic voids and determined maximum values between 1.0 and $4.5\text{ }^{\circ}\text{C}$ depending on the defect depth and heating medium (Cheng et al. 2008). For a given defect size (10 cm) and same heat flow intensity, the defects closest to the surface had higher delta-T values. Voids were identified at a depth of 3 cm.

The analysis of these and other studies that used delta-T as a criterion to identify defects leads to the conclusion that this parameter may not be the only criterion used for this purpose since its value is strongly dependent on the relative conditions of the environment (thermal flow) and the characteristics of the elements. Therefore, the formulation of a defect identifying criterion requires the inclusion of other parameters that help to quantify some extent, the environmental conditions, as well as elements and component conditions.

More recent studies examine the defects from the perspective of the delta-T behavior throughout the day, that is, how it evolves during the day. Fox et al. (2015) analyzed the delta-T behavior at different moments to define the best moments to detect the defects. Qualitative analysis of images recorded at 20–30-min intervals showed that some sequential images were visually identical and did not help to identify the thermal changes or patterns. These authors reported that the temperature difference of the defects shown in consecutive images varied with the construction type, indicating that no single interval would suffice to cover the different situations. Therefore, it is necessary to introduce parameters that take into account the wall dimensions and heat flow. There are studies that analyze the temperature gradient between the facade interior and exterior and correlate it to heat flow to study humidity and detachments of ceramic tiles (Edis et al. 2014a, b, 2015).

The thermal events inside defective and regular (nondefective) areas change with time because heat dissipation is time dependent, among other variables associated to the defects and materials. It is necessary to choose the most appropriate thermogram (at a given moment) to identify and define the boundaries of the local defects. The selection criteria are generally based on the thermogram with the highest thermal contrast (TC). The contrast corresponds to the temperature difference between

the faulty areas over the temperature difference of a regular (nondefective) area. Maldague (2001) calls this contrast function “Thermal Contrast” (TC), which is calculated by Eq. 1. It is noteworthy that the contrast is the temperature variation in the defective area over the temperature evolution in the nondefective area.

$$TC = \frac{T_d(t) - T_d(t_0)}{T_{nd}(t) - T_{nd}(t_0)} \quad (1)$$

where

TC “*Thermal Contrast*,”

$T_d(t)$ Temperature of the defective area at time t ,

$T_d(t_0)$ Temperature of the defective area at time t_0 ,

$T_{nd}(t)$ Temperature of the regular, nondefective area at time t ,

$T_{nd}(t_0)$ Temperature of the regular, nondefective area at time t_0 ,

t_0 Initial time (beginning of cycle).

Nowak and Kucypera (2010) also used this contrast function to determine the presence of materials hidden inside walls in a laboratory study. These authors concluded that the TC is independent of the material tested, is dimensionless, and oscillates around a constant close to one in the steady-state value. It is possible to compare the results of various experiments, as it has been done by Bauer et al. (2015c).

Vavilov (2014) used the contrast function “Thermal Running Contrast” (TRC) to study the sensitivity and noise of the thermographic measurements. Basically, this contrast function is obtained from Eq. 2 and it is determined originally in the heating periods. The values are generated for each time and correspond to the evolution of the delta-T (temperature in the defective region minus the temperature in the nondefective region) in relation the evolution of the mean temperature in the studied region.

$$TRC = \frac{T_d(t) - T_{nd}(t)}{T_a(t) - T_a(t_0)}. \quad (2)$$

where

TRC “*Thermal Running Contrast*,”

$T_d(t)$ Temperature of the defective area at time t ,

$T_{nd}(t)$ Temperature of the nondefective area at time t ,

$T_a(t)$ Average surface temperature in time t ,

$T_a(t_0)$ Average surface temperature at initial time t_0 ,

t_0 Initial time (beginning of cycle).

5 Laboratory Study

5.1 Laboratory Experiment

For the experimental study, the specimen consisted of a mortar plate covered with ceramic tiles. The base plate was previously molded in cement and sand mortar, with a void created in the central area of the adhesive mortar to simulate the contact fault between the base plate and the ceramic tiles. Figure 2 shows how the ceramic tiles were applied on the base plate (Fig. 3).

The void (defective area) was approximately 40 mm wide, 155 mm long, and 2 mm thick totaling about 25 % of the total area of the tile. The ceramic tiles A and B are 4.0 and 7.5 mm thick, approximately. Figure 2 shows the specimen dimensions.



Fig. 2 Placement of the ceramic tiles with central defect

Fig. 3 Specimen developed for the laboratory test

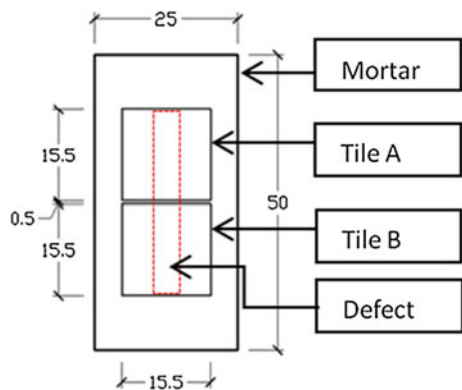
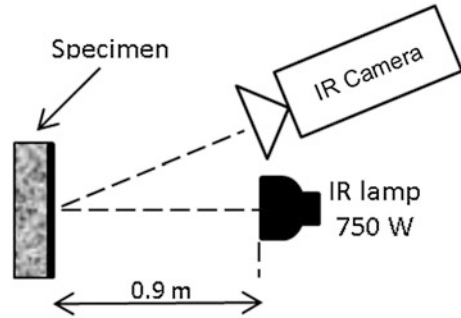


Fig. 4 Laboratory setup of the heating and cooling experiment



The specimen was subjected to a heating and cooling cycle in the laboratory, using a set of three infrared lamps of 250 W. The lamp set was positioned at a distance of 0.90 m. The heating period had a duration of 80 min, followed by the cooling down when the lamps were switched off. The cooling period had a duration of 85 min. The results presented are the average values obtained after three heating and cooling cycles (Fig. 4).

The parameters to be inserted into the infrared camera were measured for each cycle: ambient temperature, relative humidity, and the apparent temperature reflected by the corrugated aluminum method, following the procedure described in (ASTM E1862-97 2010). The emissivity was determined by comparison with the standard tape according to procedure (ASTM 1933-99 1999). The obtained average values were 0.95 and 0.93 for the mortar plate and ceramic tiles, respectively.

Thermograms were collected every 4 min with an infrared camera model FLIR T400, with a temperature range varying between -20 and 120 °C, 2 % accuracy, the spectral range from 7.5 to 13 μm , 320×240 pixels resolution, 25° lens, and 1.36 mrad IFOV.

Three behaviors were studied during the heating up and cooling down cycles, temperature (of the defective and nondefective areas), delta-T (between the defective and nondefective regions), TC, and TRC.

5.2 Results of the Laboratory Studies

Figure 5 shows the temperature evolution of the defective and nondefective areas for both tiles (A and B). It can be seen that the temperature evolution curves are similar in all four cases. Figure 5b shows the delta-T obtained in both phases. The delta-T originates from the thermal resistance difference between the defective area (empty space, air) and the surrounding area. Note that during heating, the temperature of the defective area is greater than that of the regular area from the beginning of the experiment, yielding positive delta-T values. At the start of the cooling process, the temperatures of the two areas decreased, and within 90 min, the values became the same. Subsequently, the temperature of the defective area

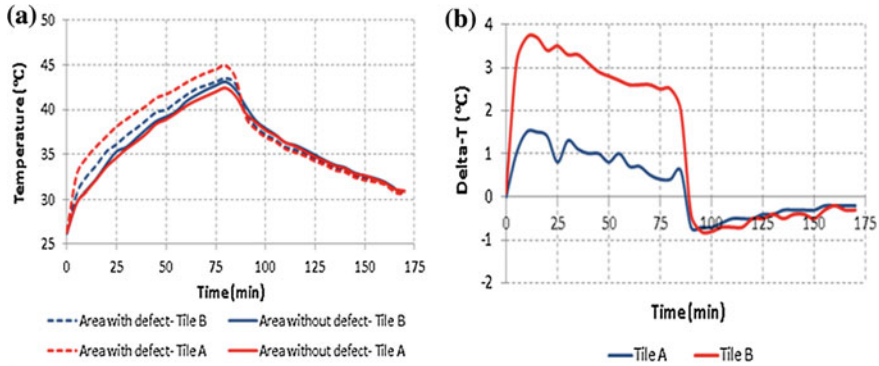


Fig. 5 Heating and cooling cycles. **a** Evolution of temperatures in the tiles' regions; **b** delta-T evolution

was lower than that of the nondefective area, with a negative delta-T, and an absolute value lower than that of the heating step.

It can be seen that the delta-T is higher for the thinner ceramic tile, B. This same behavior is seen in the cooling stage, although to a lesser degree. In this case, the delta-T (in absolute value) was also higher for the B ceramic tile. This behavior during the heating and cooling phases is similar to that reported in other laboratory studies (Freitas et al. 2014).

It was observed that the delta-T decreased over time during the heating and cooling phases (Fig. 5b). During heating, the temperature increase causes the thermal resistance of the air layer in the defect to decrease, thus decreasing the delta-T between the defective and nondefective areas, as well. During cooling, the delta-T was smaller, and in this phase, the heat flows due to dissipation of the heat in the plate, thus decreasing flow rate over time.

The thermograms of Fig. 6 show a clear difference between tiles A and B. Tile B allows better visualization of the defective area at all times, except for the thermal

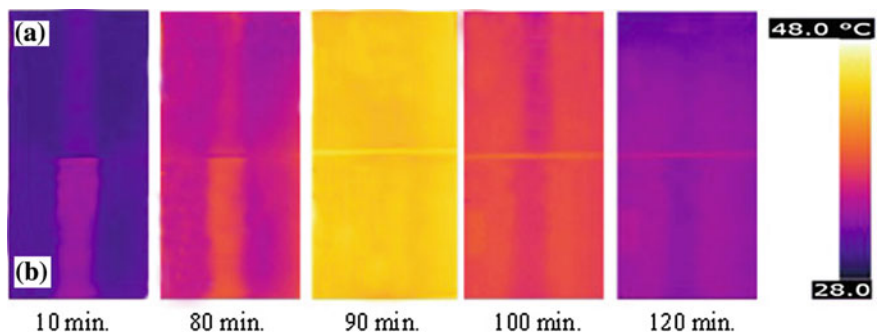


Fig. 6 Thermograms obtained at different times during the cycle

image at 90 min (for cooling), which shows identical temperatures in the defective and nondefective areas (Fig. 5a, b). It is interesting to note that the delta-T criterion identifies less clearly the defect in the cooling phase. Accordingly, the thermogram that shows the highest cooling delta-T at 100 min has similar visualization of the defects. On the other hand, the visualization of defects is already differentiated in the 120-min thermogram. This result shows that applying the delta-T criterion alone to identify the defects is inconclusive.

The analyses of TRC (thermal running contrast) and TC (thermal contrast) are shown in Fig. 7. The cycles were separated in the heating (7a) and cooling (7b) stages, and analyzed independently.

The TRC evaluates the delta-T response as a function of the average temperature variation of the tile. Thus, in the heating stage, the TRC increases as the delta-T increases quickly at the start of heating (proportionally to the increase of the average temperature of the tile). In practical terms, this means an increase of defect visibility condition. Figure 7 shows that this happens at the beginning, about 5–10 min into the cycle, for both tiles. This is how long the delta-T required to reach its maximum value, as shown in Fig. 5b. As delta-T becomes stable and decreases after this time (Fig. 5b), TRC reduces gradually until the end of the heating phase. The difference between the TRC of the tiles is directly correlated to the delta-T difference as shown in Fig. 5b. To this end, Fig. 6 shows that the defect is much sharper in ceramic B at 80 min (final heating), coinciding with the data at the end of heating (Fig. 7a).

In the cooling stage (Fig. 7b), the direction of delta-T is inverse (decreases). Assuming $t(0)$ as the time when the temperatures become the same during cooling, a strong contrast enhancement is also observed due to the decreasing delta-T.

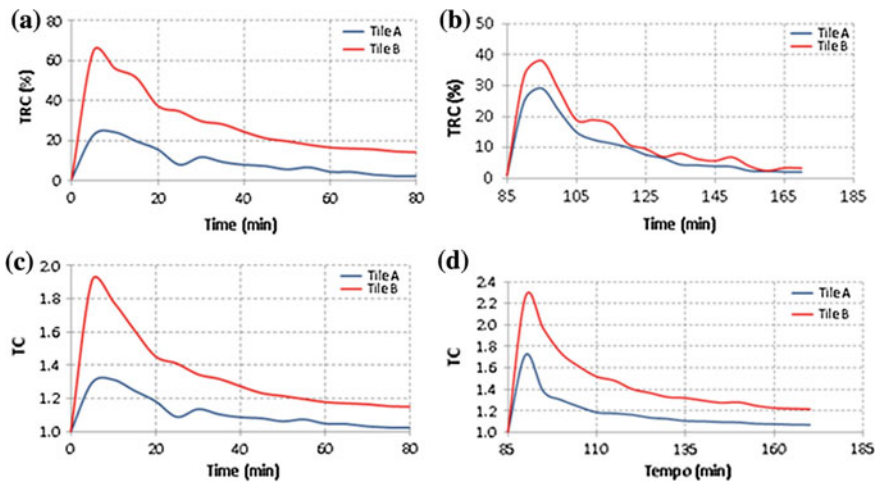


Fig. 7 Running thermal contrast (TRC) at **a** heating and **b** cooling. Thermal contrast (TC) at **c** heating and **d** cooling

Figure 5b shows that ΔT drops steeply in the first 5–10 min of the cooling stage, thus increasing the TRC value. The heat flow in the system (the cycle change from heating to cooling) seems to allow identifying more clearly the variation of ΔT . At this time (5–10 min), the TRC values peak in both tiles (A and B) due to the decreasing temperature of the specimen with cooling. However, TRC peak values were significant for both tiles. It is also observed that tiles A and B displayed very similar trends in the rest of the cooling cycle, with a gradual reduction of ΔT and TRC, which was always higher for ceramic B (thinner).

The TC evaluates other aspects. The initial temperatures in the defective and nondefective areas are analyzed. It is observed in the first reading that the contrast is higher than 1 for both heating and cooling stages (Fig. 7c, d), which also seems to associate with the ΔT . The TC peaks and the highest absolute ΔT value occurred at the same time. As the ΔT dropped in the heating phase, TC also tended to drop. Similar behavior was observed in the cooling since ΔT drops by cooling. The fact that TC approaches 1 at the end of the cycles shows that it becomes more difficult to visualize the defect, since the temperature difference between the defective and the regular areas becomes smaller.

The defects are best visualized at TC and TRC peak, i.e., at the start of heating and cooling. The type of defect in the specimen greatly affects the observed behavior. The defect manufactured into the specimen was a relatively large discontinuity (25 % of the area of the sample), constituting an empty air space capable of inducing some peculiar behavior, which is also observed in facade inspections. The decrease of ΔT during the warming up is one difficult aspect in the identification and interpretation of defects by thermographic analysis. Both TRC and TC contrast functions showed that the best time to identify defects is at the beginning of heat flows (either heating or cooling). It is noteworthy that the contrast functions peak at times when the surface temperature increases or decreases rapidly (areas with and without defect), which indicates that the facade defects are best visualized at moments when surface temperatures increase or decrease more intensely.

It was also observed that the geometrical aspects, such as the thickness of the ceramic tiles, affect heat flow, which obviously influence the heating and cooling patterns, requiring attention when executing thermographic inspections of facades.

6 Field Study

The field study was conducted in a building in Brasília, Brazil (Fig. 8). The studied facade was east-oriented with visible detachments. However, the studied area had no visible detachments since the objective was to evaluate the suitability of thermography in defect identification. The facade received direct sunlight during the morning, with no building or element nearby that could cause reflection problems in the thermal imaging. The same infrared camera was used in the lab and field study. The thermal imaging was performed hourly, from 8:30 to 18:30, to analyze ΔT

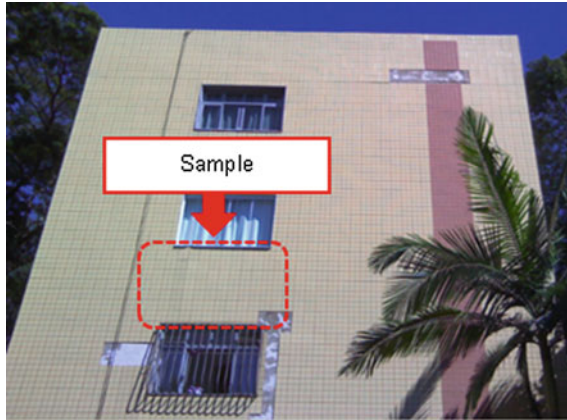


Fig. 8 Digital image of the facade showing the study area

behavior and the contrast functions under the effect of direct solar radiation and after sunset. The camera parameters related to the temperature and relative humidity were set before each image. The reflected apparent temperature was determined by the aluminum corrugated blade method, according to the standard procedure (ASTM E1862-97 2010).

Figure 8 shows the digital image of the studied facade. The red-dotted line shows the study area (sample). It is noteworthy that in this area, it is not possible to visualize detachment by visual inspection only.

Figure 9a shows the temperatures of the areas with and without defects. Figure 9b shows the delta-T values for each analyzed time.

The highest delta-T values are observed in the early morning (8:30) when the temperature rises intensely under sun exposure (Fig. 9b). From that moment on, the delta-T decreases until noon. Similar behavior was observed in the laboratory study when the rising of the temperatures slowed down in the defective and nondefective areas. Then, the delta-T decreased significantly. This fact indicates that it is necessary to conduct a preliminary study to determine the building temperature profile, which is orientation dependent, to indicate the likely time of maximum delta-T.

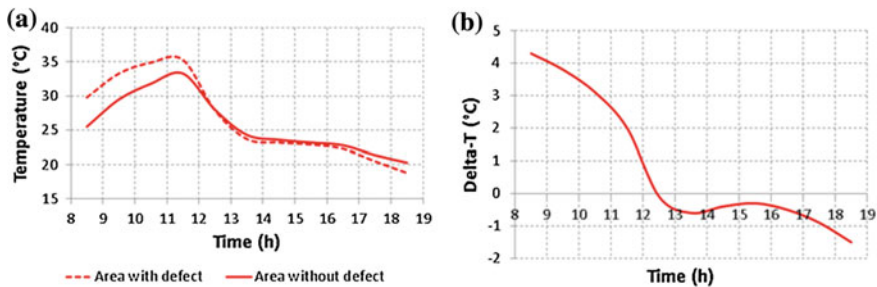


Fig. 9 Temperature analysis of the facade. **a** Evolution of temperatures in defective and nondefective areas; **b** delta-T evolution

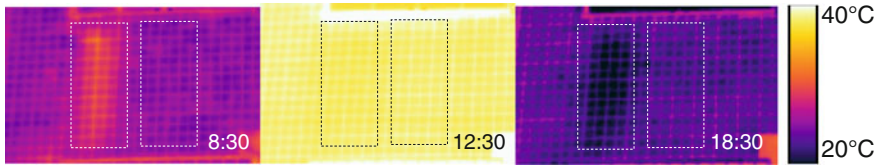


Fig. 10 Thermograms of the facade study area obtained at different moments

Figure 10 shows that the defects were better visualized in the early morning (8:30) and late afternoon (18:30). The maximum delta-T value in the cooling step did not appear instantly after reversal heat flow (Fig. 9b). In this case, the maximum value appears in the late afternoon, when the differences in temperature between the outside and the inside of the facade are greater. The different behaviors observed between the laboratory specimen and the facade are due to the wall dimensions compared to the specimen (tile), and the fact that the facade is exposed to a changing external ambient temperature. The flow reversing process takes longer because the thermal inertia of the thicker wall is greater and the defect takes longer to appear. The decreasing external temperature causes the heat flow to move from inside to the outside of the building at higher rate in the late afternoon, causing the delta-T value to keep rising.

The main source of heat on the facade is the sun, which stops shining on the facade at 12:10. Therefore, the defect no longer appears in the thermal image at 12:30 as shown in Fig. 10.

7 Conclusions

The results and the above considerations allow the following conclusions:

- The use of passive thermography to define and identify a defective area in a building subjected to different solar incidences is complex and requires an approach associated with the heat flow, especially regarding its direction (direct or inverse);
- Delta-T alone is not a consistent criterion to identify the anomalies since it depends on the characteristics of the defects (geometry, wall thickness) while the heat flow is directly dependent on the sunlight;
- To study the evolution of the temperature along the day is inappropriate as inspection technique, due to the complexity of the analysis. The results suggest that the thermograms should be obtained at times when the TC is maximum. This period coincides with the beginning of the heat flow, direct (heating) or inverse (cooling).
- The heat flow should be studied previously (before inspection) by analyzing the solar charts or by thermohygro-metric simulation. The obtained information is a

valuable tool to detect the moment of maximum contrast. Thus, it becomes possible to establish a reference inspection methodology based on thermographic inspection at times when the visualization of the defects is maximized.

References

- ASTM E1862-97 (2010) Standard test methods for measuring and compensating for reflected temperature using infrared imaging radiometers
- ASTM 1933-99 (1999) Standard test methods for measuring and compensating for emissivity using infrared
- Barreira E, de Freitas VP (2007) Evaluation of building materials using infrared thermography. *Constr Build Mater* 21(1):218–224
- Barreira E, Almeida RMSF, Freitas de VP, Soares T (2015) Sensitivity analysis of quantitative infrared thermography. In: 1st international symposium on building pathology, Porto, Portugal, 6
- Bauer E, Pavón E (2015) Termografia de infravermelho na identificação e avaliação de manifestações patológicas em edifícios. *Concreto & Construções*, (Jul-Set): 93–98
- Bauer E, Castro EK, Hildenberg A, Pavon E (2014) Critérios para a aplicação da termografia de infravermelho passiva como técnica auxiliar ao diagnóstico de patologias em fachadas de edifícios. *Rev Politec (Instituto Politec Bahia)* 26:266–277
- Bauer E, de Freitas VP, Mustelie N, Barreira E, de Freitas SS (2015a) Infrared thermography—evaluation of the results reproducibility. *Struct Surv* 31(3):181–193
- Bauer E, Pavon E, Hildenberg A, Castro EK (2015b) Erros na utilização de parâmetros termográficos da argamassa e da cerâmica na detecção de anomalias em revestimentos. XI Simpósio Brasileiro de tecnologia das Argamassas. SBTA, Porto Alegre, 12
- Bauer E, Castro EK, Pavon E, Oliveira AHS (2015c) Criteria for application and identification of anomalies on the facades of buildings with the use of passive infrared thermography. In: Freitas VP (ed) 1st international symposium building pathology, Porto, Portugal, p. 12
- Bisegna F, Ambrosini D, Paoletti D, Sfarra S, Gugliermetti F (2014) A qualitative method for combining thermal imprints to emerging weak points of ancient wall structures by passive infrared thermography—a case study. *J Cult Herit* 15(2):199–202
- Broberg P (2013) Surface crack detection in welds using thermography. *NDT E Int* 57:69–73
- Cardeira F, Vázquez ME, Collazo J, Granada E (2011) Applicability of infrared thermography to the study of the behaviour of stone panels as building envelopes. *Energy Build* 43(8):1845–1851
- Cheng C-C, Cheng T-M, Chiang C-H (2008) Defect detection of concrete structures using both infrared thermography and elastic waves. *Autom Constr* 18:87–92
- de Freitas SS, de Freitas VP, Barreira E (2014) Detection of façade plaster detachments using infrared thermography—a nondestructive technique. *Constr Build Mater* 70:80–87
- Dufour MB, Derome D, Zmeureanu R (2009) Analysis of thermograms for the estimation of dimensions of cracks in building envelope. *Infrared Phys Technol* 52(2–3):70–78
- Edis E, Flores-Colen I, de Brito J (2012) Passive thermographic inspection of adhered ceramic claddings: limitations and conditioning factors. *J Perform Constr Facil*: 258
- Edis E, Flores-Colen I, De Brito J (2014a) Building thermography: detection of delamination of adhered ceramic claddings using the passive approach. *J Nondestruct Eval*, 34
- Edis E, Flores-Colen I, de Brito J (2014b) Passive thermographic detection of moisture problems in façades with adhered ceramic cladding. *Constr Build Mater* 51:187–197
- Edis E, Flores-Colen I, de Brito J (2015) Quasi-quantitative infrared thermographic detection of moisture variation in facades with adhered ceramic cladding using principal component analysis. *Build Environ* 94:97–108

- Fox M, Coley D, Goodhew S, de Wilde P (2014) Thermography methodologies for detecting energy related building defects. *Renew Sustain Energy Rev* 40:296–310
- Fox M, Coley D, Goodhew S, De Wilde P (2015) Time-lapse thermography for building defect detection. *Energy Build* 92:95–106
- Freitas JG De, Carasek H, Cascudo O (2014) Utilização de termografia infravermelha para avaliação de fissuras em fachadas com revestimento de argamassa e pintura. *Ambient Construido* 14(1):57–73
- Kominsky JR, Luckino JS, Street NH, Martin TF (2007) Passive infrared thermography—a qualitative method for detecting moisture anomalies in building envelopes. *Tedford Pond*: 1–11
- Kylili A, Fokaides PA, Christou P, Kalogirou SA (2014) Infrared thermography (irt) applications for building diagnostics: a review. *Appl Energy* 134:531–549
- Lai WL, Kou SC, Poon CS, Tsang WF, Lai CC (2010) Characterization of the deterioration of externally bonded cfrp-concrete composites using quantitative infrared thermography. *Cem Concr Compos* 32(9):740–746
- Lai WL, Lee KK, Kou SC, Poon CS, Tsang WF (2012) A study of full-field debond behaviour and durability of cfrp-concrete composite beams by pulsed infrared thermography (irt). *NDT E Int* 52:112–121
- Larsen SF, Hongn M (2012) Termografía infrarroja en la edificación: aplicaciones cualitativas. *Av en Energías Renov y Medio Ambient* 16:25–32
- Jerma JL, Cabrelles M, Portalés C (2011) Multitemporal thermal analysis to detect moisture on a building façade. *Constr Build Mater* 25(5):2190–2197
- Jerma C, Mas Á, Gil E, Vercher J, Peñalver MJ (2013) Pathology of building materials in historic buildings. Relationship between laboratory testing and infrared thermography. *Mater Construcción* 60
- Madruca FJ, Ibarra-Castanedo C, Conde OM, López-Higuera JM, Maldague X (2010) Infrared thermography processing based on higher-order statistics. *NDT E Int* 43(8):661–666
- Maldague X (2001) *Theory and practice of infrared technology for nondestructive testing*. Wiley, NY
- Martínez E, Castillo A, Martínez I, Castellote M (2013) Metodología para la intervención en elementos históricos: el caso de la espadaña del convento de nuestra señora de la consolación (alcalá de henares-madrid-españa). *Inf la Construcción* 65(531):359–366
- Menezes A, Glória Gomes M, Flores-Colen I (2015) In-situ assessment of physical performance and degradation analysis of rendering walls. *Constr Build Mater* 75:283–292
- Nowak H, Kucypera M (2010) Application of active thermography for detecting material defects in the building envelope. *InfraMation Proc Proc*, pp 1–12
- Pascu A (2011) Non-destructive inspection of composite structures using active ir-thermography methods. *Bul științific Ser D Mech Eng* 73(1):1–14
- Taylor T, Counsell J, Gill S (2014) Combining thermography and computer simulation to identify and assess insulation defects in the construction of building façades. *Energy Build* 76:130–142
- Vavilov V (2014) Noise-limited thermal/infrared nondestructive testing. *NDT&EInt* 61:16–23

Diagnosis of Moisture Movements in Massive Dolostone Walls of Medieval Churches

Lembit Kurik, Targo Kalamees and Urve Kallavus

Abstract The current study presents one of the dielectric methods, reflection of the microwaves from material, used for diagnosis of moisture content of massive dolostone walls in Estonian medieval churches. Cold and humid climate, porous materials, absence of rainwater pipes, absence of waterproof layers avoiding rising damp leads to moisture damages in massive walls. The problem is relatively complex and cannot be modeled easily due to inhomogeneity and complex shapes of walls. Therefore, main tool for diagnostics is determination of the distribution of moisture in walls and its change over the time by moisture content measurements. The microwave method for determination of moisture content in massive walls is nondestructive and therefore very suitable for the diagnostics of moisture problems in buildings of national heritage importance. Graphically presented results are easily readable even for a nonspecialist and expedite significantly analysis of problem. Measurements of moisture content of walls in medieval churches with different measuring heads during different seasons were carried out over a 10 year period. Seasonal and long period changes of moisture content were analyzed.

Keywords Microwaves · Dolostone · Moisture content mapping · Long period moisture movements · Medieval churches

L. Kurik (✉)

Department of Physics, Tallinn University of Technology, Ehitajate tee 5,
19086 Tallinn, Estonia
e-mail: lembit.kurik@ttu.ee

T. Kalamees

Chair of Building Physics and Energy Efficiency, Tallinn University of Technology,
Ehitajate tee 5, 19086 Tallinn, Estonia
e-mail: targo.kalamees@ttu.ee

U. Kallavus

Centre for Material Research, Tallinn University of Technology, Ehitajate tee 5,
19086 Tallinn, Estonia
e-mail: urve.kallavus@ttu.ee

1 Introduction

Moisture damages in unheated medieval churches in the island of Saaremaa (Estonia) have been a problem for centuries. Various biological, chemical and mechanical processes related excessive water (see Fig. 1) in and on the walls have destroyed most of wall paintings, caused much damage to plaster (see Fig. 2). Frequently applied various face-lift and repair works lack desired results since the causal factors were not eliminated.

Figure 3 illustrates the sources of excessive water, movements of moisture in the walls and between the walls and surrounding environment.

Even though the walls may be protected from water poured from roof or driving rain, moisture content remaining in walls may still cause damages. Therefore, together with moisture mapping appearance of different damages on interior surfaces were surveyed. As an example, the degradation process caused by salt



Condensed water on the top of algal growth
(Kaarma Church)



Salt precipitation and algal growth
(Püha Church)



Ice formation on walls (Pöide Church)



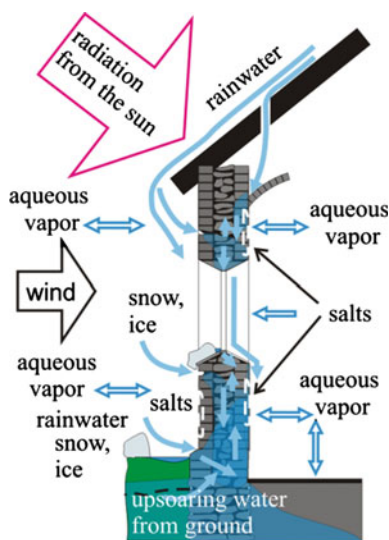
Pink bacteria and algae on
window sill (Muhu Church)

Fig. 1 Events of damages



Fig. 2 Partially damaged wall paintings in Muhu (*left*) and Valjala (*right*) churches

Fig. 3 Moisture movements in walls of medieval churches



(KNO_3) efflorescence in the test-field occurred over the 10 years in Kaarma church, is presented in Fig. 4.

In 2005, a long period measurements of moisture content of the walls in Kihelkonna and Kaarma Churches (island Saaremaa) were started.

Microwave aquametry was chosen from a large set of measurement methods (Derome et al. 2001) because it is harmless to object, allows measuring of moisture content deep inside of the walls, and has low sensitivity toward dissolved salts. The measuring process is relatively quick thereby making mapping of moisture content in large wall surfaces easy. The above-mentioned method was first introduced shortly after the World War II and has been developing constantly (Okamura 2000).

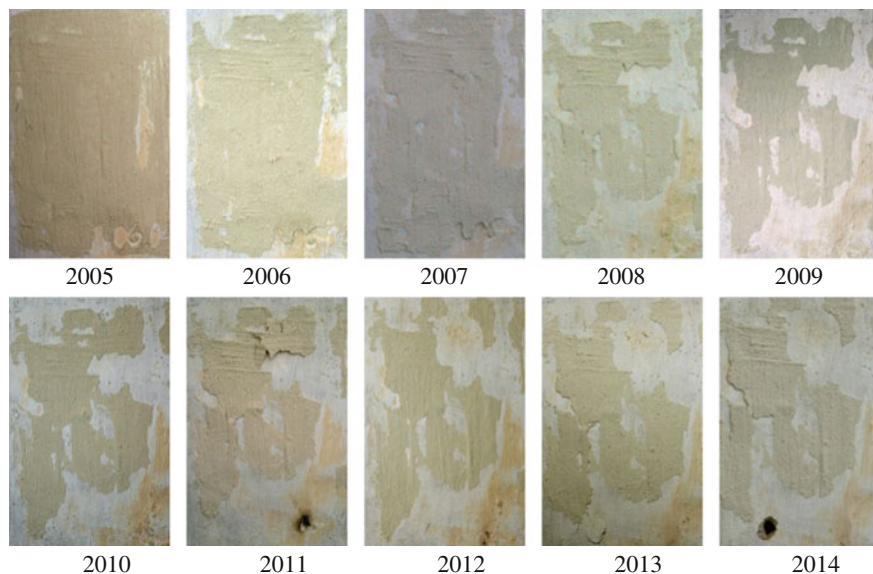


Fig. 4 Test field for the determination of behavior of lime paint in the presence of the salt efflorescence (Kaarma Church)

Unfortunately, this method allows measuring only liquid water what is free. Other methods should be additionally used to examine the bound water layers present in porous wall materials and also crystal water in salts. Perspective for this task options are Nuclear Magnetic Resonance (NMR) and dielectric spectroscopy methods (Senni et al. 2009; Capitani et al. 2009; Di Tullio et al. 2010), what are not easily put into field measurement practice.

Sometimes absolute values of moisture content are required. Carrying out such measurements is not an easy task since analyzed objects are far from being homogenous (different materials, cavities, metal pieces and wires present in walls), wall surface is usually uneven, calibrating is relatively complex and gravimetric control measurements are prohibited due to heritage protection requirements.

In many cases obtaining so-called “moisture maps” of the surface is enough informative for understanding nature of moisture displacement and sources. Furthermore, observing changes in time-lapse moisture maps taken from the same site yields in valuable information about the behavior of old stone wall. In several papers moisture maps of churches walls have been presented, but for the single moments only (Capitani et al. 2009; Larsen 2004; Curteis 2004). Present study analyzes results of long-term moisture content measurements carried out in several quite similar churches. These results allow making some general assumptions.

2 Method

2.1 Method for Moisture Measurement and Presentation of Results

2.1.1 Theory

It is a well-known fact that the dielectric permittivity of water is much higher than the permittivity of most building materials (correspondingly 80 and 4–8). The simplest model for wet material is a case, where water fills spherical pores in the main material. For this kind a simplified two-phase system effective dielectric permittivity of wet material ϵ_{eff} is possible to calculate according to Maxwell Garnett formula (Garnett 1904; Sihvola 2005):

$$\epsilon_{\text{eff}} = \epsilon_m + 3f\epsilon_m \frac{\epsilon_w - \epsilon_m}{\epsilon_w + 2\epsilon_m - f(\epsilon_w - \epsilon_m)},$$

where f —volumetric water content, ϵ_w —water dielectric permittivity, ϵ_m —dry material dielectric permittivity. For known materials according to this relationship is sufficient to measure ϵ_{eff} to determine water content in the material.

Microwave moisture measurement method utilizes hereinbefore described relation and fact that microwave reflection coefficient depends directly on dielectric permittivity of the material, Fig. 5. It means that amplitude value of reflected microwave signal contains information about water content of material.

This method is applicable only at temperatures above 0 °C and it is not possible to measure crystal water in salts, also the ~2...3 molecules thick water layers adsorbed in the pores of the building materials. Temperature and size of pores affects the results in some extent (Kaatze 2005).

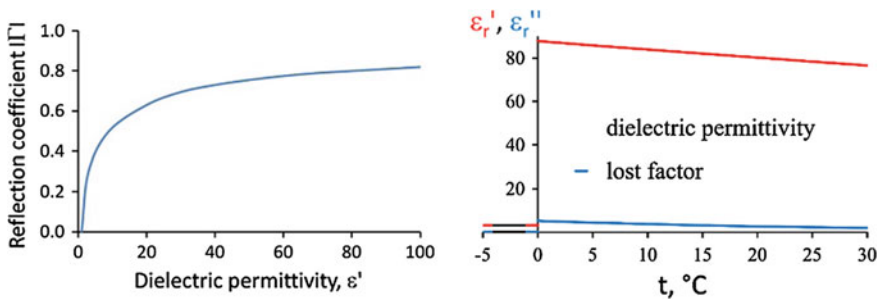


Fig. 5 Relationship between the dielectric permittivity of material ϵ and microwaves reflection coefficient Γ (left) (Agilent 2005) and temperature dependence of dielectric permittivity of water and ice at 2.45 GHz (right, calculated on the basis of Kaatze 2005)

2.1.2 Instruments

In this study, we used a handheld moisture meter “Moist 200” with surface and volume type measuring heads: Moist R (measuring depth up to 3 cm, measuring volume 20 cm³), Moist R2 M (7 cm, 150 cm³), Moist DM (11 cm, 2 l), Moist P (30 cm, 10...15 l) and Moist D (80 cm, 40...50 l). Figure 6 shows maximum penetration depths for microwaves and measuring volumes for the different sensor heads (according to producer datasheets). More detailed information about this method and measuring hardware is presented in Göller et al. (1999) and Göller (2001).

2.1.3 Presentations of the Measurements

For getting easily readable and usable data to help building moisture conditions diagnostics, mainly raster measurements with steps 1 × 1 m on external wall were used. First, moisture index was measured and then, moisture content was calculated (according of the calibration curve). Measurement results are presented as a map of the moisture distribution, Fig. 7. Colors on the map indicate gravimetric moisture content *W* values with steps of 2 % (on dry material bases). Numbers on the left

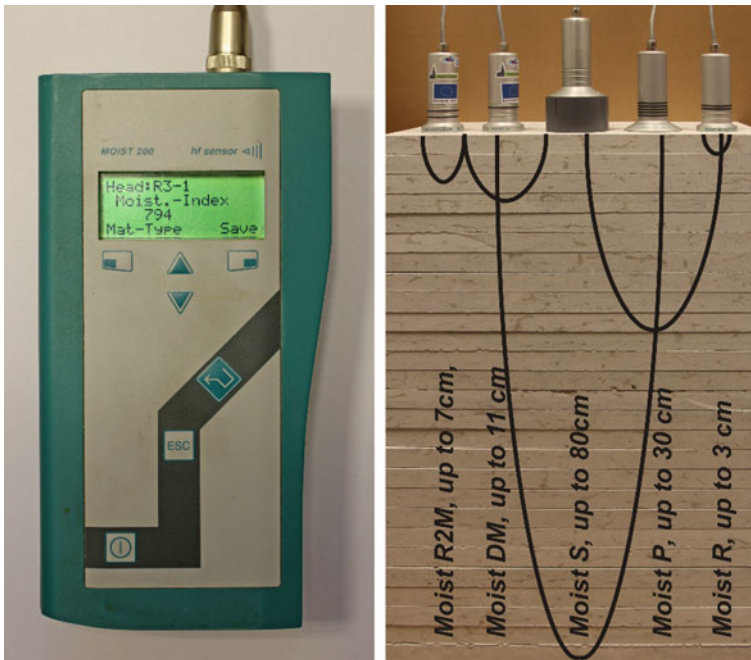


Fig. 6 Handheld moisture meter Moist 200 (*left*) with measuring heads and their penetration depths (*right*)

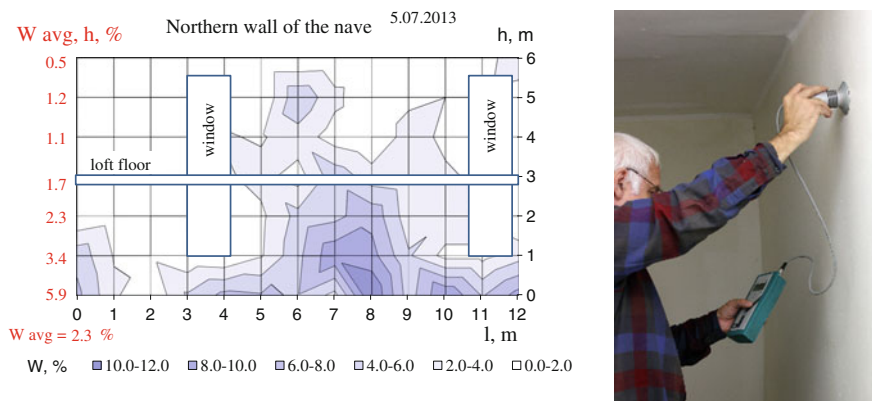


Fig. 7 Typical result of the moisture mapping. Measuring steps— 1×1 m. W—moisture content, % (left). Measurement in practice (right)

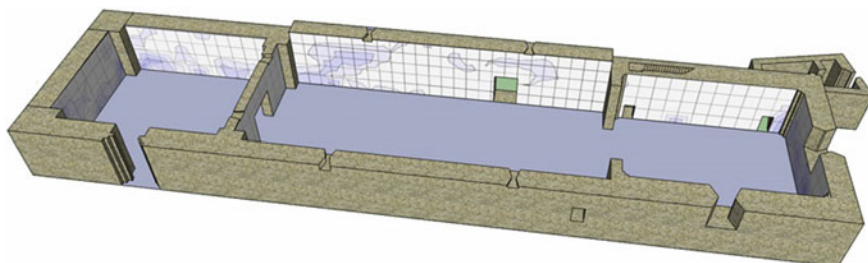


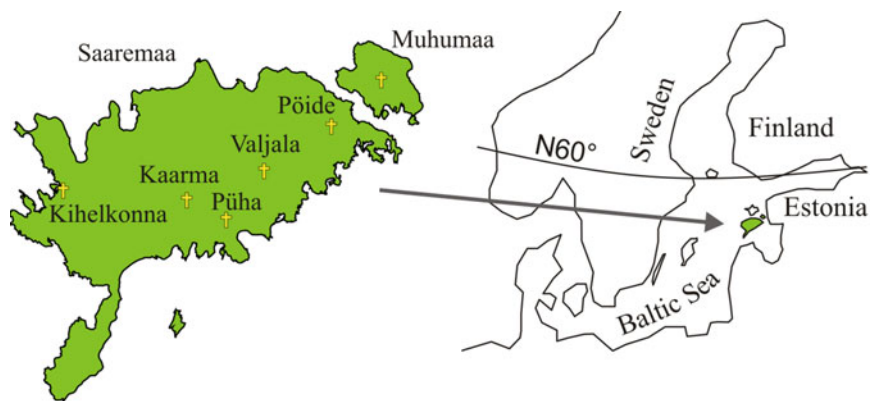
Fig. 8 Moisture content maps of the Põide Church presented on the cross-cut of the 3D model of the church (model created with Google SketchUp)

side of chart are average moisture content values at different levels from the floor and average moisture content for the entire wall.

Mainly for all figures in this paper the same color steps and measurement raster 1×1 m are used. Very informative is presenting moisture content measurement results on a 3D model. In that case, all measurements of the building are in the single easily rotated and zoomed package, Fig. 8.

2.2 Buildings Under the Survey—Medieval Churches in Estonian Islands

Microwave moisture measurement method was used in islands of Saaremaa and Muhumaa in medieval churches that are built mainly in thirteenth and fourteenth centuries (see Fig. 9). They all have complicated history—survived from



Kihelkonna
St. Michael's Church, ~1250



Kaarma Church of Saints Peter and Paul, ~1270



Põide St. Mary Church, ~1270



Püha St. James Church, ~1350



Muhu St. Catherine's Church, 1267



Valjala St. Martin Church, ~1227

Fig. 9 Medieval churches under the investigation

Reformation, several wars, rich, and poor periods. Nowadays they have been obtained great historical value. Valjala Church is probably the oldest preserved church in Estonia.

Main building material of all of these medieval churches is porous Kaarma dolostone and local dolostones, quarried from the local stone-pits nearby of the each church Fig. 10.

Estonian dolostone porosity varies from 8.3 to 25 % (Trikkel et al. 2012). Information about widely used Kaarma dolostone is presented in Table 1. For comparison information for Lasnamäe limestone is added—traditional building material for historic buildings in Northern Estonia. A big difference in water absorption properties of these stones explains much bigger moisture damages of the buildings in dolostone region.

In order to get a better idea about moisture behavior in walls of unheated churches, parameters of indoor climate of the building must be known. For the typical church under investigation—changes of indoor climate of a typical church Muhu are displayed on Fig. 11.

One can clearly see that parameters of indoor climate of this church are ominous for the building itself and people inside it. Relative humidity is very high and



Fig. 10 Main building material in churches of Saaremaa, well workable Kaarma dolostone and local building stones

Table 1 Moisture linked properties of traditional building materials for western and northern Estonia

Material	Density (kg/m ³)	Porosity (%)	Water absorbency (%)	CaO (%)	MgO (%)
Kaarma dolostone	2220 ^a 2080–2290 ^c 1960–2240 ^b	21.9 ^a	8.9 ^a 8.9 ^c Up to 10.4 ^b	26–31 ^c	14–20 ^c
Lasnamäe limestone	2650 ^a 2590–2760 ^c	2.6 ^a	0.9 ^a 1.0–1.9 ^c	45–46 ^c	4–7 ^c

^a<http://www.lossikivi.ee/index.php?a=lasnamae&lang=eng>, last accessed 28.10.2015

^bBased on measurements of samples of Kaarma dolostone

^cPerens, H. 2003, *Paekivi Eesti ehituses I. Üldiseloostus. Lääne Eesti*, Eesti Geoloogiakeskus

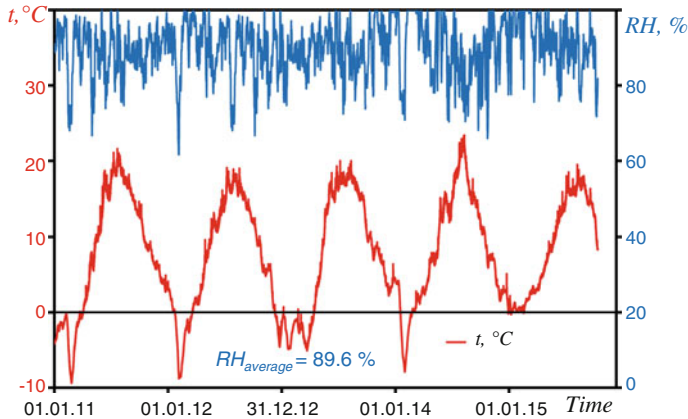


Fig. 11 Indoor climate in 5 year period of Muhu St. Catherine’s Church, typical for all unheated dolostone churches in Saaremaa—very high relative humidity, long time negative temperatures at winter period (excl. year 2015)

reaches 100 % quite often. This means that the important source of moisture in walls is condensed water.

3 Results of Measurement

High porosity of dolostone, rough building stones and large gaps between them may cause risk for high moisture content in walls: over 10 % humidity by mass or over 20 % humidity by volume. Usually this risk also realizes resulting extensive moisture damages. In order to work out solutions for renovation, one needs to know the origin and movement of water. In the following we describe how we can determine this by using microwave aquametry.

3.1 Detecting Moisture Sources

Movement of moisture from the basement upward was detected in almost all measured walls. Origin of this water is mainly rainwater from the roof and rising damp from foundation, Fig. 3. At the bottom of the wall moisture content is very high—building material is nearly saturated with water. If only rising damp is present, then in higher levels (from 2 or 3 m and up) moisture content is low, Fig. 12.

In complicated cases, there are several water sources, see Fig. 13.

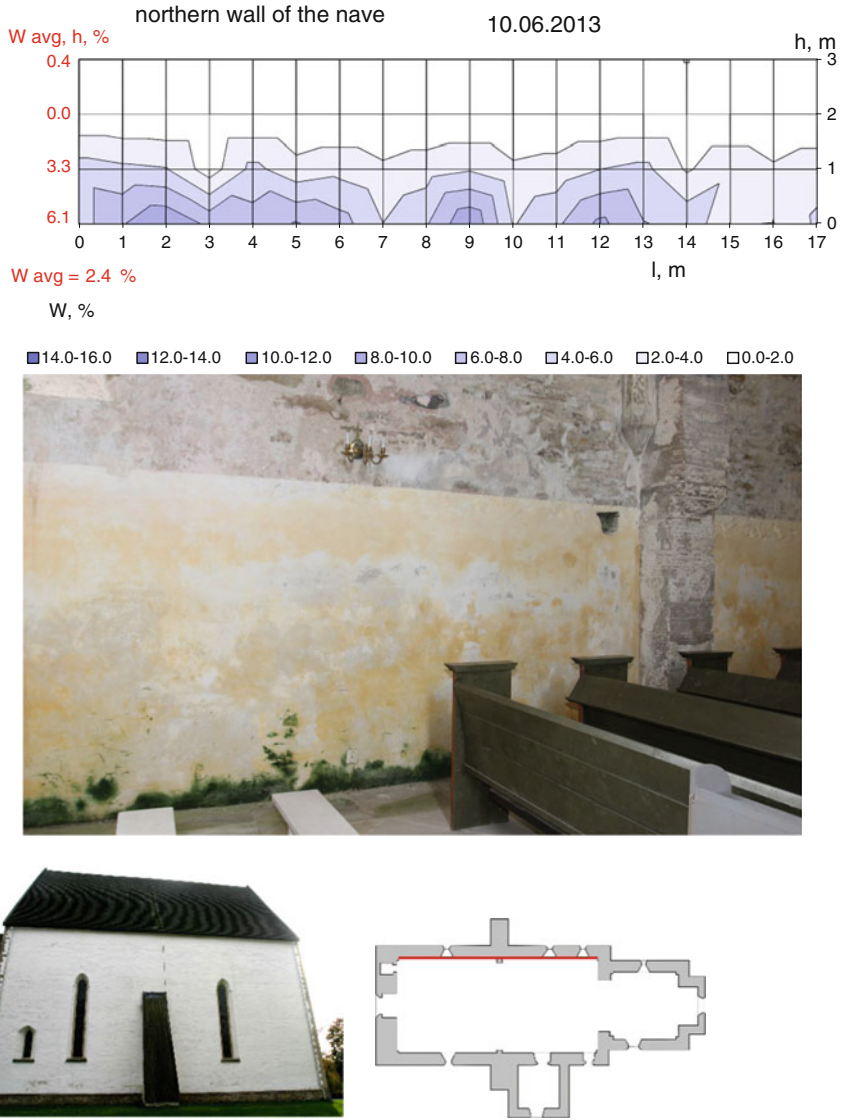


Fig. 12 Typical picture of rising damp, Muhu Church, measuring depth up to 30 cm (*up*). Picture of the part of the wall what moisture content was measured (*middle*). Outside of the same wall and measured wall location on the church plan (*down*)

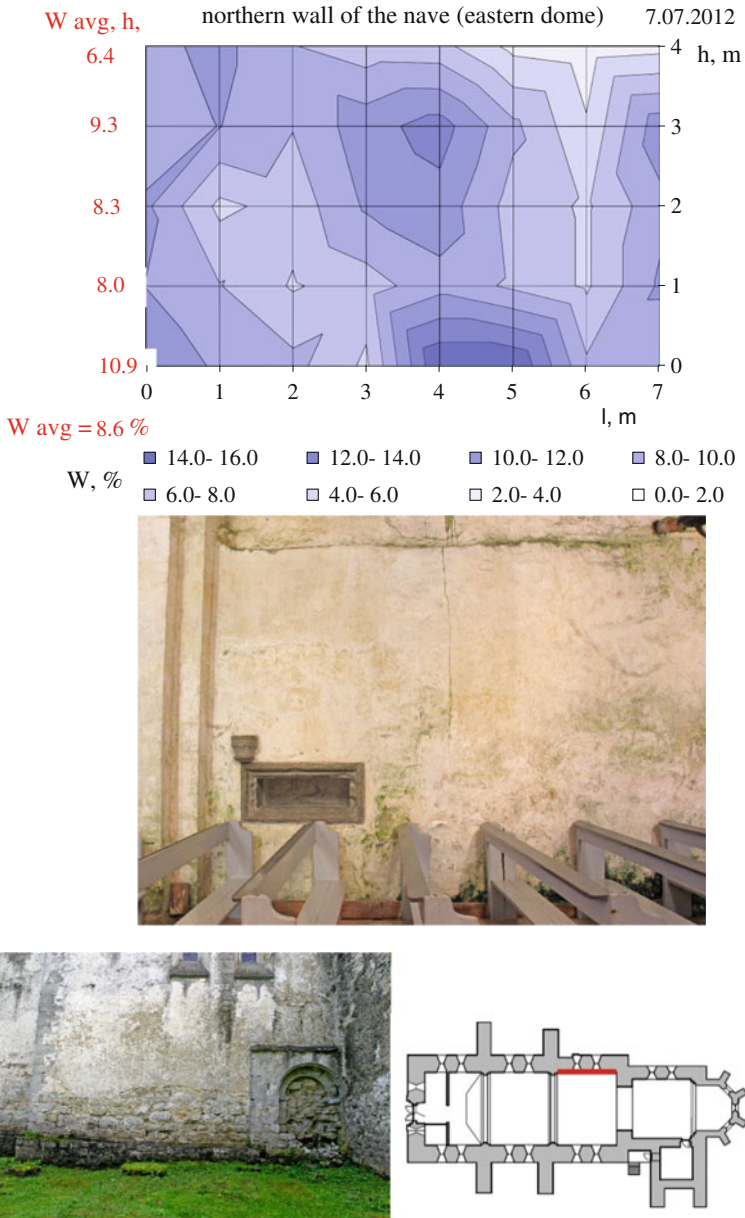


Fig. 13 Multiple water sources in this case: rising dump, condensed water, leakage through the wall and windows, Valjala Church. Measuring depth up to 30 cm. Pictures of wall from the inside and outside; wall location on church plan

3.2 Long Period Moisture Changes in Walls of Kihelkonna Church

Moisture movement out of massive walls is slow and depends on many factors: outdoor and indoor climate, moisture conditions of soil, restoring and conservation works etc. In some of the churches moisture mapping has been done over many years. In Kihelkonna Church, we started measurements already in 2005 to determine the initial conditions before the start of conservation works. For this church, we have the longest time series of moisture measurement of walls.

Southern wall of the choir Fig. 14 was in the second part of 2005 restored and partly newly plastered. By time outside ground level became too high relative to church basement level. To decrease the level of ground water covered by tent ditch was excavated around the church. Moisture content of the wall from May 2005 to October 2015 are presented on Figs. 15 and 16. We do not see major changes, only moisture content at higher levels from the ground was substantially decreased. On the levels below the covering moisture situation stayed practically the same. There was no positive effect from the temporary ditch.



Fig. 14 Southern wall of Kihelkonna Church from inside and outside (on the right side covered ditch is visible)

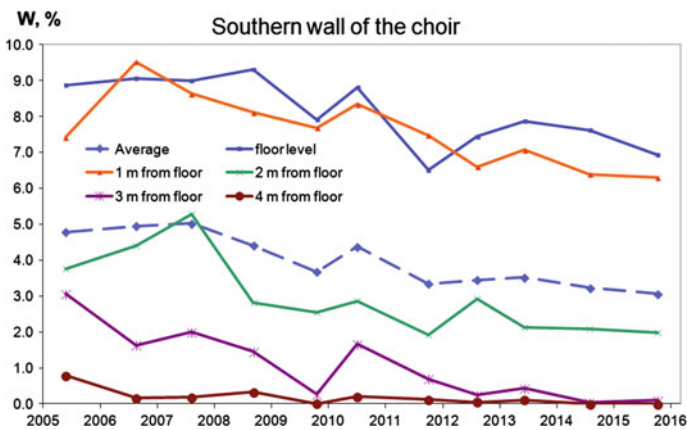


Fig. 15 Timelines of average moisture content of the southern wall of the choir at different levels from the ground

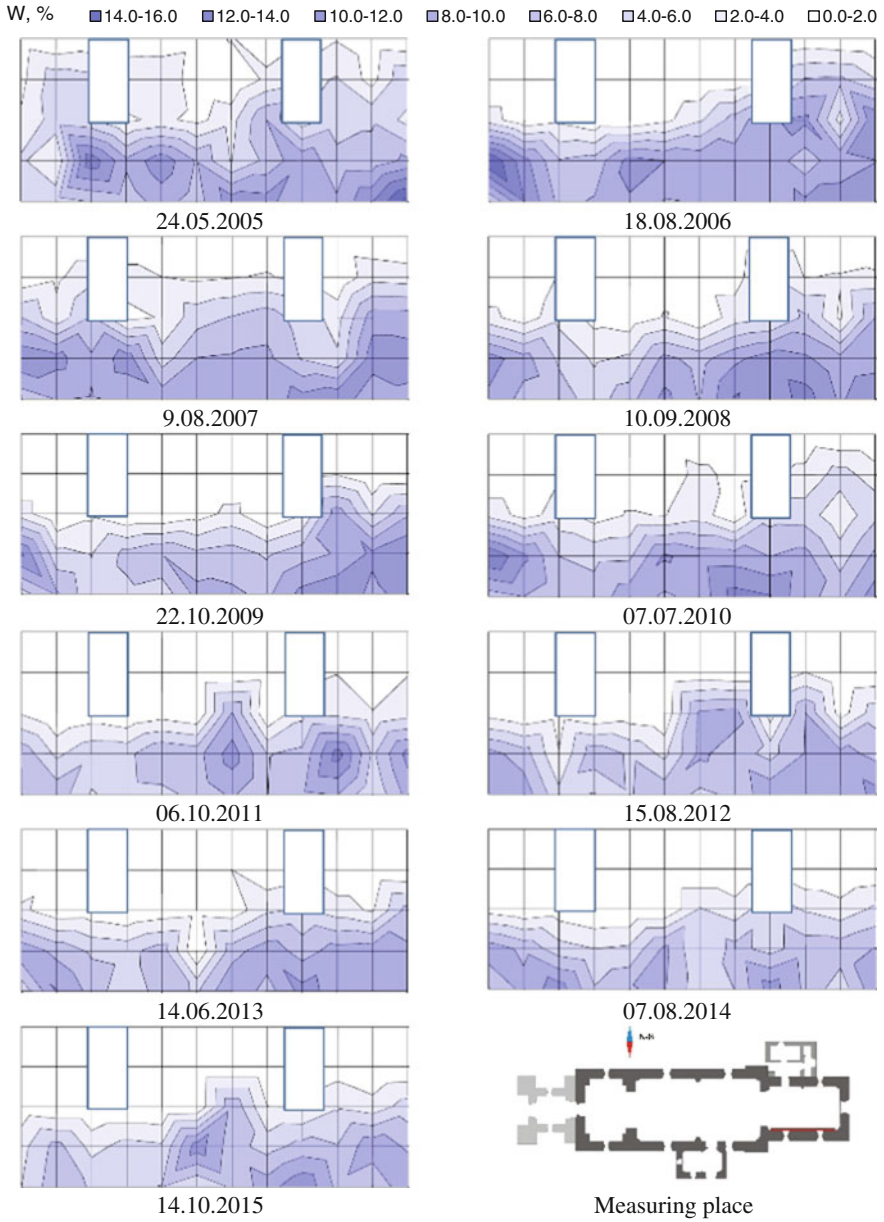


Fig. 16 Moisture maps of the southern wall of choir in Kihelkonna Church, measuring depth up to 30 cm

The nave walls of the church was covered with cement-based plaster and wooden panels that were removed during conservation works in 2005. Left upper graph in Fig. 17 presents the situation in the beginning of conservation works. Initially, the wall was very wet. Due to the restoration activities the situation became clearly better (see Figs. 17 and 18).

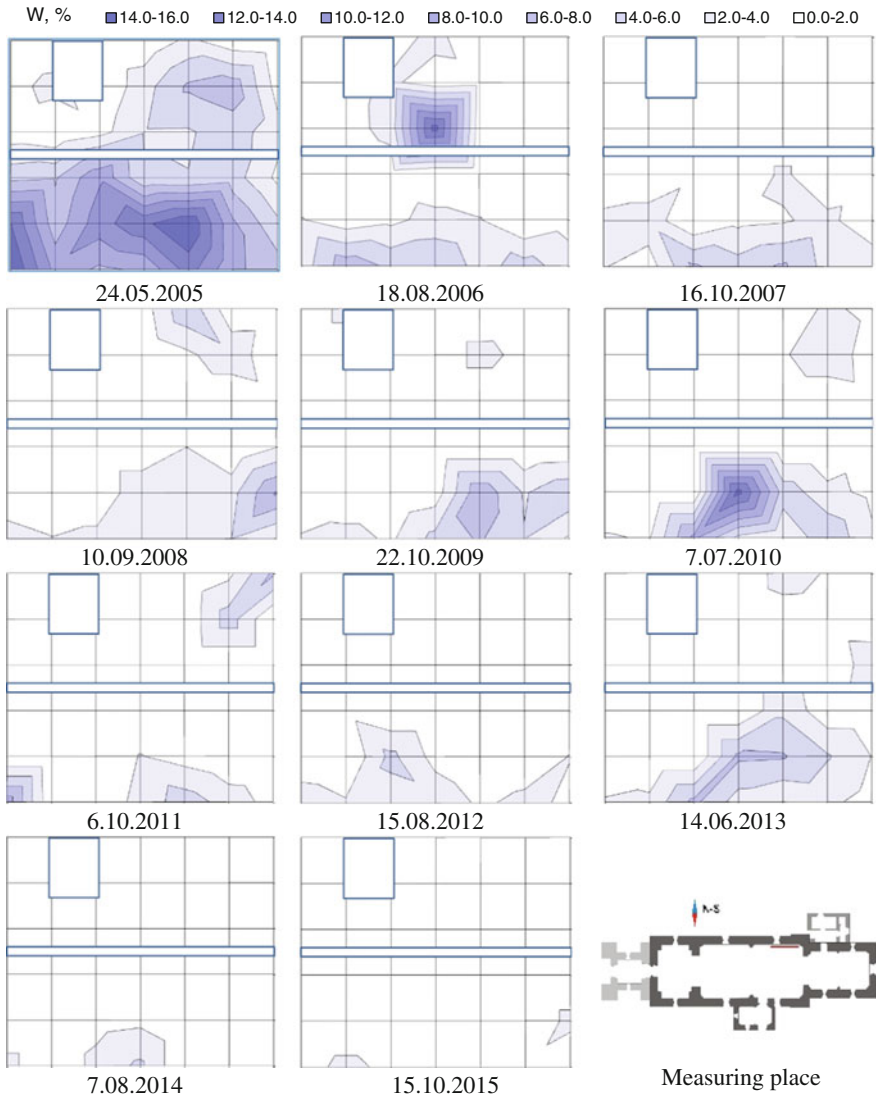


Fig. 17 Moisture distribution changes in northern wall of the nave in the Kihelkonna Church (moisture content measuring depth up to 30 cm)

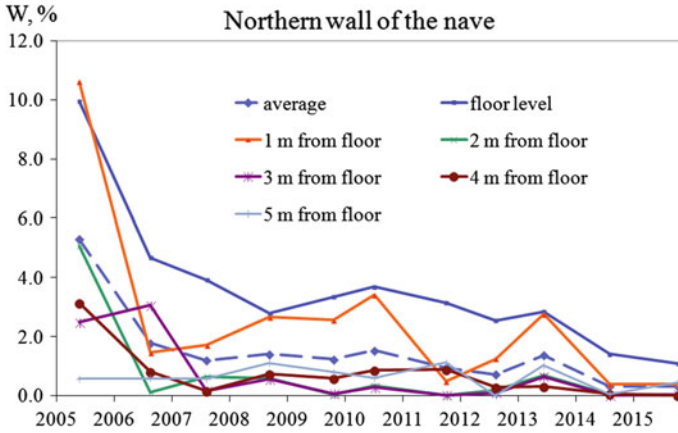


Fig. 18 Decrease in moisture content in wall on the levels up to 5 m from the floor level after conservation works in 2005 in Kihelkonna church

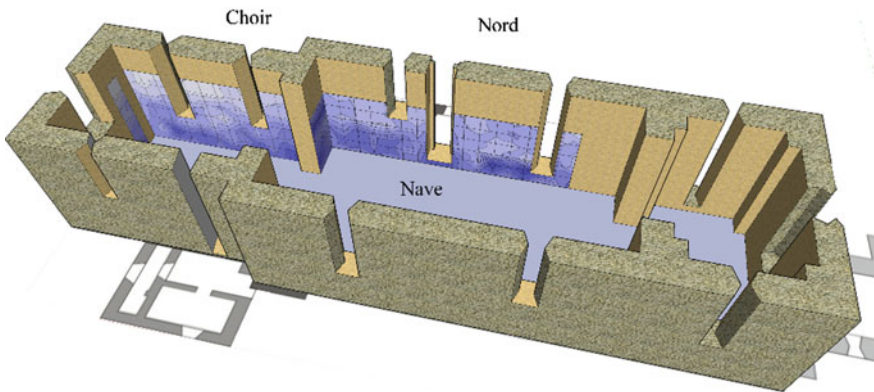


Fig. 19 Moisture content maps of the Kihelkonna Church presented on 3D model of the church

Moisture content maps made at the same time were placed on the 3D model of the church to understand better moisture problems in the church. Presenting moisture content changes over the times it is possible present moisture maps for different time moments at the different layers of model by changing visibility of layers in 3D model (Fig. 19).

3.3 Seasonal Changes

Long period measurements revealed clear fluctuations in moisture content. Main reason for that were seasonal changes in moisture content of the walls. Moisture

content changes throughout the year in northern wall in the nave in Püha Church (typical for moist Saaremaa churches) are presented on Fig. 20. Most of the moisture settled typically in lower part of the wall with maximum in the middle or second part of the summer. For this period, a lot of water was accumulated into the walls. Later, temperature of the walls stayed quite stable and little warmer from the outdoor air temperature. Moisture content started to drop and reached minimum in winter. Due do the condensed and hygroscopic water the moisture content maximum for the higher parts of the walls was at springtime. Higher parts of the walls started to warm earlier and moisture levels dropped in summer. When overall moisture content was low, then the maximum was in spring or in first part of summer, Fig. 20.

Not always the changes in seasonal moisture content were similar to the previously represented data of Püha Church. In another church, Kaarma, the maximum water content in southern wall of choir was typically achieved in October.

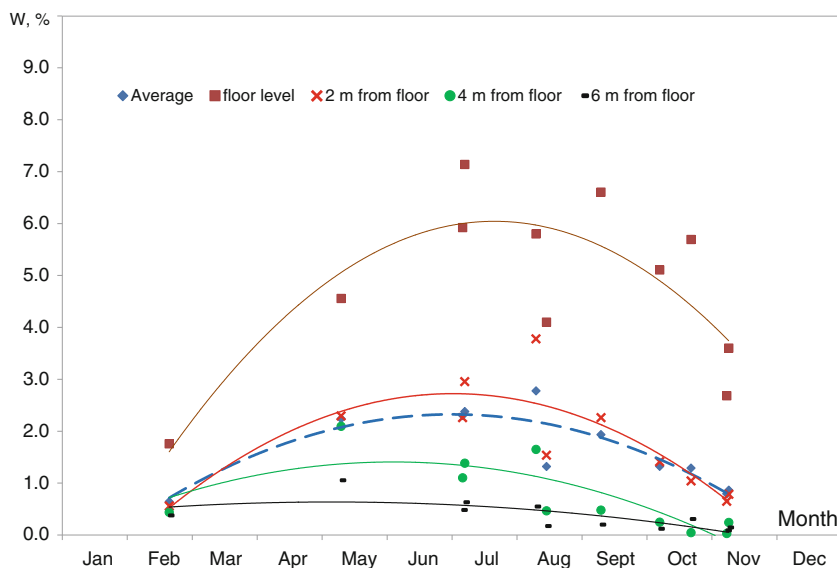


Fig. 20 Seasonal moisture content changes in the wall on the different levels from the floor

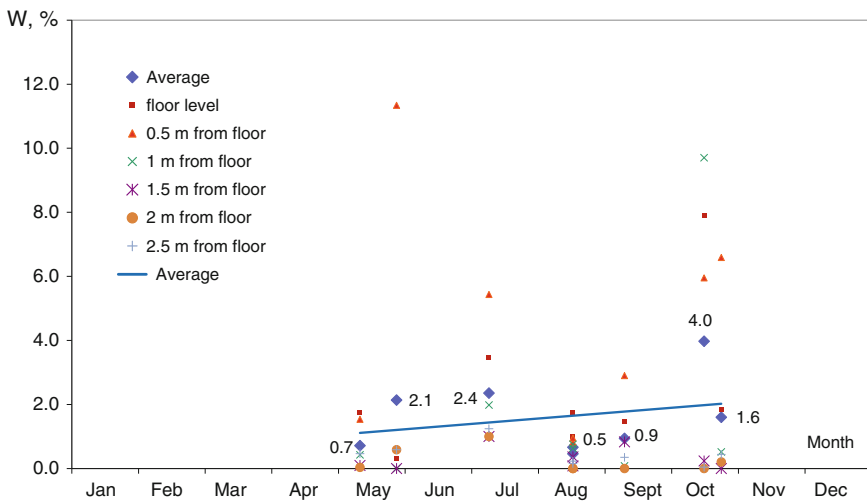


Fig. 21 Average moisture content of the southern wall in choir of the Kaarma Church is low (~2 %), but sometimes peaks up

The primary reason for it was direct rainwater leakage from outside at rainy days. Usually this wall maintains low water content (Fig. 21).

3.4 Influence of Tent (Awning)

In Sect. 3.2, we showed that temporary awning is not good for the wall health. It is not always so. In Pöide Church beside of the northern wall about 15 years old temporary awning is located. This awning reaches far from the wall and may be this was a reason why on that level inner side of the wall was dry (see Fig. 22). Awning what was originally built for the protection of ongoing archeological excavations, served as well for the protection of church health.

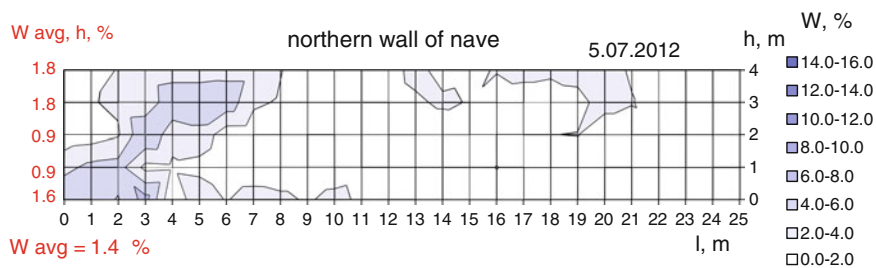


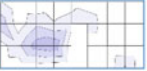
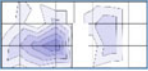
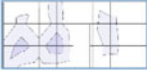
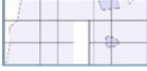
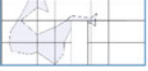

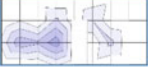



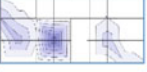
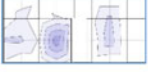








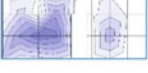





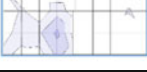
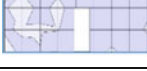

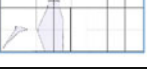









Fig. 22 Moisture content is low under the temporary awning (from the year 2000) covering the ongoing archeological excavations

3.5 Three-Dimensional (3D) Measurements

Using sensor heads with different penetration depths gives us possibility to investigate moisture distributions in several depths of the wall. Table 2 presents that kind of measurements in Püha Church what were carried out over two years period. Inside of this wall in the depth more than ~ 10 cm are two quite stable wet spaces. On the same level the surface mold was developing. It is quite difficult to understand, why such kind localization was realized for the mold development, because in the surface layer of 3 cm thickness measured moisture distribution was different. Placing measuring sensors on rough wall surface can produce incorrectly interpreted results. Better results could be achieved by combining data from different sensors. In some complex cases the only option is to carry out measurements in a hole drilled into wall. The last is not well acceptable by heritage administrators. Therefore, interpreting results of 3D measurements needs further analysis.

Table 2 3D moisture distribution in northern wall of the Püha Church

Time	Measuring depth				
	Up to 3 cm*	Up to 7 cm	Up to 11 cm	Up to 30 cm	Up to 80 cm
14.08.12					
07.11.12					
20.02.13					
9.05.13					
05.07.13					
08.11.13					
06.08.14					
15.10.15					

* only moisture index for this sensor head was used (calibration problems with this sensor)

4 Conclusions

Moisture content assessment by the reflection of the microwaves is informative and not very laborious task to receive large number of data to draw maps of moisture content distribution in the walls. This method is very suitable for diagnosing nature of the moisture problems of buildings with high value for national heritage. Results presented as 2D moisture distribution maps are easily readable even for a non-specialist and expedite significantly analysis of problem. More complex and easier understandable for everyone is the way to present all 2D moisture maps of a building on the 3D model of the building.

Periodically repeated measurements (with different measuring depth—up to 80 cm) over 10 year period in medieval churches in Estonian islands allowed to analyze seasonal and long period changes of moisture content in walls. At winter period, walls were typically dry. Maximum water content at low heights was achieved on the second half of summer and at higher levels on May. Based on long period measurements it was possible to reveal the effect (good, bad or neutral) of the restoring works for the health of building.

Acknowledgments The research has been conducted as part of the projects IUT1-15 “Nearly-zero energy solutions and their implementation on deep renovation of buildings” financed by Estonian Research Council and utilizes the measurement results from projects “Sustainable Management of Historic Rural Churches in the Baltic Sea Region” of Central Baltic IVA Programme 2007–2013 and “Damp and salt damages of stone walls of Estonian churches” financed by National Heritage Board of Estonia.

References

- Agilent (2005) Basics of measuring the dielectric properties of materials. Agilent Technologies, Inc, USA
- Capitani D, Proietti N, Gobbino M, Soroldoni L, Casellato U, Valentini M, Rosina E (2009) An integrated study for mapping the moisture distribution in an ancient damaged wall painting. *Anal Bioanal Chem* 395:2245–2253
- Curteis T (2004) Environmental conditions in Historic Churches: examining their effect on wall paintings and polychrome surfaces. *Trans Ecclesiastical Archit Surveyors’ Assoc* 5:36–46
- Derome D, Teasdale-St-Hilaire A, Fazio P (2001) Methods for the assessment of moisture content of envelope assemblies. In: *Proceedings of Buildings VIII*, Clearwater Beach, FL, USA
- Di Tullio V, Proietti N, Gobbino M, Capitani D, Olmi R, Priori S, Riminesi C, Giani E (2010) Non-destructive mapping of dampness and salts in degraded wall paintings in hypogeous buildings: the case of St. Clement at mass fresco in St. Clement Basilica, Rome. *Anal Bioanal Chem* 396:1885–1896
- Garnett JCM (1904) Colours in metal glasses and in metal films. *Philos Trans Roy Soc Lond CCIII*: 385–413
- Göller A (2001) Moisture mapping—getting 2D and 3D moisture distribution by microwave measurements. In: *Proceedings of the 4th international conference on electromagnetic wave interaction with water and moist substances*, Weimar
- Göller A, Handro A, Landgraf J (1999) A new microwave method for moisture measurement in building materials. In: *Proceedings of the 3rd workshop on electromagnetic wave interaction with water and moisture substances*, Athens, Georgia, USA
- Kaatze U (2005) Electromagnetic wave interactions with water and aqueous solutions. *Electromagnetic aquametry*. Springer, Berlin Heidelberg, pp 15–37
- Larsen PK (2004) Moisture measurement in Tirsted church. *J Archit Conserv* 1:22–35
- Okamura S (2000) Microwave technology for moisture measurement. *Subsurf Sens Technol Appl* 1(2):205–227
- Senni L, Casieri C, Bovino A, Gaetani MC, De Luca F (2009) A portable NMR sensor for moisture monitoring of wooden works of art, particularly of paintings on wood. *Wood Sci Technol* 43:167–180

- Sihvola A (2005) Model systems for materials with high dielectric losses in aquametry. Electromagnetic aquametry. Springer, Berlin Heidelberg, pp 93–112
- Triikkel A, Kaljuvee T, Soesoo A, Kuusik R (2012) Estonian dolomites: occurrence, resources, characterisation and new prospects for application. In: Veress BSJ (ed) Horizons in earth science research, vol 7. Nova Science Publisher Inc, New York, pp 147–196

The Wind-Driven Rain and the Buildings: Directional Driving Rain, Experimental Simulation and Quantification of Wetness Areas

Lais Zucchetti, Patricia Poyastro, Silvia Trein Heimfarth Dapper, Angela Borges Masuero and Acir Mércio Loredo-Souza

Abstract The theme involving the driving rain has been the subject of various studies that seek to contribute to the understanding of this phenomenon and its interaction with the buildings. In this sense, research discusses some aspects related to driving rain, such as the development and application of a methodology for quantifying wetting areas on models exposed to experimental driving rain, and the determination to the direction of the driving rain, in Porto Alegre city—Brazil, through the use of semi-empirical method, more specifically, a wind-driven rain relationship formula. The findings of this study demonstrate that the building facades oriented to the East/South quadrant have higher incidence level of driving rain, considering the Porto Alegre City-RS-Brazil. Furthermore, considering the application of the methodology, it was found, based on the images obtained in the experimental tests that both the building shape and the surroundings influence the degree of driving rain wetting on the models facades. In this way, the model with a square base and without surroundings showed the least amount of wet area when compared to the others.

Keywords Wind-driving rain · Semi-empirical method · Quantification of wetness areas in building

L. Zucchetti (✉) · P. Poyastro · S.T.H. Dapper · A.B. Masuero
Federal University of Rio Grande do Sul, Porto Alegre, Rio Grande Do Sul, Brazil
e-mail: laiszucchetti@yahoo.com.br

P. Poyastro
e-mail: patypoyastro@gmail.com

S.T.H. Dapper
e-mail: silviadesign@gmail.com

A.B. Masuero
e-mail: angela.masuero@ufrgs.br

A.M. Loredo-Souza
LAC/PPGEC/UFRGS, Porto Alegre, RS, Brazil
e-mail: acir@ufrgs.br

1 Introduction

The water from the driving rain is the most important source of moisture as it affects the hygrothermal durability and performance of the facades of the buildings (Blocken and Carmeliet 2004). In this sense, also, the weather resistance design of building facades requires adequate knowledge on the wind and rain environments around the building (Choi 1993).

Currently, several studies have sought to identify and measure the contribution of the wind-driven rain in the emergence of pathological manifestations in buildings (Robinson and Baker 1975; El-Shimi et al. 1980), since it is considered by many authors as the main source of external moisture acting on the facades of a building (Blocken and Carmeliet 2004; Straube and Burnett 2000). Choi (1999), identified in their study that originated pathological manifestations of rainwater have been, for some time, recognized as the main problem in maintaining the buildings.

Thus, the proper design of building facades requires that personnel involved has adequate knowledge about the behavior of the wind and the rain, for example, information about the wind velocity, rainfall intensity, droplet size, and duration of the rain event on the building (Choi 1993, 1994a b). Other authors, beyond these parameters, consider that the amount of driving rain that falls on the facades is also influenced by other factors such as the position the building facades, the building geometry, the geometrical configuration of panel types; the material properties and surface characteristics, topography of site, among others (Choi 1994; Blocken et al. 2002; El-Shimi et al. 1980).

The study of driving rain in civil engineering is divided basically into two parts: the measurement loads of driving rain and the study of the building response of these loads (Blocken and Carmeliet 2004). Regarding the quantification of driving rain, three main methods are available: experimental methods, numerical methods and semi-empirical methods (Blocken and Carmeliet 2004). This work will initially employ a semi-empirical method, followed by the analysis of the experimental method developed by Poyastro et al. (2012).

The quantification methods of driving rain called semi-empirical, relation basically, data concerning winds with those related to rain, this information usually comes from weather stations that provide speed and wind direction data in conjunction with the precipitation information. These methods emerged from the need of knowing the level of exposure of facades related to driving rain, through the establishment of relationships between rain and wind data (Blocken and Carmeliet 2004).

Several studies have attempted to develop methods for quantification of driving rain, the basic difference between the wind-driven rain index and the wind-driven rain relationship is that the last one considers the direction that the rain reaches the vertical plane of the wall. All methods of quantification of driving rain are based directly or indirectly in the wind-driven rain index (Blocken and Carmeliet 2004; Freitas 2011). Some studies have been published with the driving rain index of different countries (Chand 2002; Giarma and Aravantinos 2011; Sahal 2006; Pérez-Bella et al. 2013).

Several authors have proposed equations for the wind-driven rain relationship. Freitas (2011) identified in his work that there are several semi-empirical methods to evaluate the amount of driving rain, and this leads to great difficulty in deciding the most appropriate model for each query. In this work it was used the Rydock method (2006) allowing comparisons to other studies conducted in Brazil, such as the Giongo (2007), Melo Junior (2010) and Heerdt and Back (2013).

From the identification of the preferred driving rain direction incidence in Porto Alegre, through the Rydock method, the facades considered in the experimental tests will be precisely those who receive greater addressed rain index. In this regard it should be emphasized that no study was developed in order to identify the wind-driven rain relationship for Porto Alegre city, using this specific method proposed by Rydock (2006).

Thus, the results of the tests made by Poyastro et al. (2012), have been analyzed by using image processing software, in order to measure the extension of the wetted facade, for each building section and each setting of its immediate surroundings. A detailed description of the tests and their settings can be found in Poyastro et al. (2012; Poyastro 2011).

Important to emphasize that the measurement of these areas, until then, had not been realized, due to the almost complete lack of published experimental tests with driving rain in wind tunnel (Poyastro et al. 2012; Inculey et al. 1994; Rupp 2010), especially considering the recent years, where technology involved in the processing and image processing allows us to make a quantification very close to the wind-driven rain affected and protected areas in buildings facades.

The problem of quantifying the areas affected by driving rain in experimental environment was one of the gaps presented in the work of Inculey (Inculey et al. 1994). In this sense, the use of processing and treatment software has helped in the development of different researches in the civil engineering field, mainly related to the analysis of the microstructure of cementitious materials (Bernal et al. 2010) and in the studies where analyzes interfacial contact between mortar and substrate (Stolz and Masuero 2015).

2 Methodologies

The method adopted to estimate the driving rain is based on the definition of the driving rain index and was developed by Rydock (2006); it consists in the Eq. (1) below

$$I_0 = 0.206 \sum_{D=\beta-80^\circ}^{\beta+80^\circ} R_D \cdot V_D \cos(D - \beta) \quad (1)$$

Where I_0 is the driving rain index for vertical wall (mm/year), R_D is the average annual rainfall in the direction D (mm), V_D is the average annual wind speed in the

direction D (m/s), D is the wind direction in degrees from north (D°) and β is the angle between North and the direction normal to the wall (β°).

The data used in this analysis were provided by the Meteorological 8th District, located in Porto Alegre, RS, Brazil, and, encompassed the years 2001–2012, considering hourly information as rainfall (mm), velocity (m/s) and direction wind (D°).

In a second step, the quantification of rain was addressed through analysis of images of experimental tests developed by Poyastro (2011), according to the configurations shown in Fig. 1, with three different base shapes of building (square base, cross-shaped base and H base) and three different settings surrounding area (without buildings, buildings with half the height of the model and with buildings of the same height of the model evaluated).

With respect to experimental tests, the height of the evaluated building models was 46 m, which corresponds to approximately 16 floors. To the surrounding buildings, heights of 23 m and 46 m were used, roughly corresponding to 8 floors and 16 floors, respectively. These heights correspond to half-height and the same height of the buildings studied.

The distance considered in real scale of buildings, around each other and of the surrounding buildings with the main building was 15 m. The tests were performed in Joaquim Blessmann Wind Tunnel of the Building Aerodynamics Laboratory (LAC) of Federal University of Rio Grande do Sul (UFRGS). This wind tunnel allows simulation of the main characteristics of natural wind (Poyastro et al. 2012).

The evaluated models were produced at 1:150 scale, in white acrylic. The scale models of the surroundings were made of crystal acrylic (colorless) to be able to see the rain through them during testing. The equipment used for rain simulation consists of a set of nozzles selected to reproduce the dimensions of the drops. These

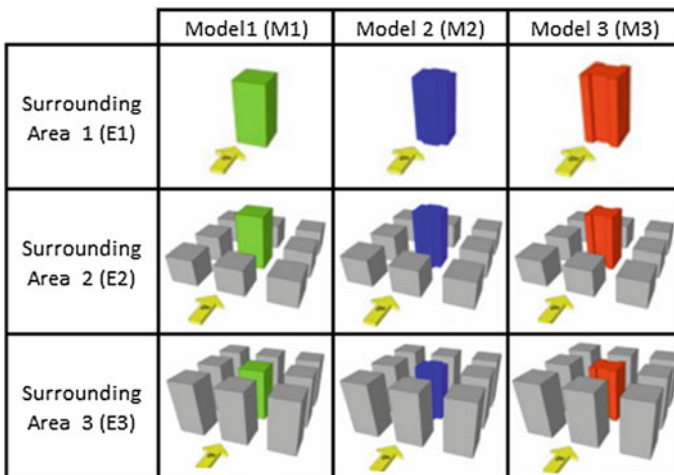


Fig. 1 Experimental test models with different base shapes and environments with different heights

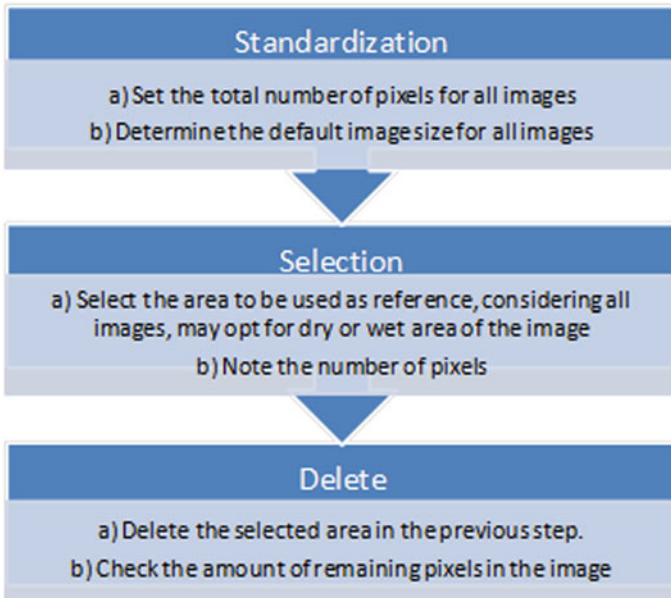


Fig. 2 Methodology developed and applied to quantify dry and wet areas, whereas the images of the experimental tests carried out by Poyastro (2011)

nozzles were arranged to create a uniform distribution of simulated rain. The speed of the final test wind was 25 km/h at the top of the building in full scale (Poyastro et al. 2012).

Images analyzes were performed using the methodology presented in Fig. 2 which initially consists in standardizing the images considering its size and quality (number of pixels). Then it is necessary to determine a standard point for all images, whether wet or dry, which will be used as reference for the analysis of all records images of the tests, from this decision, noting the amount of pixels selected in this dry or wet area. The next step relates to the removal of the selected image area so that it can be accounted for the remaining area of this image.

Thus, in studies that employ water sensitive papers, altering its color from yellow to blue as wetted by rain, such as Poyastro (2011), can be selected from the different areas of this methodology. Below, in Fig. 3, one can see the application of this methodology in the analysis of the image of the building with square base and surrounding area with the same height of the tested model.

For the evaluation of the images was used CC Adobe Photoshop software, where images have been treated to make them all of the same dimensions, these being 800 px × 352 px, resulting in a total of 281.600 pixels, as shown in the first image of Fig. 3 (left). Soon after, we used the color selection tool called “Color Range” of Photoshop CC. The fuzziness level was set to be 200, which was considered by the authors as satisfactory for color separation.

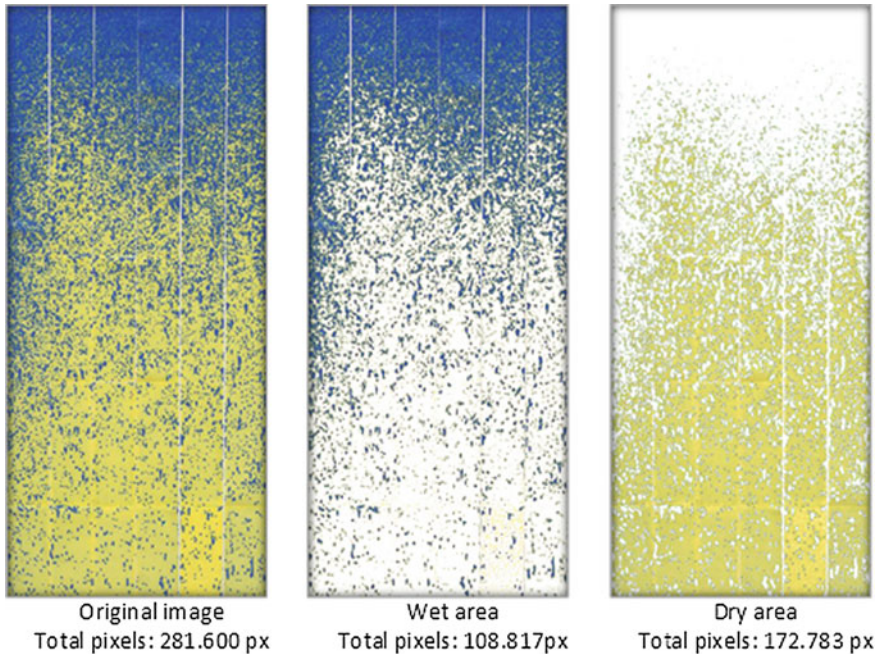


Fig. 3 Example of application of the methodology for quantification of wet and dry areas on models submitted to driving rain in the wind tunnel

With this process, at first, we can delete the yellow color (dry area), leaving only the wet area represented by blue pixels. The “histogram” tool was revealed the number of pixels composing this color which resulted in 108.817 pixels (image located in the middle of Fig. 3). Secondly, by inverting the selection, can carry out the same process with the color yellow (dry area) by excluding the color blue (wet area), resulting in 172.783 pixels. In other words, we obtained a greater number of pixels quantified as dry area (yellow pixels) compared to the area affected by the wetness, represented by blue pixels. This image editing process was performed with all samples of tests.

3 Results

Considering the vertical wall directed rain amount, calculated from the wind-driven rain relationship formula proposed by Rydock (2006) and shown in the graph in Fig. 4, the walls of the facades of buildings oriented to the South/East quadrant receive higher incidence of driving rain against other orientations, which in general, considering the North/East and North/West quadrant have similar levels of driving rain in the city of Porto Alegre, Brazil.

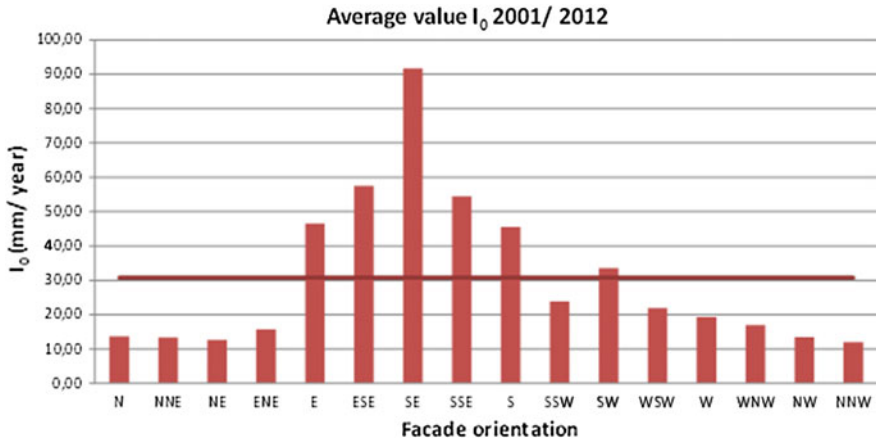


Fig. 4 Amount of driving rain on a vertical wall originated from the data of the Porto Alegre City

Thus, the direction with highest rainfall index directed vertical wall in the city of Porto Alegre, based on the application of the Rydock formula, was the Southeast with an average of I_0 above 90 mm/year, and its derivations for East and West, more precisely in the directions East-Southeast (57.5 mm/year) and South-Southeast (54.5 mm/year). In contrast, the direction that received the lowest amount of rain based on these same parameters was North-Northwest with an average value of $I_0 = 12.0$ mm/year, followed by the Northeast with $I_0 = 12.6$ mm/year, both related to the North quadrant.

In this sense, from the identification of the most susceptible facade to the incidence of wind-driven rain in the city of Porto Alegre, the areas of the models submitted to driving rain tests, based on experimental tests developed by Poyastro (2011), were quantified employing the methodology already presented. In Fig. 5, we can see the application of the methodology for some the models with square base (M1).

For all image analysis, the following nomenclature was adopted: M1 for the model with a square base, M2 for the model with a cross-shaped base, M3 for the model with a H-shaped base, and E1 for the next surrounding area without buildings, E2 for the surrounding area construction with the half-height of the model and E3 for the environment with buildings with the same height as the model evaluated. This same nomenclature referring to the building model shape and its surroundings was used in the configuration of the graphics and the analysis of results.

In Fig. 6, we can observe the methodology applied to the second model (M2) with cross format base. In these images, we can see that the wetness of this model with the environment 1 (E1) is lower compared to 2 (E2) and 3 (E3). In this case, we can still observe the wetting in parabola shape, as evidenced in the analysis with Model 1 (M1).

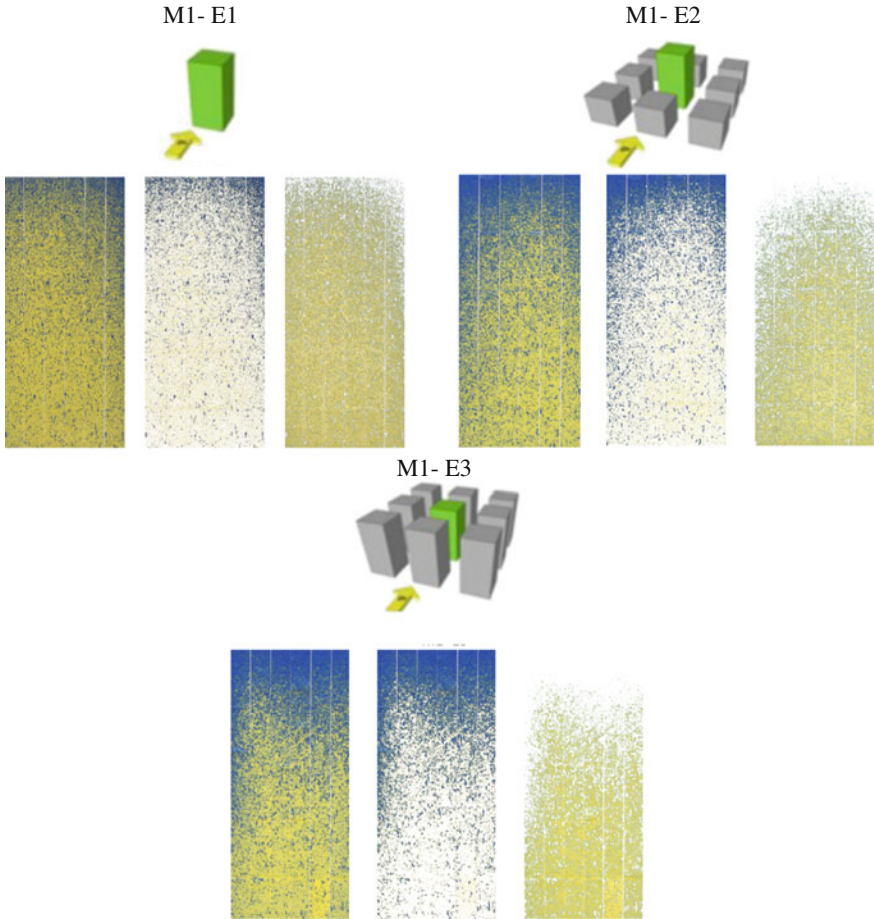


Fig. 5 Proposed methodology application for the model with square base (M1) and different surroundings

The analyzes carried out with Model 3 (M3), with H base format, may be observed in Fig. 7 and show, as in the others analysis, that the wetting caused by the environment 1 (E1), without building, is smaller than the other environments (E2 and E3) characterized by buildings with different heights.

From the image analysis, can identify the wetting of the models in parabola shape, characteristic of driving rain, which mainly affects the areas of the top and sides of the model, getting the central parts of the building more protected from wetness, caused by driving rain, simulated in the wind tunnel.

Similarly, we can observe the change in amount of wetness, when the settings related to the model format and its surroundings are modified, so, these parameters directly influence in the wetness level of the facades considering the models evaluated in this research.

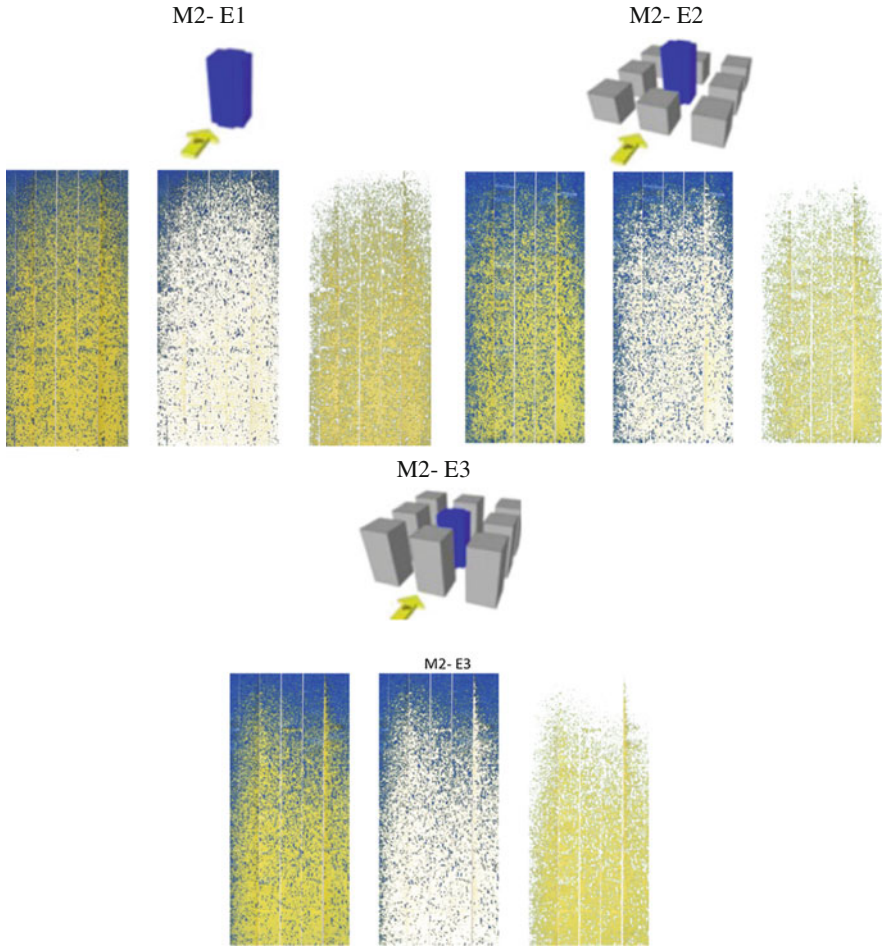


Fig. 6 Proposed methodology application for the model with cross base (M2) and different surrounds

Thus, in Figs. 8 and 9, we can see the graph that reproduces the amount of rain wetting the affected area, considering the tested models according to each surrounding area reproduced. In it can be seen that the wet area of all models increases as the composition of the buildings surrounding changes, and for all the models surrounding area 1 (no buildings) was the one that represented the lowest rates of wetting, in contrast, the surrounding area 3 (E3) over all models, had higher percentages of wet area, showing the surroundings 2 (E2) behavior very close to that found in the surrounding 3 (E3).

In the graph shown in Fig. 9, we can observe the behavior of the models in terms of each configuration surrounding area, so it appears that the model 1 (M1), with square base features for all configurations of the surrounding area smaller

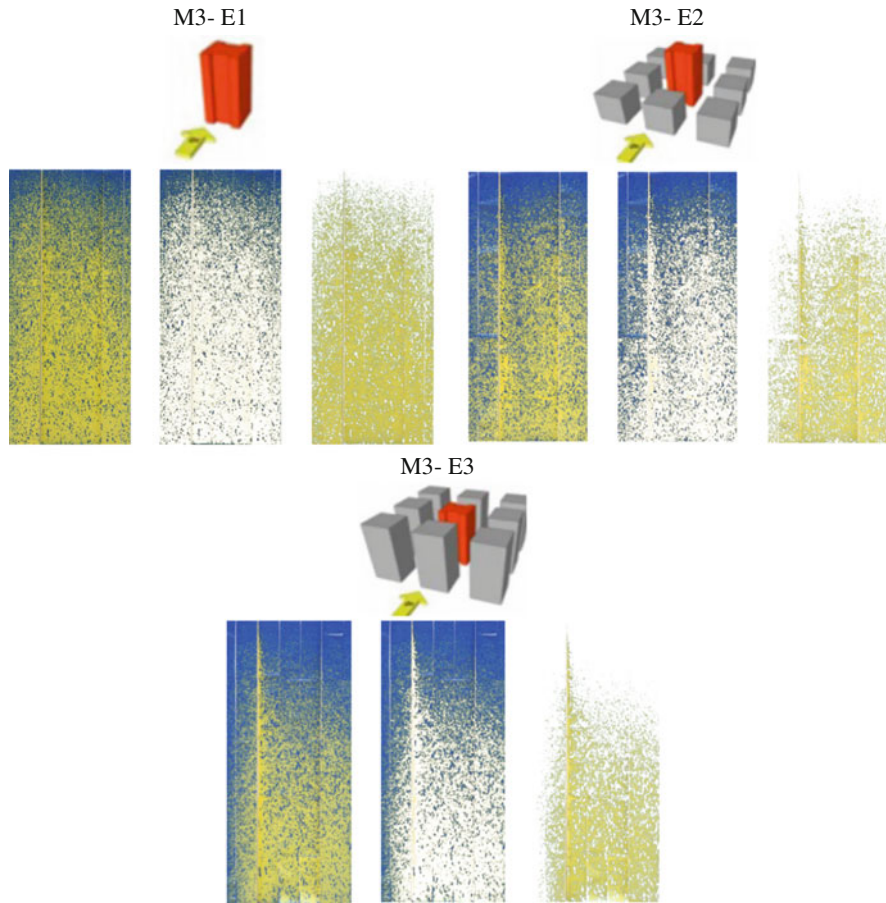


Fig. 7 Proposed methodology application for the model with H format base (M3) and different surrounds

percentage of wetness, contrary model 3 (M3) among these, is the one with higher rates of wetting, leaving the second model (M2), with cross-shaped base, with a median behavior between M1 and M3.

Thus, we can observe that both the base shape of the building and the configuration of the surrounding areas influence in the level of wetness of the facade of the models. Model with square base (M1) and no surrounding buildings had lower rates of wet areas. In contrast, model 3 (based H-shaped) with the surroundings of the same height as the model analyzed, yielded higher percentages areas of wetness coming from driving rain simulation in the wind tunnel.

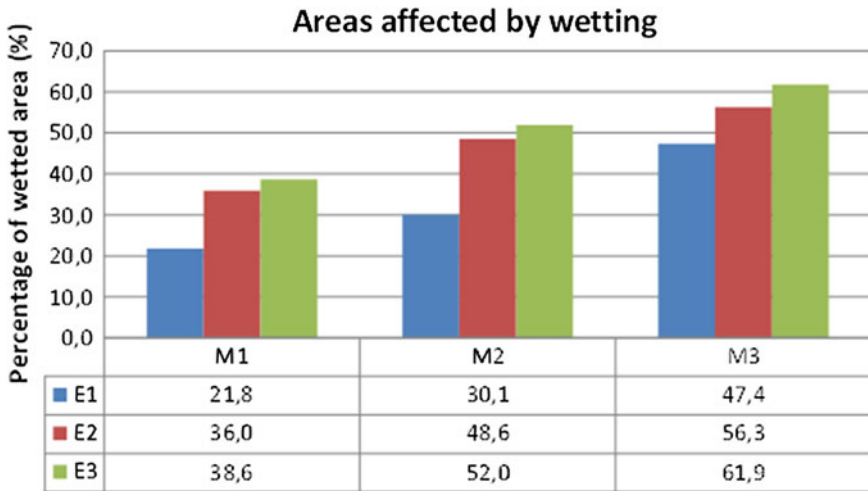


Fig. 8 Wet areas quantified in the model considering the behavior of the surrounding area in terms of the shapes of the buildings

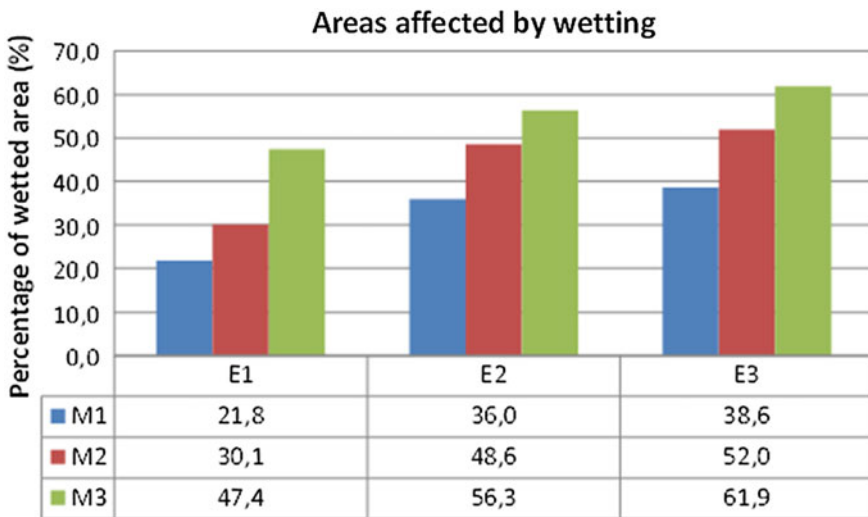


Fig. 9 Quantification of the wet area of models considering the influence of the base shape in the building model

4 Conclusions

Considering the quantification based in the wind-driven rain relationship and on the data analyzed, it was found that the facades of the buildings located in the Porto Alegre city, Brazil, are subject to a higher level of wetting due to the incidence of

wind-driven rain when oriented to quadrant East, it was found that the facades of the buildings located in the Porto Alegre city, Brazil, are subject to a higher level of wetting due to the incidence of wind-driven rain when oriented to quadrant East/South, with greater incidence for facades oriented to the southeast direction.

Taking into account the quantification of driving rain in the models subjected to wind tunnel experimental tests, based on the work of Poyastro (2011) and applying the methodology proposed in this paper, it was found to influence the base shape of the building and its immediate surroundings, in the level of wetness of the facades of the model. Whereas the configuration with the model of square base and without surrounding buildings was one that had lower wetted area, in contrast, the configuration with H-base building and surrounding area of the same height of model resulted in higher rates of hit by wind-driven rain.

Thus it was found that both the base shape of the building/model and the configuration of the immediate surroundings influence the level of wetting of the facades of buildings. Moreover, this paper proposed, developed and applied methodology that proved to be adequate, since it allowed the quantification of the areas affected by the wetness of driving rain, simulated in wind tunnel and can be reproduced in other works that have the same goals.

References

- Bernal J, Vilarino F, Sanchez J (2010) Feature detectors and feature descriptors: where we are now. Computer Vision Center and Computer Science Department UAB Campus UAB, Edi_ci O, 08193, Bellaterra, Barcelona, Spain, 6 Sep 2010
- Blocken B, Carmeliet J (2004) A review of wind-driven rain research in building science. *J Wind Eng Ind Aerodyn* 92(13):1079–1130
- Blocken B, Hens H, Carmeliet J (2002) Methods for the quantification of driving rain on buildings. *Ashrae Trans* 108(2):338–350
- Chand I, Bhargava PK (2002) Estimation of driving rain index for India. *J Build Environ* 37(5):549–554
- Choi ECC (1993) Simulation of wind-driven-rain around a building. *J Wind Eng Ind Aerodyn* 46 &47:721–729
- Choi EC (1994a) Determination of wind-driven-rain intensity on building faces. *J Wind Eng Ind Aerodyn* 51:55–69
- Choi EC (1994b) Parameters affecting the intensity of wind-driven rain on the front face of a building. *J Wind Eng Ind Aerodyn* 53:1–17
- Choi ECC (1999) Wind-driven rain on building faces and the driving-rain index. *J Wind Eng Ind Aerodyn* 79(1/2):105–122
- El-Shimi M, White R, Fazio P (1980) Influence of façade geometry on weathering. *Can J Civ Eng* 7:579–613
- Freitas ASSLA (2011) Avaliação do Comportamento Higrotérmico de Revestimentos Exteriores de Fachadas devido à Acção da Chuva Incidente. Dissertação (Mestrado em Engenharia Civil). Faculdade de Engenharia da Universidade do Porto. Porto, Portugal
- Giarna C, Aravantinos D (2011) Estimation of building components' exposure to moisture in Greece based on wind, rainfall and other climatic data. *J Wind Eng Ind Aerodyn* 99:91–102
- Giongo M (2007) Análise do Nível de Exposição das Edificações à Chuva Dirigida para Florianópolis. 2007. 107 f. Dissertação (Mestrado em Engenharia Civil)—Programa de Pós-Graduação em Engenharia Civil, Universidade Federal de Santa Catarina, Florianópolis

- Heerd G, Back AJ (2013) Determinação da chuva dirigida para região sul catarinense. Universidade do Extremo Sul Catarinense. Available <http://repositorio.unesc.net/bitstream/handle/1/1150/Graziela%20Heerd.pdf?sequence=1>. Accessed 10 sept 2013
- Inculey D, Surry D, Skerlj PF (1994) The experimental simulation of wind and rain effects on the building envelope. In: IRC-NRC-BLWTL conference on curtain wall the boundary layer wind tunnel laboratory. The University of Western Ontario, London, Ontario, Canada
- Melo Junior CM (2010) Influência da Chuva Dirigida e dos Detalhes Arquitetônicos na Durabilidade de Revestimentos de Fachada. 204 f. Goiânia, 2010. Dissertação (Mestrado em Geotecnia)—Programa de Pós-Graduação em Geotecnia, Construção Civil e Mecânica das Estruturas, Universidade Federal de Goiás, Goiânia
- Pérez-Bella JM, Domínguez-Hernández J, Cano-Suñén E, Del Coz-Díaz JJ, Alonso-Martínez M (2013) Global analysis of building façade exposure to water penetration in Chile. *Build Environ*
- Poyastro PC (2011) Influência da volumetria e das condições de entorno da edificação no manchamento e infiltração de água em fachadas por ação de chuva dirigida. Dissertação (Mestrado em Engenharia Civil)—Escola de Engenharia Civil, Universidade Federal do Rio Grande do Sul, Porto Alegre
- Poyastro PC, Masuero AB, Loredo-Souza AM (2012) Influência da volumetria e das condições de entorno da edificação no manchamento e infiltração de água em fachadas por ação de chuva dirigida. 4º Congresso Português de Argamassas e Etics, Coimbra, 2012. Available in: http://www.apfac.pt/con-grosso2012/comunicacoes/Paper%2050_2012.pdf. Accessed 25 Nov 2014
- Robinson G, Baker MC (1975) Wind-driven rain and buildings. Technical paper no. 445, Division of Building Research, National Research Council, Ottawa, Canada
- Rupp LH (2010) Simulação Experimental da Interação Vento-Chuva. Dissertação (Mestrado em Engenharia Civil)—Escola de Engenharia Civil, Universidade Federal do Rio Grande do Sul, Porto Alegre
- Rydock JP (2006) A look at driving rain intensities at five cities. *Build Environ* 41(12):1860–1866
- Sahal N (2006) Proposed approach for defining climate regions for Turkey based on annual driving rain index and heating degree-days for building envelope design. *Build Environ* 41:520–526
- Stolz CM, Masuero AB (2015) Analysis of main parameters affecting substrate/mortar contact area through tridimensional laser scanner. *J Colloid Interface Sci* 455(1):16–23
- Straube JF, Burnett EFP (2000) Simplified prediction of driving rain on buildings. In: Proceedings of international building physics conference, Eindhoven, Netherlands, pp 375–382

A Performance Assessment of Prefabricated Bathrooms Installed in the 1990s

Martin Morelli and Erik Brandt

Abstract This chapter describe the design and build up of wet rooms (bathrooms and rooms with similar exposure to water and high relative humidity) in Denmark with emphasis on wet rooms made as part of a Danish research project—Project Renovation. In this project, 19 different types of bathrooms were made in new untraditional ways. A number of these bathrooms covering 11 different types were surveyed after approximately 20 years of use. The survey aimed at evaluating the bathrooms' condition based on a non-destructive inspection. In general, the bathrooms are in good condition and perform well compared with traditionally made bathrooms. The paper describes the methodology developed to assess bathrooms and gives examples of the results.

Keywords Pre-fabricate · Bathroom · Wet room · Inspection methodology

1 Introduction

In the 1990s, urban renewal was undertaken on a large scale in Denmark and especially in the major cities, e.g. Copenhagen. The aim was to improve the sanitary conditions in apartment buildings constructed in the late nineteenth century. These buildings were normally constructed with solid masonry walls, front—and backstairs, floor divisions of wooden beams and apartments with 2–3 rooms. The apartments could have been built with a small toilet in the apartment or would otherwise have shared toilets located on the backstairs or in the backyard with their

M. Morelli (✉) · E. Brandt
Danish Building Research Institute, Aalborg University, A.C. Meyers Vænge 15, 2450
Copenhagen, Denmark
e-mail: mmo@sbi.aau.dk

E. Brandt
e-mail: ebr@sbi.aau.dk

neighbours. In connection with the urban renewal, bathrooms were installed in many apartments; nevertheless, today 8 % of apartments in Copenhagen are still having insufficient sanitary conditions.

In term of construction, bathrooms are perhaps the most complicated rooms to build. Many professions have to collaborate, thus functions, technical service installations, tiles, joints, etc., must fit together. Constructing bathrooms in new buildings are easier compared with establishing bathrooms or refurbishing bathrooms in existing buildings. Therefore, the bathroom is also the most expensive room per square metre to construct regardless of whether it is a new building or refurbishment of an existing building. Normally, in existing apartments buildings there is very limited space available for establishing a bathroom.

The many functions and installations require that special care is taken to minimise the risk of damage and especially water leakage. Given that bathrooms are exposed to water on floor and walls and to high relative humidity, it is often necessary to install a watertight membrane in order to protect vulnerable materials. In general, constructions of inorganic materials are considered as resistant against moisture in contrast to organic materials which deteriorate if exposed to regular water exposure or high relative humidity. For instance, wood in a construction is vulnerable to decay and mould, if water penetrates through a leak in floor coverings, wall coverings or installations. Such water-caused damage may lead to costly repairs, if it is not detected and eliminated within reasonable period of time. Therefore, it is necessary to inspect constructions and installations on a regular basis, e.g. as a part of regular maintenance.

Eriksen et al. (1991) surveyed 44 newer bathrooms and reported 205 failures related to the zone with the highest water load. These 205 failures were divided into seven typical groups, i.e.

1. Leakage at pipes passing through wall, floor and ceiling (59 failures)
2. Joint defects (44)
3. Moisture accumulation (30)
4. Cracks (25)
5. Lack of adherence (20)
6. Depression and lump (16)
7. Subsidence (11)

The findings from the 44 investigations established a need for improving the quality of bathrooms. Hence, a development programme called Project Renovation was initiated in 1994–1998 with the intention of improving the quality of bathrooms and simultaneously limit the cost of construction. Despite the initiative in Project Renovation, Brandt (2005) reported that for a number of years bathrooms had been number 1 as regards failures.

The most important properties related to service life of bathrooms are according to Brandt (2008); watertightness, water vapour permeability, resistance to mechanical loads, dimensional stability against changes in relative humidity and temperature and compatibility of materials. According to Brandt et al. (2011), reduced service life of bathrooms is often caused by the failures (lack of

watertightness) around penetrations of pipes and floor gullies, hence ingress of water in the construction. These common failures are caused by incorrect mounting of floor gully or unsuited/wrong floor gully used.

Failures are seen both in

- Traditional bathrooms made from concrete, masonry or lightweight concrete—these materials are rather tolerant to minor mistakes.
- Lightweight bathrooms with constructions made from board materials, e.g. gypsum boards, calcium silicate boards or plywood—these materials/constructions are often vulnerable to even small amounts of water.

Brandt (2005) reported that for the traditional bathrooms, the most common failures occur when changing the floor surface without changing the floor gully to an adequate type or securing the joint between floor and walls. These two failures cause water penetration into the floor construction and to the room below. For a lightweight bathroom of board material, the failures are water penetration through walls and/or floors caused by unsuited materials, e.g. board materials with insufficient properties, watertight membrane missing or too thin and failures around details especially floor gullies.

1.1 What Is Project Renovation?

The Project Renovation programme was initiated to promote trade and was implemented from 1994 to 1998, aiming to develop and test models for industrialised refurbishment, which embraced products, methods and processes. Within the framework of Project Renovation, nine categories of projects were identified, where bathrooms was one of them. Project Renovation was conducted during a period where major urban renewal took place in Copenhagen. The urban renewal aimed at improving the quality of housing and thereby bringing toilets and showers from the back stairs or small broom cupboards and backyards into each apartment, cf. Fig. 1.

Common for Project Renovation was the use of prefabricated bathrooms and in total 19 different bathroom solutions were installed. The bathrooms can be grouped as light- or heavyweight bathrooms with further three subdivisions, i.e. in situ, assembly kit and whole cabins. A 5-year inspection report prepared in connection with Project Renovation (Danish Ministry of Housing, Urban and Rural Affairs 2004) concluded that 90 % of the bathroom solutions were implemented in practice. For some of the bathrooms, the watertightness was investigated in laboratory before the bathroom was installed in buildings. Furthermore, an advantage of prefabricated bathrooms is that large parts of the quality control of the components are implemented at factory production. Nevertheless, a follow up on the performance of these 19 bathrooms projects was never executed.

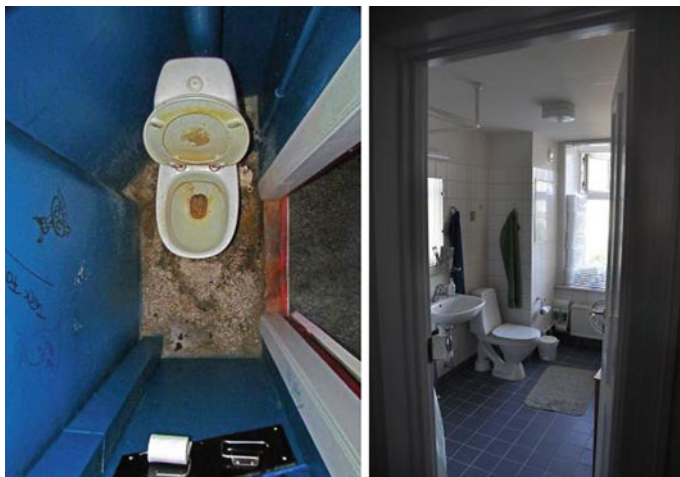


Fig. 1 *Left* Example of a common toilet in the apartment or on the back stairs before urban renewal. *Right* An enlarged bathroom after urban renewal with the shower to the left of the door

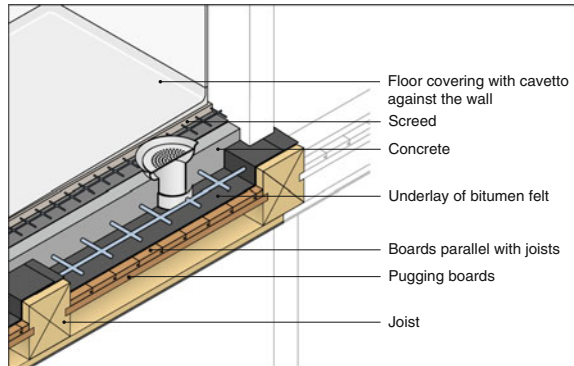
2 Construction Principles for Bathrooms

Traditionally, bathrooms and other wet rooms in Denmark were made solely from inorganic materials, e.g. masonry, concrete or lightweight concrete. The advantage of these materials is primarily that they are not vulnerable to water and besides some of the materials are watertight in themselves. Experience showed that wet-room constructions made from inorganic materials and with a watertight—or in some cases just water repellent—surface functioned satisfactorily, i.e. with the pattern of bathing at that time. For renovation purposes, new bathrooms were often made by casting a concrete slab on the old wooden floor joists—cf. Fig. 2. The experience with these and similar constructions are generally good.

In the 1970s, it was allowed to use lightweight constructions in bathrooms, e.g. stud walls with cladding of gypsum boards and floor constructions with plywood as subfloor. In floor constructions, wood-based materials were permitted on condition that they were impregnated and protected with a water-resistant and watertight surface. The objective was to make the constructions cheaper and at least to some extent to make the building process faster.

During the 1970s and 1980s, further relaxations were introduced, e.g. allowing wood-based materials without impregnation against dry rot and fungi. It was a condition, however, that floor and wall coverings should be in accordance with directions approved by the Danish Ministry of Housing or in accordance with an approval of a specific construction (system) at that time also granted by the ministry.

Fig. 2 Structure of a traditional wet-room floor established on existing floor divisions with wooden beams with pugging (Brandt and Morelli 2015)



At that time, the guideline approved by the Danish Ministry of Housing was SBI Direction 109, “*Floors on wooden floor joists and linings on stud walls in wet rooms*” (three editions the last one valid until 1991) (Kjerulf et al. 1984). A prerequisite for the use of lightweight constructions was that the constructions were accessible from beneath so that any leaks could be detected as soon as possible.

2.1 Requirements for Bathrooms in the 1990s

In the 1990s, the use of lightweight constructions was widespread with several different possibilities for wall as well as floor constructions. The constructions were described in SBI Direction 169 “*Floors and walls in wet rooms – in new dwellings and in connection with renovation*” (1991) (Brandt and Nielsen 1991).

Based on experience gained from using lightweight constructions stricter rules were introduced for some constructions, e.g. only approved plywood and chipboard could be used for floors. Besides glass fibre reinforced polyester was withdrawn from the guideline due to health reasons and the use of lightweight construction was prohibited for wet rooms with an exposure higher than in ordinary dwellings.

Experience gained from its use showed that some of the constructions and surface coatings were vulnerable especially in social housing where the exposure in many cases is harsh. In 1995 further requirements were introduced to improve the quality and service life of wet rooms. The most important change was that a wet and a moist zone in wet rooms were introduced. Only the most resistant constructions and surfaces were allowed in the wet zone, i.e. the area around the shower and the bathtub, see Fig. 3. Ordinary gypsum boards were prohibited and a new type with silicone impregnated core was developed. Surface coatings with paint and wooden boards were from that time only allowed in the moist zone.

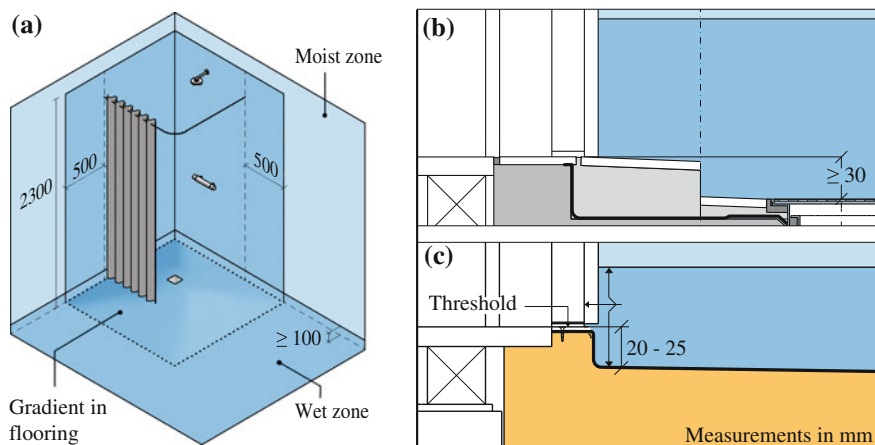


Fig. 3 a Moist and wet zones in a bathroom with a shower unit, where the wet zone encompasses the entire floor and walls around the shower unit until 500 mm from its demarcation. Wet zone on walls are from floor to ceiling, however, in tall rooms the area above normal room height can be considered as a moist zone. No penetration of pipes in the floor is allowed in the most water-exposed area—marked with a *dotted line*. This is normally also the area with the largest slope of the floor towards the floor gully. The room is designed as a “basin”, i.e. either as shown in b 30 mm height difference between the top of the drain and the floor at the door or alternatively c 20–25 mm between floor surface and lower edge of threshold (Brandt and Morelli 2015)

In 1993, SBi Direction 180 “Bathrooms” (Eriksen 1998) was issued giving some examples on planning, designing and execution of especially good solutions for wet rooms.

In the same period a number of projects—under the umbrella Project Renovation—were launched trying to develop new, simpler, cheaper and safer constructions for wet rooms especially for renovation projects. These projects were of many different types and did not necessarily have to fulfil usual requirements and directions including today’s requirements. However, all the projects had to fulfil the most important performance requirement, namely water tightness.

2.2 Requirements for Bathrooms in 2015

Figure 3 illustrates how—especially lightweight—bathrooms today are divided into a wet and a moist zone. The wet zone is where surfaces are expected to be exposed to water on a regular/daily basis, whereas the walls in the moist zone are only expected to be exposed to high relative humidity and only occasionally to water. However, if the bathroom is smaller than 3.25 m² or less than 1.3 m wide, all the walls are considered to be the wet zone (Brandt and Morelli 2015). In the wet zone, requirements to watertightness and robustness are stricter than in the moist zone.

Wet rooms in Denmark are also classified dependent on the category of building they are intended for. The lowest category is wet rooms in single-family houses, second homes, etc. (class L—Low). The middle category is dwellings in blocks of flats (social housing) (class M—Middle), and the third category is for uses with exposure beyond normal dwellings, e.g. washrooms in sports halls or industrial kitchens (class H—High). In class H, only inorganic constructions are allowed.

In dwellings, the most used light/semilight constructions are

Floors

- Wooden floor joists with plywood, watertight membrane and ceramic tiles (class L)
- Wooden joists with chipboard and PVC (with heat welded joints) (class L)
- Wooden joists with plywood + watertight board, watertight membrane and ceramic tiles (class M)
- Concrete slab on wooden joists with membrane and ceramic tiles (class M)—the most commonly used floor construction for renovation

Walls

- Stud walls with a cladding of boards (gypsum boards, cement-based boards, etc. but NOT plywood or chipboards), membrane and ceramic tiles (class M)
- Stud walls with chipboard and PVC (with heat welded joints) (class L)
- Stud walls with watertight boards, membrane and ceramic tiles (class M)
- Aerated concrete (class M)

Besides a new double-floor construction has been introduced consisting of two independent watertight membranes separated by a thin layer of water resistant lightweight concrete. Both membranes are drained to the floor gully, i.e. if the upper layers fail there is still a watertight membrane below. This construction was invented because the foundation for some of the old buildings is not able to carry the extra load from thick concrete slabs.

3 Types of Bathrooms Installed During Project Renovation

The 19 types of bathrooms in Project Renovation are all installed in typical apartment buildings built around the late 1800s. Two approaches were used to build in bathrooms in apartments constructed with floor division of wooden beams with clay pugging. The first approach was to install bathrooms as individual cells in each apartment, implying that the load from the bathroom should be carried by the existing floor division. The second approach was to build self-supporting cabins, where the existing floor division was demolished and new foundations constructed for the tower of cabins. Figure 4 shows the two approaches, and Table 1 describes the 19 different types of bathrooms developed during Project Renovation.



Fig. 4 *Left* Self-supporting cabins with foundation in basement, and *right* Bathrooms installed as cells in each apartment on existing floor division of wooden beams

3.1 *Lightweight In Situ*

Bathroom #3 (Danish Ministry of Housing 1994) was constructed with a horizontal steel surface in the entire bathroom floor area. In larger bathrooms the bottoms of the bathroom were delivered in pieces and welded on site. The edges of the steel surface were folded and finished at least 60 mm above the floor surface, cf. Fig. 5. The wall membrane had to overlap the steel with at least 60 mm at the wall-floor assembly.

The steel surface acts as a traditional watertight membrane; however, it is much more robust during installation as compared with PVC floor coverings or membrane with tiles. The slope towards the floor gully was built up with screed laid out on the steel surface. With a thickness of 1–2 mm, the steel surface had no rigidity and the underlay for the steel tub had to have sufficient rigidity to apply, e.g. tiles on the floor.

Penetrations were welded to be waterproof and mountings for the toilet were also welded ensuring that no screws or bolts penetrated the steel tub. Stainless steel was used to minimise the risk of moisture degradation of the surface, and to avoid damage by corrosion, identical materials were used for all pipes.

During the development of the floor it was found that a steel thickness of 1.5 mm induced deformation as lumps from heat. Therefore, the thickness was increased to 2 mm. In large bathrooms or where all walls were kept, the steel had to be delivered in smaller pieces and then welded at the construction site, ensuring that the watertightness had to be tested on site.

Table 1 Overview of bathrooms after construction principle with a short description and number of surveyed bathrooms

Construction principle	#	Description	Surveyed
Lightweight in situ	1	Bathroom with a shower cabin with ceiling, 3 walls and basin made of steel	0
	2	Bathroom with subfloor of wood and PVC finish/veneer/surface	0
	3	Bathroom with horizontal waterproof steel surface on entire floor	3
Lightweight assembly kit	4	Bathroom with horizontal waterproof steel surface on entire floor and steel membrane in walls	2
	5	Prefabricated horizontally sandwich element with a steel surface as membrane	4
	6	Fibre reinforced concrete elements for walls, floor and ceiling	7
	7	Bathroom with horizontal waterproof steel surface on entire floor	0
Lightweight whole cabins	8	Fibreglass cabins produced as elements	0
	9	Bathroom with horizontal waterproof steel surface on entire floor with cylindrical steel shower unit	3
	10	Bathroom with horizontal waterproof steel surface on entire floor with cylindrical steel shower unit	0
	11	Cabin with lightweight concrete floor and walls with steel studs	4
Heavyweight in situ	12	Concrete floor in situ	0
Heavyweight assembly kit	13	Prefabricated concrete bathrooms floor with 85 cm high walls	1
	14	Fibre reinforced concrete floor element with aerated concrete walls	3
Heavyweight whole cabins	15	Concrete cabins for two apartments	2
	16	Concrete cabins for one apartments	0
	17	Lightweight concrete cabins for one apartments	0
	18	Concrete cabins for two apartments bathroom and kitchen bay	4
	19	“Light” steel/gypsum cabins including bathroom and kitchen for one apartment	2

3.2 *Lightweight Assembly Kit*

Bathroom #4 (Danish Business and Housing Authority [2004b](#)) built on the floor principle of Bathroom #3, focusing on development of walls with steel membranes similar to those existing for floors.



Fig. 5 *Left* Steel surface on entire floor with a reduced height of the edge in the *front right* for a door. The *two white parts* are for the toilet and behind it is the floor gully. *Middle* The folded edge at the assembly between steel floor and wall and the assembly of two steel plates. *Right* Structure of floor with tiles and screed around the floor gully. Pictures from Danish Ministry of Housing (1994)

The prefabricated room-high panels consisted of a steel membrane with calcium silicate boards and tile surface. The wall elements could then be assembled with the steel tub floor with an overlap of 50–100 mm; thus water penetrating into the wall would be led to the bathroom floor in the cavity between the calcium silicate board and the stainless steel plate, as shown in Fig. 6. The watertightness between elements was ensured by applying a neoprene sealant tape on assemblies.

The water installations were placed in service shafts and led to above the ceiling. Water pipes to the shower and washbasin were led through the cavity between the steel membrane and the calcium silicate board. This can be done without penetrations of the membrane.

The concept of Bathroom #5 (Danish Ministry of Housing and Urban Affairs 2001a) was to develop lightweight prefabricated floor elements to be installed directly on the existing floor division and afterwards assembled with lightweight stud walls. The first generation of the floor element consisted of welded steel



Fig. 6 *Left* Section in floor and wall showing where the steel membranes are overlapping. *Middle* Assembly of wall and floor at the door, where the steel height is reduced. *Right* Red painted steel frame above ceiling for fastening the walls steel plates, see marking. Pictures from Danish Business and Housing Authority (2004b)

profiles with integrated slope, onto which a plywood board and steel plate with floor gully and upstand for the wall/floor junction was placed. This first floor was too heavy (>150 kg) and a second generation floor was developed (ca. 50 kg). Furthermore, initial tests revealed problems with the watertightness of the assembly between the stainless steel membrane and the bottom plate, due to different impacts from heat and high pressure during foaming. Therefore, the floor element was designed with only materials of stainless steel.

This second floor element was still a sandwich construction but the steel profiles and plywood were substituted with stainless steel plates at top and bottom with integrated slope and between the plates was polyurethane (PU) foam. The top plate had a slope of 20 mm towards the welded-on floor gully. The floor element had a floor/wall junction to secure watertightness to the lightweight steel stud walls. The walls consisted of two layers of calcium silicate boards and tiles, cf. Fig. 7.

Bathroom #6 (Danish Business and Housing Authority 2002; Danish Ministry of Housing 1997) was developed in two generations (hereafter referred to as #6.1 and #6.2). The bathrooms # 6.1 consist of fibre reinforced elements for floor, walls, corners and ceiling. The elements had a fixed height of 2.1 m; however, the large walls were divided horizontally into two elements due to the weight issue. The elements were assembled with bolts that connected the floor with the ceiling through the corner elements, cf. Fig. 8. The watertightness of the elements was ensured by applying a membrane and tiles. The second generation of the bathroom was an improvement on the solution developed in bathroom #6.1, e.g. reducing the weight and improving the quality of the elements.

The lessons learned from development of Bathroom #6.1 was that the assemblies were sufficiently developed to be used in other projects. However, the finish of the surfaces was not good enough due to the large tolerances between the elements. Furthermore, a reduction in the density of the heaviest elements was needed for improving the working environment.



Fig. 7 *Left* Floor element seen from the top, *Middle* floor gully at bottom plate and *Right* installation of walls to the floor. Pictures from Danish Ministry of Housing and Urban Affairs (2001b)



Fig. 8 *Left* Principle of the shower cabin showing the different elements in the bathroom. *Middle* Fibre reinforced concrete floor element with hole for fixing of bolts. *Right* Bolts above the ceiling for assembling the elements. Pictures from Danish Business and Housing Authority (2002), Danish Ministry of Housing (1997)

3.3 *Lightweight Whole Cabins*

For Bathroom #9 it was required that the solution should be lightweight due to the conditions of the foundation which did not allow heavy bathrooms. The floor, including the concave moulding, as well as the cylindrical shower, was constructed in stainless steel, and was delivered to site as a unit. The floor was kept in stainless steel but glass-blown to give a non-slip surface. The steel stud walls are covered with calcium silicate boards with an applied waterproof coating as the walls have no direct exposure to water, cf. Fig. 9.

Bathroom #11 (Danish Ministry of Housing and Urban Affairs 1998c) was a prefabricated cabin with a floor element of lightweight concrete and walls of steel studs with gypsum and calcium silicate boards. It was a precondition that the cabin

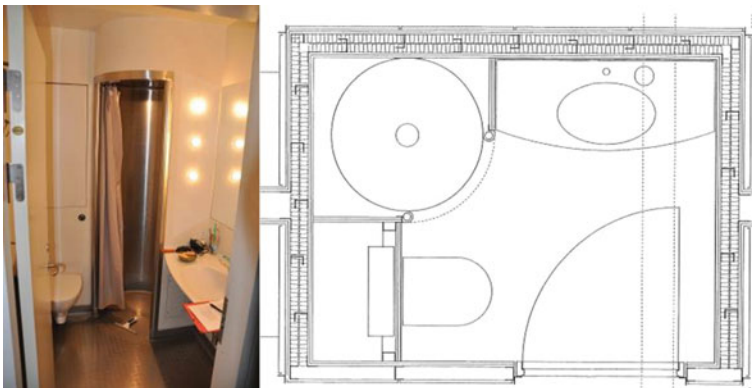


Fig. 9 *Left* Picture of the bathroom after approximately 20 years of use. *Right* Horizontal section of the bathroom. Pictures from Danish Ministry of Housing, Urban and Rural Affairs (1999b)



Fig. 10 *Left* Demolished façade prepared for the insertion of cabins and cabin. *Middle* Installation of cabin. *Right* Cabins after installation with visible installations. Pictures from Danish Ministry of Housing and Urban Affairs (1998c)

could be supported by the existing wooden beams in the floor division. The floor was a reinforced, waterproof concrete slab with a thickness varying from 60 mm at the floor gully to 90 mm at the door. Furthermore, the floor element had a 40 mm plinth onto which the steel stud walls with calcium silicate boards were constructed. On the entire floor and the walls intended to be exposed to direct water impact, a watertight membrane applied in liquid form and tiles were mounted.

The bathrooms were installed by rolling the cabins on the existing wooden beams; however, this required a floor gully with horizontal outlet and the trap placed inaccessible in the service shaft outside the bathroom, cf. Fig. 10.

3.4 *Heavyweight Assembly Kit*

The solution for Bathroom #13 (Danish Ministry of Housing and Urban Affairs 1998a) was to combine a prefabricated concrete floor element—designed as a basin with 850 mm high walls—with prefabricated concrete walls. The elements were installed on the existing floor division. The 850 mm high walls of the basin were determined by the width of the window, through which the elements were brought into the apartments. The inner surfaces had membrane and tiles mounted at the factory except over the joint where the basin and walls were assembled, cf. Fig. 11. The assemblies between basin-walls and wall-wall were the only places that needed waterproofing on site. This was done by applying a liquid membrane (with reinforcement over the joint) covering two rows of tiles.

Bathroom #14 (Danish Business and Housing Authority 2004a) consisted of a fibre reinforced floor element with embedded floor gully and a plinth on to which an aerated concrete wall was built on site. The bathrooms were installed on a new floor division of steel and gypsum, hence the existing kitchens and toilets including the wooden beams were demolished, cf. Fig. 12.



Fig. 11 *Left* Floor element with 850 mm high walls. *Right* Assembly between floor and walls with applied membrane (dark colour). Pictures from Danish Ministry of Housing and Urban Affairs (1998a)



Fig. 12 *Left* Opening in the building after demolishing kitchen, toilet and floor division. *Middle* Inner frame of new floor structure for carrying the bathroom and new kitchen. *Right* Fibre reinforced floor element with a plinth. Pictures from Danish Business and Housing Authority (2004a), Danish Ministry of Housing, Urban and Rural Affairs (1999b)

3.5 Heavyweight Whole Cabins

The solution of Bathrooms #15 (Danish Ministry of Housings 1997) and #18 (Danish Ministry of Housing and Urban Affairs 1999a) was to install two room-sized concrete bathrooms with fully mounted interior fittings. The bathrooms could be stacked on top of each other to form a self-supporting structure that was placed on a new separate foundation in the basement. The system required the roof and floor divisions to be demolished to make room for the cabins in the building, cf. Fig. 13.

Contrary to Bathrooms #15 and #18, Bathroom #19 (Danish Ministry of Housing and Urban Affairs 1998b) was constructed as a light structure of steel studs and gypsum boards. Each cabin was constructed with walls, floor and ceiling

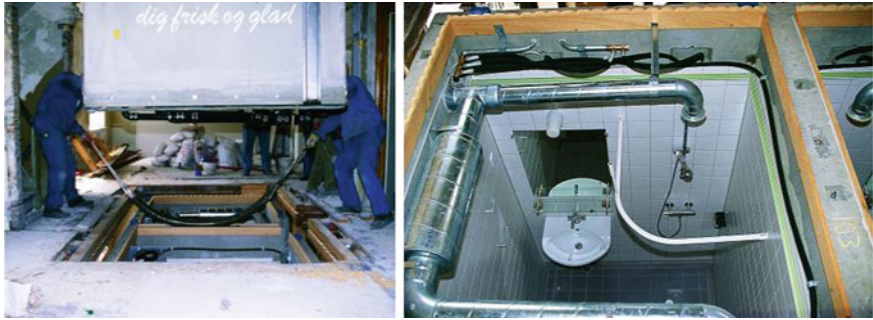


Fig. 13 *Left* Installation of two cabins as Bathroom #15 with placing of apartment boundary in the middle. *Right* Installed Bathroom #15 cabin seen from above. Pictures from Danish Ministry of Housings (1997)

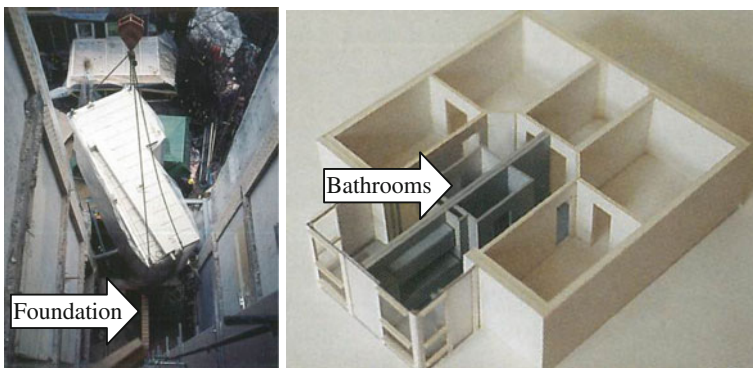


Fig. 14 *Left* Installation of a kitchen and bathroom. At the ground, a brick foundation can be seen. *Right* Principal sketch of the kitchen placed in a bay and the bathroom inside the apartment after renovation. Pictures from Danish Ministry of Housing and Urban Affairs (1998b)

elements combined with rigid corners. Furthermore, the solution was a cabin that also included the kitchen and not the neighbouring bathroom as was the case for Bathrooms #15 and #18, cf. Fig. 14. The surfaces were covered with tiles on floor and walls, and similar to the cabin shown in Fig. 13 right.

4 Systematic Field Investigation

A systematic condition assessment was developed for inspection of the bathrooms. The condition assessment related to damage investigation and described the procedure used for field investigation of bathrooms. An inspection scheme was developed based on the methodology described in Nordtest Report (Brandt 1997).

The methodology was developed in order to reveal normally seen defects in bathrooms, thus a consistent evaluation of each bathroom was achieved independent of the investigator. By means of the scheme, visual inspections were performed systematically to register the conditions and damage of several predefined items.

The items included in the condition assessment are listed as bullets, and an excerpt of the inspection scheme is given in Table 2.

- Bathroom layout, number of users, size, photos
- Constructions—flooring, wall covering, ceiling, doors and windows as well as construction configuration
- Installations—water and drainage including pipe penetrations, electrical, ventilation and service shafts
- Measureable conditions—e.g. moisture content in wooden items and cracks in tiles

The systematic condition assessment included a five-step ranking of condition and interrelated degree of consequence for the structures and installations, as shown in Table 3. The ranking was conducted for floor, walls, ceiling, doors/windows, building services in bathrooms and service shaft. Furthermore, the inspection scheme included a plan drawing of the bathroom and other general information, e.g. size and users.

The bathroom inspections were conducted in randomly chosen apartments, where the only criterion was that the bathrooms were constructed during Project Renovation. The inspector was independent and unconnected with the property and apartments, and therefore no destructive investigations were conducted. However, moisture content in wood and crack width and length was measured, if appropriate.

Table 2 Excerpt of an inspection scheme for a flooring assessment

Subject	Condition	Assessment/observation
<i>Floor</i>		Tiles small
Surface material condition	2	One tile cracked at gully
Watertightness of floor and wall	0	
Basin	0	5 cm, approx. 3 cm resilient silicone sealant
Joints/welded joints	0	Resilient silicone sealant at arc-corner and floor/wall
Resilient silicone sealant	1	Modest mould growth
Surface easy to clean	1	Small tiles
Position of floor gully in proportion to wall	0	
Slope on floor, even, back fall, towards floor gully	0	
Loose tiles/floor covering	0	
Suitable floor covering for underlying structure	0	

Table 3 Ranking of condition and interrelated degree of consequence for the inspected structures and installations

Condition N/A	Not applicable or it is not possible to do the inspection
Condition 0	Very good: No signs of abnormal wear or damage
Condition 1	Good: Need for minor maintenance
Condition 2	Bad: Need for maintenance and minor repair
Condition 3	Very bad: Visible symptom of failure or damage repair needed

If possible, inspections were conducted in three bathrooms for every type of bathroom. The chosen bathrooms were selected based on the occupant's willingness to participate in the project. This random selection was considered sufficient to obtain bathrooms with different use patterns and damage.

5 Lesson Learned from Inspection After Approx. 20 Years of Use

For the bathrooms with an age of approximately 20 years, the general quality is high compared with traditional bathroom built in situ. 35 bathrooms were inspected of which 27 were smaller than 3.25 m², and on average the bathrooms were used by 1.7 occupants with a maximum of three occupants. All the bathrooms were designed as a basin with at least 30 mm difference from threshold to floor gully and equipped with mechanical ventilation. Some of the bathrooms also had windows. These issues correspond with the requirement for bathrooms built in 2015.

The failures reported by Eriksen et al. (1991) from surveying 44 newer bathrooms their two most critical failures were leakage at pipes passing through wall, floor and ceiling as well as joint defects. From our inspections the most critical failures registered were mould-infested resilient silicone sealant, cracks and holes in wall and floor covering as well as issues related to the service shaft.

Many of the failures registered could have been avoided with increased maintenance, e.g. replacing tiles with cracks and resilient silicone sealant infested with mould growth. One reason for the high quality of the bathrooms relates to their layout, where the wet zone is separated from critical assemblies, e.g. doors, and moisture sensitive materials such as wooden panels are kept in the moist zone instead of in the wet zone. Another reason for the bathrooms' high quality can be explained by the watertightness test that was conducted during the development process of several of the bathroom types. If the test failed, changes to the bathroom design was made and hence the installed bathrooms are in principle with documented and improved watertightness.

5.1 Cracks and Holes

In many of the bathrooms small cracks and holes were observed, however, these minor defects are assessed not to be significant, because the watertightness is not affected—mortar joints are not waterproof. These defects were often found in the wet zone, i.e. where they are exposed to water. In a few cases, cracks caused by movements were also seen and these cracks were close to exterior walls, however, not in the shower unit.

In bathroom #14, a heavyweight assembly kit of fibre reinforced concrete bottom with a plinth, perhaps the most critical crack was registered. In the three surveyed bathrooms on top of each other, a crack was registered at different places on the wall in the shower unit, about 30 mm above the floor. This crack might be related to the plinth on the bottom element, cf. Fig. 15, and caused by movements in the building, even though a new steel frame was constructed for the bathrooms and kitchens, cf. Fig. 12.

5.2 Mould Growth

Mould growth was seen primarily on resilient silicone sealant, which was applied in the assemblies between walls and floor or around floor gully. The mould was mainly present in wet zones with a regular water exposure, i.e. long periods of high relative humidity. The reason for this is that the resilient silicon sealant contains an anti-mould agent, which after 1–2 years will be washed away and mould will start growing.



Fig. 15 *Left* Fibre reinforced bottom plate with a plinth marked with a *black line*. *Right* The *black line* indicates the crack, which was found on different walls in the bathroom above and below the apartment on the picture. *Left* Picture from Danish Ministry of Housing, Urban and Rural Affairs (1999b)



Fig. 16 *Left* Bathroom #4, the corner of the door, wall and floor assembly where the rusty *red* colour is anticipated to be mould growth as it is the same colour as seen on the silicone sealant. *Right* Rusty *red* colour at each corner at the interface of the shower unit and floor, see also Fig. 9

In the bathroom with stainless steel bottom, mould growth was also seen, cf. Fig. 16. This might also be rust, but it was not further investigated.

The influence of mechanical ventilation is important to the indoor environment in these small bathrooms, as most bathrooms are installed inside the apartment not allowing the room to have windows. In several cases, the mechanical ventilation was either blocked or dirty, and therefore not performing satisfactory. This creates an increased risk of mould growth in the bathroom as the relative humidity is kept on a high level for a prolonged time. In one building, three apartments were inspected all connected to the same ventilation exhaust. The one bathroom with a very low ventilation exhaust had dark stains in the ceiling, which is assessed to be mould growth, contrary to the two bathrooms with a high exhaust rate which had no stains in the ceiling, cf. Fig. 17.



Fig. 17 Two bathrooms connected to the same ventilation exhaust, but where the one (*left*) has a *low rate of extraction* and *dark stains* in the ceiling, whereas the other (*right*) has a *high rate of extraction* and *no dark stains* in the ceiling

This risk of mould growth as a consequence of low ventilation exhaust might be related to the occupant's maintenance of the bathroom and the ventilation system, i.e. the fan.

5.3 Service Shafts

A variation of the design of the service shafts was registered, i.e. size of hatches, accessibility and space for future installations, cf. Fig. 18. Access to the installations was not as carefully designed as most of the bathrooms were. In many cases it was very difficult to access the most important installations, which was also mentioned by the operating staff. Only a few of the 11 inspected bathroom types had an alarm system to report if installations leaked. For the heavyweight concrete cabins described in Bathroom #18, drain pipes were led from each shaft to the basement, however, in the basement there was still no alarm system other than a possibility of visual inspection.

It can be questioned whether the visual inspections are adequate for an evaluation of the construction of bathrooms. The inspection did not reveal any underlying failure in the construction of the building, which could have a high economic impact for the occupant or building owner. However, the inspections of the bathrooms are conducted on a uniform basis with a predefined rating system. The developed scheme encompasses the most important items for a conditions assessment of bathrooms. For the 35 inspected bathrooms, the damage seen have not given rise to consider destructive inspections.



Fig. 18 *Left* Access to installations through a hatch in the ceiling. *Middle* A small cabinet gives access to the installations. *Right* Access to the installations through a door in the bedroom

6 Conclusion

The inspections led to the conclusion that in general the conditions of the 35 inspected bathrooms were good considering their age of approximately 20 years. All bathrooms were designed as a basin and the shower area was placed away from areas with moisture-sensitive materials or critical assemblies.

The resilient silicone sealants were often observed to be infested with mould growth especially in the wet zone. A number of tiles were observed to have cracks or holes from screws (mainly on walls) and in a few cases cracked tiles were observed close to the floor gully. Finally, it is concluded that mechanical ventilation is important for bathrooms placed in the middle of apartments to ensure the extraction of moist air, hence decreasing the risk of mould growth.

However, as only visual inspections were undertaken, a need for a destructive investigation might be needed in some cases where the reason for the damage is not clear.

Acknowledgments The research is financially supported by the Landowners' Investment Association. This support is gratefully acknowledged. Furthermore, we would also like to thank Johan Elsass Nørby from The building damage fund for urban renewal for all the help provided for this study; ranging from help collecting literature, finding contact information and assisting on building inspections. Finally, we would like to express our appreciation to all the people making the inspections of bathrooms possible.

References

- Brandt E (1997) Systematik til feltundersøgelse af baderum (English: Methodology for field investigation of bathroom), Nordtest report: NT techn report 366. Nordtest, Espo
- Brandt E (2005) Reduced service life due to common failures in Denmark. 10DBMC International Conference on Durability of Building Materials and Components. Lyon, France, 17–20 Apr 2005
- Brandt E (2008) Service life of light weight bathrooms. 10DBMC international conference on durability of building materials and components. Istanbul, Turkey, 11–14 May 2008
- Brandt E, Morelli M (2015) SBI-anvisning 252: Vådtrum (English: SBI Guideline 252: Wet room). Danish Building Research Institute, Aalborg University, Copenhagen, Denmark (in Danish)
- Brandt E, Nielsen CW (1991) SBI-anvisning 169: Gulve og vægge i vådrum—i nye boliger og ved renovering. (English: SBI Direction 169: Floors and walls in wet rooms—in new dwellings and in connection with renovation.). Danish Building Research Institute, Hørsholm, Denmark (in Danish)
- Brandt E, Møller EB, Hansen EJdP (2011) Reduced service life of bathrooms due to leaks Around Floor Gullies and Pipe Penetrations. 12DBMC International Conference on Durability of Building Materials and Components. Porto, Portugal, 12–15 Apr 2011
- Danish Business and Housing Authority (2002) Komponentbadeværelser-2—PL Box lette komponentbadeværelser i fiberbeton (English: Component bathrooms 2—PL Box light-weight component bathrooms in fibre reinforced concrete), Project Renovation report no. 281. Copenhagen, Denmark (in Danish)
- Danish Business and Housing Authority (2004a) Let façade-og etagedæk-system til renovering (English: Simple façade and floor division system for renovation), Project Renovation report no. 290. Copenhagen, Denmark (in Danish)

- Danish Business and Housing Authority (2004b) Rationel, let byfornyelse (English: Rational, simple urban renewal), Project Renovation report no. 157. Copenhagen, Denmark (in Danish)
- Danish Ministry of Housing (1994) Lette baderum (English: Light bathroom). Copenhagen, Denmark (in Danish)
- Danish Ministry of Housing (1997) Komponentbadeværelser (English: Component bathrooms), Project Renovation report no. 015. Copenhagen, Denmark (in Danish)
- Danish Ministry of Housing and Urban Affairs (1998a) Præfabrikerede lave baderum (English: Prefabricated low shower room), Project Renovation report no. 194. Copenhagen, Denmark (in Danish)
- Danish Ministry of Housing and Urban Affairs (1998b) Tårnelementer—præfabrikerede rumstore tårnelementer (English: Tower elements—prefabricated room sized tower elements), Project Renovation report no. 234. Copenhagen, Denmark (in Danish)
- Danish Ministry of Housing and Urban Affairs (1998c) Vandret indbygning af præfabrikerede lette badeværelser (English: Horizontal building-in of prefabricated lightweight bathrooms), Project Renovation report no. 260. Copenhagen, Denmark (in Danish)
- Danish Ministry of Housing and Urban Affairs (1999a) Badetårn—Badeværelsestårn med køkkenkarnap (English: Bath tower—bathroom tower with kitchen bay), Project Renovation report no. 283. Copenhagen, Denmark (in Danish)
- Danish Ministry of Housing and Urban Affairs (2001a) Lette præfabrikerede badeværelselementer: Lette stålunde (English: Lightweight prefabricated bathroom elements: lightweight steel bottom). Copenhagen, Denmark (in Danish)
- Danish Ministry of Housing and Urban Affairs (2001b) Lette stålunde (English: Lightweight steel bottom). Copenhagen, Denmark (in Danish)
- Danish Ministry of Housing, Urban and Rural Affairs (1999b) Vådtrum—Bedre brug af gode totalløsninger for opbygning af bade- og wc-rum (English: Wet room—better use of good overall solutions for construction of bath- and wc-rooms), Project Renovation report no. 242–02. Copenhagen, Denmark (in Danish)
- Danish Ministry of Housing, Urban and Rural Affairs (2004) Projekt renovering—5 årseftersyn (English: Project renovation—5 years inspection report). Copenhagen, Denmark (in Danish)
- Danish Ministry of Housings (1997) Badekabiner (English: Shower cabins), Project Renovation report no. 021. Copenhagen, Denmark (in Danish)
- Eriksen SS (1998) SBI-anvisning 180: Badeværelser: Eksempler på planlægning, projektering og udførelse af badeværelser i nye og gamle boliger. (SBI Direction 180: Bathrooms: Examples of planning, design and construction of bathrooms in new and old housing), Danish Building Research Institute, Hørsholm, Denmark (in Danish)
- Eriksen SS, Hommel-Hansen O, Nielsen CW, Ovesen K (1991) Nye vådrum i gamle boliger. Erfaringer fra en undersøgelse af 44 nyere vådrum. SBI-meddelelse 87 (English: New wet rooms in old apartments. Experience from an investigation of 44 new wet rooms. SBI Communication 87). Danish Building Research Institute, Hørsholm, Denmark (in Danish)
- Kjerulf K, Brandt E, Nielsen PA (1984) SBI-anvisning 109: Bygningers vådrum. Gulve på træbjælkelaag og beklædninger på skeletvægge, 3rd edn. (English: SBI Direction 109: Wet rooms in dwellings. Floors on wood joists and linings on stud walls). Danish Building Research Institute, Hørsholm, Denmark (in Danish)

Good Practice: Analysis of the Vulnerability of Seven Churches in Monza. From an Information Model to a Geodatabase

Cecilia Bolognesi

Abstract The topic regards a project submitted for funding, and then realized, with a plan of action to “promote the rationalization and renewal of Cultural Heritage”. The project’s proposal is the promotion of good practice in the prevention and preservation of historical and architectural heritage (Bandi Cariplo 2013). It is about some historic churches of the city of Monza, where the religious buildings occupy a prominent place in the central area; owing to their visibility, historical and artistic importance, cultural and social value and appreciation of the services provided the preservation of these building is a public theme. The writing describes the whole method taken on the organization of a contest to select researchers and the outline of a method to be followed/the identification of precise degeneration of the building to be studied/the selection of researchers appropriate to the specific themes previously identified/the organization of the researches/the organization of the results in a national database/the construction of a 3D model/the use of a 3D model as database for information itself.

Keywords Best practice · Survey · Risk map

1 The Project as a Method

This is the description of the method adopted by a project submitted for funding by the Association of Engineers and Architects of Milan¹ on a specific theme: the analysis of the vulnerability of seven churches in Monza and the project of their maintenance, renovation and collection of information in a db. The adopted method

¹<http://www.collegioingegneriarchitettimilano.it>. It is a voluntary association of Engineers and Architects devoted to diffusion of the project’s culture.

C. Bolognesi (✉)

Department Architecture, Built Environment and Construction Engineering—ABC,
Politecnico di Milano, Milan, Italy
e-mail: cecilia.bolognesi@polimi.it

was divided into different phases: (1) a preliminary phase with a panel of experts for a first collection of interesting building with architectural peculiarity spread in the centre of the town; (2) a first check of the macro problems regarding each specific building; a possible list with the possible researches required before planning the conservative interventions; (3) the organization of a contest for the selection of study groups specialized in heritage with ability in databases and connections between data sheets and portals, the groups where chosen to obtain materials and information regarding the churches, each of the studies with an attention to the specific damage; (4) an in-depth selection for further investigations such as the approval of the static calculations for a bell tower, thermography images for diagnostic purposes, 3d model obtained with laser scanner and photogrammetry to survey damages during the years, measurement of repositioning of the structure with beating radar; and (5) the additions of all the studies into a national Data Base,² la Carta del Rischio, where are included all the monuments aim of the study in Italy.

The project's goals are:

- start the study of churches and holy architectural complexes, which are the most significant in the urban area of Monza, in order to plan the interventions of maintenance according to their needs;
- give a first implementation of the “Guidelines for the assessment and reduction of seismic risks of the cultural heritage in line with the new technical standards for construction [d.m. 14/01/08]” (2008) particularly with regard to the knowledge of the cultural object and the simplified models for the evaluation of seismic safety;
- carefully classify the damage and any vulnerabilities with a superior level of analysis than the simple visual one, through the use of instrumentation choice depending on the specific pathologies;
- share the knowledge on a platform of free information for all the experts such as “La Carta del Rischio” (appointed Risk chart then); and
- verify new possibilities of sharing data through 3d models, as vehicle of information added.

2 The Architectures

The scientific committee was aimed at the definition of the research lines of the study of churches and architectural complexes built between the eleventh and twentieth centuries in order to formalize a preliminary proposal for monitoring and planning the conservation.

²La carta del Rischio: <http://www.cartadelrischio.it/>.

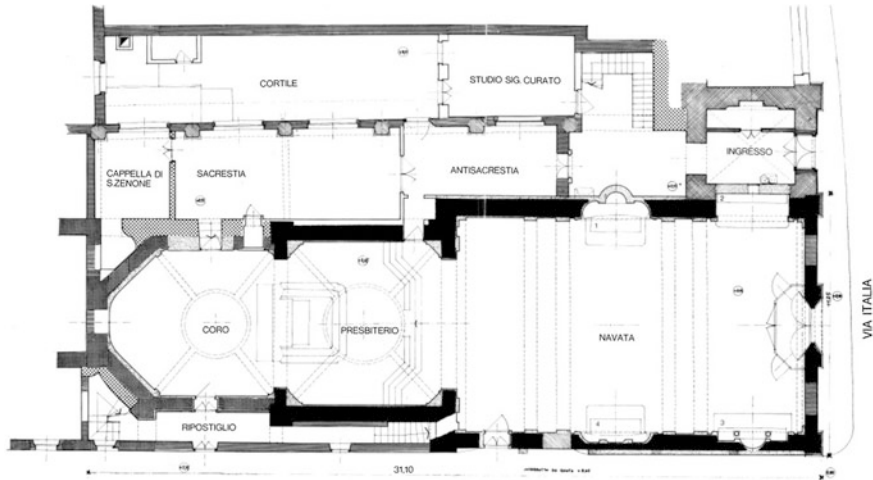


Fig. 1 Plan of the church of Santa Maria in Strada with location of different walls according to different periods: (S. Maria in Strada, 1925) the *black ones* the most ancient of the original building

The object of the study was located in terracotta bricks and buildings built with this material; the reason of the choice is the dissemination of the material and construction technique throughout Lombardy, in a geographical area bordered by the rivers Ticino, Adda and Po, which provided for centuries the raw material for its production.

Seven churches were identified:

- “Santa Maria in Strada” (see Fig. 1); it has a façade in brick and ashlar moulded fabric; it was built in the fifteenth century on a former convent of the Franciscan Friars called “Penance”. The construction was begun in 1357. Next to the church is a small cloister. At the very beginning it was a single rectangular hall with a plain apse and a truss ceiling. During 1421 it was enlarged and enriched with a choir, the sacristy and the bell tower.
- “San Giovanni Battista”, Monza’s Cathedral (see Fig. 2); it was built mainly between fourteenth and sixteenth centuries with texture walls of eras from the tenth century to the fifteenth century in mixed blocks of local stone furnace; the cathedral preserves the famous Iron Crown which, according to tradition, contains one of the nails used for the crucifixion of Christ. The church recognizes it with a value of a relic, which is the reason why it is preserved in the church in a famous and renovated chapel. The cathedral is classified as a complex asset formed by the church itself, the bell tower, the cloister and the Lombardic tower. Each single element was studied by itself and well classified in the risk chart.
- Dominican San Pietro Martire: a church built in local ashlar facade and colonnades; the church of St. Peter Martyr is a fourteenth-century church of Monza. The first news of the church go back up to 1369, but it is very likely that

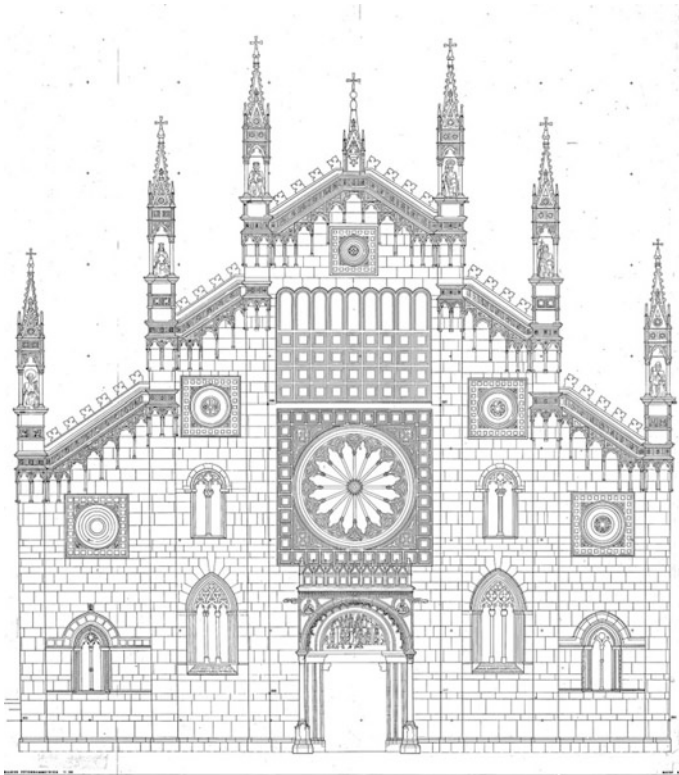


Fig. 2 The cathedral: main elevation. This drawing is a part of an elevation survey already done in 2000 and now in the “Historical archives of Diocesi” previous study. It is one of the documents uploaded in the platform of the Risk chart

the building is even older. The original apse was rebuilt in 1645. In 1776 the adjoining convent was suppressed. The apse was amended again in 1817 and the same year was also remodelled the belfry. The building underwent further changes during the twenties of the twentieth century. From the left nave a door leads into the cloister of the fifteenth century.

- Carrobiolo (see Fig. 3): it is a complex asset too, the church, the convent and the bell tower, where the buildings are stratified with baked brick ashlar plastered ever since the seventeenth century; the first church of Santa Maria del Carrobiolo belongs to the community of the Humiliated and dates back to 1232; in that year the archpriest of Monza authorized the construction of a chapel dedicated to God and to the Virgin. In 1571 the order of the Humiliated was suppressed by Pope Pius V: the complex of the church and its convent was assigned to Barnabite Fathers that, in 1573, began to renew it, whilst maintaining the structures of the church, the bell tower and the cloister. In 1584 San Carlo Borromeo consecrated the temple and many of the works of remodelling followed.

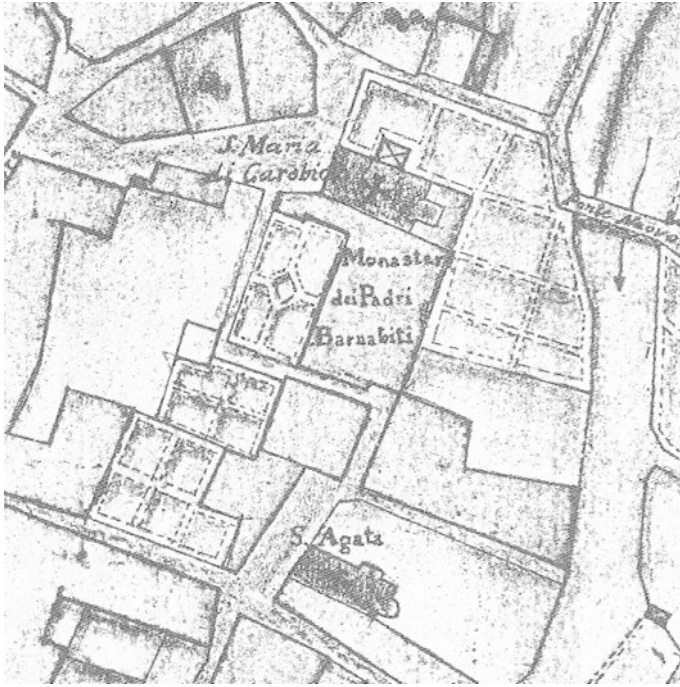


Fig. 3 Historical map of the complex of Carrobiolo. One of the files uploaded in the platform of the Carta del Rischio, Historical section. It is part of a map of 1721 from Giovanni Filippini, then redrawn in 1738 by Carlo Porta (Filippini 1722)

- “San Maurizio” Monastery (see Fig. 4), former Santa Margherita’s: it has a brick façade; and it is a reconstruction of the eighteenth century; the present building stands on the site of the former monastery of Santa Margherita (Gaeta 1787), founded by Humiliated in the thirteenth century and occupied by the nuns of the order. In 1469 a new church dedicated to the holy Margaret and Catherine occupied the site of the mediaeval oratory (Bertotti 1836). The monastery is famous for the story of Marianna de Leyva (1575–1650), the nun of “Promessi sposi”. In 1736, it was necessary for its complete revision. In 1785, the monastery was demolished and the church desecrated; various buildings in the complex were sold. The cloister is partly demolished and then, from 1956, a private residential building occupies most of the surfaces of the ancient monastery.
- “San Rocco” is a Parish Church made in the modern era with terracotta; it was built in the twentieth century; according to some documents in the place there was a chapel whose construction dates back to 1402. In 1848 the parish was created and the actual construction began in 1931.
- “Santa Maria of the Angels” is a church built in the early seventeenth century in Baroque style. It was destroyed and rebuilt in neo-Gothic style in the late nineteenth century.

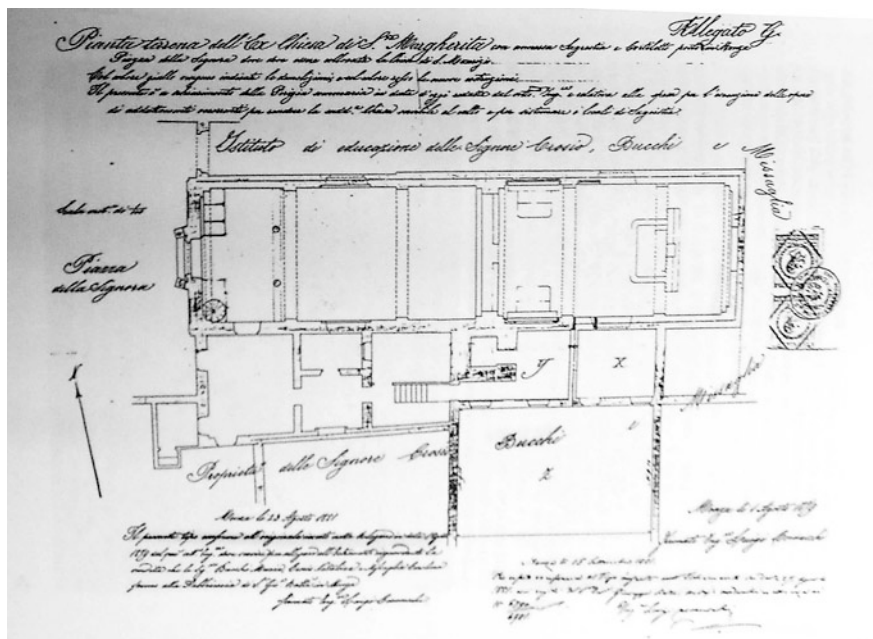


Fig. 4 Plan of the church of San Maurizio in a document of 1879 now in “Historical archives of Diocesi” of the Dome, the author is Cernuschi L 1879

3 The First Data Collection

The proposed case, therefore, becomes a case study model to plan the conservation of many Lombard urban centres, their architectural heritage, during a considered period of time, which embraces about one thousand years of history; it allows a systemic study reactions in the works according to the different parameters, and gives an indication of the brick structures’ dynamics evolution in a frame of reference for buildings with similar constitution or construction period.

Dealing with this specific theme, the project’s study was examined in several buildings, through the following main aspects:

- the dressed stone’s size and appearance used in different eras;
- the mortar junction’s composition and the consistency;
- the construction technique of the building obtained through the arrangement and composition (Opus) of segments;
- the static and structural features, obtained with state of the art materials used;
- the degradation problems from fatigue and ageing of the materials;
- the problems of degradation due to environmental causes and to exceptional events of a physical nature or man-made;
- the setting up of a systematic and coordinated monitoring instrumental;

- the proposal of ordinary and extraordinary maintenance and restoration that can be applied.
- the possibility to share the study and the various artefacts in order to plan the conservation and valorize the sites for tourism.

The first step of the research was to create a dossier for each monument with previous and new documents; some data already processed and stored in different archival locations were divided into the following:

- essential data for identification;
- historical researches in archives: contracts, documents...;
- floor plans, design documents, drawings, photographs, ...;
- macroscopic analysis, in relation to the object of investigation, the type of material, size, appearance, quality and quantity;
- investigation of the chemical and physical processes, depending on the type of 'opus' adopted;
- survey campaign of macro- and micro-climatic factors with particular attention mapping temperature and humidity; and
- collections of structural movements;

The main intention was to add to these studies all the other causes of degradation, stratified by historical periods, in order to assess the influence of particular and contingent facts.

Each building was specifically investigated and for everyone was given the assessment to fill in the Risk chart, in addition to the collection of materials from the previous databases. The goal was to complete the study and data acquisition, to enrich the knowledge of these monuments focused on the fired clay brick, to organize the criteria of operational methods of restoration or plan projects to prevent and correct the identified risk factors, but also to use and possibly renew the way to collect data not only with a public informatics platform.

4 The Deeper Investigation

The main risks on territory of Monza and Brianza, what damages the building in its static and decorative components, are a series of reasons as follows:

- Seismic risk (moderate);
- Hydro-geological risks (floods, changes in the level of groundwater);
- Climatic risk (winds, rain showers, winter frosts);
- Micro-climatic risk (variation of thermal factors in relation to moisture, microclimate altered by infiltration, condensation, lifts, prolonged exposure to the sun); and
- Anthropogenic risks (pollution, direct modifications, environmental changes).

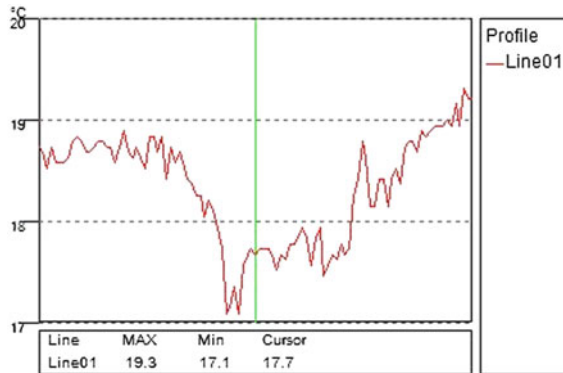


Fig. 5 The graph shows the thermal linear trend in temperature between the surface in good state of preservation and the area with the presence of moisture, with a thermal gradient of about 2 °C

The proposed methodology offered monitoring of the factors of potential deterioration of the goods, or direct (temperature and humidity mapping, micro-movements), or discrete (see Fig. 5).

In this second case, a periodicity default (laser scanner on major points to be checked, ambient vibration-based investigations) needed a systematic collection of the results to be correlated in a database (see Fig. 6).

The investigations planned were different. This method allows improving the predictive capabilities on the degradation of structures and time schedule for the conservation interventions. The aim is, between others, an appropriate standardization of the model collection that will allow, in the future, extending to a large number of buildings the acquisition of the data to compare the evolutionary dynamics over time, with considerable economic savings and increase the reliability of forecasting models.

Specifically, each church was examined by the scientific committee of the competition; the question was which parts of the building needed a deeper investigation and what about the instruments needed in relationship with its peculiar state of being.

Two examples before the others are Santa Maria in Strada and San Pietro Martire.

The thermographic investigations conducted within the church of Santa Maria in Strada in Monza were conducted with the aim to verify from the presence of moisture due to capillary rise within the structure to phenomena of infiltration by the roof covering.

The vault appears with localized abrasions of the painting. It is protected by a net installed to prevent falls of parts; it runs longitudinally. On the surface you can notice the effects of a probable infiltration of meteoric water from the roof. Mural decoration presents abrasions localized area, moisture stains and whitening. The scientific committee decided for a thermographic monitoring that started in May 2014. To evaluate the environmental changes inside the building temperature

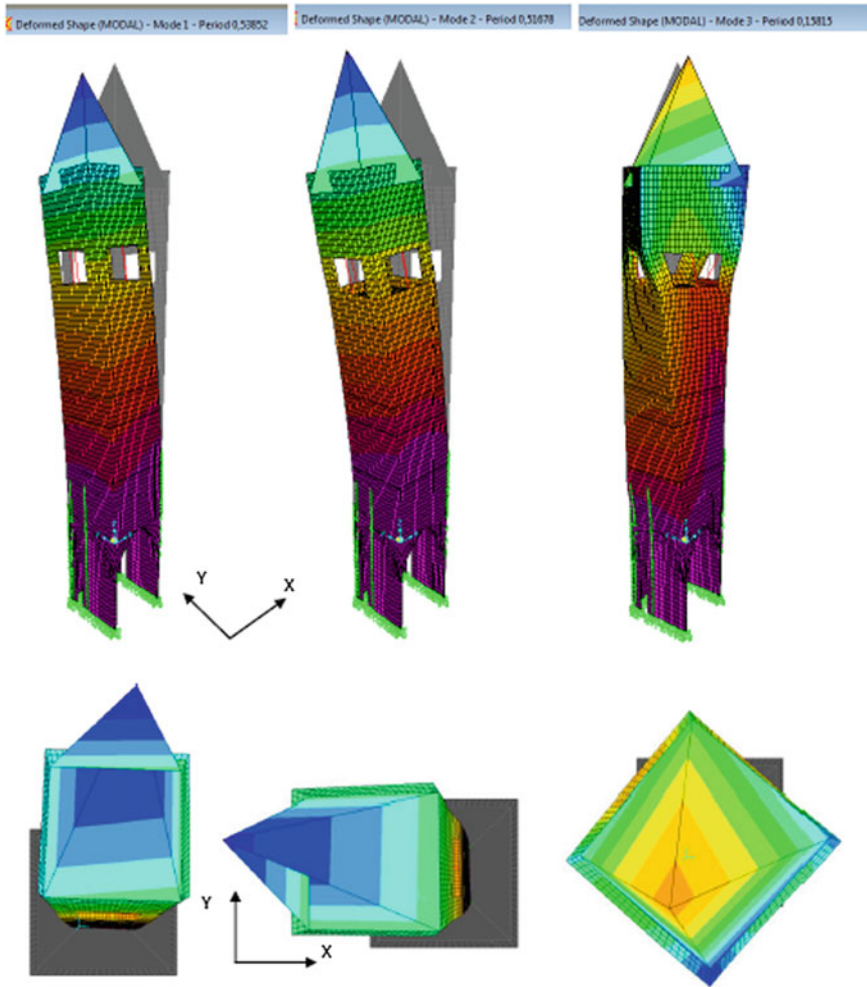


Fig. 6 This image comes from the exam of the static and seismic bell tower played by the group of L. Jurina. The *picture* shows the first three modes of vibration, in the Y-direction (MODE 1), i.e. along the axis of the church, in the X-direction (SO₂), which is perpendicular to the axis of the church, and torsional (MODE 3)

detectors and data logger were placed. The aim was to monitor the cyclical variations in relation to climate change external.

Relevant weather data of the year 2013–2014 registered for the city of Monza were also collected and graphed relevant.

The thermographs were executed passively, in conditions of stability of the structure with the surrounding environment. The thermal images observed distinctly shown and clearly defined by the perimeter, and demonstrate in the vault an area at a lower temperature than the surrounding area.

The presence of moisture in the structure is due to an active infiltration of rainwater from roofs.

In San Pietro Martire the bell tower needed an investigation on the structural conditions. A specific assessment procedure was organized including full-scale ambient vibration testing, modal identification from ambient vibration responses, finite element modelling and dynamic-based identification of the uncertain structural parameters of the model (Gentile, Saisi 2011). A good match between theoretical and experimental modal parameters was reached.

The tower is characterized by the presence of major cracks on the load-bearing walls and the need to produce checks was recommended by the presence of these obvious vertical cracks in the walls. These cracks are possibly attributable to excessive vertical stress of the masonry at the base of the tower. Loads transferred from the vault and the arch itself adds up. The only 50 cm of masonry below the arch are not adequate to transfer vertical loads in the foundation of the entire north face of the tower. The horizontal thrust of the arches is not countered by the presence of neither spurs nor chains. In order to achieve an adequate level of knowledge of geometrical and mechanical parameters of the existing masonry, some diagnostic tests were conducted, as much as possible non-invasive and non-destructive.

The cathedral of San Giovanni Battista has a main importance among the chosen monuments. Given to the historical significance of the building analysed, and the significant documentation, some specific choices were made, with the aim of offering an overview of the building as much as possible complete and comprehensive.

The identification of the material to be included in the Risk chart preferred selected technical material dating from the last two decades (especially reports, data static monitoring and consolidation work performed), not available in the traditional bibliography of the Dome. These materials are plenty and full of information: the risk is that such richness is not considered in its entirety and remains unknown: from here the necessity of a db such as Risk chart.

The main areas of intervention in the Dome in recent decades are as follows:

- Rebuilding of the roof;
- Adoption of an anti-dampness;
- Structural consolidation of the bell tower in successive batches, according to the plan by prof. Claudio Modena;
- Consolidation Tower Structural Lombard, according to the plan by Prof. Lorenzo Jurina (see Fig. 7); and
- Renovation and retrofit of technological systems.

After the collections of historical or recent documents an inspection was carried out in situ, in order to identify any weaknesses and vulnerabilities in the building.

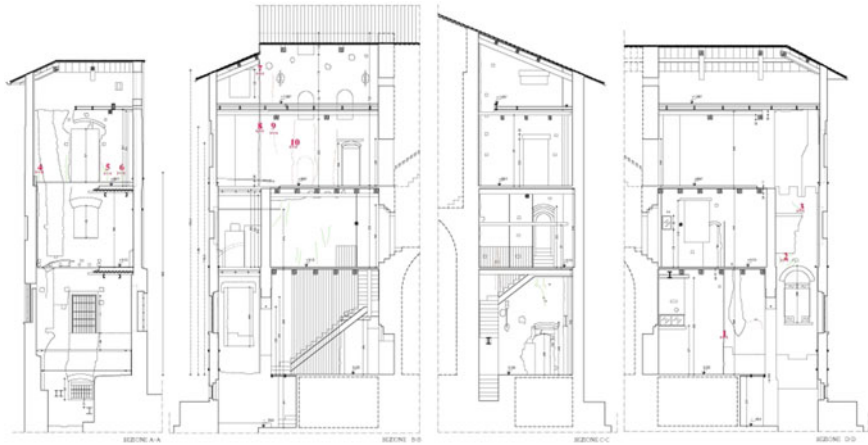


Fig. 7 Consolidation Tower Structural Lombard, according to the plan by Prof. Lorenzo Jurina; one of the documents collected in the Carta del Rischio

The following aspects were considered:

- Visible structures: the structural elements for inspection reports on any past or current instability;
- Decorations: the decorative elements were analysed in order to point out any degradations disseminated; and
- Facilities: we assessed the consistency of the electrical, water and security, based only on visual inspection and documents archive.

From the point of view of structures, it was observed how the interventions of consolidation performed in recent past “froze” the situation of instability that had occurred, especially the Bell Tower and the Lombardic Tower.

However, it was noted the presence of some cracks found in the attic and in the sacristy.

4.1 The Specific Case of the Church of San Maurizio

Specifically, the church of San Maurizio proved to be the most relevant case from the point of view of the deterioration hygrometer consequences of detectable damage on the state of the frescoes, plaster and wooden structures. In the case study of the church of San Maurizio, the following surveys have been done: essential data identifying, historical research, laser scanner survey of the interior, photogrammetric survey of the wall and vault, thermographic analysis and specific structural calculation.

The church of San Maurizio in Monza is located on the site of the former monastery of Santa Margherita, founded by Humiliated in the thirteenth century and occupied by

the nuns of the order. [Documents in public and private libraries.] In 1736 the early eighteenth century the church pours in a precarious state of preservation, so as to make need her makeover in 1736, since the monastery was suppressed and deconsecrated in 1785, which was followed by the construction of various buildings around the building. Since 1881 the church belongs to the Cathedral Monza, who transferred the dedication of the ancient nearby church of San Maurizio, demolished previously. The interior of the church has a single nave and preserves paintings of the church of Santa Margherita that the demolished church of St. Maurice, in addition to successive decorations added in the eighteenth century (Filippini 1722).

The survey of the interior of the church was carried out using laser scanner (Leica HDS7000) and photographic camera (Canon 5DMarkIII, lens 35 mm).

The survey required three days in the field and about 2 weeks for processing data.

The elaborations are the final result of the survey executed from the floor level and it was not possible to have scaffolding or other means to get up.

The laser scanner survey was carried out by setting a scan resolution of 3 mm–10 m, ensuring in this way a medium resolution on the object of about 5 mm; this resolution allows restitution to a 1:20 scale. It was necessary to acquire five different scans, to complete, without holes, the model of the whole church (see Fig. 8). The targets, appropriately placed, allowed the correct georeferencing of point clouds and then the creation of a single point cloud describing the interior of the church.

The availability of the 3D model in point cloud format allows the extraction of information anytime, at a later time to the survey itself (see Fig. 9). You can make simple measurements of distances and 3D coordinates.

At the same time the laser scanner survey was done by a photogrammetric survey (see Fig. 10). We acquired about 700 images, respecting the restitution to a maximum scale of 1:20. To ensure proper illumination of the church has been

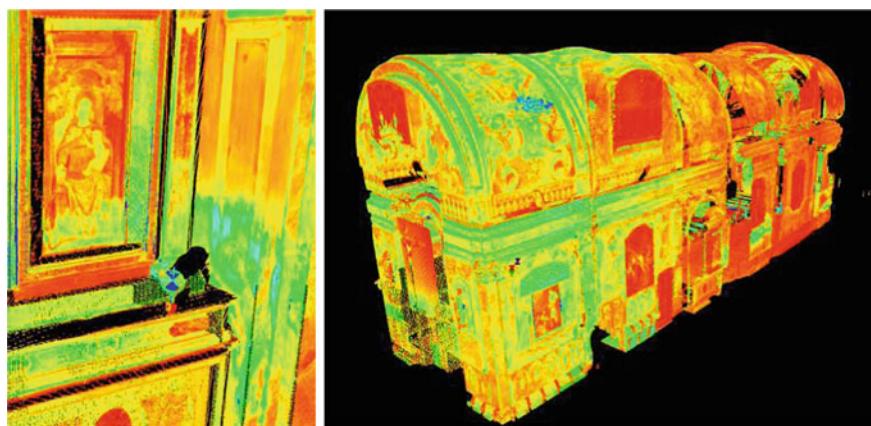


Fig. 8 One of the five scans, one of the targets used for the alignment of the scans and the cloud complete

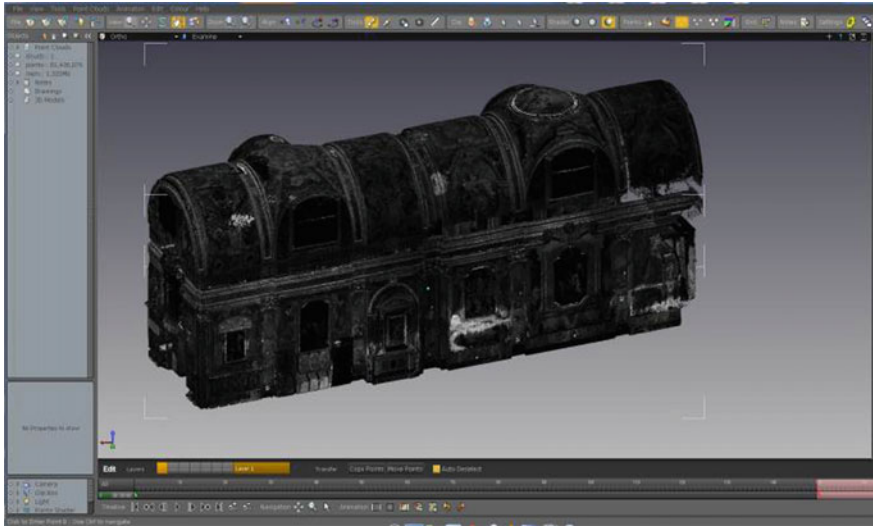


Fig. 9 The complete point cloud of the church's interior (software Bentley Pointools), to the right a distance measurement directly on the model



Fig. 10 North elevation: photogrammetric survey

employed a professional lighting system (Faro Sirocco2, Airstair international, 575 W HMI) that generates uniform illumination with light calibrated 5600 K constant. This allows restitution with faithful colour and shadow reduction. From the photogrammetric model were extracted orthophotos of the four walls and the vault (see Fig. 11).

The conservation status of the nave of the church is rather problematic, especially in the lower part of the walls, in which are present murals with volutes and frames that have been visibly recovered and repainted. These have undergone in the last century, the intervention detachment and relocation of wall decorations, that you do not currently have the information and documentation (see Fig. 12).

Probably, the surgery was performed to try to solve previous problems of rising damp which, unresolved, recur over time. On the lower part of the walls was placed



Fig. 11 Orthophoto of the vault



Fig. 12 North elevation

a marble plinth which has brought the level of capillary rise at a greater height for venting against moisture evaporation.

The main degradation phenomena visible in these areas are caused by the spread salt efflorescence, led to bleaching superficial abrasion of the paint film and gaps of the layers of plaster. One can observe how all these phenomena are localized mainly along the edges intervention detachment relocated, making it particularly recognizable compared to the top of the walls.

Through the gaps in the plaster it was possible to observe the stratigraphic succession of detachment: on a tarred sheet, applied on the substrate as brick, were made more layers of plaster in which was immersed a metal mesh to stiffen the structure on which the painting was relocated mural.

The layers that constitute this structure are gradually losing adhesion and cohesion, because of the persistent humidity and the related phenomena. In particular, the network mechanical is oxidized and presents with gross distortion due to the efforts of tension and the weight of the structure.

The north wall of the oriented nave shows itself in a worse state of conservation, especially the third span, in which there are serious problems of detachment and where the paint film is extensively abraded (see Fig. 13). The same phenomena are also visible in the first span of the same side.

The south wall shows an initial level of degradation, but with phenomena similar to the wall opposite.

The general state of profound deterioration in facing the property has decreed the choice of a relief with laser scanner for a presentation of the state of the artefact on the present day.

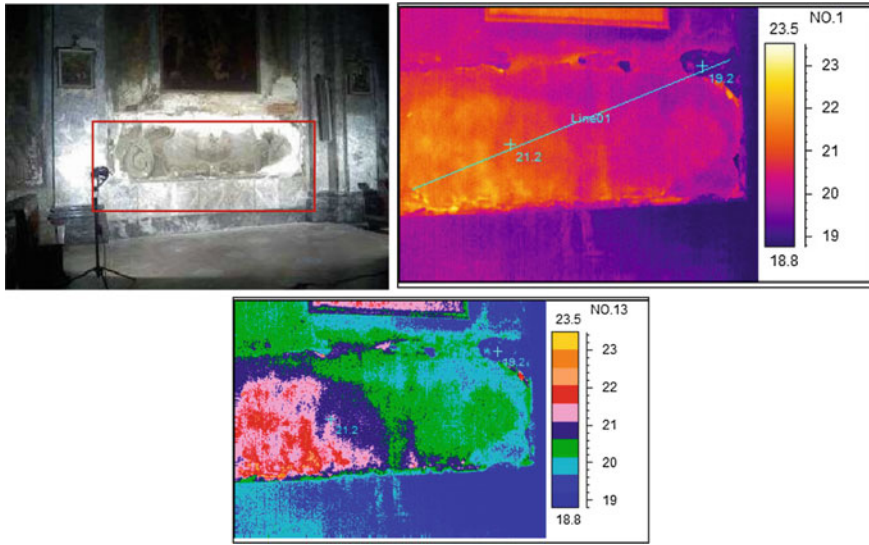


Fig. 13 North elevation, third span. The thermographic investigation was carried out in active thermography to highlight the different behaviours of the surfaces with respect to the induced heating and subsequent cooling

5 Conclusions

5.1 Databases for a Free Fruition

The results of the investigations carried out by the project ‘good practice’ on the churches of Monza fully satisfy the need for documentation of built heritage expressed by the ‘Risk Map of Cultural Heritage’: an information system that supports decisions related to the historical national architectural, in the monitoring of risk. The GIS is a database system, rich in alphanumeric and cartographic data, capable of exploring and processing information about potential risk factors that affect the cultural heritage (see Fig. 14).

It is therefore necessary that all activities undertaken at national level ‘converge’ to the risk map, thus sustaining the database and increasing the quality of the intervention to be implemented directly on the built heritage.

For the construction of the risk model of the db it was adopted a statistical approach, based on which the individual assets are valued as “units” of a “statistical population” of which the aim is to assess the level of vulnerability and risk.

Risk factors were divided into the following:

- Individual vulnerability, which is a function that indicates the level of exposure of a given item to the aggression of territorial environmental factors; and
- Hazard territorial, i.e. a function that indicates the level of potential aggressiveness of a given territorial area, regardless of the presence or not of goods.

The screenshot displays the 'Carta al Rischio' software interface. The top section features an aerial map of a city with a red line indicating a risk boundary. Below the map is a data entry form with various fields for building characteristics. The bottom part shows a detailed view of three damage descriptions with their respective severity and urgency levels.

Descrizione: Danno (1)		
Tipologia del danno:	Gravità:	Diffusione (%):
A	1	5
Grado di urgenza:	Intervento:	
1	MONITORAGGIO	
Concentrato/Diffuso: LOCALIZZATO		
Localizzazione: spallata campata sinistra, in corrispondenza della mezzera dell'arco de		
Legenda della tipologia di danno: A = danno strutturale B = dispersione materiale C = usidità D = attacchi biologici E = abrasione degli stmi superficiali F = parti mancanti		

Descrizione: Danno (2)		
Tipologia del danno:	Gravità:	Diffusione (%):
B	2	40
Grado di urgenza:	Intervento:	
3	OPERE PROVVISORIALI O PRONTO INTERVENTO	
Concentrato/Diffuso: DIFFUSO		
Localizzazione:		
Legenda della tipologia di danno: A = danno strutturale B = dispersione materiale C = usidità D = attacchi biologici E = abrasione degli stmi superficiali F = parti mancanti		

Descrizione: Danno (3)		
Tipologia del danno:	Gravità:	Diffusione (%):
C	2	30
Grado di urgenza:	Intervento:	
3	OPERE PROVVISORIALI O PRONTO INTERVENTO	
Localizzazione:		
Legenda della tipologia di danno: A = danno strutturale B = dispersione materiale C = usidità		

Fig. 14 The Risk chart (cf. footnote 2) is a computer database for data collection and return information about the index of vulnerability of a building. The chart is a national and local (cf. footnote 1) public apparatus available to anyone under the guidance of the direction of the Ministry of Culture (Urbisci, Mozzi 2007). Here are some illustrations showing the steps of in-depth knowledge of the good. The last shot shows the index of vulnerability processed by the system regarding the church of San Maurizio

For this purpose, the data entered in the system have been acquired at different times and in different ways depending on the projects that have taken place over the years, often with research projects in collaboration with various Italian universities and institutional organizations, or with the acquisition of the detection of damage on goods.

All the material produced during the investigation on the seven churches in Monza was then uploaded in the information system of the Carta del Rischio. Detailed information of the case study and georeferencing are processed through its indices; vulnerability of the object is processed in order to bring out the situations which require further investigation, restoration or conservation work.

5.2 *What Is the Next Step*

When we face with increasingly complex db, the Risk map in 1994, the fear is that the research of documents in the future will become increasingly complex and process of vulnerability of the object will be complicated also by an increasing population of data. The current challenge is the management of complexity to achieve an improvement in output. One consideration dominates over the other: the monuments themselves are witnesses and guardians of their memories.

This opens the door to situations in which the 3D model of the monument can itself become a container of information studies georeferenced to its parts as a BIM system.

As a second option, every building contains its own chip as an ID cards as a collection of studies useful for its maintenance, among them his virtual model too.

Researches are currently underway.

References

- Bertotti P (1836) Monastero della Signora di Monza, Monza, Pianta topografica Città di Monza, Monza, Civica Raccolta di Stampe Bertarelli
- Cernuschi L (1879) Pianta terrena dell'ex chiesa di S. Margherita, Archivio del Duomo di Monza D.m. 14/01/08, G.U. n. 29 feb 2008, Allegato A, LVI
- Filippini G (1722) Monza e il suo territorio, Archivio di Stato di Milano
- Gaeta G (1787) Pianta del monastero e della Chiesa di Santa Margherita, Archivio di Stato di Milano
- Gentile C, Saisi A (2011) Radar-based vibration measurement on historic masonry towers. In: 5th conference on emerging technologies in non destructive testing, Ioannina, Greece
- Plan of S. Maria in Strada, Private archive of Fabbrica della Basilica di San Giovanni Battista, Nr 212/1925
- <http://www.fondazioneCARIPLO.it/it/bandi/index.html> "Gli edifici religiosi in concio d'argilla nel tessuto urbano di Monza", Bandi Cariplo 2013, piano d'azione 'Promuovere la razionalizzazione e il rinnovamento dell'offerta culturale', promuovere buone prassi di prevenzione e conservazione del patrimonio storico e architettonico
- Urbisci S, Mozzi E (2007) La Carta del Rischio del Patrimonio Culturale lombardo on-line, in Atti della 11° Conferenza Nazionale ASITA, Torino
- <http://www.lombardiabeniculturali.it/architetture>

On the Use of Infrared Thermographic Measurements for Evaluating the Airtightness of the Building Envelope

Katrien Maroy, Nathan Van Den Bossche, Marijke Steeman
and Sven Van De Vijver

Abstract Infrared thermography (IRT) is a non-destructive evaluation technique that is used to visualize construction deficiencies, e.g. thermal bridges. In combination with a pressurization fan, IRT is also used to detect air leakages. The surface temperature change caused by the leakage air can be monitored by taking multiple IR images. Is it possible to assess the severity or quantify the flow of air leakages with this method? In order to link infrared images to the magnitude of air leakage flow, all influencing factors on the change in the surface temperature were examined in simulation models, laboratory and in situ measurements. The research showed that the visibility of an air leak is dependent on the position of other surfaces nearby. Consequently, the amount of air leakage flow cannot be related to the surface temperature change viewed on multiple IR images. Next to visibility issues, the change in surface temperature is proven to be smaller at large air leakage spots. This is due to the constant influence of the leakage air on the surface temperatures. Thermography is a sufficient technique for the visualization of air leakages that cause a clear surface temperature pattern under a pressure difference. However, it is not possible to derive the quantity of the air leakage flow.

Keywords Infrared thermography · Airtightness · Building envelope · Measurements · Simulation

K. Maroy (✉) · N. Van Den Bossche · M. Steeman · S. Van De Vijver
Faculty of Engineering and Architecture of Ghent University, Ghent, Belgium
e-mail: Katrien.Maroy@UGent.be

N. Van Den Bossche
e-mail: Nathan.Vandenbossche@UGent.be

M. Steeman
e-mail: Marijke.Steeman@UGent.be

S. Van De Vijver
e-mail: Sven.Vandevijver@UGent.be

1 Introduction

Thermography is a non-destructive measurement technique that visualizes surface temperatures of objects, by means of infrared radiation emitted from the surface of these objects. In building pathology, infrared thermography (IRT) has potential to evaluate the condition of new built and renovated buildings. Construction deficiencies such as thermal bridges, air and moisture inclusions and air leakages are easily visualized. However, it is not clear to what degree information can be derived from an infrared picture. Building deficiencies are indeed visible with thermography, but is it also possible to assess the severity of building pathologies with an IR picture?

For a proper analysis of thermographic images, a good understanding of the principles behind this technique is indispensable (Sect. 2.1). Next to that, many boundary conditions such as the weather and surface characteristics influence the surface temperatures and thus the image created with an IR camera (Sect. 2.2).

In this research, the focus lies on the application of thermography for airtightness evaluation (Sect. 3). The current standards give little information about the pressure and temperature difference necessary for a thermographic assessment in combination with a depressurization test. For example, in (NBN EN 13187), there are no specific boundary conditions mentioned for this specific application of thermography. On the other hand, ongoing research revealed the potential to analyse thermographic images of air leakage spots in order to receive information about the severity (Kalamees 2007) and the dimensions of an air leak (Bérubé Dufour et al. 2009).

It is clear that the change in surface temperature is the main indication of the presence of an air leak. By taking multiple IR images, the change in surface temperature and pattern can be visualized. Does this change give information about the severity of an air leakage flow? Before starting the research, the influence of the pressure and temperature difference on the surface temperatures was clarified (Sect. 4). Subsequently, the relation between the surface temperature change and air infiltration flow through one single air leak was examined by means of simulations, laboratory and in situ measurements (Sect. 5).

2 Thermography in Building Pathology

2.1 *General Principles of Infrared Thermography*

All objects with a temperature above 0 K emit electromagnetic radiation, including infrared rays. In the electromagnetic spectrum, infrared radiation is situated between the visible light and microwaves, in the wavelengths from 0.75 to 1000 μm (Fig. 1). Thermographic cameras only receive radiation in the wavelengths from 0.7 to

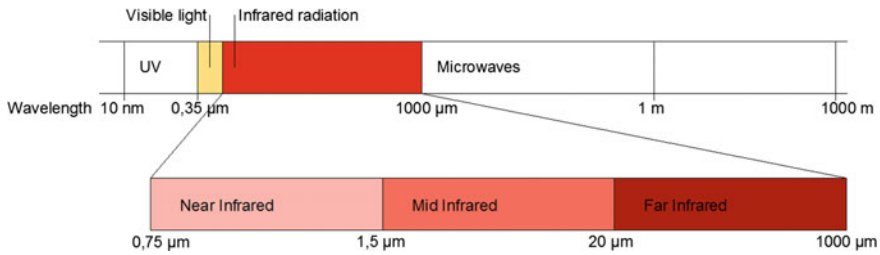


Fig. 1 Overview of the electric magnetic spectrum, based on Barreira et al. (2013)

15 μm, which is in the reach of the near- and mid-infrared field (Willockx 2010; Barreira et al. 2013).

Not every object emits the same amount of radiation in all wavelengths. For example, the radiation of a light bulb consists of a small share of visible light and a large amount of infrared radiation, whereas sunlight consists of visible light and UV rays. The amount of electromagnetic radiation per unit wavelength emitted by a black body is described by Planck’s law (1) (Jewett and Serway 2008).

$$I_{(\lambda,\theta)} = \frac{2\pi hc^2}{\lambda^5 (e^{(hc/\lambda k\theta)} - 1)} \tag{1}$$

In (1), h Planck’s constant is (6.626×10^{-34} J s), c the velocity of light (3×10^8 m/s), k the Boltzmann constant (1.381×10^{-23} J/K), λ the wavelength (μm) and θ the temperature of the black body (Kelvin).

A black body absorbs all incident radiation. By consequence, the black body emits radiation in all directions, which originates from its temperature only. The total amount of energy emitted by the black body is described by the Stefan–Boltzmann law (2). In this formula, the temperature of the black body is the only variable (Eads et al. 2000; Jewett and Serway 2008).

$$W = \sigma\theta^4 \text{ (W/m}^2\text{)} \tag{2}$$

where W the amount of energy emitted by the black body (W/m^2), σ the Stefan–Boltzmann constant (5.67×10^{-8} $\text{W/m}^2/\text{K}^4$) and θ the temperature of the black body (Kelvin).

In reality, however, radiation emitted by ordinary objects originates partially from its own temperature. The other part is reflected from the environment on the surface or, in the case of transparent materials, transmitted through the objects. Therefore, the Stefan–Boltzmann law needs to be adjusted (3) by a factor ϵ , which symbolizes the emissivity of an object.

$$W = \epsilon\sigma\theta^4 \text{ (W/m}^2\text{)} \tag{3}$$

The emissivity of a material is a characteristic that expresses the ability of an object to emit radiation originated from its own temperature. The emissivity always has a value between 0 and 1 (Jewett and Serway 2008) and is described in (4) (Dall'O 2013; Meola and Carlomango 2004).

$$\varepsilon = \frac{W_{\text{obj}}}{W_{\text{bb}}} (-) \quad (4)$$

W_{obj} symbolizes the energy emitted from an object with emissivity ε (W/m^2), whereas W_{bb} expresses the energy emitted from a black body with a temperature equal to that of the object. The relation between the emissivity ε , reflectance ρ and transmittance τ is described in (5). For opaque materials, τ is zero.

$$\varepsilon + \rho + \tau = 1 \quad (5)$$

With the help of a thermographic camera, radiation emitted from an object is recalculated to a matrix of surface temperatures, which composes the IR image. The calculation is described by the main law of thermography and involves all the principles mentioned above (Dall'O 2013; Charlier 2007; FLIR Systems 2012).

$$W_{\text{tot}} = \varepsilon \cdot \tau_{\text{atm}} \cdot W_{\text{obj}} + (1 - \varepsilon) \cdot \tau_{\text{atm}} \cdot W_{\text{amb}} + (1 - \tau_{\text{atm}}) \cdot W_{\text{atm}} \quad (6)$$

W_{tot} is the total radiation captured by the thermographic camera (W/m^2), W_{obj} the object radiation (with object temperature) (W/m^2), W_{amb} the ambient radiation (with the reflected temperature of environment) (W/m^2), W_{atm} the atmospheric radiation (with atmospheric temperature) (W/m^2), τ_{atm} the transmission of the atmosphere [-] and ε the emissivity of the material [-].

The transmission of the atmosphere τ_{atm} symbolizes the amount of radiation that the air between the camera and the objects transmits, which is dependent on the relative humidity of the air and the distance between camera and object. Fortunately, the wavelengths in which τ_{atm} equals 1 are in the range of 3–5 μm and 8–14 μm , the same ranges in which IR cameras operate. Consequently, (6) can be simplified to:

$$W_{\text{tot}} = \varepsilon \cdot W_{\text{obj}} + (1 - \varepsilon) \cdot W_{\text{amb}} \quad (7)$$

Once the emissivity ε and the reflected temperature of the environment (to calculate W_{amb}) are determined, the thermographer is ready to perform a thermographic survey with a reliable temperature measurement. The methods to determine the emissivity and reflected temperature of the environment are described in ASTM E1993-99a (2005) and ASTM E1862-97 (2002), respectively. Most building materials have an emissivity above 0.90.

2.2 General Boundary Conditions for an Optimal Visibility of Building Pathologies with Thermography

With thermography, the variation in the surface temperature of building components is easily visualized. In the case of thermal bridges, the deficiency becomes visible when a large temperature difference across the building component is present. Therefore, thermography is mainly applied in the winter season. Next to the temperature difference between inside and outside, the emissivity of the surface and reflected temperature of the environment, the weather conditions also have an impact on the measured surface temperatures.

For example, Fig. 2a shows an infrared picture of a brick cavity wall, orientated towards the east. At the bottom of the wall, higher surface temperatures indicate a thermal bridge at the foundation–wall interface. The measurement was executed before sunrise, under clear sky conditions. Figure 2b shows an IR image of the same façade when the surface was exposed to sun radiance. On that moment, the thermal bridge at the foundation–wall interface shows as a colder zone. This is caused by the shadow of a neighbouring building. However, one can see that the sun radiance clearly has an impact on the surface temperatures of the brick façade. Because of the high heat capacity of the surface, the surface temperatures remain higher than the steady state, even after clouds have appeared. Without notification of this effect, building deficiencies can remain unnoticed.

The period of time in which the surface temperature of a building component is influenced by sun radiation can be related to the thermal effusivity (8).

$$b = \sqrt{\lambda \rho c} \text{ (J/m}^2 \text{ K}\sqrt{\text{s}}) \tag{8}$$

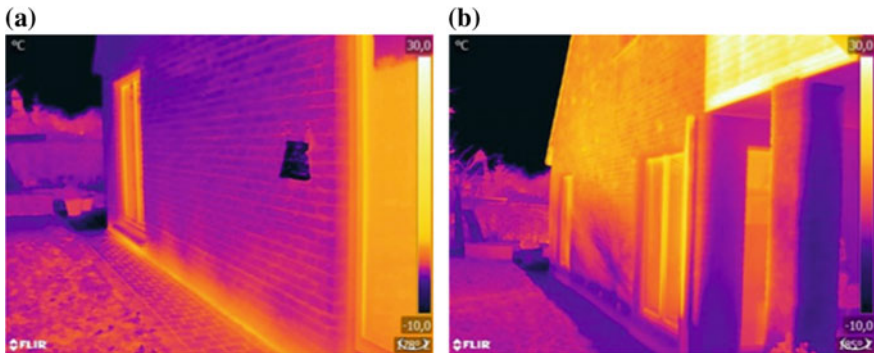


Fig. 2 *Left* A thermal bridge at the foundation–wall interface of the East façade, clearly visible before sunrise. At the moment of the measurement, a temperature difference of 19 °C was present. *Right* IR picture of the same façade, at 10 a.m. After sunrise, the façade was exposed to radiant heat from the sun. Because of the heat capacity of the bricks, the outside surface temperature of the construction remains influenced by the sun radiance by which thermal bridges can become invisible

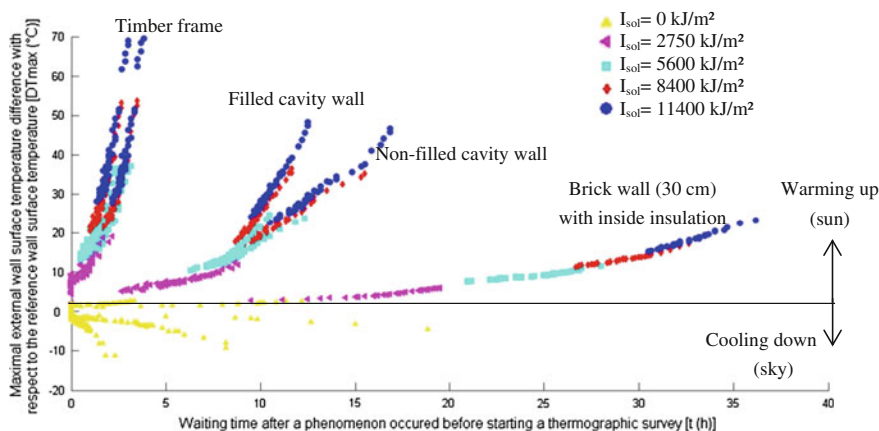


Fig. 3 Maximal external wall surface temperature deviation from the steady state and waiting time for 6 types of building components. The *horizontal axis* shows the period of time in which heavy clouded weather should occur before it is possible to measure surface temperatures closer than 0.5 °C to the steady state

In (8), λ is the conductivity (W/m K), ρ the density (kg/m^3) of the material and c the specific heat capacity of the material (J/kg K). Materials with a high thermal effusivity act more as a heat storage medium (Hens 2012).

After sun or clear sky radiation, the surface temperature of a building component is increased or decreased, respectively, compared to the steady state. The duration of this deviation was studied for six different types of walls frequently used in Belgium (Van De Vijver et al. 2014) (Fig. 3).

Figure 3 shows the period of time (horizontal axis) in which heavy clouded weather should occur before it is possible to measure surface temperatures closer than 0.5 °C from the steady state. The vertical axis shows the maximum temperature deviation between the surface temperature under a specific weather condition and under steady-state conditions. For a timber frame construction ($U = 0.22 \text{ W/m}^2 \text{ K}$, $b = 32.40 \text{ J/m}^2 \text{ K}\sqrt{\text{s}}$), only four hours of heavy clouded weather is necessary to measure surface temperatures close to the steady state. For a massive brick wall with a thickness of 30 cm and inside insulation ($U = 0.22 \text{ W/m}^2 \text{ K}$, $b = 2500.00 \text{ J/m}^2 \text{ K}\sqrt{\text{s}}$), a period of 37 h with heavy clouded windstill weather is required before surface temperatures close to the steady state can be measured.

In general, sun radiation is the main weather condition that should be avoided before and during the assessment. The sun caused the highest surface temperature deviations for all construction types (Fig. 3). Because the thermal effusivity is much higher for a massive wall than for a timber frame construction, the period in which the massive wall releases heat is much longer.

Consequently, sun radiation also has a negative impact on the visibility of construction deficiencies with thermography. Consider, e.g., a thermal bridge in a filled cavity wall (Fig. 4). During sun radiation, the surface at the thermal bridge

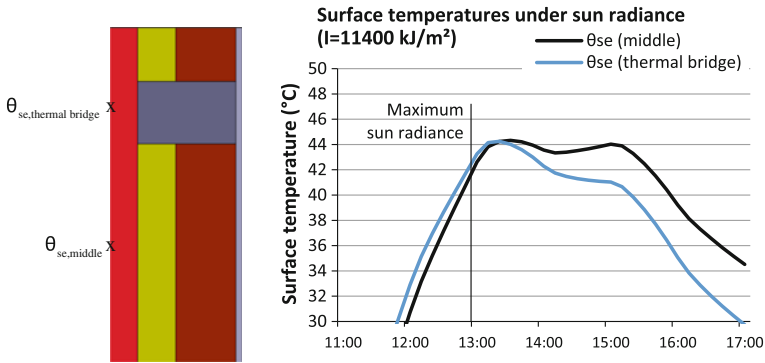


Fig. 4 Simulation model of a thermal bridge in a filled cavity wall, exposed to sun radiance. The graph shows the current of the outside surface temperatures

heats up slower than the surface at the insulation. After all, the concrete in the thermal bridge has a higher heat capacity and thermal effusivity than the insulation in the cavity wall. Hence, the surface temperature differences disappear, and the thermal bridge is no longer visible.

On the other hand, during a night with clear sky, the outside surface at the thermal bridge will show higher surface temperatures because the concrete cools down slower than the insulation. Consequently, a thermal bridge will be more visible in clear sky conditions.

In some case, however, a heat source is necessary to visualize air or moisture inclusions beneath a surface. Again, because of a different thermal effusivity, the surface at the air inclusions will heat up and cool down faster. In the case of moisture inclusions, the surface temperatures there will increase and decrease faster. This technique is also called active thermography and is used for the inspection of, e.g., stucco surfaces in monumental buildings or the surfaces of flat roofs (Fig. 5).

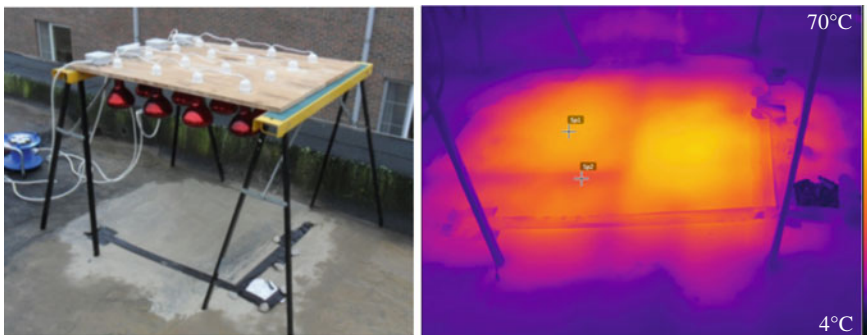


Fig. 5 *Left* IR light bulbs can be used to create a radiant heat source for the inspection of a membrane on a flat roof. *Right* After heating up the surface with the IR light bulbs, a colder area becomes visible under the surface. This indicates that there is possibly water between the insulation panels under the roof membrane

For thermography for airtightness inspection, the thermal effusivity also has an impact on the change in surface temperatures during the (de)pressurization test. Depending on the weather conditions before and during the survey and the heat capacity of the surface at the leak, the change in surface temperatures goes slower or faster. In general, it is advised to perform thermography for airtightness assessment at the inside of the construction to avoid additional external influences (sun, wind). Next to that, in some constructions, e.g. cavity walls, it can be expected that the air leak will remain invisible.

3 Thermography in Airtightness Surveys

3.1 The Change in Surface Temperature

Figure 6 illustrates an airtightness survey of a window–wall interface using IRT. These pictures were taken from the inside, while the building was depressurized with a constant pressure difference of -50 Pa. Cold air from outside infiltrated at the window–wall junction, cooling down the surface locally.

Figure 6 shows the irregular purple pattern that changes in time. This typical characteristic allows to distinguish air leakage spots from other building deficiencies such as thermal bridges. The latter have a geometrical form and a constant surface temperature.

When the outside wind pressure is rather high and a sufficient temperature difference between inside and outside is reached, the most important air leakage spots can be visualized with a thermographic camera without the use of a pressurization fan. When one is interested to visualize also the smaller air leakage spots, a pressurization fan is recommended.

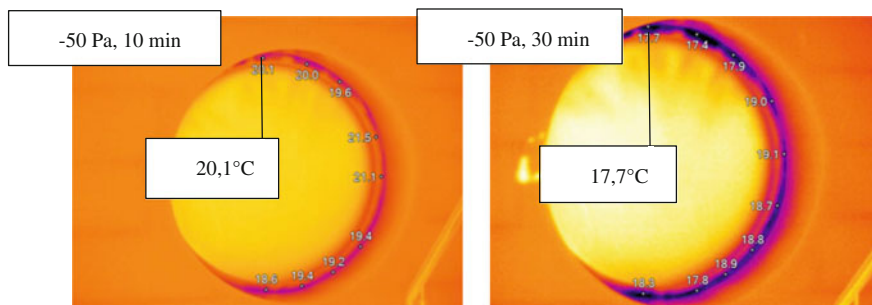


Fig. 6 IRT-survey at the inside of a window–wall intersection under a pressure difference of -50 Pa. The image on the *left* is taken after 10 min, while the image on the *right* displays the surface temperatures after 30 min. *Blue spots* are the coldest and *white spots* are the warmest zones on the image. Due to the change in surface temperature, it is clear that this is an air leakage spot and not a thermal bridge

3.2 *State of the Art*

The current standards provide a set of recommendations for thermographic surveys. For air leakage assessment, it can be expected that the temperature and pressure difference between the inside and outside environment will play an important role. However, rarely, a distinction is made between air leakage measurements and thermal bridge detection with IRT. And when there are specific boundary conditions listed, the standards mention various temperature differences (Table 1). These standards also advise to depressurise the inspected building in order to spot air infiltrations indoor.

In spite of the lack of clear guidelines in the standards, ongoing research revealed the potential to analyse thermographic images in order to assess the severity of air leakage spots. For example, in Kalamees (2007), airtightness measurements of 32 of Estonian houses were analysed. First, the airtightness of each building was measured using a standardized pressurization fan. Then, the typical air leakage spots were determined using a thermographic camera in combination with a pressurization fan, providing a negative pressure difference of 50 Pa. It appeared that the typical air leakage places were ceiling–floor–wall interfaces, the window–wall interfaces and the junctions of separating walls with the external walls or roof. As mentioned before, the irregular shape of the temperature pattern reveals the presence of an air leak. The impact of the air leakage spots were examined through calculation of the temperature factor. This factor indicates the risk of condensation (Senave et al. 1990).

In a second study, a first step towards quantitative airtightness measurements using thermography was taken (Bérubé Dufour et al. 2009). Here, the experimental set-up consisted of a pressurized box with a crack with known dimensions in the middle of the box. With the thermographic pictures, the authors tried to make a reconstruction of the geometry of the crack. A first method consisted of detecting the edges of a deviating surface temperature pattern to derive the opening width and length. In the second method, a correlation was developed between maximum deviation and attenuation in the temperature pattern. This was suitable for smaller widths.

Table 1 Overview of the standards that mention specific boundary conditions for an airtightness survey with IRT

	Temperature difference	Pressure difference
RESNET (2012)	>1.7 °C	>10–20 Pa
ASHRAE Journal (Eads et al. 2000)	>3 °C	
BSRIA (Pearson 2011)	>5 °C	

4 Design of Experiment: Ideal Pressure and Temperature Difference

Because of the lack of clear guidelines for the pressure and temperature difference between inside and outside, the first step consisted of determining these boundary conditions for the laboratory and in situ measurements.

4.1 Characteristics of the Model

To simulate the impact of the pressure and temperature difference, an air leakage path with a height of 1000 mm and a width of 10 mm was modelled along a window–wall intersection in VOLTRA (Fig. 7). This simulation programme allows to study 3D dynamic heat transfer using a finite element method (Physibel 2008). The wall is composed of 15 mm of gypsum at the inside surface, 190 mm reinforced concrete, 100 mm insulation with thermal conductivity = 0.025 W/m K and 90 mm of masonry at the outside surface. The surface temperatures were simulated along profile L0 in Fig. 7.

Both overpressure and underpressure were examined with changing pressure differences from 20 Pa up to 100 Pa and changing temperature differences from 10 °C up to 30 °C. Environmental factors such as the sun, wind and rain were neglected, as IRT measurements for air leakage detection are usually performed indoor. The power law formulation (9) was used to estimate the air flow rate entering the building through the crack (NBN EN 13829 2001).

$$V = C \cdot \Delta P^N \text{ [m}^3\text{/h]} \quad \text{with } C = \frac{V_{50W}}{\Delta P^N \cdot 1\text{m}} \text{ [m}^3\text{/h.Pa}^N\text{]} \quad (9)$$

where V is the air flow rate [m³/h], ΔP the pressure difference [Pa], C the air flow coefficient [m³/(h Pa)] and N the air flow exponent [–]. In this simulation, the air

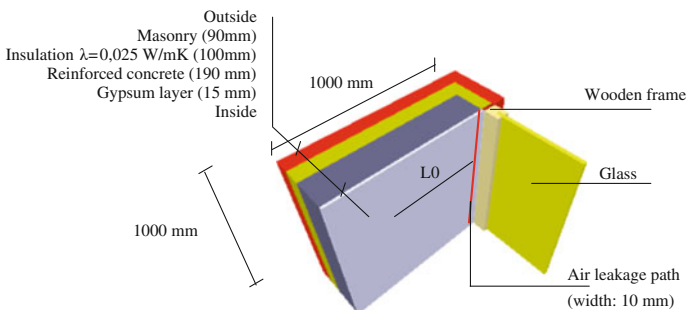


Fig. 7 Simulation model of the window–wall interface to determine the ideal temperature and pressure difference for the IRT-survey

flow exponent was set to 0.66, as a standard value between 0.6 and 0.7 is suggested in the standards (AIVC 1994).

The air flow coefficient C was calculated based on V_{50W} , the maximal acceptable air loss at the window–wall interface, which is 10 % of the overall building leakage V_{50} . For newly built detached residential buildings in Flanders, the average building airtightness n_{50} is 6 h^{-1} (Van Den Bossche et al. 2012). Based on this observation, the maximal acceptable air loss at the window–wall interface (V_{50W} in (2)) was set to $3.3 \text{ m}^3/\text{hm}$ at 50 Pa by which C was calculated. For example, for a simulation model with a window–wall interface of 1 m at 50 Pa pressure difference, this gives a C value equal to $0.25 \text{ m}^3/\text{h Pa}^N$.

4.2 Pressure Difference

In Fig. 8, the temperature profile along L0 obtained with a pressure difference of 20 and 100 Pa is displayed. The temperature difference remained constant at $20 \text{ }^\circ\text{C}$ during this simulation. It can be noticed that the pressure difference does not have a significant influence on the course of the surface temperature. The inside surface temperature at 0 mm from the air leakage spot was decreased with $2 \text{ }^\circ\text{C}$ after 10 min when a pressure difference of 100 Pa was used. In the simulations with 20 Pa pressure difference, the inside surface temperatures were decreased with $1 \text{ }^\circ\text{C}$ after 10 min.

The deviation between 20 and 100 Pa was only $1 \text{ }^\circ\text{C}$ after 10 min, and it remained constant during the simulation (line after 30 min). Compared with the absolute measurement accuracy of most IR cameras ($\pm 2 \text{ }^\circ\text{C}$), it can be concluded from this simulation that the amount of pressure difference is not significant for the temperature change near the junction.

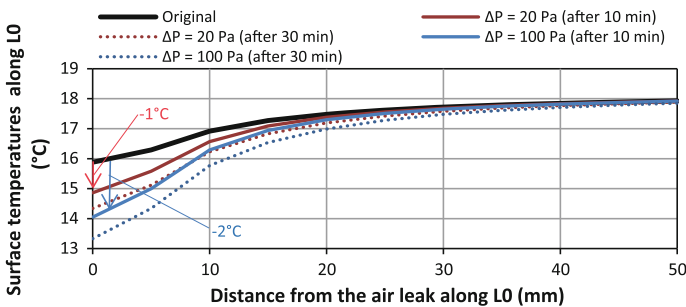


Fig. 8 The pressure difference has a limited influence on the surface temperatures near the joint. At the air leakage spot, the resulting surface temperature difference between 20 and 100 Pa was $1 \text{ }^\circ\text{C}$ throughout the whole period of depressurization in the models

In practice, however, there is always a minor pressure difference present, often increased by the wind. When this happens hours before the assessment, the decrease of surface temperatures during a depressurization test will be limited (Sect. 5.3).

4.3 Temperature Difference

In a second step, the window–wall junction was simulated with temperature differences of 5, 10, 20 and 30 °C. The indoor temperature and the pressure difference in the model (Fig. 7) were kept constant at 20 °C and 50 Pa, respectively. The outside temperature varied from −10 °C until 15 °C. Figure 9 shows the resulting temperature profiles along L0, after 0 and 25 min. It can be seen that the temperature difference has a much greater influence on the obtained surface temperatures near the junction than the pressure difference, where the surface temperature drops varied from 0.5 to 3 °C, depending on the temperature difference between inside and outside. Based on this simulation model, a thermographic survey can be executed with an indoor–outdoor temperature difference of 10 °C, when a surface temperature drop of minimum 1 °C in 25 °C is premised.

For the visibility of an air leakage spot, it is clear that a pressure difference and temperature difference are necessary for a clear surface temperature pattern on the IR image and to see a change in the surface temperatures. However, concluding from this simulation, only the amount of temperature difference between inside and outside is an influencing boundary condition on the change rate of the surface temperatures. Next to that, there are other influencing factors that have a larger impact on the surface temperature change rate than the pressure difference and temperature difference (Sect. 5).

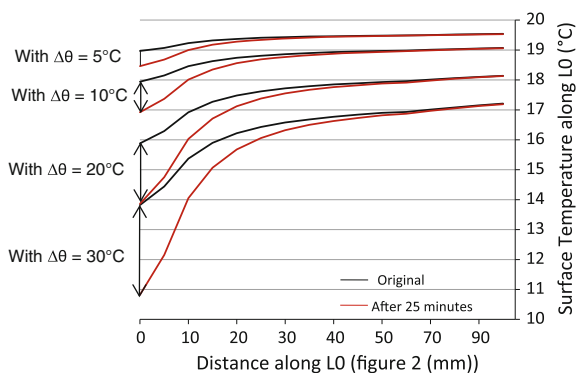


Fig. 9 Effect of the temperature difference on the change in surface temperature. A minimum temperature difference of 10 °C is advised when using IRT to assess air infiltration spots. With this difference, a change in surface temperature of 1 °C after 25 min is obtained

5 Influencing Factors of the Surface Temperature Change Rate

A change in the surface temperature throughout the depressurization test indicates the presence of an air leak (Fig. 6). But does this characteristic also give information about the severity of the air leakage spot or the infiltration flow? To examine the influencing factors of the change in surface temperature, a roof–wall and wall–wall junction were simulated in VOLTRA (Sect. 5.1) (Physibel 2008). In these models, it was possible to examine the impact of the width of the junction and the joint assembly.

Of course, a simulation model is a simplification. In reality, an air leakage spot leaves an irregular pattern and the air leakage flow is never a fixed value. Therefore, laboratory measurements on the same roof–wall and wall–wall junction were executed simultaneously (Sect. 5.2). Lastly, this research was completed with in situ measurements, showing the impact of wind and dimensions of air leakages. (Sect. 5.3).

5.1 Impact of the Geometry and Joint Assembly: Simulation Models

5.1.1 Assumptions in the Simulation Models

To investigate the impact of the joint assembly and geometry on the surface temperature change rate near the air leakage spot, a roof–wall junction and a wall–wall junction were modelled in VOLTRA (Fig. 10). To model the air flows, a ventilation path from the outside air (fixed at 18.5 °C) to the modelled air leak was determined. The temperature of the inside air was fixed at 40 °C.

It is clear that these models are only a simplification of the reality. For example, the infiltration air does not enter the indoor climate directly (Physibel 2008). Also, the surface temperature pattern that originates from the infiltration air is in reality

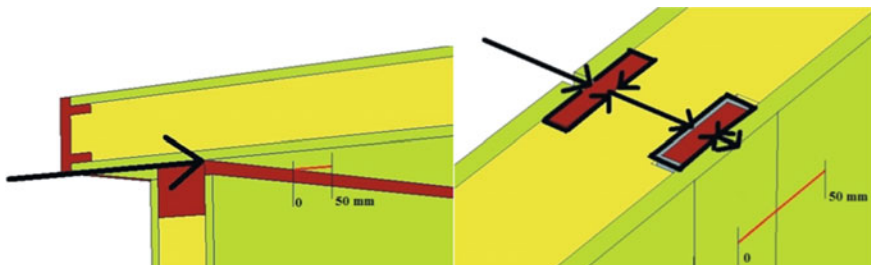


Fig. 10 *Left* Roof–wall junction. *Right* Wall–wall junction. The air flow was a fixed value in the simulations. Along the *red lines* on the figures, the simulated temperature profile was plotted

irregular. In the simulation, this is a regular pattern. The air flow used in the simulations is a fixed value, whereas in reality, infiltration air flows fluctuate constantly.

As an input for the simulation models, the measured air flow through the junctions was used, which was determined in the laboratory on a test house with identical junctions (Sect. 5.2). The varying parameter was the air leak width, which was alternately estimated on 0.5 and 1 mm. These widths directly influence the air velocity and the convective heat transfer coefficient (CHTC) in the model.

Finally, to calculate the CHTC (10), the turbulent correlation for forced convection was used (Loveday and Taki 2001). Using this correlation, the CHTC varied under changing air flow velocities, of which the latter is related to the changing dimensions of the air leak. Figure 11 shows the changing CHTC correlated to the velocity of the air flow, calculated for leak widths of 0.5 mm. In the wall-wall junction, the CHTC was lower due to lower air flows measured in Sect. 5.2. When executing the simulation with a leak width of 1 mm, the air velocity and thus the CHTC were decreased by half.

$$CHTC_{\text{Turbulent}} = (0.023 \cdot R_E^{0.8} \cdot P_r^{0.3}) \cdot \left(\frac{\lambda_{\text{air at } 29^\circ\text{C}}}{\text{hydraulic diameter}} \right) \quad (10)$$

$$\text{With } R_E = \left(\frac{\rho \cdot \text{hydraulic diameter} \cdot v}{\text{dynamic viscosity}} \right) \quad (11)$$

In (10) and (11), P_r is the Prandtl number (-), λ the thermal conductivity (W/m K), ρ the density (kg/m^3) and v the velocity of the air (m/s).

In this simulation, we only wanted to study the impact of the air leakage width, assuming the air flow rate is a fixed value for the measurements. Therefore, there was only a correlated CHTC used for the surfaces inside the modelled air leak. Across the inside and outside surfaces, the models had a uniform CHTC of $25 \text{ W/m}^2 \text{ K}$ on the outside and $7.70 \text{ W/m}^2 \text{ K}$ on the inside, while it is shown that the CHTC at the outside surface increases proportionally to the height (Blocken et al. 2009). Also, the effect of corners on the CHTC was not taken in account. Finally, the used correlation in this research was purely based on turbulent convection, while in reality, the air flow shows both laminar and turbulent characteristics.

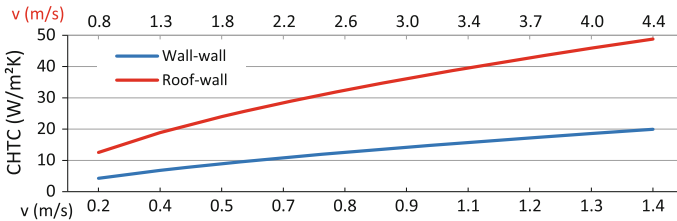


Fig. 11 CHTC ($\text{W/m}^2 \text{ K}$) correlated to the speed of the air flow, calculated with a leak width of 0.5 mm

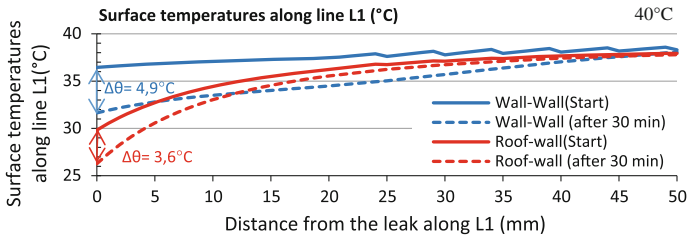


Fig. 12 Simulated surface temperatures (°C) at 50 Pa pressure difference, simulated with a width (w) of 0.5 mm (full line). These profiles are taken along the black line shown in Fig. 6

5.1.2 Impact of Thermal Bridges in the Joint Assembly

In Fig. 12, the resulting temperature profiles at the surface near the joint with an air leakage width of 0.5 mm are displayed. It was observed that the temperature was lower closely to the leak in the roof–wall junction (27.3 °C) than at the wall–wall joint (31.8 °C) after 30 min. The same trend was observed in the laboratory measurements (Sect. 5.2.3). However, the effect in the simulations was more likely caused by a difference in insulation characteristic at the joints.

In the roof–wall junction, only a wooden beam with a conductivity of 0.180 W/m K formed the separating component between inside and outside. The air infiltration path was also straight. On the other hand, the wall–wall junction was more complex with two wooden slats and an insulation layer with a conductivity of 0.050 W/m K. The images in Fig. 13 show that the inner surface at the wall–wall junction is higher before imposing a pressure difference, because of a better thermal insulation.

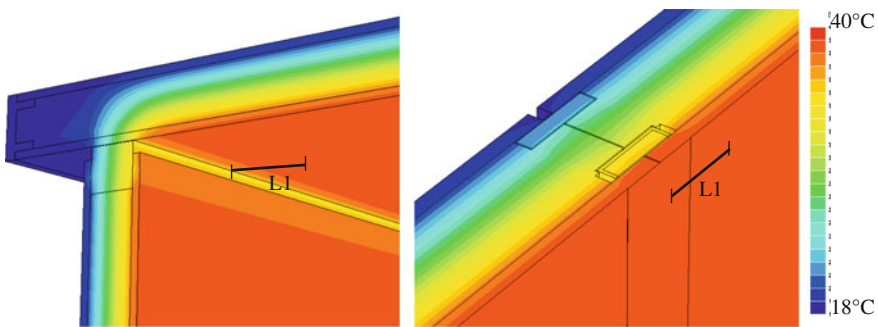


Fig. 13 Temperature distribution inside the simulation models, before depressurization. The surface temperature in the roof–wall junction is already lower due to the high conductivity of the wooden beam between the roof and wall panel

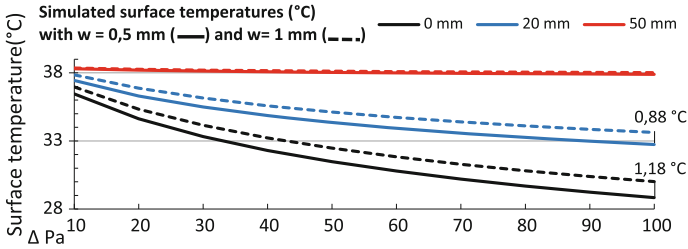


Fig. 14 Simulated surface temperatures of wall–wall junction. The *horizontal axis* shows the different pressure differences, and the *vertical axis* shows the surface temperatures at 0, 20 and 50 mm distance of the air leak. The maximum difference between the simulated results with both widths is 1.18 °C, at 0 mm from the leak with pressure difference 100 Pa

5.1.3 Impact of Width of the Air Leak, Assuming a Fixed Infiltration Flow

In the simulation model, a fixed air infiltration flow was assumed. By consequence, the width of an air leak had a direct influence on the air velocity through the air leak, which affected the CHTC and the resulting surface temperatures. Figure 14 shows the results of the wall–wall junction with a width (w) of, respectively, 0.5 and 1 mm, at different distances from the air leak. These surface temperatures were derived from the model after 3 h of depressurization, in order to have the maximum temperature change of the surface.

The surface temperatures showed that a more narrow width corresponded with lower surface temperatures after depressurization, due to a higher air velocity and a higher CHTC. The maximum difference in surface temperature between 0.5 and 1 mm width was 1.18 °C, at 100 Pa pressure difference near the air leak. At a distance of 20 mm, the temperature difference resulting from both simulations was similar (0.88 °C). Eventually, a wider air leakage spot will show a smaller decline in surface temperature on the inside surface. Therefore, a large air leakage spot will seem less severe than a narrow air leakage spot if they had the same air flow rate on an IR image after a period of depressurization.

5.2 Impact of the Location: Laboratory Measurements

5.2.1 Test House Set-up

With the boundary conditions determined in Sect. 4, laboratory measurements were executed on a small test house with a range of different air leakage spots. The test house with $2.4 \times 3.6 \text{ m}^2$ ground surface was constructed with structural insulated panels (SIP) in the laboratory (Fig. 15). The panels consist of a PUR insulation layer with a thickness of 74 mm, covered on both sides with an OSB panel of

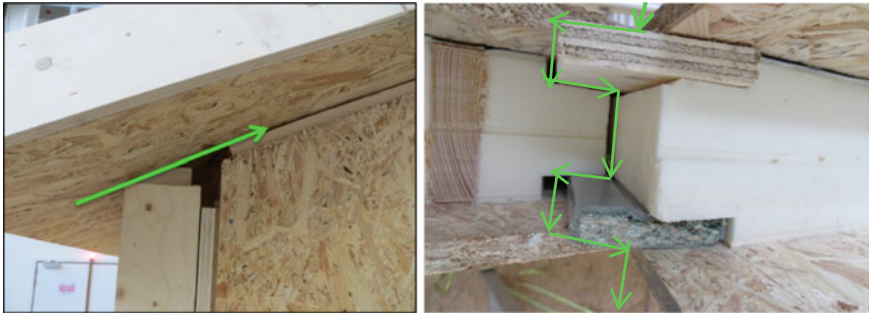


Fig. 15 *Left* Section of the roof–wall junction. *Right* Picture of the wall–wall junction with grey PVC foam brace at the inside. The expected air infiltration path from outside to inside is indicated with a *green arrow*

12 mm thickness. The airtightness system adopted between two wall panels is illustrated in Fig. 15 (right). It contains two small pieces of plywood, from which the inside plank was covered with a grey PVC foam brace. The house had a lean to roof with a maximum height of 3.959 m and a minimum height of 2.500 m. In this chapter, a roof–wall and a wall–wall junction are discussed.

The test protocol consisted of 4 steps:

1. The test house was both pressurized and depressurized to determine the initial air infiltration flow, according to NBN EN 13829 (2001). As pressurization apparatus, a Lindab LT600 was used. The pressurization took place in steps from 10 to 100 Pa, increasing the pressure difference level with 10 Pa. During the first test, all junctions which were to be examined were left unsealed.
2. Inside the test house, the temperature was increased up to 40 °C using two convectors. The temperature in the laboratory remained at 18.5 °C. The temperature difference of 20 °C is sufficient to clearly detect air infiltration, as was concluded from the simulations in Sect. 2. In order to mix the inside air and avoid thermal stratification, a small fan was placed inside the test house.
3. Throughout a period of 30 min, the air infiltration at one junction was monitored with a thermographic camera (Flir TB640x), secured on a tripod inside the test house. While taking pictures, the inside of the test house was depressurized with –50 Pa. Every 30 s, a thermographic picture was taken.
4. After completion of the thermographic measurements, the junction was sealed and the test house was again pressurized and depressurized according to NBN EN 13829 (2001). After subtracting the measured air flow from the measured air flow in step 1, the air infiltration flow at the examined junction was known.

For each junction, the whole procedure was repeated. Air flows through the junctions were calculated by subtracting the measured air flows before and after sealing of the examined joint. Evidently, the resulting flow rate was converted to standard conditions concerning temperature, relative humidity and absolute

pressure. In this chapter, only the results of the depressurization test were used in the simulations, as the IRT images were made in this condition.

After each thermographic measurement, a time span of 20 h was respected to raise the inside temperature at least 15 °C above temperature level in the laboratory. This was realized with two convectors and one fan for mixing the inside air. This time span also ensured the SIPs to attain a thermal equilibrium with the climate inside and outside the heated test house.

As shown in Kalamees (2007), the temperature factor f_{Rsi} (12) is an interesting tool to compare multiple air leakage spots.

$$f_{Rsi} = \frac{\theta_{si} - \theta_e}{\theta_i - \theta_e} \quad (12)$$

In formula (8), θ_{si} is the inside surface temperature measured with thermography, θ_i is the temperature inside the test house (approximately 40 °C) and θ_e is the temperature in the laboratory (approximately 18 °C). The inside temperature (θ_i) was monitored with a Hobo-logger in the test house. The temperature in the laboratory (θ_e) was also measured with a Hobo-logger, placed closely to the test house in the laboratory.

5.2.2 Experimental Results

Figure 15 shows the configuration of the roof–wall and wall–wall junction in detail. Without sealing, one can presume the roof–wall junction will not be airtight. The amount of air through the roof–wall joint was 4.724 m³/hm at –50 Pa pressure difference. The junction length measured 1.05 m. The other joints were sealed with an airtight tape. The wall–wall junction was left open over the entire height of the panel, which was 2.70 m. Despite the airtightness system in this joint, air flows up to 1.444 m³/hm at –50 Pa pressure difference were measured. Table 2 shows the results per pressure difference.

Table 2 Air flow per current metre (m³/hm) through the joints, calculated from the depressurization tests by subtracting the air flow before and after sealing of the joint. Also, the maximum and minimum possible air flow within the 95 % confidence interval is displayed

Δ (Pa)	–10	–20	–30	–40	–50	–60	–70	–80	–90	–100
Roof–wall (m ³ /hm)	1.438	2.402	3.240	4.007	4.724	5.403	6.054	6.680	7.285	7.873
V + s95 %	1.449	2.418	3.261	4.032	4.753	5.436	6.090	6.718	7.327	7.917
V – s95 %	1.428	2.385	3.219	3.981	4.694	5.371	6.018	6.641	7.244	7.829
Wall–wall (m ³ /hm)	0.377	0.673	0.943	1.199	1.444	1.680	1.910	2.134	2.354	2.569
V + s95 %	0.442	0.794	1.121	1.432	1.732	2.024	2.309	2.589	2.863	3.134
V – s95 %	0.312	0.551	0.766	0.966	1.155	1.336	1.511	1.680	1.844	2.005

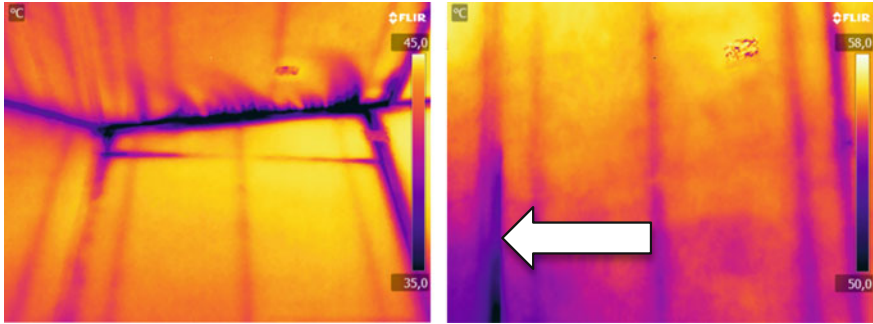


Fig. 16 *Left* Roof–wall junction thermogram. *Right* Wall–wall junction (indicated with an *arrow*). Images taken at 30 min with –50 Pa pressure difference

Figure 16 shows the thermographic pictures of both joints after a pressure difference of 50 Pa was applied for a period of 30 min. The air infiltration pattern was clearly visible at the roof–wall junction, due to the perpendicular placement of the surfaces. The cold air brushes against the roof surface causing the surface temperatures to decrease near the junction. This causes an irregular surface temperature pattern. The wall–wall junction only showed traces of air infiltration in the lower part of the joint. Due to the regular pattern, one might assume that this is a thermal bridge in the wall–wall junction.

5.2.3 Analysis of Laboratory Measurements

In order to compare the thermographic measurements of both junctions, the temperature factors (f_{Rsi}) at the surfaces near the joints were calculated. Next to that, the effect of the air infiltration over time was visualized by subtracting the temperature factors of subsequent thermographic pictures from each other (Fig. 17). This

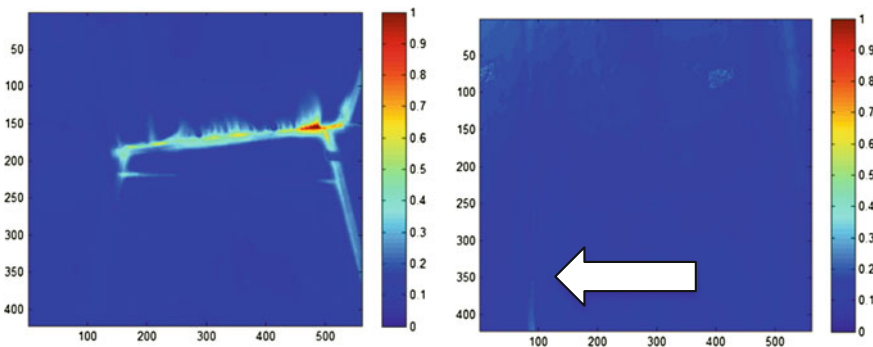


Fig. 17 Change in temperature factor relative to the first image after 30 min. *Left* Roof–wall junction. *Right* Wall–wall junction

approach enabled to eliminate the impact of geometrical thermal bridges in the construction. Only the effect of air flows was visible in the figures. Consequently, it is possible to compare multiple IR images taken in slightly different circumstances as it normalizes the measured surface temperatures.

Figure 17 shows the resulting diagrams of both junctions after 30 min. The red zones are the most affected by the air leak.

In Fig. 17, one can see that the air infiltration pattern was far more outlined in the roof–wall junction as compared to the wall–wall junction. This effect can of course be explained by the air infiltration flow, which was larger at the roof–wall junction (Table 2). Next to that, in this junction, the cold air brushed against the roof surface, making the surface temperatures drop faster at locations further away from the joint. Due to the perpendicular placement, the cold air caused an irregular pattern on the IR image. In this case, the largest air leakage spot is indeed more visible on the temperature factor diagram. However, in practice, it is shown that the change rate in surface temperature is not representative for the dimensions of the air leak (Sect. 5.3).

Concerning the wall–wall junction, one could presume that this joint is not airtight based on the measured leakage flow. On the other hand, from the temperature factor diagram, it seems that there is no air leakage spot at all. This shows that not all air leakage spots have an influence on the surface temperature. Therefore, it is not possible to visualize and quantify all air leakage spots with thermography.

In this particular case, the air leakage flow in the wall–wall junction entered the interior at the end sides of the wall–wall joint. The cold air infiltrates in the ends of the junction, passing the airtight PVC brace to the inside surface. By consequence, the lower and upper end of the wall–wall junction was affected by the infiltrating air.

5.3 Impact of Wind and Large Air Leakages in Reality: In Situ Measurements

In this research project, two case studies were executed in order to test the conclusions from Sects. 5.1 and 5.2 in practice. Case 1 showed that it is impossible to assess the severity of air leakage spots because of the wind prior to the survey. The surface temperature near an air leakage spot was already influenced by the cold air that infiltrated before the start of the survey. By this, the surface temperatures did not change further during a depressurization test. Air leaks in inner corners (e.g. Fig. 18) will be visible even before the depressurization test started (Dewulf and Goetelen 2015).

In a second case study, the effect of a large air leak causing an irregular pattern was compared with a small air leak that was only detected through depressurization. In this case, it was again shown that the surface at large air leakages does not

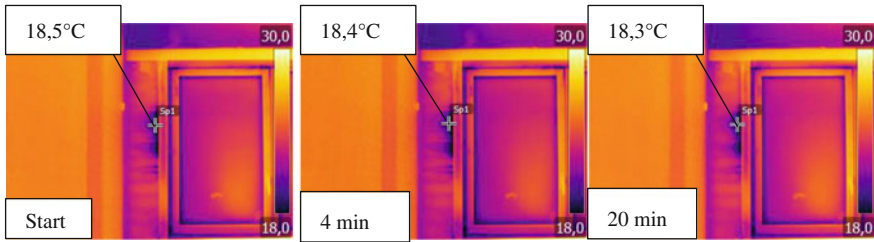


Fig. 18 All pictures were taken with $\epsilon = 0.90$ and reflected environment temperature of $19\text{ }^{\circ}\text{C}$. There was no change in the pattern visible, but due to the irregular shape, this was clearly an air leakage spot

decrease much in temperature during the depressurization test. But in contrary to the simulation model, the surface temperature remained nonetheless constant because the surface was already adapted to the constant infiltration of cold air prior to the survey. A small air leakage spot in the same building kept decreasing in surface temperature throughout the whole test (Dewulf and Goetelen 2015). Again, all these effects make it practically impossible to estimate an air leakage flow on surface temperature change alone.

5.3.1 Case 1: Effect of Wind During the Survey

The first case study was situated in a high-rise residential building. An apartment on the 5th floor was heated to $25\text{ }^{\circ}\text{C}$ before the test. The outside temperature was on average $10\text{ }^{\circ}\text{C}$ during the inspection. The pressurization test was executed with a Blowerdoor (230 V). During the test, the wind velocity reported from a weather station nearby was 3.35 m/s from a reference height of 10 m , coming from the north east in the hours before and during the measurement. Note that the yearly average reference wind velocity is 4 m/s . All inspected windows were on the north-east side of the building and thus on the windward side of the building (Dewulf and Goetelen 2015).

Air leakages that cause an irregular pattern are then directly visible from the inside. The air leakage spot in Fig. 18 was already visible when entering the apartment on the 5th floor. Depressurizing the building further had no use, as the surface temperatures near the air leak were already influenced by the cold wind and had reached a thermal equilibrium. There was no significant change in surface temperature pattern after 20 min of depressurization at 20 Pa pressure difference (Dewulf and Goetelen 2015).

5.3.2 Case 2: Large Versus Small Air Leakage Spots

The second case was located in a small residential building, situated in a courtyard in an urban environment. The building was heated to $23.3\text{ }^{\circ}\text{C}$, while the outside

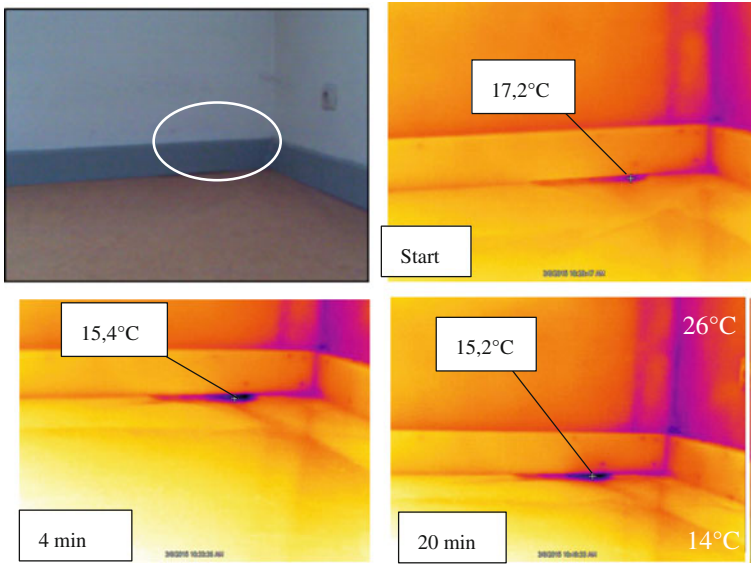


Fig. 19 Infrared images under -20 Pa pressure difference of a large air leak, visible with the eye. After 4 min of depressurization, the surface temperatures remained nonetheless constant. All pictures were taken with an emissivity of 0.90 and reflected temperature of 20.0 °C

temperature was 5 °C. The building was shielded from wind, due to its location in a courtyard.

Figure 19 shows the monitoring of a large air leak during a depressurization test at -20 Pa pressure difference. The air leak was visible with the eye. Figure 20 shows the monitoring of a small air leakage spot at a window, during the same depressurization test. Before imposing a pressure difference, the surface at the large air leakage was already influenced by the cold air that constantly infiltrates through this spot. In Fig. 20, on the other hand, no traces of an air leakage were visible on the infrared image before the depressurization test. It was only after the depressurization test that it became clear there was an air leak at the window–wall interface.

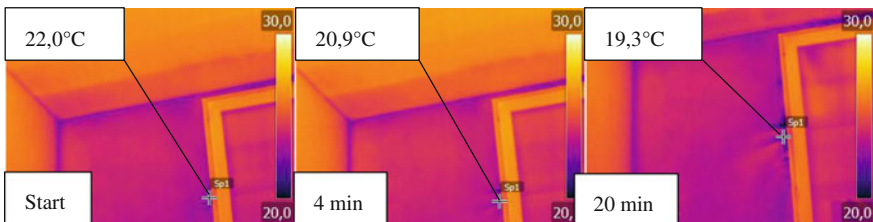


Fig. 20 Infrared images under -20 Pa pressure difference. All pictures are taken with $\varepsilon = 0.90$ and reflected environment temperature of 19 °C. The surface temperatures kept decreasing until the end of the test

When comparing Figs. 19 and 20, it can be seen that the temperature decreased faster at the small air leakage. In contrast, at the large air leakage spot, the surface temperature remained nonetheless constant after 4 min (Dewulf and Goetelen 2015). This again shows that it is practically impossible to assess the severity of air leakage with the change rate in surface temperatures.

6 Conclusions

Thermography is an interesting tool for the detection of construction deficiencies, e.g. thermal bridges, moisture and air inclusions and air leakage spots. A thermographic camera receives the infrared radiation emitted by the surface of a building component. With the emissivity of the building component and reflected temperature of the environment as input, the camera calculates the surface temperatures and generates an image by which the building pathology is visualized. Additionally, the weather conditions and thermal effusivity have a large impact on the visibility of building pathologies. Because of the thermal effusivity, the surface at a building pathology heats up faster or slower. For example, under sun radiance, the temperature difference diminishes and the building pathology will no longer be visible with an infrared camera.

Nowadays, thermography is often used in combination with a pressurization fan to identify the exact location of the air leakage spot. Although the current standards give little to no information about the boundary conditions necessary for this kind of survey, ongoing research revealed the possibility to go further than visualization only. An air leakage spot is characterized by the change in surface temperature during a (de)pressurization test. Therefore, is it possible to assess the severity of an air leakage with the change rate of surface temperatures? To examine the influential factors of this change rate, simulations, laboratory and in situ measurements were executed.

Firstly, in order to determine the ideal pressure and temperature difference for the measurements, a window–wall intersection was modelled in VOLTRA (Physibel 2008). It was found that the temperature difference should be at least 10 °C to observe a sufficient change in surface temperatures within a reasonable amount of time. In the simulation in Sect. 4, the surface temperature decreased 1 °C after 25 min with a pressure difference of 20 Pa and a temperature difference of 10 °C. Next to that, the amount of pressure difference has no influence on the surface temperatures change rate. In reality, the surface near an air leak is constantly influenced by cold infiltration air, due to the minor natural pressure difference. In practice, imposing a larger pressure difference is sufficient to make air leaks visible with IRT.

In the second step, the influencing factors of the surface temperature change rate were examined. Through simulation of a roof–wall and wall–wall junction, the impact of air leakage width and assembly was researched. It is shown that the geometry of the joint plays a major role in the surface temperature change near the

joint. When a fixed air infiltration flow is assumed, large air leakages cause lower air velocities through the leak and lower CHTCs at the surfaces in the leak. Next to that, large air leakage spots also work as a thermal bridge. The surface temperature is already lower before a pressure difference is imposed, and by consequence, only the surface temperatures show minor changes during the depressurization test.

In the laboratory, the roof–wall and wall–wall junction were also compared. Air leakage spots in an inner corner (roof–wall) leave an irregular pattern on the surfaces nearby, whereas an air leakage spots in the plane (wall–wall) only moderately influence nearby surfaces. In this particular case, the air leakage flow originated from the end sides of the junction.

Finally, in situ measurements showed the influence of wind and the width of air leakage spots on the change in surface temperature, monitored with IRT. The wind makes air leakages in the corner visible before the survey. By consequence, during a depressurization test, the surface temperature hardly changes. Next to that, at large air leakage spots, the change rate is much slower because the surface there is already influenced by cold air that is infiltrating constantly.

All these influencing factors render it impossible to derive an air leakage flow or even assess the severity with the surface temperature change rate. Although this method seems to have the potential for quantitative analysis of the buildings airtightness, it is not possible to derive the air infiltration flow from IRT-images.

Acknowledgments The research has been financed by the Flemish Institute for the Promotion and Innovation by Science and Technology in Flanders (IWT 130210). Their financial support is greatly acknowledged. Next to that, the authors would also like to thank Bieke Dewulf and Cleo Goetelen, who executed the in situ measurements for their master dissertation.

References

- AIVC (1994) Technical note 44—an analysis and data summary of the AIVC's numerical database. Air Infiltration and Ventilation Centre
- ASTM E1862-97 (2002) Standard test method for measuring and compensating for reflected temperature using infrared imaging radiometers. ASTM American society for testing and materials
- ASTM E1993-99a (2005) Standard test method for measuring and compensating for emissivity using infrared imaging radiometers. ASTM American society for testing and materials
- Barreira E, de Freitas S, de Freitas V, Delgado J (2013) Infrared thermography application in building diagnosis: a proposal for test procedures. In: *Infrared thermography application in building diagnosis*. Springer, Heidelberg, pp 91–117
- Bérubé Dufour M, Derome D, Zmeureanu R (2009) Analysis of thermograms for the estimation of dimensions of cracks in the building envelope. *Infrared Phys Technol* 52:70–78
- Blocken B, Defraeye T, Derome D, Carmeliet J (2009) High-resolution CFD simulations for forced convective heat transfer coefficients at the facade of a low-rise building. *Build Environ* 44(12):2396–2412
- Charlier L (2007) Utilisation de la thermographie infrarouge pour la détermination des déperditions thermique d'un bâtiment. Université de Liège, Liège

- Dall'O G (2013) Infrared Audit. In: Green energy audit of buildings. Springer, London, pp 111–125
- Dewulf B, Goetelen C (2015) Opsporen en kwantificeren van luchtlekken in de gebouwschil aan de hand van thermografie. Universiteit Gent, Vakgroep Architectuur en stedenbouw, Gent (in Dutch)
- Eads L, Epperly R, Snell J (2000) Thermography: practical guide. ASHRAE J 51–55
- FLIR Systems (2012) Thermal camera guide for research professionals. FLIR, Boston
- Hens H (2012) Building physics-heat, air and moisture. Ernst & Sohn, Berlin
- Jewett J, Serway R (2008) Physics for scientists and engineers with modern physics. Thomson Higher Education, Belmont
- Kalamees T (2007) Airtightness and air leakages of new lightweight single-family detached houses in Estonia. *Build Environ* 42:2369–2377
- Loveday D, Taki A (2001) Section 3: heat transfer. In: Compton P, Jones W, Loveday D, Purvis M, Watson A (eds) Reference data, CIBSE guide C. Butterworth-Heinemann, London, pp 84–92
- Meola C, Carlomango G (2004) Recent advances in the use of infrared thermography. *Measure Sci Technol* 15:27–58
- NBN EN 13187 (n.d.) Thermal performance of buildings—qualitative detection of thermal irregularities in building envelopes-infrared method. Bureau voor Normalisatie, Brussels
- NBN EN 13829 (2001) Thermal performance of buildings-determination of air permeability of buildings-fan pressurization method. Belgisch Bureau voor normalisatie, Brussels
- Pearson C (2011) Thermal imaging of building fabric (BSRIA Guide 39). BSRIA 30
- Physibel V (2008) 3-dimensional dynamic simulation tool using the finite element method (Version 7.0 ed), Maldegem
- RESNET (2012) Interim guidelines for thermographic inspections of buildings. RESNET Residential energy services network
- Senave E, Standaert P, Walley B, Wouters P (1990) Annex 14 condensation and energy. The International Energy Agency (IEA)
- Van De Vijver S, Steeman M, Van Den Bossche N, Carbonez K, Janssens A (2014) The influence of environmental parameters on the thermographic analysis of the building envelope. QIRT, Bordeaux, p 10
- Van Den Bossche N, Huyghe W, Moens J, Janssens A, Depaep M (2012) Airtightness of the window-wall interface in cavity brick walls. *Energy Build* 45:32–42
- Willockx A (2010) Using the inverse heat conduction problem and thermography for the determination of local heat transfer coefficients and fin effectiveness for longitudinal fins. Doctoral paper, 283. Universiteit Gent, Gent

Evaluation of Moisture Transfer to Improve the Conservation of Tiles Finishing Facades

Silvia Erba, Bruno Daniotti, Elisabetta Rosina, Antonio Sansonetti and Riccardo Paolini

Abstract The research of methodologies and tools to improve the durability of building components has the aim to find out the strategies to increase the service life, minimizing the environmental impacts. The paper refers on clinker facades, especially after the repairs of mortars due to severe damages. The authors achieved on-site investigations on a prominent study case in Leonardo Campus, at Politecnico di Milano, and laboratory tests to study the interaction between moisture and cement mortars, the decay effects, and the protective treatments to improve the mortar durability. The research sharpens the methods for the evaluation of water absorption and moisture transfer in external building components and proposes possible strategies of intervention. The methodology focuses on the characterization of the water behavior in mortars by different tests, the experiments in laboratory on mortars samples, to study the hygroscopic and capillarity absorption properties, and on site, through visual analysis and nondestructive techniques. The researchers studied a water-repellent protective treatment to apply on the finishing surface and evaluated it in terms of water-repellent efficacy, compatibility with the substrate, vapor permeability, and color stability. The investigations provide input data, useful for simulating the moisture transfer, validating the experimentations, and modeling the physical mechanisms, which occur on the façade. In addition, the method

S. Erba (✉) · B. Daniotti · E. Rosina · R. Paolini
Politecnico Di Milano, Milan, Italy
e-mail: silvia.erba@polimi.it

B. Daniotti
e-mail: bruno.daniotti@polimi.it

E. Rosina
e-mail: elisabetta.rosina@polimi.it

R. Paolini
e-mail: riccardo.paolini@polimi.it

A. Sansonetti
Consiglio Nazionale delle Ricerche, Istituto per la Conservazione e Valorizzazione dei Beni Culturali (National Research Council, Department for the Conservation and Valorization of Cultural Heritage), Milan, Italy
e-mail: a.sansonetti@icvbc.cnr.it

analyses also the optical characteristics of the surface, with the aim to detect any change due to the application of further protective treatments and for aging process.

Keywords Moisture · Cements · Mortars · Water-repellent treatment · Durability

1 Introduction

The research of methodologies and tools to improve the durability of building components aims to find strategies to increase the service life, minimizing the environmental impacts (Nicolella 2003).

For existing buildings, the *residual service life* is the time span remaining after considering a specific moment. To assess the residual service life of an inspected building or component is crucial to *reconstruct its conservation history*, i.e., data on the original performance values, information on the installation, maintenance, trends of deterioration, etc.; several difficulties and the lack of information regarding the initial state prevent the complete achievement of this task. The process of assessment of the residual service life allows also to plan the remaining part of the service life, the performance levels to maintain equal or higher than the accepted threshold of the decreased service (Daniotti 2009).

As regards the listed contemporary buildings, a mandatory issue drives to the preservation of the original materials and features, together with keeping the residual service life of their components and system; therefore, the preservation criterion overcomes the functional criterion of maintaining the performance level by replacing the components before the end of their service life.

Therefore, the evaluation of risk factors and damage processes is the most important step for preventing decay, planning the effective routines for the early detection of anomalies, and constantly protecting the weakest part of the system.

The paper refers to a research aimed at improving the durability of clinker facades, especially after the repairs of mortars after severe damages. The authors achieved on-site investigations on an important study case in Milan and laboratory tests to study the interaction between the moisture and cement mortars, the decay effects, and the treatments to improve the mortar durability.

2 Planning Conservation Works in Humid Environment

The facades cladding is composed of cement mortar layers on which clinker tiles are applied. Therefore, the complete system of finishing includes the superimposition of mortar layers with different compositions and surface morphology. Moreover, the line between the tiles edges and the mortar constitutes a possible gap in the outer layer and therefore a vulnerable line for the infiltration of water, and it increases the risk of triggering damages.

The application of water-repellent treatments on the mortar is a new frontier for the conservation plans of cultural heritage. The protective treatment has the requirement to guarantee a hydrophobic performance, reducing the presence of water on the surface and near-surface regions. At the same time, a proper protective layer guarantees the water vapor permeability (Amoroso and Fassina 1983). These treatments slow the transformations of the materials due to the decay processes, caused by aggressive external agents, and the imbalances in the boundary conditions.

The researchers tested two different mortar mix designs based on cement, performing several tests to evaluate the water transport phenomena and the radiation properties. At a second step, they applied a water-repellent polymeric treatment on the mortar surface; after an appropriate curing time, they repeated the same tests.

In other words, the authors evaluated the water-repellent effectiveness through a series of laboratory tests and computer-based simulations, including the evaluation of the compatibility with the substrate, the color variations, and the permanence of the vapor permeability. A further step of the research will include the assessment of the durability of the system substrate/polymer through accelerated aging cycles varying temperature, relative humidity, and solar irradiance and also the investigations on the real site.

3 Case Study

3.1 *Città Studi, Sustainable Campus; Monitoring the Klinker Facades*

The case study here presented is a building inside the “Leonardo Campus,” Politecnico di Milano, see also Fig. 1, on which the researchers assessed the state of conservation within the research “Città Studi, Sustainable Campus.”¹ The Campus is representative of many typologies of contemporary buildings. The study case has an exterior cladding system of tiles. The facades materials, exposed to excessive rainwater infiltration or critical moisture content, show a visible damage and have a consequent reduction of their durability. Scientific literature reports the prediction about exterior finishing and cladding systems service life and the use of degradation models (Sousa 2008; Emídio 2012). In each case study, the phase of diagnostic knowledge represents an essential step aimed at the definition of the correct strategies of intervention to prevent the occurrence of failure and maintain, manage, and valorize the building components.

The researchers developed and validated the investigative procedure on some buildings with tiles cladding systems (buildings *n* 12, 14, 15, see Fig. 1), and later, they applied the procedure on buildings with plaster finishing (buildings *n* 1, 2, 3).

¹<http://www.campus-sostenibile.polimi.it/home>.

Fig. 1 Map of Leonardo Campus



Stoneware tiles cladding is a diffused rendering practice in Italy since the 1950–1960s, due to the good wear resistance, high temperatures stability, hardness, tenacity, and thermal inertia. Moreover, the durability of the ceramic materials, their low cost, and low sensitivity to the effects of pollution are some of the reasons of their application in the middle-southern region of Europe (Velosa et al. 2011). After 50 years of usage, the façades present a severe decay pattern, such as delaminations, missing tiles, and discoloration; this is due to the action of atmospheric agents, loss of adherence at the interfaces tile/mortar/support, and the absence of a correct maintenance. Giò Ponti, one of the most famous architects of 1950–1980s, designed some buildings in the Campus, and at present, their facades urgently require maintenance. The assessment of these façades is an important issue both for the economic aspects related to the costs of maintenance and for the repair project that deals with contemporary buildings having high historical–artistic value. From this side, preserving the authenticity of the building is a critical issue. At the current state of the debate, restorers generally accept that the repair should be clearly identifiable from a short distance. On the contrary, a “mimetic” solution, with the substitution of materials and elements with new ones “à l’identique,” is a practice that does not fit the conservation requirements. Therefore, the need to limit as much as possible the substitution rises up, preventing the damage by reducing the risk factors (environment, building techniques, use, lack of maintenance, etc.) by monitoring the degradation phenomena evolutions, and by means of a conservation plan.

Delamination, as defined by ICOMOS glossary (International Scientific Committee 2008), is the detachment process affecting laminated stones. It

3.2 Description of Building 12 and Diagnostics of the State of Conservation

Building 12 has an exterior stoneware tiles cladding (Fig. 3, left). The ceramic elements, flamed at high temperature (producer Italian Society of Grès, now Italcementi s.p.a.), are no longer under production. The body of the material is compact, and the superficial layer presents the typical glaze obtained through a vitrification while firing; the glaze thickness is around 50 μm , except for the corner tiles where it is enhanced at 150 μm (Fig. 3, right). The underneath layer is a cement mortar bedding 4 cm thick.

IRT was used after 2 h of solar heating on building 12. The thermal anomalies due to clinker tile delaminations were the target of the investigation.

This time span permitted to obtain the better contrast between delaminated areas and sound ones.

Cladding thickness and thermal characteristics, the presence and depth of defects, and environmental conditions (air T and RH, wind speed, solar irradiance) play a prominent role in the heat diffusion through the cladding itself.

As a result of the surveys phase, a series of pathological failures have been listed and classified according to the associated damage. The most spread and severe damage resulted the detachment, since it represents a source of danger in particular in the case of public buildings, such as a university; hence, the delamination requires a timely intervention for safety reasons (Re Cecconi 1996).



Fig. 3 Building 12 in Campus Leonardo (*left*); details of the tiles of building 12 (*right*)

Incorrect design and application are supposed to cause the majority of detachments and missing tiles. The areas where design errors caused the damages are mainly located close to the windows: the loss of adherence could be due to water infiltrations through the sill and the mullions, in the junction between the wall and the window frames. Rainwater can remain stagnant at the top of the window frames, because of the profile insufficiently leaning, causing the corrosion of the steel frames. Execution errors mainly deal with the mortar and to its high thickness (around 3–4 cm) where the several layers are not always adherent to each other's.

Cracking are also supposed to be mainly related to unsuitable design and application, because of the excessive shear stresses between tiles and support (due to the lack of the expansion joints) and the wrong choice and laying of the adhesive and substrate.

In addition to the IRT scanning and thermal analysis, the researchers completed the diagnostics by analyzing some samples of the facades materials and their decay products. Microscopic observations confirmed that the body of the tile is a compact ceramic material, very similar to earthenware, and the tiles have a finishing glazed layer; corner tiles do not differ from the others. EDS analyses of mortar samples resulted a common cement binder and sand as aggregate.

4 Moisture and Protective Treatments

4.1 Moisture Transport Mechanisms and Damages

The penetration of water in the structures causes a general decrease of their mechanical performances, depending on the absorption ability of the materials and their level of soaking (Coppola 1996). The causes of damage range from mobility of soluble salts, their crystallization inside the pores structure, freeze and thaw cycles, hydric expansion, and biological growth. Damage is located mainly on the surfaces (exfoliation, pulverization, efflorescence); otherwise, it can reach the bulk, causing cracks even across the section of the walls depending on the time of weathering exposure, the typology of building material, and the thickness of masonry. National and international standards provide the appropriate procedures to measure the specific parameters, which are helpful to evaluate the physical decay mechanisms and kinetics. In fact, the source of water infiltrations, their path into the structure, and their transport cycles in a short time determine the potential increasing of the existing damage.

Because of the previous surveys and analysis, the researchers chose two cement mortars (CEM I and IV) for bedding and prepared 36 specimens (18 of each type; dimensions 5 × 5 × 2 cm) for the laboratory investigations.

4.2 Consolidation and Protective Treatments

The use of consolidation and water-repellent treatment on natural stones is well known (Toniolo et al. 2002; Tsakalof et al. 2007). Many different organic compounds have been used as coatings for building materials (Horie 1987; Amoroso and Camaiti 1997) such as natural and synthetic waxes, acrylic resins, siloxanes perfluoropolyethers, fluorinated polyolefin, and fluoroelastomers. These different polymeric materials have been often used without an adequate knowledge of the properties of the polymer/stone system; therefore, the application did not reach an optimal formation of the final system. As a result, the treatment resulted not satisfactory for the insufficient protection effectiveness and/or the permanence on the substrate.

The term protective treatments identifies a range of products, materials, and structures, which play a defense action on building components against natural weathering or human actions. Systems, materials, and procedures can achieve the protective function, based on both active and passive interventions. The passive protection prevents the beginning of a process of degradation, acting on the causes of the degradation and/or around the component. This category includes screens, roofs or barriers (provisional or definitive), canopies, flashings, and overhangs. The active protection consists in the application of products on the surface to improve (reach) the water repellency of the protected matter. Hence, the protective treatments seek to slow the probability of transformations of the materials, because of aggressive external agents transported by water and imbalance with the surrounding environment.

In some cases, the protective products display properties similar to those of the ones under protection; nevertheless, their first requirements is to ensure water repellency and water vapor permeability.

The water repellency reduces the absorption of water into the material porosity. A good permeability allows the water vapor to pass through the material, avoiding any “barrier effect” which should accumulate water in a localized area.

4.2.1 Siloxane Treatments

Among the different protective products available on the market at present, the experimentation focuses on siloxanes, which are used since 1960 on natural stone; despite the application since a long time, less investigation focused on their application on artificial materials (Maravelaki-Kalaitzaki 2007; Allen et al. 1992). Siloxanes are organosilicon compounds; they form usually the backbone of the so-called silicones, and they are able to impart water repellency when applied to any surface. They show their chemical stability due to the Si–O bond. Once cured, they abate the penetration of water inside the pore structure, allowing a good water vapor permeability. Moreover, they are stable at atmospheric agents and do not change the substrate color, and they are not toxic. Nevertheless, there are also negative aspects,



Fig. 4 Application of the water-repellent siloxane treatment on the outer surface of cement mortar samples (CEM I and IV)

among which the scarce durability in the presence of sulfur dioxide (Mavrov 1983). The researchers chose the product CTS SILO 111, which substituted the less recent CTS 111, due to its common use in the restoration field (Fig. 4). Moreover, a vast bibliography exists, and it supports the study of its performances in several different conditions, comparing their performances with the ones of other products.

Different parameters affect the choice of a protective treatment:

- water-repellent effectiveness,
- chemical inertia with respect to the substrate,
- long-lasting vapor permeability,
- resistance to thermo-hygrometric variations,
- heat resistance,
- UV aging resistance, and
- penetration ability.

Erba (2015) refers about many investigation on the water-repellent effectiveness through a series of laboratory tests and computer-based simulations, the compatibility with the substrate and the chromatic alterations, and the permanence of the vapor permeability after the application of the product, all evaluated at the so-called time t_0 (after the curing of the polymeric treatment). In the following, the authors present and discuss the results of the laboratory tests and simulations.

4.3 Treated Mortars Properties for the Protection of Humid Walls

According to the German standard DIN4108-3 (Künzel et al. 2004), adequate plaster and protective layers for the protection of humid walls must present the following properties:

- water vapor diffusion-equivalent air layer thickness (S_d) lower than 2 m,
- water absorption by capillarity (A) lower than $0.5 \text{ kg/m}^2 \text{ h}^{0.5}$, and
- product of S_d and A lower than 0.2.

To fulfill these requirements, the authors tested different mixture for mortars by performing absorption tests such as the absorption by capillarity and the water vapor transmission tests. After this first step, they placed on the mortars' surface a water-repellent polymeric liquid treatment, and the tests were repeated.

5 Experimental Setup, Tests for the Characterization of Water Transport Phenomena, and Radiation Properties of Treated/Untreated Samples

The first step of the experimental research concerned the characterization of the water transport phenomena. The specimens for each type of mortars, having dimensions $5 \times 5 \times 2$ cm, were tested before and after the application of the protective treatment. The second part reports the results of the color and solar spectral reflectance test.

List of the laboratory tests:

- hygroscopic absorption (UNI EN 12571),
- water absorption by capillarity (UNI EN 15801),
- water absorption by partial immersion (UNI EN ISO 15148),
- long-term water absorption by immersion (UNI EN 12087),
- water vapor transmission (UNI EN ISO 12572), and
- color measures (UNI EN 15886).

In the following, the paper shows the adopted procedures and the results for the tests, underlying the differences between untreated and treated samples. In fact, after the first phase without the treatment, the researchers repeated the tests on the samples with SILO 111 CTS in white spirit 10 %, (applied by brush until reaching the condition of surface saturation). They left the specimen at laboratory conditions ($T 22 \pm 3$ °C; $RH 50 \pm 10$ %) for 30 days to guarantee the complete curing of the polymeric product, according to the UNI 10921.

5.1 Hygroscopic Absorption

The absorption test was executed in a climatic chamber, according to UNI EN ISO 12571 (2001) (Daniotti et al. 2014a, b) (Fig. 5). The researchers could not obtain the sorption curve values at relative humidity >90 % due to the technical features of the climatic chamber. The missing values will be obtained in the following part of

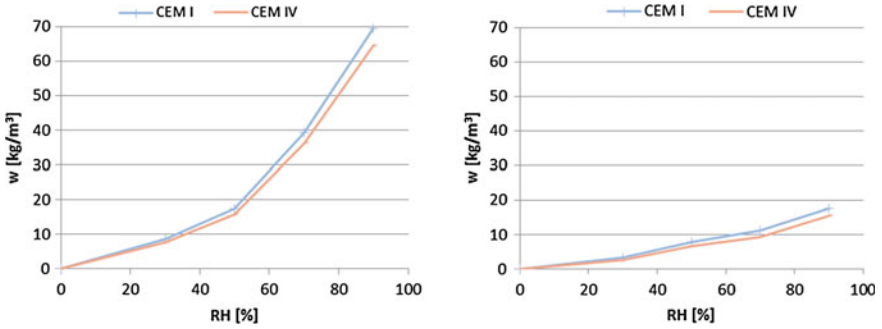


Fig. 5 Relative humidity–moisture content mass by volume (untreated specimens: *left*; treated specimens: *right*)

the research, through long-term water absorption by immersion (UNI EN 12087 thermal insulating products for building applications).

Observing the curves is possible to remark the reduction of the moisture content, due to the presence of the product: the tests performed on the specimens resulted with a high difference, and the moisture content decreases from around 70 to 20 kg/m^3 .

5.2 Water Absorption by Capillarity

The researchers determined water absorption by capillarity applying the standard UNI EN 15801 (2010) (Fig. 6).

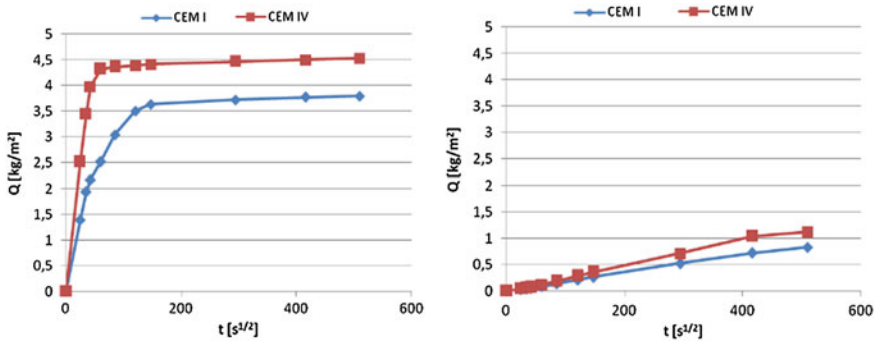


Fig. 6 Curves of capillary water absorption for cement mortars (untreated specimens: *left*; treated specimens: *right*)

Table 1 Capillary water absorption coefficient for the mortars specimens (untreated–treated)

Type of mortar	AC ($\text{kg/m}^2 \text{s}^{0.5}$) before treatment	AC ($\text{kg/m}^2 \text{s}^{0.5}$) after treatment	ΔAC ($\text{kg/m}^2 \text{s}^{0.5}$) before–after treatment
CEM I	0.065	0.002	0.063
CEM IV	0.100	0.003	0.097

The diagrams show that the siloxane treatment causes an abatement of the absorbed water. Table 1 shows the value of the absorption coefficient for the different mortars.

It is possible to notice that for both the mortars, the coefficient decreases from untreated to treated mortars. The test result on CEM IV shows the highest reduction in terms of AC value.

5.3 Water Absorption by Partial Immersion

The researchers compared the water absorption values obtained by capillarity and by partial immersion, determining the water absorption coefficient by partial immersion, according to the UNI EN ISO 15148, 2003. The samples were sealed with a sealant to prevent bypassing of the coating.

The main interest of this test was to find out the differences between the AC value and A_w value, since the thermo-hygrometric simulations in WUFI require the results from partial immersion tests.

Figures 7 and 8 show a faster absorption of water (see the darker color of the surface) in the specimens of CEM I with respect to the ones of CEM IV. After 40 min, the water reaches the outer surface.

The water absorption by partial immersion showed results very similar to those performed through capillary tests. The curves have the same trend, and the

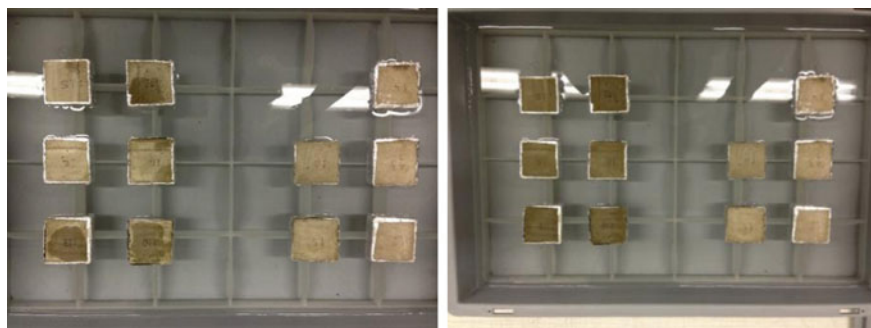


Fig. 7 In each photo, the samples on the *left* of the basin are untreated, and those on the *right* are treated. In the photo on the *left* CEM I specimens after 5 min and in the photo on the *right* after 40 min

application of the water-repellent treatment reduces the water absorbed from 5–6 kg/m² to 1–2 kg/m² (Fig. 9).

Table 2 shows the values of the water absorption coefficient for the two cement mortars. Table 3 shows the differences in terms of water absorption coefficient between the values obtained by capillarity and by partial immersion.

The coefficients obtained by partial immersion are always higher than those obtained by capillarity. This is probably because the specimens' surfaces are

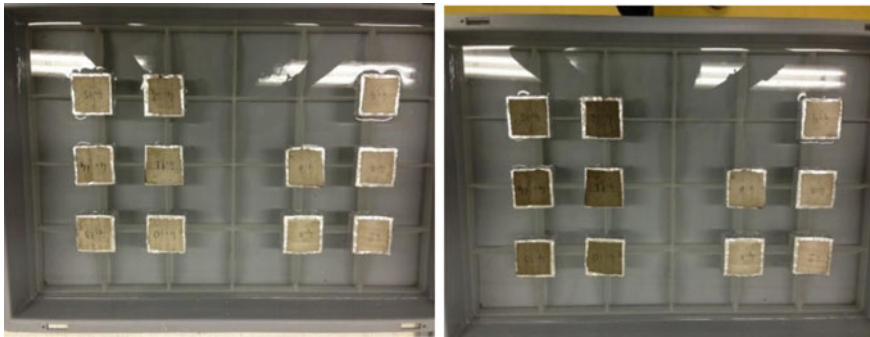


Fig. 8 In each photo, the samples on the *left* of the basin are untreated, and those on the *right* are treated. In the photo on the *left* CEM IV specimens after 5 min and in the photo on the *right* after 40 min

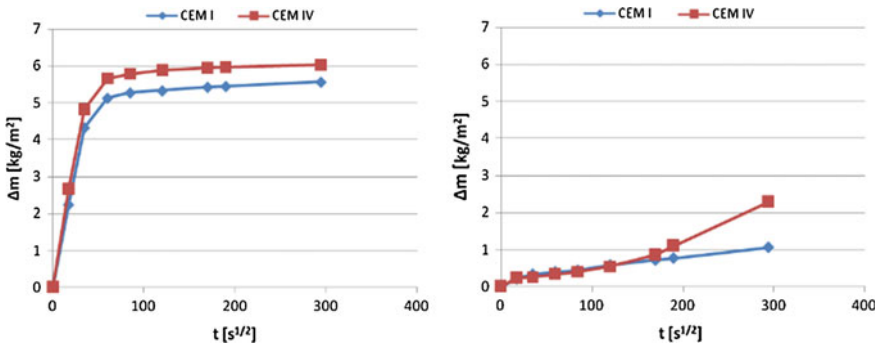


Fig. 9 Curves of water absorption by partial immersion for cement mortars (untreated specimens: *left*; treated specimens: *right*)

Table 2 Water absorption coefficient by partial immersion for the mortars specimens CEM I and CEM IV (untreated–treated)

Type of mortar	Aw (kg/m ² s ^{0.5}) before treatment	Aw (kg/m ² s ^{0.5}) after treatment	ΔAw (kg/m ² s ^{0.5}) before–after treatment
CEM I	0.125	0.003	0.122
CEM IV	0.139	0.005	0.134

Table 3 Differences between the water absorption coefficients by capillarity/partial immersion for the mortars specimens (untreated–treated)

Type of mortar	Aw (kg/m ² s ^{0.5}) before treatment	Aw (kg/m ² s ^{0.5}) after treatment	AC (kg/m ² s ^{0.5}) before treatment	AC (kg/m ² s ^{0.5}) after treatment	ΔAw-AC (kg/m ² s ^{0.5}) before treatment	ΔAw-AC (kg/m ² s ^{0.5}) after treatment
CEM I	0.125	0.003	0.065	0.002	0.060	0.001
CEM IV	0.139	0.005	0.100	0.003	0.039	0.002

Aw water absorption coefficient by partial immersion

CA water absorption coefficient by capillarity

directly in contact with water in the test of absorption by partial immersion, while in the test by capillarity, there is a layer of interposed paper. The differences between the two coefficients are negligible when considering treated samples, while for untreated samples, in particular for CEM I, the difference is quite significant.

5.4 Determination of Water Vapor Transmission Properties

The researchers tested the specimens following the standard UNI EN 15803, 2010, after the desiccation at 60 °C until reaching constant mass, to avoid alterations, especially once applied the water-repellent treatment (Fig. 10).

Table 4 shows the results of the mean values of water vapor resistance factors for the different types of mortars before and after the application of the siloxane product.

It is possible to notice that the values with and without the water-repellent treatment are almost equal, and therefore, the application of the product SILO 111 on cement samples does not add resistance to the flow of vapor.

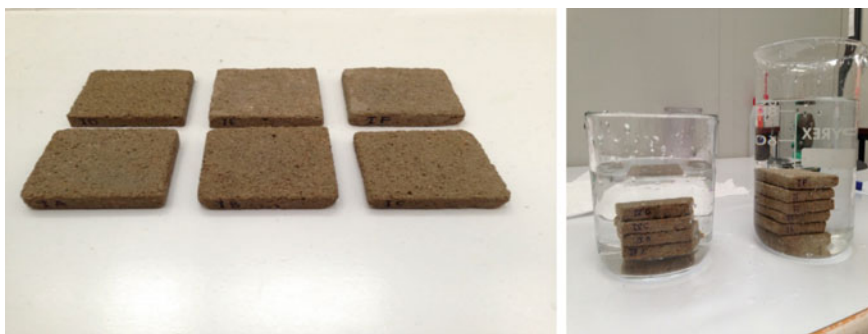


Fig. 10 Preparation of the sample for the evaluation of water vapor transmission properties: The images shows the cement samples placed in a container of deionized water

Table 4 Water vapor resistance factor for untreated/treated samples

Type of mortar	μ [-] before treatment	μ [-] after treatment
CEM I	13	14
CEM IV	10	12

5.5 Determination of Long-Term Water Absorption by Immersion

The determination of long-term water absorption by immersion has been performed following the standard UNI EN 12087, 2013.

The researchers studied the coefficient of long-term water absorption by immersion only for untreated cement samples. The long-term water absorption by total immersion is determined by measuring the change in mass of the test specimen, totally immersed in water, over a period of 28 days (Table 5).

Figure 11 shows the long-term water absorption by total immersion.

5.6 Color Test

The color measurement has the aim to evaluate the chromatic alterations caused by the application of the water-repellent treatment SILO 111 on the mortar specimens.

The researchers carried the measures out according to the standard UNI EN 15886, 2010. The method is based on the reflectance measures, which express the color as a number. Colors are represented in a solid or “color space” in which each point is univocally defined by three spatial coordinates to which correspond a defined color of the visible spectrum.

Table 5 Long-term water absorption value W_f by total immersion

Specimen	W_f (kg/m ³)
CEM I	224.7
CEM IV	260.7

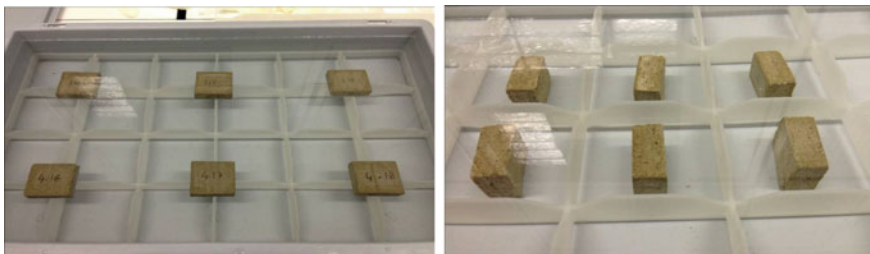


Fig. 11 Long-term water absorption performed on cement samples

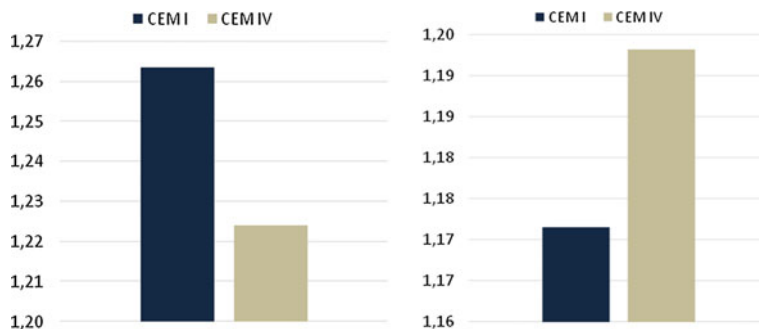


Fig. 12 Total color difference ΔE (left) and total shade difference ΔH (right) between the two cement types

In this test, the system of measurement of the color is the CIE $L^*a^*b^*$ (1976) according to the Commission Internationale de l'Éclairage (1931). The system is based on the mathematical transformation of the CIE space in a three-dimensional Euclidean space.

The variable L^* represents the measure of the brightness in a range from 0 to 100; a^* and b^* are the coordinates of the point of color in a Cartesian plane. Their values can be positive or negative, or can be equal to zero for both values for a neutral color (white, gray, black). The measurement was taken with a colorimeter Minolta Cr-200. The test procedure involves 25 measures for each specimen. The values of L^* , a^* , and b^* are the mean values of the 25 measures, taken to minimize the error due to the presence of chromatic irregularities on the surfaces of the specimens (Fig. 12).

The diagram shows that the application of the water-repellent treatment does not affect the surface color (ΔE ranging from 1.20 to 1.30). In fact, values around 1 are considered very good and not perceivable by naked eye.

5.7 Solar Reflectance

Spectrophotometry is the quantitative measurement of the reflection or transmission properties of a material as a function of the wavelength. The study aims to investigate the changes in reflection of mortars when the siloxane treatment is applied. The following graph of absorption versus wavelength (spectrum) presents the results on untreated and treated cement mortars specimens.

The solar reflectance tests follow the standard ASTM E903-12 (2012). The researchers selected 20 cement specimens CEM I and 20 cement specimens CEM IV: specimens 1.2–1.6 and 4.2– 4.6 have a siloxane treatment, while from 1.10 to 1.21 and from 4.10 to 4.21 are untreated. For each specimen, two measures have been carried out. The spectral reflectance was measured with a Perkin-Elmer Lambda 900 Spectrophotometer.

The machine was equipped with a 150-mm Spectralon-coated integrating sphere, a photomultiplier tube, and lead sulfide detectors. The authors measured the reflectance and compared the measurements to a Spectralon-calibrated reference in the 300–2500-nm wavelength range with a spectral resolution of 5 nm (Paolini et al. 2014). Two points of each sample lit by the measurement beam were used for the analysis; thus, the surface variations were considered. For each cement type of mortar (untreated–treated, CEM I–IV), the researchers computed the average spectral curve and then the integrated values.

Focusing on the spectral data, the portions of the solar spectrum where the treatment has the largest impact on the variations in reflectance can be determined (Fig. 13).

The main differences between CEM I and IV are visible at NIR; nevertheless, in general, the distance among the curves is constant along all the wavelengths. The trend of the measures of untreated and treated specimens is almost equal at NIR and becomes evidently different at VIS and UV, where it decreases for both the types of cement.

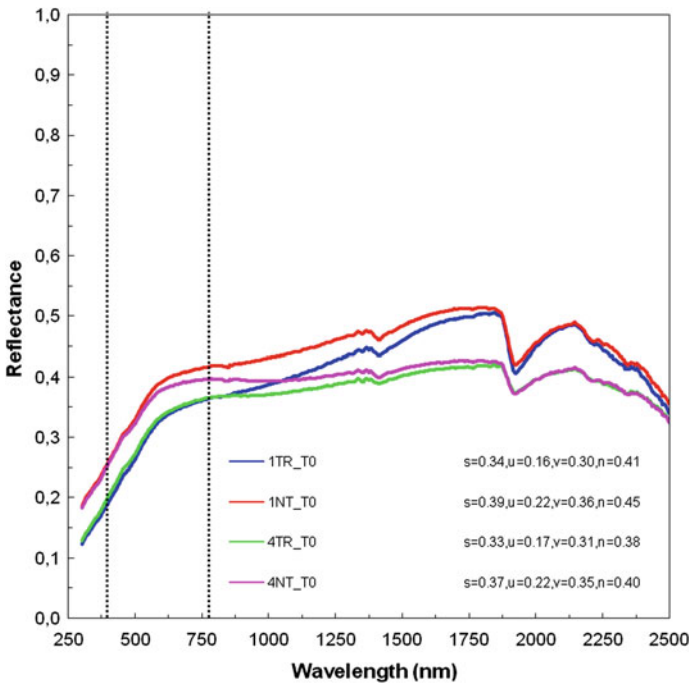


Fig. 13 Spectral and computed solar (*s*), UV (*u*), visible (*v*), and near infrared (*n*) reflectance performed before exposure; the curves of the specimens with siloxane treatment are TR, whereas the untreated are NT

6 Heat and Moisture Transfer

The research has shown that the conservation of historic building facades is closely linked to the moisture control and to the water transfer inside the components. An adequate evaluation of these factors is unavoidable to produce accurate and timely interventions. However, the experiments in laboratory and on-site are time- and money-consuming, and the possibility to trust on computer-based simulations would be useful and would guarantee savings (Künzel 1995; Krus 1996).

For this reason, the last part of the research deals with the validation of the results through computer simulations and the development of a set of data for the investigated building materials, and in particular, cement mortars evaluated with a water-repellent protective treatment.

The researchers used the program WUFI (Wärme und Feuchte instationär—Transient Heat and Moisture), developed by Fraunhofer Institute for Building Physics. It allows the use of data derived from outdoor and laboratory tests for the development of realistic simulations of the transient hygrothermal behavior of building materials and components, exposed to natural climate conditions.

The first step for the assessment of moisture transfer by numerical simulation has been the search through laboratory tests of the necessary material data set, which have been evaluated according to the standard UNI EN 15026 (2008). The thermo-hygrometric characterization of the mortars performed in laboratory and on site supported the simulations with the specific data of the materials of the analyzed case studies. However, during the simulations, the researchers used also the data of materials already existing in the database to catch the differences and understand the influence of the characterization data on the results. Moreover, they referred to the database for the characterization of the other materials composing the walls, which did not go under investigation in this research.

The specific boundary conditions have been referred to Milan and compared to the available data. The dynamic simulations are fundamental in case of the external layer evaluation, which is directly affected by the microclimatic variations occurring in the environment (Marra 2011).

Aim of the simulation was to support the choice of the best formulation in terms of compatibility and moisture absorption, simulating the behavior of the two mortars mix design with/without the application of the water-repellent treatment. For the sake of the research, the authors considered only the stratigraphy in correspondence with the mortar joints, and therefore, the model of the hygrothermal behavior of the components has been performed using WUFI-1D. A further development of the study implies 2D simulations especially in the case of tiles cladding systems, where the two sections of the finishing (mortar joints/tiles and embedded mortar) contribute in a different way to the final moisture balance of the façade.

The researchers investigated the northern façade of building 12, Campus Leonardo, and in particular focused the simulations on the bedding mortar layer. In fact, the thermographic analysis performed on the elevation underlined the presence

of adhesion problems distributed on the external cladding system. They assume a constant geometry of the mortar layer without swelling and shrinkages.

6.1 Material Properties and Boundary Conditions

According to the standard UNI EN 15026, 2008, Table 6 shows the list of the material properties, which are necessary for the simulations. The list of the hygrothermal properties are for both untreated and treated materials, according to the laboratory tests availability. The tests described in the previous paragraphs provided the measured values, which correspond to the following:

- bulk density ρ (kg/m³).
- moisture storage function (sorption curve) $w\phi$, according to the UNI EN ISO 12571, 2001.
- diffusion resistance factor μ . For the sake of the research, aimed at evaluating the permanence of the vapor permeability by the treatment, the researchers followed the standard UNI EN 15803, 2010. Actually, the values used for the simulations in WUFI are those obtained by dry-cup tests, according to the UNI EN ISO 12572, 2006. For these reasons, the measured values were verified with tabulated ones (ISO 10456 2007) and performed a sensitivity analysis. The values are comparable and do not affect the final results.
- liquid conductivity K that has been determined by the approximations using the water absorption coefficient by partial immersion (UNI EN ISO 15148, 2003). Moreover, the differences between the coefficients by partial immersion and capillarity observed for cement mortars appear not significant, especially for treated samples. For this reason, the researchers decided to use the values obtained from water absorption by capillarity test.

Table 6 Material data set and properties used in the simulations

	CEM I	CEM IV	
ρ (kg/m ³)	1928	1867	Measured
ε (m ³ /m ³)	0.3	0.3	Tabulated
c_p (J/kg K)	850	850	Tabulated
λ (W/m K)	1.2	1.2	Tabulated
μ [-] NT	13	10	Measured
μ [-] TR	14	12	Measured
A_w (kg/m ² s ^{0.5}) NT	0.125	0.139	Measured
A_w (kg/m ² s ^{0.5}) TR	0.003	0.005	Measured
AC (kg/m ² s ^{0.5}) NT	0.065	0.100	Measured
AC (kg/m ² s ^{0.5}) TR	0.002	0.003	Measured
α [-] NT	0.61	0.63	Measured
α [-] TR	0.66	0.67	Measured

The untreated mortars are defined as NT, whereas the treated ones as TR

- free water saturation (kg/m^3) taken from the laboratory tests according to the standard UNI EN 12087, 2013.
- shortwave (solar) radiation absorptivity [–] available for untreated cement mortars, according to the standard ASTM E903—12, 2012.

The other parameters [porosity ε (m^3/m^3), specific heat capacity of dry material c_p (J/kg K), and thermal conductivity of dry material λ (W/mK)] have been defined considering the standard ISO 10456, 2007.

The boundary conditions are defined in relation to the simulation to be modeled. The first analysis has regarded the validation of the laboratory test about hygroscopic absorption, and therefore, the researchers set up the boundary conditions according to the specific temperature and relative humidity inside the climatic chamber.

The second set of simulations regarded the evaluation of the real behavior of the mortars, in order to verify the efficacy of the water-repellent treatment in terms of water absorption reduction.

6.2 Simulation Modeling

The first analysis performed with WUFI-1D has been modeling the hygrothermal behavior of the mortar specimens obtained in the laboratory, to verify the data resulted from experimental tests (Marra 2011).

This series of simulation has been developed considering a mortar layer 2 cm thick, which corresponds to the thickness of the mortars specimens used in the laboratory. In the case of treated surfaces, the mortar has been divided in two parts: In the first, the researchers inserted the values obtained on the treated specimens and in the second the untreated ones, since the researchers assumed that the protective treatment properties are to be considered in the first centimeter of product penetration. They have defined the boundary conditions considering constant temperature at 20 °C, while imposing different steps in the relative humidity, corresponding to those used in the climatic chamber during the hygrothermal absorption tests (0, 30, 50, 70, and 90 %). The initial relative humidity of the component has been zero since the specimens remained in the desiccator until they reach the constant weight before the test.

The duration of the desiccation was two week (336 h) for the first two RH steps (30, 50 %) and of four weeks (672 h) for the remaining steps (70, 90 %).

In the analysis, the conditions imposed on both the sides of the samples are equal since the specimens were freely in contact with the environment inside the climatic chamber. In this case, it should be noted that in WUFI, only two surfaces are considered at the moisture balance, while in the laboratory tests also the sides contributed to the hygroscopic exchanges.

In the second set, the researchers simulated the presence of a plastic film, since during the laboratory tests a plastic waterproof paraffin film sealed the boundary of the specimens, leaving only one free surface exposed toward the environment. They considered 3 measurement points placed, respectively, on the surface (0 m) at 0.05 m in depth and in the center of the sample (0.01 m) to monitor the trend of relative humidity along the thickness of the layer.

Figure 14 shows the simulations for CEM I mortar; nevertheless, the results were similar also for CEM IV.

In general, it is possible to notice that the component reaches the equilibrium with the environment in a longer time when relative humidity is increasing.

Adding the waterproof layer, the time to reach equilibrium increases with respect to the simulations considering free specimens, since the area exposed is reduced. Treated specimens reach faster the equilibrium.

The second objective of the simulations was to verify the best mortar mix design in terms of the lowest moisture absorption among those investigated. In the following, the researchers have performed simulations on treated mortars to verify the effectiveness of the applied siloxane water-repellent treatment (SILO 111) (Fig. 15).

The graph shows a reduction of absorbed water and in the water content peaks in the specimens treated with the siloxane product SILO 111 with respect to the untreated mortar.

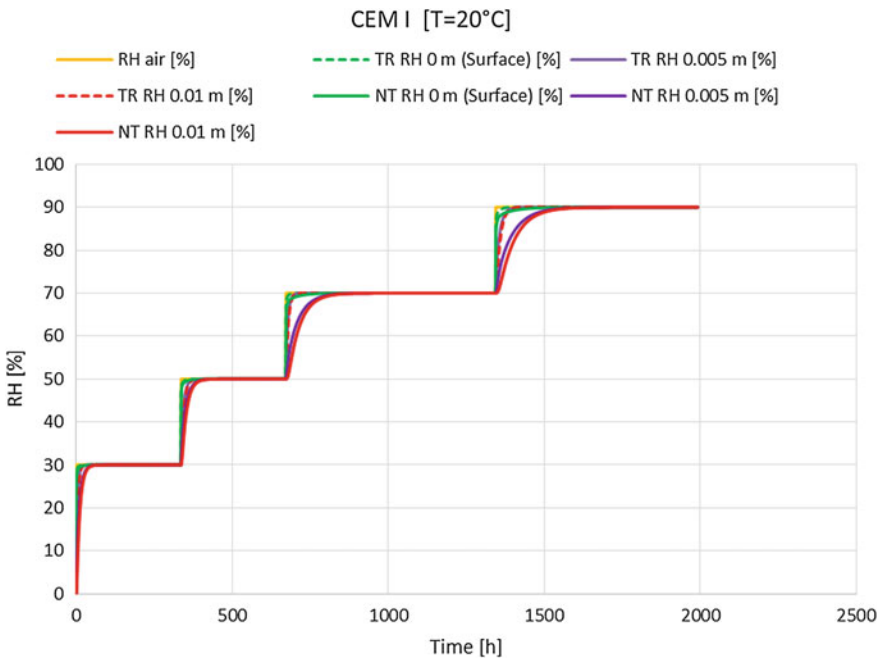


Fig. 14 Comparison of the RH trends for untreated/treated cement (CEM I) specimens

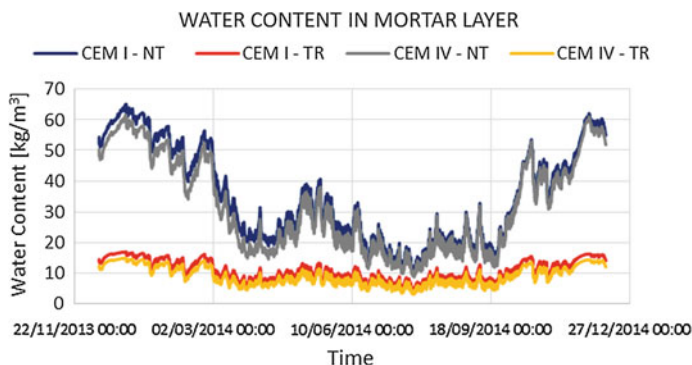


Fig. 15 Comparison of the water content trend in the external mortar (joints-section) for treated/untreated cements specimens

The trend for the two cement mortar types is equal even if CEM IV shows a higher reduction both in the treated and in the untreated curve.

Moreover, from the reported graphs, the dependency on the seasons of the trend of water content is apparent in the untreated specimens: in spring/summer, it is equal to 20 kg/m^3 , while in autumn/winter, it is around 50 kg/m^3 . Instead, for the treated specimens, it is almost constant. These simulations have shown the efficacy of the treatment in terms of absorbed water in the external mortar layer.

7 Conclusions

The presented work suggests a methodology for the evaluation of moisture transfer in bedding mortar layers to improve the conservation of clinker facades. Besides, the results of the monitoring and of the experiments provide effective indications for the correct strategies of maintenance (Daniotti et al. 2014a, b).

The investigations on the application of the water-repellent siloxane treatment SILO 111 show that the analyzed mortars fulfill the requirements necessary for the protection of humid walls (Künzel et al. 2004). Moreover, the treatment has shown its water-repellent effectiveness and its vapor permeability: the water vapor resistance factor, obtained through the experiments in laboratory, basically, remains constant between untreated/treated samples. Besides, it is resistant to thermo-hygrometric variations, it does not provoke chromatic alteration on the surfaces, and it is compatible with the substrate. The computer simulations on moisture transfer validated the results obtained through the laboratory tests and verified the effectiveness of the siloxane protective treatment in terms of reduction of absorbed water.

References

- Allen NS, Edge MD, Horie CV (1992) *Polymers in conservation*. Royal Society of Chemistry, Cambridge
- Amoroso G, Camaiti M (1997) *Scienza dei materiali e restauro*. Alinea Editrice
- Amoroso GG, Fassina V (1983) Stone decay and conservation. *Materials Science Monograph*, 11
- ASTM E903-12 (2012) Standard test method for solar absorptance, reflectance, and transmittance of materials using integrating spheres
- Caglio S, Redaelli V, Gargano M, Ludwig N, Rosina E (2011) The surfaces of contemporary architecture: characterization of clinker by IRT. In: *Proceedings of 11th international workshop on advanced infrared technology and applications*. L'Aquila, pp 1–10
- Coppola L (1996) Umidità nelle costruzioni: diagnosi e rimedi. In *Presenza tecnica*, pp 79–86
- Daniotti B (2009) *Building durability and maintenance*. Cusi, Milano
- Daniotti B, Erba S, Rosina E (2014) Development of a methodological procedure for the durability evaluation of existing exterior finishings. In: *Proceedings of XIII international conference on durability of building materials*, Sao Paulo
- Daniotti B, Erba S, Muioli R, Rosina E, Sansonetti A (2014) PPC at Lavello Convent: towards a sustainable conservation plan after the restoration. In: *Proceedings of the PPC conference: preventive and planned conservation*, Monza-Mantova
- De Freitas SS, De Freitas VP, Barreira E (2014) Detection of façade plaster detachments using infrared thermography—a nondestructive technique. *Constr Build Mater* 70:80–87
- Emídio FA (2012) *Dissertação par a obtenção do Grau de Mestre em Engenharia Civil - Aplicação do método factorial à previsão da vida útil de revestimentos de pedra natural*. Instituto Superior Técnico, Universidade Técnica de Lisboa, Lisboa, Portugal
- Erba S (2015) *Knowledge and diagnostics for the durability of external finishing systems*. Doctoral dissertation in Building Engineering, Politecnico di Milano. Supervisor: Daniotti B, Co-Tutors: Rosina E, Sansonetti A
- Horie CV (1987) *Materials for conservation*. Butterworth & Co, London
- ICOMOS International Scientific Committee (2008) *ICOMOS-ISCS: Illustrated glossary on stone deterioration patterns*. Champigny/Marne, France
- Krus M (1996) *Moisture Transport and storage coefficients of porous mineral building materials*. Fraunhofer IRB Verlag
- Künzel HM (1995) Simultaneous heat and moisture transport in building components. One- and two-dimensional calculation using simple parameters. Fraunhofer IRB Verlag
- Künzel HM, Künzel N, Holm A (2004) Rain protection of stucco facades. In: *Proceedings of the performances of envelopes of whole buildings IX conference*. Clearwater Beach, Florida
- Ludwig N, Rosina E, Caglio S, Gargano M, Redaelli V (2012) Heat diffusion in Klinker facade: the study case of a Giò Ponti building. *Adv Opt Technol*
- Maldague X (ed) (2001) *Non destructive testing handbook*, 3rd edn, vol 3: Infrared and thermal testing. ASNT Columbus (OH), USA
- Maravelaki-Kalaitzaki P (2007) Hydraulic lime mortars with siloxane for waterproofing historic masonry. *Cem Concr Res* 283–290
- Marra E (2011) *Influenza dell'ambiente sulla corrosione degli inserti di acciaio nelle murature antiche*. Doctoral dissertation in building engineering, Politecnico di Milano. Tutors: Daniotti B, Bertolini L
- Mavrov G (1983) Aging of silicone resins. *Stud Conserv* 28:171–178
- Nicolella M (2003) *Programmazione degli interventi in edilizia. Guida al libretto di manutenzione del fabbricato*. Maggioli Editore
- Paolini R, Zinzi M, Poli T, Carmiolo E, Mainini AG (2014) Effect of ageing on solar spectral reflectance of roofing membranes: natural exposure in Roma and Milano and the impact on the energy needs of commercial buildings. *Energy Build* 333–343

- Re Cecconi F (1996) Metodologie e strumentazioni per la previsione della durabilità di componenti edilizi per edifici scolastici ai fini della loro programmazione manutentiva. Doctoral dissertation. Politecnico di Milano
- Sousa R (2008) Dissertação de Mestrado Integrado em Engenharia Civil - Previsão da vida útil dos revestimentos cerâmicos aderentes em fachada. Instituto Superior Técnico, Universidade Técnica de Lisboa, Lisboa, Portugal
- Toniolo L, Poli T, Castelvetro V, Manariti A, Chiantore O, Lazzari M (2002) Tailoring new fluorinated acrylic copolymers as protective coatings for marble. *J Cult Heritage* 309–316
- Tsakalof A, Manoudis P, Karapanagiotis I, Chryssoulakis I, Panayiotou C (2007) Assessment of synthetic polymeric coatings for the protection and preservation of stone monuments. *J Cult Heritage* 69–72
- UNI EN 12087 (2013) Thermal insulating products for building applications. Determination of long term water absorption by immersion
- UNI EN 15026 (2008) Hygrothermal performance of building components and building elements. Assessment of moisture transfer by numerical simulation
- UNI EN 15801 (2010) Conservation of cultural property. Test methods. Determination of water absorption by capillarity
- UNI EN 15803 (2010) Conservazione dei beni culturali - Metodi di prova - Determinazione della permeabilità al vapore d'acqua
- UNI EN 15886 (2010) Conservazione dei Beni Culturali - Metodi di prova - Misura del colore delle superfici
- UNI EN ISO 12571 (2001) Hygrothermal performance of building materials and products: determination of hygroscopic properties
- UNI EN ISO 12572 (2006) Hygrothermal performance of building materials and products. Determination of water vapour transmission properties
- UNI EN ISO 15148 (2003) Hygrothermal performance of building materials and products: Determination of water absorption coefficient by partial immersion
- Velosa A, Veiga R, Martins G (2011) Water behaviour of old and new tiles—a contribution towards the conservation of ceramic facades. In: *Proceedings of XII DBCM, Porto, Portugal*

Analysis of Microclimate in a Historical Building to Assess the Probability of Recurrence of Filamentous Fungi

Fernanda Lamego Guerra, Eduardo Grala da Cunha and Fábio Galli

Abstract Filamentous fungi are important agents of deterioration, able to result in actual losses in many construction materials. Relative humidity (RH), surface temperature, and nutrient availability, in addition to the characteristics of substrates such as hygroscopicity and pH are critical factors in the development of related pathological manifestations. This study presents an analysis of the microclimate in a nineteenth-century historic building in the city of Pelotas, Southern Brazil, in order to verify the probability of recurrence of filamentous fungi. Eight sensors were installed in different indoor environments, for monitoring RH and temperature values in one year. The data analysis shows that, regarding microclimate, the recurrence of fungi is possible due to exposure of walls with high values of RH (above 70 %) for a prolonged period. The development of this type of analysis intended to indicate strategies to control the filamentous fungi growth from the microclimate control and ongoing maintenance of the historic building materials.

Keywords Filamentous fungi · Microclimate monitoring · Historical buildings

1 Introduction

Pelotas is a city in southern Rio Grande do Sul, Brazil. The first historical mention of the city's emergence dates from June 1758, but it was officially recognized in 1835. It has an important cultural heritage, evident in several architectural speci-

F.L. Guerra (✉)

Federal University of Rio Grande do Sul—UFRGS, Porto Alegre, Brazil

e-mail: f.lamegoguerra@gmail.com

E.G. da Cunha

Faculty of Architecture and Urbanism, Federal University of Pelotas, Pelotas, Brazil

e-mail: eduardogralacunha@yahoo.com.br

F. Galli

Conservation and Restoration of Movable Cultural Heritage, Federal University of Pelotas, Pelotas, Brazil

e-mail: fabiogallirestauro@uol.com.br

mens as well as in its urban setting. There are many buildings protected through the national conservation buildings organization, the IPHAN (*Instituto do Patrimônio Histórico e Artístico Nacional* or Institute of National Historical and Artistic Heritage).

The Pelotas Candy Museum, analyzed in this work, is part of the assets protected at a national level. This edification was constructed in 1878 and its project is attributed to Italian architect José Isella. It was part of a set of two other buildings in a Neoclassic style. Figure 1 shows the analyzed building.

The house remained closed from 2000 to 2011, when the restoration work started. During this period in which the house remained unoccupied, its state of deterioration was intensely aggravated. Several points of rainwater infiltration resulted in losses of material at various points of stucco ceilings, as well as the rotting of wooden floor in many environments. The wall coatings were ripping, deteriorated, and one could verify the presence of many spots related to biological deterioration agent growth, which was also seen on the surface of wood (Fig. 2). These conditions imposed the indispensable need for a complete restoration.

In 2011, before the beginning of the restoration work, a surface sample collection was made in 10 of the 30 rooms, in order to identify the main genera of filamentous fungi involved in the surface deterioration. The traditional identification method with a swab moistened with distilled water was used, passing over the area where stains probably related to fungal growth were visualized. The samples obtained directly from the surfaces were placed in a Potato-Dextrose-Agar (PDA) medium, (ACUMEDIA[®]), acidified (pH 4) with tartaric acid (10 %), suitable for fungi (Fig. 3). It was possible to identify nine different genera of

Fig. 1 Pelotas Candy Museum





Fig. 2 Indoor ambience before the restoration



Fig. 3 a, b, c Fungal growth example in Petri dishes from the building indoor surfaces collection

filamentous fungi involved in biodeterioration of materials collected from selected surfaces: *Aspergillus*, *Aureobasidium*, *Cladosporium*, *Fusarium*, *Paecilomyces*, *Papularia*, *Penicillium*, *Rhizopus*, and *Trichoderma*.

The mentioned traditional method of analysis used to identify the fungal genera is rather limited. The culture medium produced in the laboratory is very selective, thus it is only possible to identify agents involved in the process of deterioration. In addition, it is known that the formation of biofilm occurs on interaction between different populations and communities of microorganisms, like different types of bacteria, for example. However, fungi are among the most active microorganisms in these processes and the nature of substrate will determine the type of degradation (Arroyo 2009).

The restoration of the analyzed building was completed in 2012. Although it changed its occupation form, now being used as a museum, the natural thermal regime of exchange and ventilation was maintained. The building has walls with high thickness (about 0.50 m), which favors the natural balance of the interior microclimate, due to increased resistance to thermal exchanges. Additionally, the entire building has rooms with high ceilings (about 4.80 m), and large rates of natural ventilation provided by outward-oriented frames. All the environments are interconnected, which also favors the free circulation of the air flow.

Therefore, this study aims to evaluate the microclimate conditions in preselected indoor environments through monitoring of temperature and relative humidity (RH), in order to evaluate the probability of filamentous fungi recurrence.

It is known that buildings' natural environments are exposed to biological contaminants that are easily transported by air and by other means. When there are favorable conditions for it, especially humidity, temperature, and nutrients, the development of these microorganisms results in changes on the surfaces (Allsopp et al. 2010). Furthermore, the concentration of contaminants in the air may be associated with health problems in people who remain for a long time in such environments. Crook and Burton (2010) explain that humans are constantly exposed to fungi, usually without suffering harm to health. However, in some instances, inhalation of sufficient numbers of fungi spores can trigger symptoms of asthma, rhinitis, or bronchitis. Respiratory ill health associated with the built environment is often referred to as Sick Building Syndrome (SBS).

The proposed monitoring can help to understand the mechanisms of natural thermodynamic indoors and thus facilitate the search for microclimate control strategies, respecting the historical conditions of the building, in order to prevent further proliferation of filamentous fungi. For proper verification, the museum's occupancy routine was registered, during the monitoring period, by completing monthly spreadsheets. In order to obtain the microclimate data, a measurement sensor was installed in eight of the building's indoor environments, as well as an external sensor for checking the outside microclimate near the building. The data are obtained through HOBO model equipment: HOBO H8 RH/Temp Data Logger. The sensors were configured to obtain schedules of RH and temperature values in continuous mode.

2 Biological Growth and Decay Mechanisms in the Materials of Buildings

International researches about biodeterioration of building materials have increased in recent decades. The problem becomes more important when such materials are part of historical heritage and degradation results in priceless losses.

According to Warsheid and Braams (2000), water availability is one of the most important factors that influence biological infection and the intensity of biodeterioration of material. The evaluation of the biological contribution to decay starts

with the descriptions of the type of material and exposure conditions (e.g., rising dampness, damaged water drainage, condensational moisture) and nutrients (e.g., inorganic and organic compounds from natural or anthropogenic sources).

In a preventive way, effective control of the water and nutrient availability by and in the material is the first step to control biodeterioration, even before the adoption of treatments with biocides (Warsheid and Braams 2000).

In Brazil, some researches have been developed, mainly on the facades of historic buildings, on which the occurrence of a large microbial diversity could be verified. Crispim (2003) proposed the morphological and molecular analysis of cyanobacteria in biofilm on external surfaces in Porto Alegre, Southern Brazil; Kiel (2005) studied the bacterial diversity in external surfaces; Shirakawa (1994), Shirakawa et al. (1997, 2002, 2003), Vieira et al. (2009) did many researches on different building materials. Among the various fungi identified in the research carried out in southeast Brazil, *Cladosporium* was found to be the fungi genera most frequently recovered from field species (Shirakawa et al. 2003).

According to Caneva et al. (2000), the biological growth is strongly influenced by climatic parameters, with temperature being a conditioning factor for living organisms because it interferes with the kinetics of biochemical reactions and the structure of molecules that constitute cells. Thus, the biological development in a rather wide temperature rating is possible; however, biologically active metabolism lies in a narrower range. Therefore, it shows a distinction between the active life and survival in an inactive form as a response to environmental conditions. The microbial diversity conditioned by the climatic conditions of different regions may interfere with the development of certain species of microorganisms at the expense of others. Thus, it is increasingly important to conduct research capable of identifying the main agents responsible for deterioration of materials related to the different microclimates. Knowing the agent and the influential environmental conditions in your development, it is possible to propose strategies that minimize development.

2.1 Bioreceptivity and Construction Materials

Depending on the material nature, mineral composition, porosity and permeability, environmental factors (mainly the water availability), pH, climate exposure, and nutrients sources, the growth of certain organisms is favored over others. Materials that are mineralogically similar can be attacked by the same kind of microorganisms, using the same mechanisms. Inorganic nature construction materials such as concrete and limestone are a poor substrate nutrient for organisms that require organic sources for their metabolism, like filamentous fungi. However, the natural aging of these materials, nutritional enrichment by dirt deposits, as well as the prior growth of other microorganisms such as autotrophic bacteria can, in many cases, favor the development of other heterotrophic agents, like filamentous fungi (Warsheid and Braams 2000).

Many authors cited by Warsheid and Braams (2000) mention that limestone and marble generally consist of a dense calcareous matrix allowing mainly a superficial microbial contamination. Nevertheless, the material seems to be subject to lichens and fungal attack.

Plaster, mortar, and ceramic materials are often used in buildings and can be considered stone materials produced by humans, though its biological agent degradation mechanisms may be similar to those occurring in natural stones. In addition to the differences in chemical composition, these materials generally have a higher porosity, favoring water retention, and consequently creating a favorable substrate for the development of many kinds of microorganisms (Caneva et al. 2000).

2.2 Filamentous Fungi and the Influence Factors for Its Development

Filamentous fungi are among the most active microorganisms in biodeterioration and the substrate determines the type of degradation (Arroyo 2009).

The fungi degrade substantial amounts of organic nature materials through the action of enzymes that cause a reduction or loss of the material itself (Sterflinger 2010; Sterflinger and Piñar 2013). On surfaces of inorganic nature, however, although the material itself is not the nutritional source, the filamentous fungi structures penetrate causing the detachment of materials' surface layers. Fungi cause serious changes in the surfaces due to colony formation and secretion of pigments. Fungi develop on the material's surface, producing spores that disperse in the air. They utilize the available nutrients in the substrate, which are easily assimilated for their growth. When the ideal conditions for their growth are met, the spores germinate and the hyphae grow, forming the mycelium. This process can occur in parts of the building and on surfaces indoors, causing risks to ambient air quality and exposing the occupants to potential health hazards (Johansson et al. 2012).

Three main factors required for growth of filamentous fungi on the surface of the material are nutrients, temperature, and humidity, which must be considered simultaneously with respect to the exposition time (Sedlbauer et al. 2003). Besides these factors, Johansson et al. (2012) emphasize the pH of the surface. According to Caneva et al. (2000), many organisms and microorganisms prefer neutral conditions; however, many species of fungi are acidophilic, preferring lower pH values. The growth of filamentous fungi on surfaces results in the production of various organic acids (citric, oxalic, gluconic, glucuronic, lactic, fumaric). The degradation of the substrate by chemical solubilisation always results in a reduction in the pH on the surface of the materials. According to Sterflinger (2010), fungi play a significant

role in the deterioration of buildings due to its high enzymatic activity and its ability to grow at low values of water activity (a_w).

Most building materials, such as mortar, are inorganic in nature. Considering the need for organic compounds as a nutritional source for fungal growth, these substrates, in principle, would not support the development of this type of microorganism. However, the presence of organic matter is very common in these substrates, especially if the materials are exposed to certain conditions. For example: air pollution, pollen, debris from previous biological colonization, restoration treatments with traditional materials (waxes, oils, and casein) or new (protectors, consolidants), accumulation of dust and dirt, can all favor the development of heterotrophic microflora, as the filamentous fungi (Caneva et al. 2000; Warsheid and Braams 2000; Shirakawa et al. 2003; Arroyo 2009).

According to Arroyo (2009), fungi do not use the inorganic supports for nutrition but they do alter them deeply with synthesis products from their own metabolism, such as inorganic and organic acids. The latter can produce chelation and form complexes with metabolic cations, which are obtained from the support.

Many fungi are responsible for the formation of black crusts due to the melanin in their hyphae. This fungi structure can penetrate the limestone calcite crystal previously dissolved by enzymes (Arroyo 2009).

The fungal growth can also be influenced by the physical properties of the materials, in particular its porosity and hygroscopicity, which influences the water content of the materials. However, other phenomena such as capillary absorption and high RH, especially near the values condensation or rainwater may also increase the water content of the materials (Caneva et al. 2000).

Caneva et al. (2000) also emphasize that not all water present in the substrate is available from the metabolic point of view. The amount of water actually available for chemical and biochemical reactions of the body is defined as the water activity (a_w). This parameter values varies between 0.6 and 0.998 a_w . Most bacteria require values greater than 0.98 a_w , while fungi can tolerate lower values.

The fungal growth in museums is strongly determined by the indoor climate, the nutritional availability from atmospheric contamination and the materials themselves, as well as the availability of nutrients enabled by inadequate cleaning intervals. It considers RH 55 % as the limit to prevent the growth of fungi, therefore, the climate control should be adjusted accordingly (Sterflinger 2010).

Arroyo (2009) mentions that, after confirming the presence of filamentous fungi growing in the support, in the first place we ought to eliminate the conditions that favor their development, such as environmental conditions (humidity and temperature), nutrients, light, etc.

In the case of museums, it is important to consider the museum spaces and the collections as well. In this sense, Arroyo (2009) reports that we ought to provide the building with a suitable climate, to eliminate all the humidity sources and to keep it under stable conditions, never below 50 % or above 62 %. As regards temperature, it should never be higher than 20 °C.

3 Monitoring

The differences in the average or long-term level of humidity cause visible differences in fungi growth. A control of the hygroscopic surface parameters could lead to a profound reduction in the biological infestation. In this way, the environmental monitoring is an important tool to understand to which conditions are the materials exposed and, thus, propose correct strategies to protect the building's materials and surfaces from biological growth (Krus et al. 2007).

Therefore, considering the importance of microclimate analysis as a tool to propose strategies for environmental conditioning to contain biological growth, monitoring of the inner microclimate was held, regarding RH and temperature, as described below.

3.1 Selection of Environments

The analyzed building is located on a corner lot. It has two gardens, one located in its front and another on its backside. A small part of the house has a second floor, in which rooms were possibly rented in its original use. It has a high basement, to the full extent of the main block. The building has 43 rooms. Among them, eight environments were selected for the distribution of sensors, six on the ground floor and two upstairs. The choice took into account various conditions regarding the exterior facades, as well as the locations where main activities of the museum would take place.

3.2 Arrangement of Sensors

For proper verification of data obtained from the sensors, prior measurement was made, in order to make sure that the equipment was adequate and in appropriate conditions of use. The specifications of the sensor accuracy are indicated for the values of temperature of ± 0.7 °C and ± 5 % RH. From analysis of the measurement data, it was observed, on average, values of temperature accuracy of 0.38 °C and RH of 2.39 %, thus being appropriate for use.

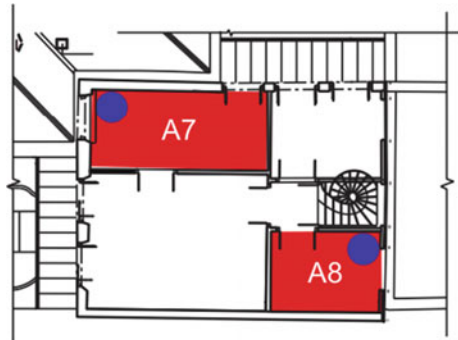
Due to the verified fragility of the lining walls, composed of handmade lime-based paint, the sensors were fixed near the side of the internal doors. Thus, the occurrence of any superficial detachment would be easier to repair, with the benefits of the discreet location. The sensors were fixed at a height of 2 m from floor level.

Considering the importance of checking the occupancy routine and use of the house, a worksheet for monthly notes was made, referring each of the environments analyzed and forwarded to the administrative staff of the museum. The spreadsheet



Fig. 4 Environments monitored on the ground floor

Fig. 5 Environments monitored upstairs



contains information regarding the activities undertaken in each environment, number of occupants and round occupancy, equipment installed and in use, frequency and time of opening of doors and windows (glass and shutters), and the frequency and method of cleaning environments. Figures 4 and 5 show the ground and upper floor plan of the building. The rooms hatched in red are the ones selected as monitoring environments; the blue marks indicate the prominent place of installation of the sensors.

The environments named *A1*, *A2*, *A3*, and *A4* are occupied with temporary expositions and sometimes with academic activities proposed by the museum. The elaborate design of the museum reserves these environments for use as exhibits for the arrangement of artistic elements, leaving surfaces free of spaces, which together compose the collection itself. The *A5* environment is a busy bookstore, featuring shelves of books that cover the surfaces of the walls of the environment. The *A6* is the cafeteria. The *A7* and *A8* of the top floor rooms are occupied by the administrative part of the museum.

The building was visited regularly and the data were unloaded from the sensors on average every 2 months. The downloading of data was done using BoxCar Software, which provides the files in a format compatible with Excel Software, allowing reading, tabulation, and graphical formulation for the analysis of micro-climatic data of the building.

4 Results and Discussion

The spreadsheet data formulated for routine monitoring of the building shows that environments *A1* (showroom) and *A6* (coffee shop) have the greatest number of occupants. The first one has been used for conducting classes of orchestra musicians from the local university. It receives, on average, 15–20 people daily. The *A3*, *A4*, and *A5* environments remain unoccupied most of the time. The administrative sector (*A7* and *A8*) is occupied by a maximum of two people. The only equipment installed in environments are lamps for ambient lighting, except for the *A7* and *A8* environments that have computers. The windows of the museum are open Monday through Friday during morning and evening lighting. Natural ventilation occurs when there is presence of occupants, such as when using the administrative part, bookstore, and cafeteria. Natural ventilation is provided only when the weather presents mild temperatures. The house is swept daily, and wax is applied on the wooden floor once a week. The windows are cleaned once a month.

Based on what was observed, the edification was not yet fully occupied. The plans for the museum to this moment have not yet been implemented. However, there is an attempt to use the edification, even with activities unrelated to the ones it was designed for, in order to allow the building to remain open and thus have better conditions for its preservation.

The ventilation and thermal conditioning of the house are controlled in a natural way. Prior to the monitoring, there was no knowledge of the microclimate inside the building. The natural mechanism for controlling the temperature and humidity inside has been thought of empirically. Only from the analysis of the data obtained in the monitoring will it be possible to devise strategies for the control of micro-climate variations.

Following, the RH and temperature sensors data for indoor and outside in the period from February to January is presented, considering a period of 12 months. Figure 6 shows a graph with hourly measurements for the months of February and March. Table 1 shows the minimum and maximum values, as well as the mean RH and temperature for each of the monitored environments for this period.

Based on Fig. 6, the oscillation between the minimum and maximum values of RH presents greater amplitude for the data collected on the outside of the building compared to inner values, both for February and March. The indoors means of RH have been above 60 % for the two months, with temperature averages around 25 °C. However, the outside sensor data showed that about 48 % of the time the RH was above 80 % in February. In March, the outside RH was on average 59 % of the

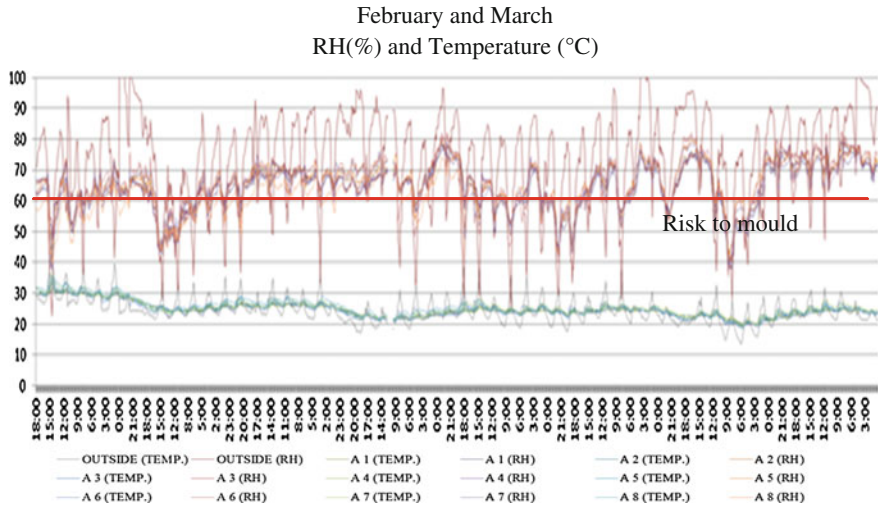


Fig. 6 RH and temperature sensors for indoor and outside from February to March

Table 1 Minimum, maximum, and mean values for RH and temperature in February and March

			A1	A2	A3	A4	A5	A6	A7	A8	Outside
February	RH (%)	Min.	38	44	43.4	42.7	40.6	37.6	37.5	39.2	22.5
		Max.	70.2	72.7	73.9	73.1	74.4	75.9	76.1	70.2	>100
		Mean	61.9	64.1	63.5	63.6	64.9	64.4	63.9	60	73.6
	Temp. (°C)	Min.	21.7	21.3	21.7	22.1	21.3	20.9	21.7	22.1	17.1
		Max.	35.3	33.2	31.1	31.9	34.8	36.1	36.1	35.3	45.9
		Mean	26.5	26.4	26.2	26.3	26.8	26.3	26.8	27.5	25.9
March	RH (%)	Min.	37.7	40.3	39.3	37.1	41.1	35.3	38.5	40.7	24.7
		Max.	77	79.2	81.9	79.3	79.4	82	78.2	74.1	>100
		Mean	64.5	66.2	66.9	66.2	66.4	65.4	65	64.4	73.6
	Temp. (°C)	Min.	19.8	19.4	19.8	20.2	18.6	18.3	19	21.3	13.7
		Max.	27.1	26.7	25.7	25.2	27.5	27.9	28.3	29.5	38.7
		Mean	23.6	23.5	23.2	23.3	23.8	23.8	24.3	24.2	23.5

time above 80 %. In both months condensation occurred in certain periods. Thus, it would be prudent to prevent this moisture from the outside air to stay retained indoors. It can increase the risk of condensation with the reduction in the indoor air temperature. For the reporting period, there is the risk of fungal recurrence if other requirements are met, particularly in relation to nutritional conditions.

Figure 7 shows a graph with hourly measurements for the month of April and May. Table 2 shows the minimum and maximum values, as well as the mean RH and temperature for each of the environments monitored for this period.

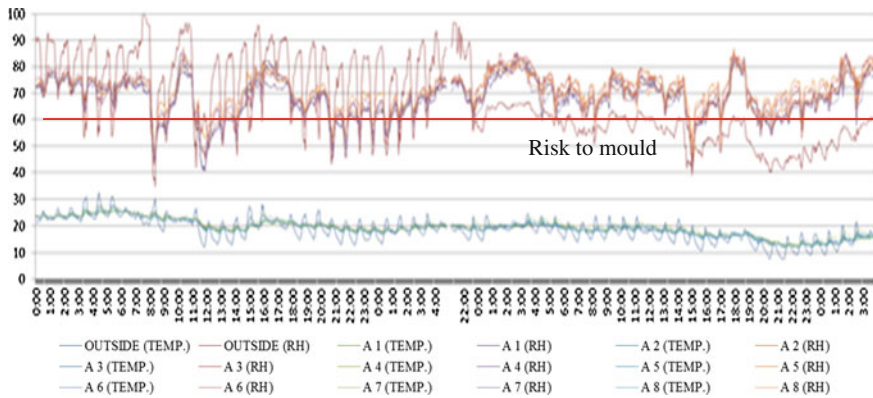


Fig. 7 RH and temperature sensors for indoor and outside from April to May

Table 2 Minimum, maximum, and mean of the values for RH and temperature in April and May

			A1	A2	A3	A4	A5	A6	A7	A8	Outside
April	RH (%)	Min.	41.3	43.2	44.1	40.5	47.3	42.7	44.1	–	34.7
		Max.	80.6	87.2	85.2	83.5	83.5	87.2	85.2	–	>100
		Mean	66.4	67.9	67	67.1	69.9	67.9	67	–	76.4
	Temp. (°C)	Min.	17.9	16.8	17.5	17.9	16.8	16.8	17.5	–	12.6
		Max.	25.6	27.5	27.5	25.6	26.7	27.5	27.5	–	32.3
		Mean	21.3	21.4	21.9	21.2	21.2	21.4	21.9	–	20.8
May	RH (%)	Min.	40.7	42.9	44.1	40.1	48.4	38.6	48.5	47.3	40
		Max.	83.7	83.5	85.3	85.2	87.1	85.3	83.6	83.8	96.6
		Mean	69	70.5	71.1	69.8	73.8	72.2	69	70.2	57.1
	Temp. (°C)	Min.	12.2	12.2	12.9	12.9	11.7	11.7	11.7	11.7	7.4
		Max.	22.9	21.3	20.6	20.9	21.7	22.5	23.2	22.5	24.4
		Mean	17.3	17.3	17.2	17.3	17.3	17.3	17.3	18.3	17.6

Between April and May, there was a small rise in indoor RH. It is believed that due to the natural ventilation mechanism adopted in the building, the wet air outdoors could be conducted to the interior environment, increasing the RH. However, the maximum interior was still maintained below the outside.

In April, the outer RH was over 80 % about 52 % of the time. In May there was a considerable reduction in the external RH, with the occurrence of a few days with incidence above 80 %. However, inside RH remained high and temperature remained higher regarding the values obtained abroad, which presents itself as a favorable aspect, due to the increase in RH values. Thus, remained the risk of recurrence fungi, which tends to be intensified since the moisture being retained within the environments and the temperature period on them tends to be gradually reduced, increasing the risk of condensation on surfaces.

Between April and May, there was a small rise in indoor RH. It is believed that due to the natural ventilation mechanism adopted in the building, the wet air outdoors could be conducted to the interior environment, increasing the RH. However, the maximum interior was still maintained below the outside.

In April, the outer RH was over 80 % about 52 % of the time. In May there was a considerable reduction in the external RH, with the occurrence of a few days with incidence above 80 %. However, the inside RH remained high and temperature remained higher regarding the values obtained abroad, which presents itself as a favorable aspect, due to the increase in RH values. Thus remained the risk of recurrence fungi, which tends to be intensified since the moisture being retained within the environments and the temperature period on them tends to gradually reduce, increasing the risk of condensation on surfaces.

Figure 8 shows a graph with hourly measurements for the months of June and July. Table 3 shows the minimum and maximum values, as well as the mean RH and temperature. During this period, the interior RH values kept rising, staying on average above 70 % due to the reduction in temperature values in indoor environments, increased by the risk of moisture surface condensation from the indoor air. It is possible to verify in early June that the outside RH was about 59 % of the time below 60 %. However, this reduction in outside RH was not accompanied in the indoor environment. This reveals that moisture remained trapped within environments.

Figure 9 shows a graph with hourly measurements for the months of August and September. Based on the collected data it is possible to assess that in about 80 % of the time, the average indoor RH among all ambiances was above 60 %. Furthermore, in about 60 % of the time, RH was above 70 %. Since there is the

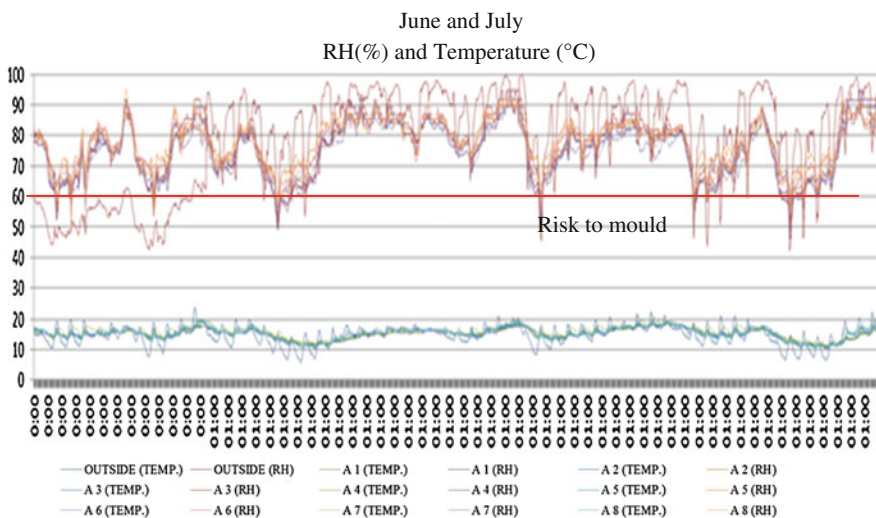


Fig. 8 RH and temperature sensors for indoor and outside from June to July

Table 3 Minimum, maximum, and mean values for RH and temperature in June and July

			A1	A2	A3	A4	A5	A6	A7	A8	Outside
June	RH (%)	Min.	48.9	50	53.6	51.4	56.8	52.1	55.5	47.7	42.4
		Max.	89.2	89.2	91.8	91.7	89.3	91.8	91.7	94.8	98
		Mean	74.7	76.1	76.8	75.2	78.2	76.7	74.8	77	72.9
	Temp. (°C)	Min.	11	11.4	11.7	11.7	10.2	10.6	11	10.2	5.8
		Max.	17.5	18.3	17.5	18.3	18.7	19.8	19.4	19	24
		Mean	14.9	15	15	15.1	14.9	15.1	15.7	15.2	14.6
July	RH (%)	Min.	46.2	47	51.5	47.8	56.2	49.6	52.5	54.1	42.2
		Max.	91.8	91.8	94.9	94.9	91.8	91.8	89.3	94.9	100
		Mean	74.9	76.6	77.7	76	79.2	77	75	77.1	84.6
	Temp. (°C)	Min.	10.6	11	11.4	11.4	9.8	10.2	11	10.2	6.6
		Max.	19	19	18.3	18.7	19	19.4	20.2	19.4	22.5
		Mean	15.3	15.4	15.4	15.4	15.1	15.4	16.2	15.7	15

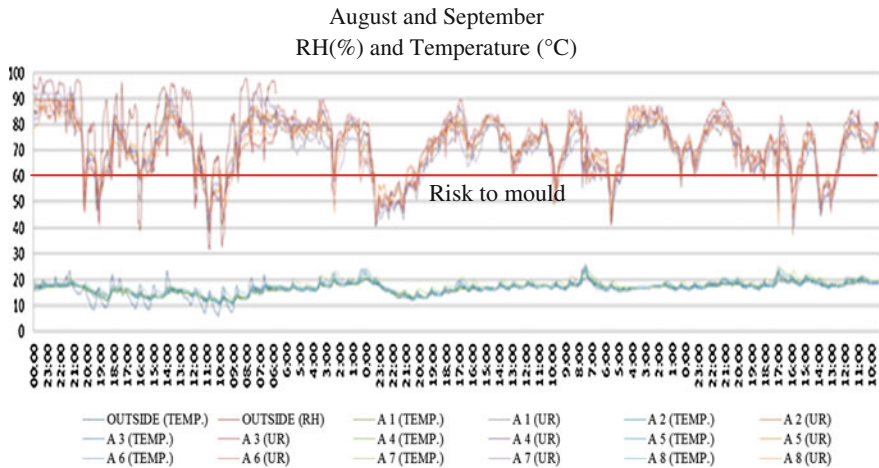


Fig. 9 RH and temperature sensors for indoor and outside from June to July

reduction in the outside temperature, accompanied by a reduction in the inside environments, there is a high risk of condensation and consequent higher moisture retention through the materials’ pores. Thus, there is an imminent possibility of recurrence of the filamentous fungi growth.

Table 4 gives the RH and temperature for each of the monitored environments. During this period a failure in the external sensor occurred. Unfortunately, the equipment could not be replaced, therefore, it was only possible to register the indoors monitoring.

For a rough check of the RH and temperature outside, data were obtained from the Meteorological Station of EMBRAPA (*Empresa Brasileira de Pesquisa*

Table 4 Minimum, maximum, and mean values for RH and temperature in August and September

			A1	A2	A3	A4	A5	A6	A7	A8	Outside
August	RH (%)	Min.	37.6	39.6	39.6	40.7	45.2	38.7	41.4	40.5	Not registered
		Max.	89.2	89.3	91.8	91.7	91.7	89.2	94.9	89.3	
		Mean	70.3	71.9	72.3	71.7	73.3	70.4	71.1	69.6	
	Temp. (°C)	Min.	10.6	11	11.8	10.6	10.6	11	11.8	11.4	
		Max.	21.3	15.6	19.8	20.2	22.9	24.0	24.0	23.6	
		Mean	15.7	15.6	15.6	15.8	15.6	15.7	16.2	16.7	
September	RH (%)	Min.	16.4	15.6	16	16	15.2	15.2	16.4	15.6	Not registered
		Max.	24.4	25.2	21.7	22.9	22.9	25.2	25.6	25.2	
		Mean	18.2	17.9	17.6	17.9	18	17.9	19.2	18.5	
	Temp. (°C)	Min.	40.8	42.1	44.2	40.9	43.7	37.1	40.4	41	
		Max.	82.2	83.6	89.3	85.3	85.3	87.1	87.1	87.1	
		Mean	68.8	71.9	73.9	71.4	72.2	71.8	69.3	71	

Agropecuária or Brazilian Agricultural Research Company of Pelotas). In September, the meteorological station found an average air temperature of 16.5 °C and an average of 86.3 % RH.

During August and September, the mean values of RH remained around 70 %, favorable condition for the growth of several species of fungi.

Figure 10 shows a graph with hourly measurements for the months of October and November. Table 5 gives the RH and temperature for each of the monitored environments.

In October, it notes that the RH stayed above 60 % (about 88 % of the time). However, in November, it is clear that the RH gradually starts to reduce (only about

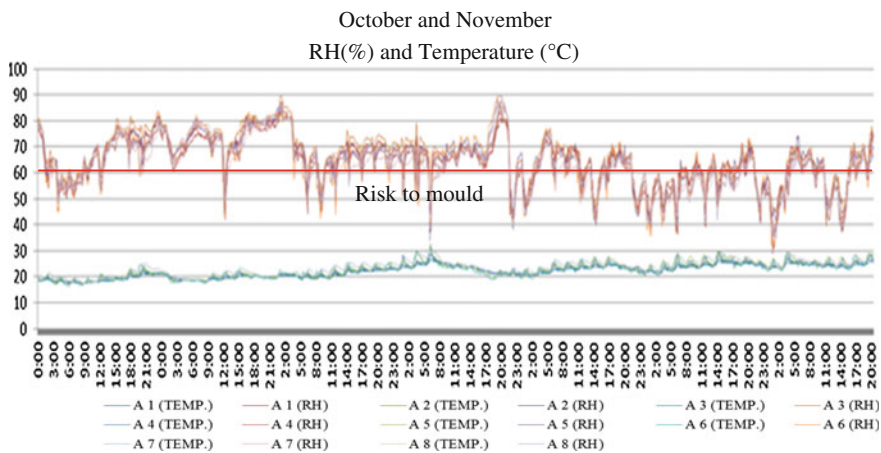


Fig. 10 RH and temperature sensors for indoor and outside from October to November

Table 5 Minimum, maximum, and mean values for RH and temperature in October and November

			A1	A2	A3	A4	A5	A6	A7	A8	Outside
October	RH (%)	Min.	36.9	36.9	47.4	44.8	42.1	39.6	44.1	33.7	Not registered
		Max.	85.2	85.2	89.3	87.1	85.2	83.6	87.1	87.1	
		Mean	66.9	69.6	71.3	68.7	68.4	68.2	67.5	68	
	Temp. (°C)	Min.	17.5	17.1	17.5	17.1	16.8	16.4	17.5	16.8	
		Max.	30.7	31.9	26.7	29.1	30.3	31.1	31.9	32.8	
		Mean	21.1	20.8	20.5	20.7	21.2	21.1	22	21.5	
November	RH (%)	Min.	28.9	38.3	39.4	32	36.6	30.6	30	34.9	Not registered
		Max.	80.6	87.1	85.2	83.5	87.1	89.4	87.1	89.4	
		Mean	58.2	61.1	61.8	61	60.5	60.6	58.8	59	
	Temp. (°C)	Min.	20.2	20.2	20.2	20.6	19.4	19	20.6	19.8	
		Max.	29.1	28.3	26.3	27.5	29.9	29.9	29.5	29.5	
		Mean	24.1	23.8	23.4	23.8	24.6	23.9	24.9	24.4	

23 % of the time with over 60 % RH). It should be noted that this time the temperature also begins to rise. This is a period in which there is a softening of the conditions which favor the growth of fungi.

For the months of October and November, the weather station found the average values of 19.4 °C air temperature and 85.10 % RH for the first month; and 21.4 °C temperature and 78.2 % RH for the second month.

Figure 11 shows a graph with hourly measurements for the months of December and January, completing 12 months of monitoring. Table 6 shows the minimum and

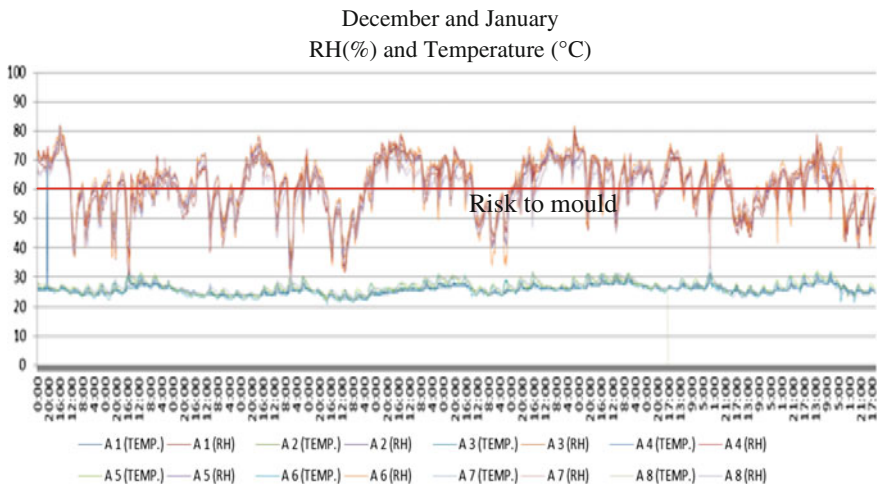


Fig. 11 RH and temperature sensors for indoor and outside from December to January

Table 6 Minimum, maximum, and mean values for RH and temperature in December and January

			A1	A2	A3	A4	A5	A6	A7	A8	Outside
December	RH (%)	Min.	29.2	31.9	36.3	32.4	33.1	30.4	29.6	27.5	Not registered
		Max.	77.9	79.1	81.9	81.9	80.4	81.9	81.9	81.9	
		Mean	59.3	61.9	62.5	61.5	60.7	61.3	59.5	58.4	
	Temp. (°C)	Min.	22.5	22.1	22.5	22.5	22.1	20.9	22.9	22.1	
		Max.	31.9	73.1	73.1	73	31.5	30.7	30.3	31.1	
		Mean	25.5	25.2	24.9	25.2	26.2	25.4	26.3	26.2	
January	RH (%)	Min.	39.9	43.7	44.1	41	40.3	33.6	32.6	40.5	Not registered
		Max.	79.1	79.1	81.9	80.4	74.8	78	77.9	73.9	
		Mean	60.4	62.3	62.9	62.2	60.9	61.8	62	60.1	
	Temp. (°C)	Min.	24	23.2	24.4	24	23.2	21.3	23.2	24	
		Max.	31.5	30.7	29.1	30.7	31.9	31.9	35.7	31.9	
		Mean	26.7	26.5	26.3	26.4	27.6	26.7	27	27.8	

maximum values, as well as the mean RH and temperature for each of the environments monitored in the period.

In December, one can see that about 58 % of the time, the RH was above 60 %, with temperature around 25 °C. In January, about 63 % of the time, the RH was above 60 %. Therefore, the microclimate favorable factors to fungal developments remains.

For the months of December and January, the weather station found the average values of 22.5 °C air temperature and 80.9 % RH for the first month; and 23.9 °C temperature and 81.6 % RH for the second month.

The eight indoor environments monitored showed similar values for both RH and temperature. However, for the whole period, it was observed that the environment A5 had, on average, higher RH values. This environment is one of the smaller ones of the building and a less open area for natural ventilation and lighting. It is used as a bookstore, having shelves and covers in all free surfaces. Therefore, in this environment, it is even more probable the recurrence of filamentous fungi.

Environment A1 presented, on average, slightly lower values for RH than the others did. Although still unoccupied, environment A1 is intended to become a showroom. This space has large and outward-oriented window frames in two of its walls. The other walls have gateways to adjacent environments. These doors remain open, allowing free circulation of air.

It is important to mention that the building is being occupied and remains open throughout the week. Constant cleaning of its environments is a part of the building's routine. A team of professionals in the field of conservation constantly monitors this building.

However, without conducting an analysis to check the behavior of the building microclimate or with a lack of understanding of the behavior of materials of the building in relation to temperature and humidity, it is often quite difficult to contain

the recurrence of problems, especially pathological manifestations related to biological growth, like filamentous fungi.

5 Conclusions

Through the analysis developed, we confirmed that there is a high possibility of recurrence of filamentous fungi because of the microclimate inside the building, especially during winter, when high rates of RH and lower values of temperature can cause the occurrence of condensation on surfaces.

In winter, when it becomes disadvantageous to open the windows for natural ventilation due to inappropriate external conditions, implementation of heaters inside the environments is needed.

In the period of heat, when the outside RH is low, it is recommended to open the doors and windows for natural ventilation and fresh air within the environments.

It is important to emphasize the necessity of performing routine cleaning with a unique character, as it is highly important to remove the dust and dirt on all surfaces of the environments observed, like the surfaces and corners of walls, ceilings, and internal and external doors and windows.

Since this is a historical building, a measure favorable for its preservation is to adopt preventive actions and continuous maintenance. The monitoring and constant observation of the environment, regarding microclimate conditions and the condition of the materials, greatly reduces the chance of recurrence and advancement of deterioration from elements. This measure protects the building's need for new restoration interventions, procedures that result in high investment costs and losses on historical materials.

References

- Allsopp D, Seal KJ, Gaylarde C (2010) Introduction to biodeterioration, 2nd edn. Cambridge University Press, New York, p 237
- Arroyo I (2009) Role of fungi in the deterioration of cultural heritage. In: *e_conservation* magazine. Issue 9, April 2009. URL: <http://www.e-conservationline.com>
- Caneva G, Nugari MP, Salvadori O (2000) La biología en la restauración. Nerea, Sevilla, 274 p
- Crispim CA (2003) Identification of cyanobacteria in biofilms on external surfaces of historical buildings: morphological and molecular analysis. Master Thesis. Post Graduate Program in Agricultural Microbiology and Environment. Federal university of Rio Grande do Sul, Brazil
- Crook B, Burton NC (2010) Indoor moulds, sick buildings syndrome and building related illness. *Fungal Biol Rev* 24:106–113
- Johansson P, Ekstrand-Tobin A, Svensson T, Bok G (2012) Laboratory study to determine the critical moisture level for mould growth on building materials. *Int Biodeterior Biodegradation* 73:23–32
- Kiel G (2005) Bacterial diversity in biofilms on external surfaces of historic buildings in Porto Alegre. Master Thesis. Post Graduate Program in Agricultural Microbiology and Environment. Federal university of Rio Grande do Sul, Brazil

- Krus M, Kilian R, Sedlbauer K (2007) Mould growth prediction by computational simulation on historic building. Museum Microclimates. National Museum of Denmark
- Sedlbauer K, Krus M, Breuer K (2003) Mould Growth Prediction a new biohygrothermal method and its application in practice. IX Polska Konferencja Naukowo-Techniczna Fizyka Budowli w Teorii i Praktyce, Conference paper, Łódź
- Shirakawa MA (1994) Estudo da biodeterioração do concreto por *Thiobacillus*. Master Thesis in Science in the Area Power and Nuclear reactors Nuclear Fuel technology. Institute of Research and Nuclear Energy—Authority associated with the University of São Paulo, Brazil
- Shirakawa MA, Cincotto MA, Carneiro AMP, Gambale W (1997) Atividade de água e biodeterioração de argamassas por fungos filamentosos. In: II Simpósio Brasileiro de Tecnologia das Argamassas—Salvador, Bahia, Brazil
- Shirakawa MA, Gaylarde CC, Gaylarde PM, John V, Gambale W (2002) Fungal colonization and succession on newly painted buildings and the effect of biocide. *FEMS Microbiol Ecol* 39:165–173
- Shirakawa MA, Beech IB, Tapper R, Cincotto MA, Gambale W (2003) The development of a method to evaluate bioreceptivity of indoor mortar plastering to fungal growth. *Int Biodeterior Biodegradation* 83:83–92
- Sterflinger K (2010) Fungi: their role in deterioration on cultural heritage. *Fungal Biol Rev* 24:46–55
- Sterflinger K, Piñar G (2013) Microbial deterioration of cultural heritage and works of arts—tilting at windmills. *Appl Microbiol Biotechnol*
- Vieira EN, Cesar RT, John VM, Barros MMSB, Shirakawa MA (2009) Influência de aditivos em argamassa de revestimento com pintura nos crescimento de fungos em condições de ciclos de molhagem e secagem. In: VIII Simpósio Brasileiro de Tecnologia das argamassas. Curitiba, Brazil
- Warsheid T, Braams J (2000) Biodeterioration of stone: a review. *Int Biodeterior Biodegradation* 46:343–368